Study of corneal ultrastructure in normal and post-LASIK human eyes

Thesis submitted to Cardiff University for the degree of

Doctor of Philosophy

Mohammad Abahussin B.Sc (Optom), M.Optom

School of Optometry & Vision Sciences

Cardiff University

2008

ProQuest LLC
789 East Eisenhower Parkway
P.O. Box 1346
Ann Arbor, MI 48106-1346

In the name of Allah (God), the most gracious, the most merciful

Acknowledgements

First and foremost, my praise and thanks are due to ALLAH. Without his blessings and guidance, this work would not have been undertaken.

I deeply appreciate and thank my supervisor Prof. Keith Meek for his continued support, valuable suggestions, endless encouragement, and never-ending patience throughout my PhD study. Keith's comments on various drafts of the thesis were extremely helpful.

I would also like to thank Dr. Sally Hayes and Dr. Craig Boote for their help and advice with the XRD experiments. Sally's smile and patience during XRD data analysis were highly appreciated. I must also thank Dr. Saeed Akhter, Dr. Rob Young, and Dr. Phil Lewis for their help and advice with TEM technique. They supported me with their TEM experience without hesitation. Special thanks must be extended to the staff of the biophysics group as well as to my friends at the school of optometry and vision sciences. Ali, Saud, Abdulaziz, and other postgraduate students: I have had a great time with you all and hope to see you become doctors in the near future. Special thanks go to my best friend Dr. Abdullah Assiri for his support during my first PhD year. Abdullah motivated and inspired me and was always in a good mood; I do not know how, really!!

A big thank you is due to the young EM expert, Dr. Anthony Hann, for his continuous help and support. Hann's words made a hard task as simple as 1-2-3. I also would like to thank the staff of the Synchrotron Radiation Source (SRS, Daresbury, UK) for their help during the XRD experiments, Dr. Val Smith from Bristol Eye Bank for providing the human corneas, and King Khaled Eye Specialist Hospital (Riyadh, Saudi Arabia) for the ectatic corneal tissues. Special thanks are also offered to Prof John Marshall and his research group at St. Thomas hospital (London, UK). Dr. Yaser Khan from John's group helped me greatly during femtosecond laser and *in vitro* LASIK experiments: thank you,

Yaser. In addition, thanks to Mr. Sheraz Daya and his research group at the Centre for Sight (East Grinstead, UK) for helping me to complete the femtosecond laser experiment.

I must also thank King Saud University for giving me the chance and support to run this PhD study. Thank you, too, to my friends in Cardiff. I spent one of the best times of my life with you. Your friendship, your help, and your encouragement will not be forgotten.

Finally, I am particularly grateful to my brothers, my sisters, and my relatives at home (Saudi Arabia) for their continued support and concern about the progress of my study and their honest prayers for me.

.....

Dedication

To my wife Asma for her patience, support, and encouragement during my PhD study. She sacrificed a lot throughout the period of my study.

To my beloved children Hanin and Ziyad. They tried so hard to be as quiet as they could, to allow me to write my thesis without disturbance.

Abstract

Laser in situ keratomileusis (LASIK) is a surgical technique used to correct refractive errors by reshaping the cornea. Although LASIK is superior to other visual correction techniques, recent clinical reports show that, in some cases, it leads to serious optical problems. Therefore, the aim of this thesis was to study the corneal ultrastructure in normal and LASIK corneas and discover a reason for the deterioration of vision in some LASIK patients. Different experiments were run, from experiments to improve understanding of the collagen fibril arrangement in the human cornea to studying the corneal changes in post-LASIK ectasia. Also, different techniques were used in this study including wide-angle x-ray diffraction (XRD), transmission electron microscopy (TEM), scanning electron microscopy (SEM), and light microscopy (LM).

XRD showed that the human cornea possesses a unique orthogonal central collagen fibril orientation that was not found in the corneas of animals, such as camels or rabbits, which were found to have unidirectional or circular collagen orientation respectively. However, all human, camel, and rabbit corneas were found to have the same collagen fibril orientation around the limbus, that is, an annulus circumscribing the cornea.

XRD was also used to study the effect of corneal full-thickness trephination on collagen fibril arrangement, trying to mimic penetrating keratoplasty (PKP) and LASIK procedures. The results indicate that central corneal trephination (at 4 mm diameter) will change the collagen fibril arrangement around the trephine-wound edges. This effect will be reduced if the trephination is made away from the centre, toward the limbus. These results may encourage ophthalmic surgeons to use a large graft diameter for PKP in order to avoid postoperative complications such as astigmatism. Also, these results may give a good explanation for the low post-LASIK astigmatism rate found in the literature.

As LASIK surgery includes flap creation and laser ablation, it was preferable to study the collagen fibril arrangement at different corneal depths (by means of femtosecond laser and XRD) in order to understand the precise effect of the LASIK technique on collagen lamellae. It was found that the first third (33%) of the corneal thickness has an irregular collagen lamellar orientation whereas the orientation clearly becomes orthogonal towards the posterior cornea (endothelium side). Thus, it can be concluded that LASIK flap creation and laser stromal ablation usually occur in the irregular collagen fibril layers. These layers have been found to be the strongest part of the cornea and are essential to maintain corneal curvature and strength. Therefore, these findings allow us to understand the reason for high astigmatism or ectasia in some LASIK patients.

In vitro LASIK was then conducted on donor human corneas to simulate the *in vivo* situation of LASIK so that the collagen fibril orientation and other corneal structural changes could be studied by means of XRD, SEM, and TEM. XRD results indicated that the collagen fibril orientation and distribution after LASIK are similar to those in normal corneas. This normal orientation was expected because the flap creation and the laser ablation usually occurred in the first third of the corneal thickness, which has been found to have an irregular collagen fibril orientation and hence, the full corneal thickness XRD cannot reveal the localised effects of LASIK. XRD on post-LASIK ectatic corneas showed that the collagen fibril orientation was also similar to that of the normal cornea, that is, it showed an orthogonal collagen orientation.

TEM, SEM, and LM of normal and ectatic LASIK corneas showed that the flap-bed interface can be detected easily regardless of the time after surgery; flap borders have been detected up to 10 years after the LASIK procedure. Moreover, the results indicate that the LASIK corneal wound healing happens superficially (epithelium healing only) and also show that the collagen lamellae do not bond with each other again after LASIK, which leaves the flap weak and, thus, explains the easy separation or dislocation of the flap from the stromal bed months or

years after surgery. Also, the results give an overview of the corneal biomechanical insults caused by the LASIK flap, which seem difficult to avoid and, in some cases, may lead to ectasia.

Interestingly, TEM shows that the collagen fibril diameter and interfibrillar spacing of both normal and ectatic LASIK corneas appear similar to those in normal corneas, which may explain the perfect visual acuity results obtained immediately after LASIK surgery and, also, indicates (according to the above results) that the reduced vision in ectatic patients is not a result of any disarrangement of the collagen fibrils, which is known to affect corneal transparency, but, instead, is a result of a corneal biomechanics insult due to the flap creation and tissue ablation.

.....

Table of Contents

.....

List of Figures

List of Tables

.....

Chapter 1. Introduction

1.1 Cornea

The cornea is a thin layer of transparent tissue surrounded by fluid (tear film anteriorly and aqueous humour posteriorly) and it covers one-sixth of the circumference of the eyeball, with sclera covering the remaining five-sixths (Figure 1.1).

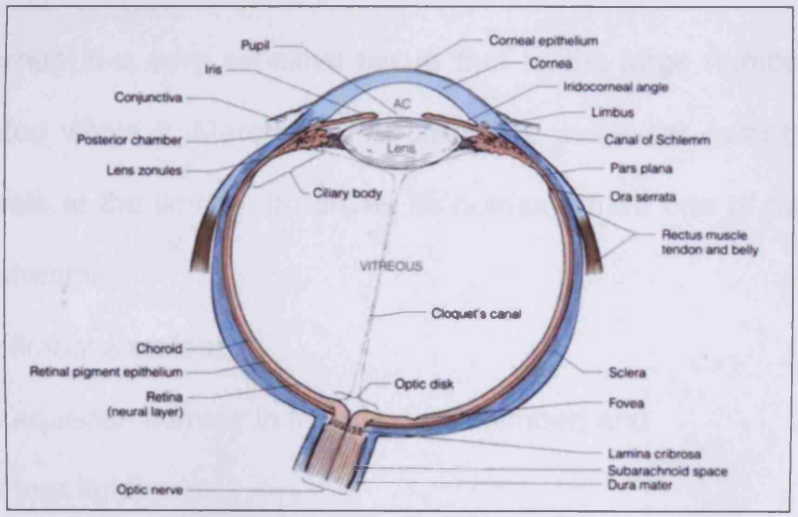

Figure 1.1: Cross section through the human eyeball revealing the major components (Forrester *et al.* 2002).

Descriptions of corneal anatomy and physiology have been published by many authors (Duke-Elder and Wybar. 1961; Maurice 1984; Kaufman *et al.* 1988; Fatt and Weissman 1992; Smolin and Thoft 1994; Bennett and Rabbetts 1998; Forrester *et al.* 2002). The main functions of the cornea are transmitting (and refracting) light to help focus the object being viewed onto the retina, and protecting the intraocular contents. The average central corneal thickness is about 540 µm, increasing to about 700 µm in the

periphery, and the cornea has a diameter, from the front surface, of about 11 mm vertically and 12 mm horizontally. The average corneal curvature in the adult cornea is approximately 7.8 mm anteriorly and 6.5 mm posteriorly. The bulk of the cornea consists of the extracellular matrix that is largely formed of collagen, plus a variety of complex molecules that are important in corneal maintenance and healing. In the extreme periphery, there is an opaque tissue called sclera. The border between cornea and sclera is known as the limbus (Figure 1.1).

The cornea is a very sensitive tissue due to the large number of nerve fibres located within it. Moreover, the cornea is avascular, with the nearest blood vessels at the limbus. It derives its nutrients from one of the following encircling streams:

- The limbal arcades;
- The aqueous humour in the anterior chamber; and
- The tear fluid.

The transparency of the cornea is its most important property. Due to its highly exposed position, it must present a clear medium to light and a tough physical barrier to trauma and infection. Any disturbance of the corneal metabolism, for example, the deprivation of nutrients or oxygen, leads to oedema and corneal swelling, and reduces transparency. The reason behind corneal transparency is still not fully understood, although many studies have been conducted to investigate the ultrastructure of the cornea, that is, the direction, diameter and organisation of the collagen fibrils (Maurice 1957; Maurice 1984; Meek and Fullwood 2001).

1.2 Corneal layers

The cornea is composed of five layers, as shown in Figures 1.2 and 1.3. From anterior to posterior they are the epithelium, Bowman's membrane, the stroma, Descemet's membrane, and the endothelium.

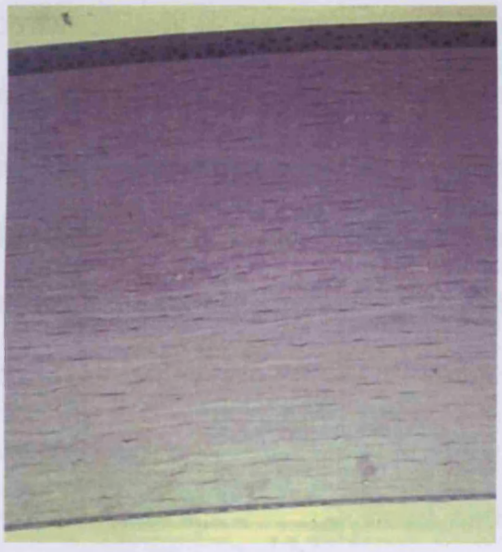

Figure 1.2: Cross section of the cornea. Light micrograph, magnification ~x100 (Efron 2001).

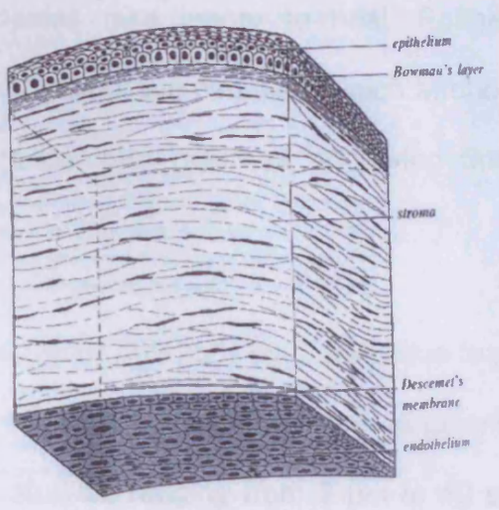

Figure 1.3: Sketch of the cross section of corneal layers (Saude 1993).

The epithelium is approximately 60 μm in thickness (Li *et al.* 1997) and is found on the outer corneal surface. It presents the first refracting interface to transmitted light. Three distinct shapes of cells are recognised in the epithelium: basal, wing, and squamous (or superficial) cells. The basal cells are the most internal and are attached to the basement membrane. The wing cells are two or three rows of cells found immediately in front of the single row of basal cells. External to the wing cells are two to three rows of flattened squamous cells. There are also cellular microprojections on the epithelial surface, that is, microvilli and microplicae, which vary between species and which are believed to be important in promoting tear stability to maintain a smooth optical surface (Collin and Collin 2000).

The life cycle of an epithelial cell has been estimated to be around seven days (Maurice 1984). In the case of layer disruption, the epithelium responds rapidly with an amoeboid sliding movement of cells on the wound margin followed by cell replication. While minor corneal abrasions heal within a few hours, severe injuries take longer to heal. Epithelial adhesion is maintained by a basement membrane complex, which anchors the epithelium to Bowman's layer via a complex mesh of anchoring fibrils and plaques (Forrester *et al.* 2002).

The epithelium is covered anteriorly by a protective tear film that can be as thick as 7 μm (Holly 1973). However, there are variations in the tear film thickness values among studies, ranging from 3 μm to 40 μm (Ehlers 1965; Benedetto *et al.* 1975; Prydal *et al.* 1992; Wang *et al.* 2003a). These

differences are due to different methods having been used in the measurement of thickness (Johnson and Murphy 2004). Tear film contains three layers: a lipid layer anteriorly to the air, an aqueous layer in the middle, and mucous layers attached to the epithelium (Johnson and Murphy 2004). Some studies, however, found that the tear film contains two layers only, as the aqueous and the mucous layers blend together and form one gel-like layer (Korb 2002). The tear film delivers oxygen to the epithelium when the eye is open; otherwise, the epithelium obtains diffused oxygen from conjunctival vessels (Friend and Hassell 1994). The tear film also serves to protect the cornea from drying out and ensures an excellent smooth optical surface for the cornea. It is therefore considered the sixth corneal layer because the cornea functions poorly without it.

Bowman's layer was described in humans by William Bowman in 1947 (Jacobsen *et al.* 1984). It measures approximately 17μm in thickness (Li *et al.* 1997) and consists of fine, closely packed, and randomly arranged collagen fibrils (Maurice 1984; Komai and Ushiki 1991). The anterior surface is separated from the epithelium by the thin basal lamina, while the posterior boundary merges with the stroma. The layer is perforated by nerve fibres arising from the stroma to supply the epithelium. In contrast to the epithelium layer, Bowman's layer cannot regenerate, which may explain recurrent erosion syndrome following refractive surgery, such as photorefractive keratotomy (PRK) or laser epithelial keratomileusis (LASEK).

The stroma is the largest part of the cornea and accounts for 90% of its total thickness. The stroma is composed mainly of water (80 %), collagen fibrils (15%), keratocytes, proteoglycans and other proteins (5%) (Duke-Elder and Wybar. 1961; Maurice 1984; Smolin and Thoft 1994). Collagen fibrils are found within 200 to 300 lamellae (see section 1.3). The stroma normally contains no blood or lymphatic vessels, but sensory nerve fibres are present in the anterior layers towards the epithelium.

Anteriorly, the stromal lamellae are slightly thinner and follow a more intertwined path, while posteriorly, the lamellae are laid down flatter. This anatomical variation between anterior and posterior lamellae may partly explain the tendency of the cornea to swell in a posterior to an anterior direction (Komai and Ushiki 1991; Radner *et al.* 1998; Muller *et al.* 2001; Radner and Mallinger 2002).

Keratocytes are the principle cells of the stroma and are responsible for the synthesis, secretion, and maintenance of the lamellar stroma (Gipson 1994). They are flat with long, extensive cytoplasmic processes and occupy 2-4% (2.4 million keratocytes) of the stroma in humans (Maurice 1984; Moller-Pedersen *et al.* 1994). The highest density of keratocytes is found anteriorly and from there the density declines in a posterior direction by as much as 30% (Moller-Pedersen and Ehlers 1995; Petroll *et al.* 1995). Further, keratocytes are arranged in a regular clockwise spiralling pattern and communicate with each other through gap junctions in both horizontal and vertical directions (Ueda *et al.* 1987; Muller *et al.* 1995). It is therefore thought

that keratocytes help keep lamellae stable in their locations (Komai and Ushiki 1991; Muller *et al.* 1995).

Descemet's membrane is a thin (8-12 μm), elastic membrane found between the posterior stroma and the endothelium. It can reform, has good resistance against infective agents, and acts as a modified basement membrane for the corneal endothelium, from which it is secreted. It has species variation in thickness and structure (Fatt and Weissman 1992; Forrester *et al.* 2002).

The endothelium is a single layer of about 400,000 cells/mm^2 and plays a critical role in maintaining corneal hydration and thus transparency by regulating stromal hydration, that is, by acting both as a fluid barrier and as a fluid pump, which removes fluid from the corneal tissue (Wigham *et al.* 1994). The endothelial cells rest on Descemet's membrane and form an uninterrupted polygonal or hexagonal array. The cells are 5-6 μm in height and 18-20 μm in diameter. These cells cannot reproduce after birth. Some cells are lost or die naturally with age. Therefore, damage to corneal endothelial cells, that is, when cell density reaches fewer than 500 cells/mm^2 in the case of, for example, corneal disease or refractive surgery, will affect the endothelium's function of driving out fluid that naturally accumulates in the cornea, thus leading to oedema and swelling of the stroma with a resultant loss of transparency (Saude 1993; Wigham *et al.* 1994; Efron 2001).

1.3 Collagen fibrils

Collagen is a fibrous protein found throughout the body and is a major component of all connective tissue, tendons, ligaments, bone, and skin. In the cornea, a number of individual collagens form natural linkages called collagen fibrils that run parallel to the corneal surface and continuous with the sclera at the limbus. Each group of collagen fibrils is joined uniformly in the lamella. The lamella measures 0.2-2.5 μm in thickness and 0.5-250 μm in width (Komai and Ushiki 1991). The corneal stroma consists of about 200-300 lamellae at the centre and about 500 at the limbus (Maurice 1957; Hamada *et al.* 1972; Radner *et al.* 1998) stacked on top of one another at different angles and surrounded by keratocytes (Figure 1.4). Usually, studies on collagen fibrils mention the thickness and width of lamellae only and do not mention the length as no lamellae ends have been detected. It is thought that the branches of lamellae merge with others to form new lamellae (Komai and Ushiki 1991; Radner *et al.* 1998). Collagen fibrils are the most critical aspects of structure needed to provide strength and rigidity to the cornea and determine its transparency (Maurice 1957; Newsome *et al.* 1981; Maurice 1984).

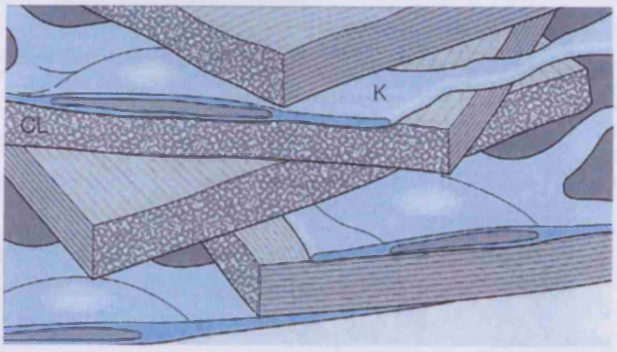

Figure 1.4: The arrangement of collagenous lamellae (CL) surrounded by keratocytes (K) (Forrester *et al.* 2002).

Pro alpha chains (pro-α chains) are the main components of collagen. After hydroxylation and glycosylation of these chains, each single collagen will have three chains of amino acids that spiral around one another to form a triple helix (Friend and Hassell 1994; Chan *et al.* 1997). The intertwined helices in a single collagen molecule form a thin strand about 1.5nm in diameter and 300nm long. Individual molecules form natural linkages, creating long assemblages of parallel molecules that are the collagen fibrils, as shown in Figure 1.5 (Burgeson 1988; Chan *et al.* 1997; Lamonde and Bateman 1997; Bores 2001). Different collagen fibril diameters are recorded throughout the literature i.e. 22-30nm due, it is thought, to the various methods used to prepare the tissue for measurement, that is, sample chemical fixation and dehydration for electron microscopy (EM) and sample unplanned dehydration before x-ray diffraction (XRD) measurements (Meek *et al.* 1991; Fratzl and Daxer 1993; Fullwood and Meek 1993). Moreover, it has been found that the collagen fibril diameters change during ageing (Daxer *et al.* 1998).

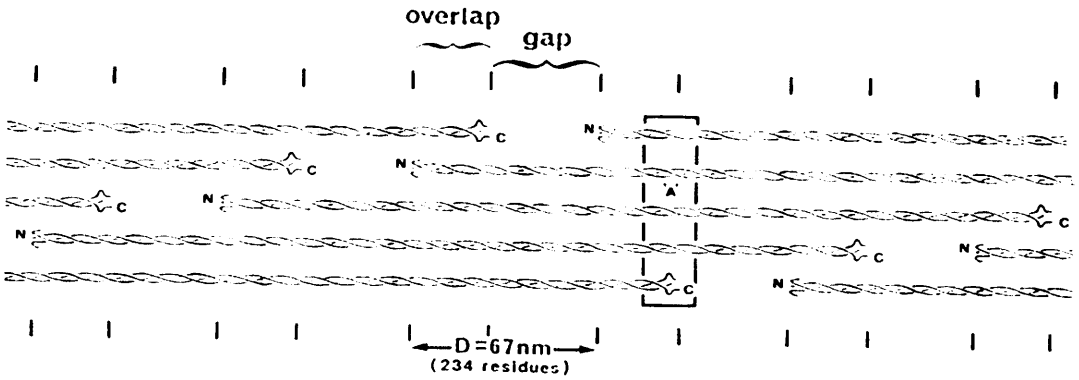

Figure 1.5: Schematic diagram shows the arrangement of triple helical collagen molecules in a fibril (Chapman *et al.* 1990).

Collagen type is defined based on the composition of the polypeptide chain (usually referred to as alpha chains) present in the triple helix. Currently, there are 26 different types of collagen recognised in vertebrates, 22 of them have been detected in the ocular tissues (Myllyharju and Kivirikko 2001; Sato *et al.* 2002; Michelacci 2003; Ihanamaki *et al.* 2004). Collagen type I is the major collagen in the cornea and comprises about 68% of the dry weight (Maurice 1984; Meek and Fullwood 2001). Types III, V, and VI are also present and comprise about 2%, 10%, and 20%, respectively, of the total collagen content (Newsome *et al.* 1982; Doane *et al.* 1992; Forrester *et al.* 2002). There are also several different types of collagen available in small quantities in each layer of the cornea as shown in Figure 1.6.

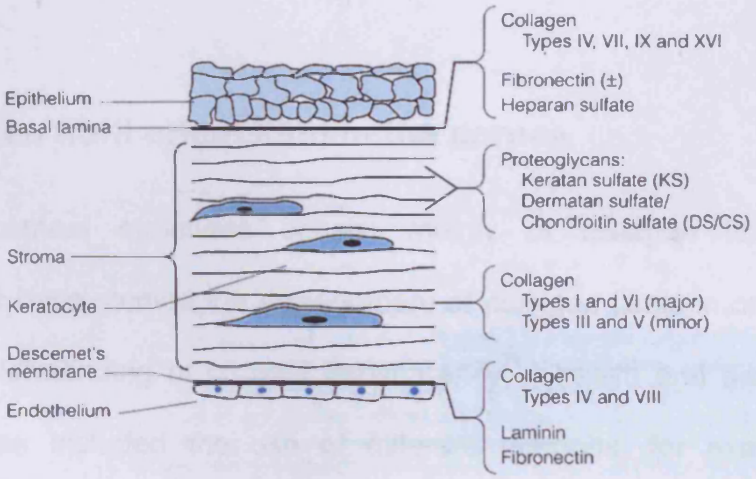

Figure 1.6: Collagen types in the cornea (Forrester *et al.* 2002).

Collagens have been classified into three types according to their molecular shapes and structural properties: fibril-forming collagen, fibril-associated collagens with interrupted triple helices (FACIT), and non-fibril-forming collagen. Table 1.1 summarises the families and types of collagen

(Zimmermann *et al.* 1986; Keene *et al.* 1991; Michelacci 2003; Ihanamaki *et al.* 2004).

Collagen family	Collagen type
Fibril-forming	I, II, III, V, XI
FACIT	IX, XII, XIV, XVI, XIX
Non-fibrillar	
Short chain	VIII, X
Basement membrane	IV
Anchoring fibrils	VII
Microfibrillar	VI
Other collagens	XIII, XV, XVII, XVIII, XX, XXI, XXII, XXIII, XXIV, XXV, XXVI

Table 1.1: Families and types of collagen (Michelacci 2003).

1.4 Collagen fibril orientation in the cornea

As corneal structures consist mainly of collagen fibrils, many investigators have studied the arrangement of collagen fibrils in order to gain a better understanding of corneal transparency in health and disease. This approach has included the use of different methods, for example, light microscopy (Duke-Elder and Wybar. 1961; Polack 1961), scanning electron microscopy (Komai and Ushiki 1991), transmission electron microscopy (Teng 1962; Maurice 1984; Klyse and Beuerman 1989), and x-ray diffraction (Goodfellow *et al.* 1978; Meek *et al.* 1981; Meek *et al.* 1987). The light microscope (LM) and electron microscope (EM) have not been as successful as x-ray diffraction (XRD) in determining or quantifying large-scale collagen

fibrils' orientations as the high magnification necessary to observe orientation is obtained at the expense of seeing the tissue as a whole. XRD, however, is well suited to providing quantitative fibril orientations. Moreover, in XRD, the tissue can be examined in its native condition whereas using LM or EM, the tissue must be fixed and dehydrated by a series of different chemical solutions to produce clear and detailed tissue images (Meek and Quantock 2001).

Most studies on collagen fibril orientation are based on the theory of transparency by David Maurice. Maurice (1957, 1984) suggested three conditions are necessary for excellent stromal transparency:

a) Constant thickness of the fibrils, arranged in parallel patterns;

b) Constant separation between the fibrils; and

c) This separation must be less than the wavelength of light.

In other words, as long as the collagen fibrils remain of uniform calibre and are not spaced further apart than $\lambda/2n$ (λ is the wavelength and n is the refractive index of the media), then the requirements for transparency are satisfied (Goldman and Benedek 1967). Intrusion of water into the stroma (swelling) upsets the arrangement of the collagen fibrils, that is, the distance between the collagen fibrils increases as the proteoglycans absorb water (Maurice 1957; Edelhauser 1994), which leads to aggregation and disorganisation of the collagen fibrils (Figure 1.7), and produces extra scattering and absorption of light, resulting in reduced corneal transparency.

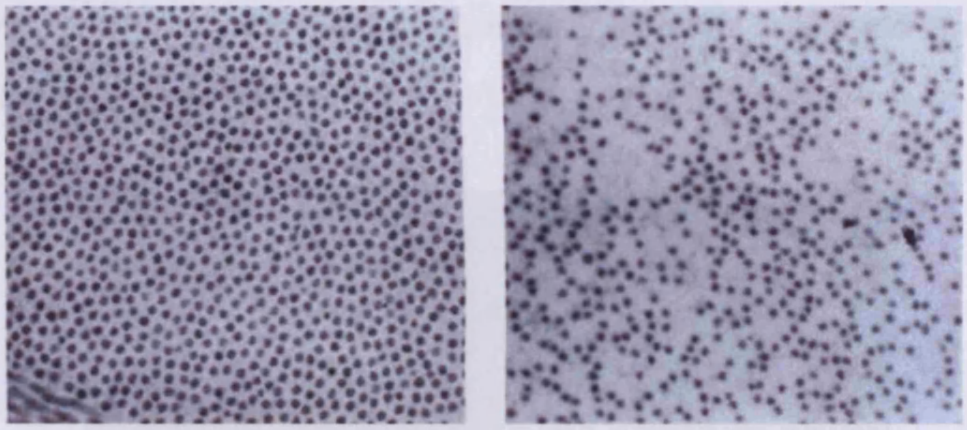

Figure 1.7: Transmission electron microscope pictures of human corneal stromal collagen fibril distribution in normal (left) and swollen (right) conditions (original magnification ~ x 50,000) (Smolin and Thoft 1994).

Using XRD, Meek *et al.* (1987) demonstrated that the collagen fibrils of the human cornea are arranged in an orthogonal shape along the horizontal (nasal - temporal) and vertical (inferior - superior) meridians. This arrangement of collagen fibrils is much more evident in the posterior stroma than in the anterior stroma. Scanning electron microscope (SEM) studies of human corneas have shown that in the anterior stroma, lamellar bundles run obliquely to the corneal surface, sometimes splitting into two or three sublayers that become interwoven (Figures 1.8 and 1.9), whereas in the posterior stroma, most of the lamellae lie parallel to the corneal surface (Komai and Ushiki 1991). Their study supports the XRD findings of Meek *et al.* (1987) that posterior stroma differ structurally to anterior stroma. Daxer and Fratzl (1997) found 66% of collagen fibrils within 45 degrees around vertical and horizontal meridians, whereas one third (34%) were at oblique angles. Another study, with slightly different findings from previous studies, reported lamellae crossed at many different angles and only occasionally at right angles, that is, only about 10% of crossed angles measured 90°. Also, the

distribution of crossed angles did not show any significant differences (Radner *et al.* 1998).

Figure 1.8: SEM image shows the anterior region of the cornea where irregular-shaped collagen lamellae run in different directions. They branched out or merge with other lamellae (arrows). Magnification x1100 (Komai and Ushiki 1991).

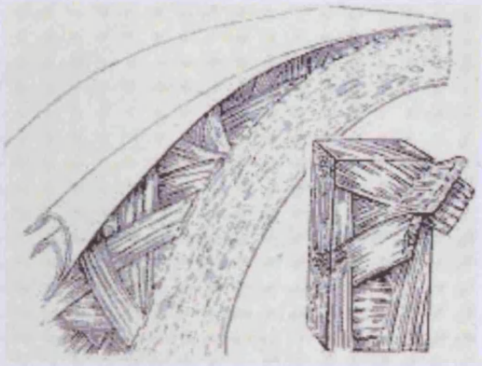

Figure 1.9: Sketch of collagen arrangement in the anterior stroma. From Grendahl Eye Associates: http://www.grendahl.com/eyeworks/eyeanatomy.html [accessed: 28 March 2008]

By using wide-angle XRD, Meek's group (Aghamohammadzadeh *et al.* 2004) was the first to generate a detailed map of the preferred collagen fibril orientations for normal human cornea (Figure 1.10). The map shows that the collagen fibril orientation remains orthogonal throughout the width of the

cornea until the region of the limbus where orientation becomes circumferential (Newton and Meek 1998a; Newton and Meek 1998b). The orthogonal orientation in the central human cornea has not been seen in other mammalian species and, instead, a uniaxial superior-inferior orientation existed (Meek *et al.* 1987; Quantock *et al.* 2003a; Boote *et al.* 2004; Hayes *et al.* 2007). However, other mammalian species have almost the same collagen fibril orientation near the limbus as have humans (Quantock *et al.* 2003a; Boote *et al.* 2004; Hayes *et al.* 2007).

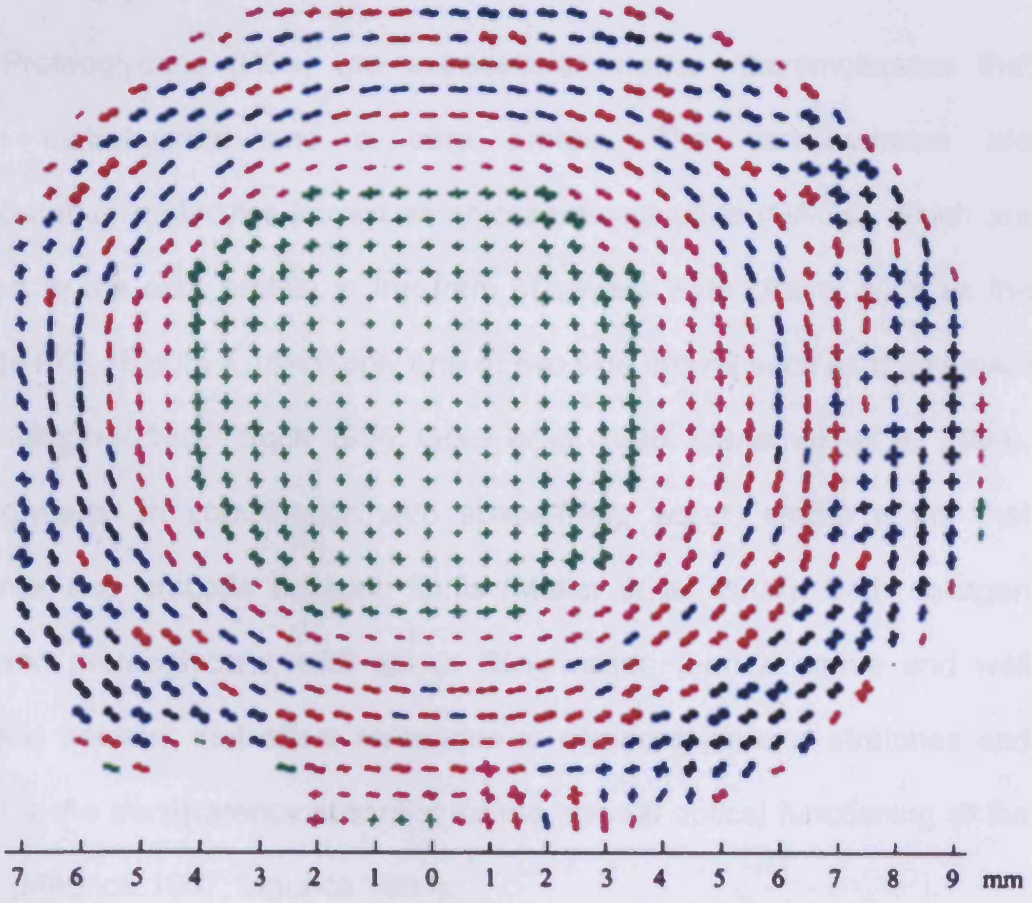

Figure 1.10: Wide-angle XRD map of collagen fibril orientation in normal human cornea. Each "propeller-shaped" plot shows the preferred collagen orientation(s) averaged throughout the tissue at that sampling point. The sizes of the plots are proportional to the amount of preferentially aligned collagen. Colours indicate the fact that as plots get larger towards the periphery, they need to be scaled down to fit on the grid. The colour key factors are: green, 1; pink, 2; red, 3; blue, 4; and black, 5 (Aghamohammadzadeh *et al.* 2004).

In the human cornea, preferred collagen fibril orientation corresponds to the directions of the insertion of the four rectus oculo-motor muscles thought to take up the mechanical forces of the eye muscles along the corneal trajectories (Daxer and Fratzl 1997). However, this conclusion does not apply to animal corneas where superior–inferior collagen fibril orientation is the dominant orientation and it is thought that most eye movements occur on the nasal - temporal muscles (Boote *et al.* 2004).

1.5 Proteoglycans

Proteoglycans (PGs) are extracellular matrix macromolecules that contain carbohydrate and a core protein. The carbohydrates are polysaccharide molecules known as glycosaminoglycans (GAGs), which are attached to the core protein in the form of several side chains such as the cartilage PGs (Figure 1.11) or only one or two side chains such as the corneal PGs (Gallagher 1989; Scott 1995; Goes *et al.* 1999; Ihanamaki *et al.* 2004). Proteoglycans, in combination with space-filling water, create a gel that surrounds and embeds collagen fibrils (Muller *et al.* 2004). Both collagen fibrils and proteoglycans, with space filling water, form a dense and well organised network that offers resistance to compression and stretches and maintains the transparency essential for the optimal optical functioning of the cornea (Maurice 1957; Maurice 1984).

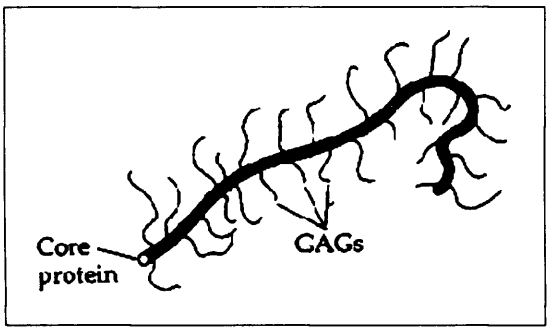

Figure 1.11: Sketch diagram shows proteoglycan with attached GAGs (Oyster 1999).

There are different types of proteoglycans according to the type of GAG side chains. The bulk of the corneal GAG (proteoglycan) is keratan sulphate, which represents about 50% of the total GAGs content in the stroma; most of the rest is chondroitin/dermatan sulphates (representing about 30% and 20% respectively), which have a closely related structure and are generally referred to simultaneously (Maurice and Riley 1970; Hassell *et al.* 1986; Scott and Bosworth 1990; Zieske 2001). The term, for example, keratan sulphate proteoglycan refers to a proteoglycan whose carbohydrate moiety consists of the GAG keratan sulphate. In addition, subsequent immunochemical and sequence analysis of the core proteins containing the keratan sulphate side chains indicates it to be lumican, keratocan, and mimecan. Also, analysis of the chondroitin/dermatan sulphate chains shows it to be decorin, the commom proteoglycan in the cornea (Li *et al.* 1992; Smolin and Thoft 1994).

GAGs have high water-binding capacity, which gives the corneal stroma a water content higher than that of connective tissue elsewhere in the body (Oyster 1999). Moreover, keratan sulphate, a more hydrophilic

proteoglycan, is prevalent in the posterior part of the corneal stroma, whereas dermatan sulphate, a much less hydrophilic proteoglycan, is prevalent in the anterior part. This proteoglycan organisation (besides the endothelial pump function) makes corneal swelling behaviour decrease gradually from the posterior to the anterior side (Scott 1995; Muller *et al.* 2001).

Proteoglycans are associated with collagen fibrils mostly at specific binding sites within the corneal collagen D-period, that is, at a, c, d, and e bands (Meek *et al.* 1986; Scott 1988; Scott and Haigh 1988). Also, it has been found that GAGs bridge and link adjacent collagen fibrils (Scott 1988). It is thought that these molecules play a role in maintaining both the relative positions and the diameter of the fibrils, both of which are required for stromal transparency (Rada *et al.* 1993; Scott and Thomlinson 1998; Meek and Fullwood 2001).

1.6 Photorefractive eye surgery

Traditionally, eyesight problems have been corrected with spectacles or contact lenses. In recent years, photorefractive eye surgery has become a popular alternative. It is performed with an excimer (excited dimer) laser machine, which uses a cool ultraviolet light beam (193 nm) to remove precisely (ablate) an exact depth of the corneal outer layer in order to reshape it (Waring and Seiler 1993; Bores 2001). Currently, there are several laser systems available in the market, such as VISX Co. (Sunnyvale, California); Summit Technologies (Watertown, Massachusetts); Bausch &Lomb

Technolas 217Z (Rochester, New York); Nidek EC-5000 (Gamagori, Japan); and Wavelight Allegretto Wave laser (Erlongen, Germany) (Sher *et al.* 1993; Bores 2001; Probst 2004). There are different vision correction procedures used by excimer laser machines, but the three most popular procedures are as follows.

Laser in situ keratomileusis (LASIK) is the most popular type of photorefractive surgery. Under this procedure, a thin layer of the cornea is sliced off to create a flap and allow the laser beam to hit the stroma directly. The flap is then replaced to its original position (see section 1.6.1 below for more details).

Laser Epithelial Keratomileusis (LASEK) is similar to LASIK, except that the surgeon cuts a flap in the epithelial layer only, instead of through the epithelium and part of the stroma. After that, the edge of the flap is loosened with alcohol. LASEK is used mostly for patients with a thin cornea who are considered poor candidates for LASIK. It is a relatively new procedure and its drawbacks include more discomfort afterwards and a slightly longer healing time than for LASIK (Ambrosio and Wilson 2003; Taneri *et al.* 2004).

Photorefractive keratectomy (PRK) was the first and standard photorefractive surgery for many years (Trokel *et al.* 1983). In PRK, the outermost layer of the cornea (epithelium) is manually scraped away and an excimer laser reshapes tissues located beneath the epithelium, that is, Bowman's layer and part of the stromal layers. Afterwards, the epithelium layer grows back. PRK is an option for those with a thin cornea, where the

creation of a corneal flap by cutting (such as in LASIK or LASEK) is undesirable. Drawbacks to PRK include a longer recovery period and more discomfort during healing than with LASIK (Lee *et al.* 2001; Randleman *et al.* 2007). The two main advantages are that PRK does not create a corneal flap using a microkeratome blade and it does not penetrate deeply into the cornea, thus reducing the risk of ectasia (Bores 2001; Lee *et al.* 2001).

In this study, I will concentrate on LASIK surgery, as it is currently the most common photorefractive surgery. Moreover, in LASIK, a large part of the anterior cornea is affected (that is, flapped and ablated), which is now believed to cause biomechanical and visual problems in the long term.

1.6.1 Laser in situ keratomileusis (LASIK)

Lucio Buratto and Ioannis Pallikaris, at the end of the 1980s, were the first to combine the use of the excimer laser and microkeratome technology (Buratto and Ferrari 1997). Burratto's original work involved performing a corrective excimer laser ablation on the back of a resected disc of corneal tissue. This disc was replaced and sutured onto the cornea. Pallikaris developed the technique of performing the excimer laser corrective ablation in the corneal stromal bed under a hinged flap. He first studied the procedure in rabbits, then in blind human eyes in 1989, and finally in sighted eyes in 1991 (Pallikaris *et al.* 1990; Pallikaris *et al.* 1991).

The LASIK procedure involves an oscillating blade and a microkeratome set at a predetermined depth, while the pressure in the eye is

maintained at a high level by a vacuum ring (Figure 1.12). A slice made by the microkeratome undercuts the optical zone perpendicular to the visual axis, creating a flap of tissue with a nasal attachment. The flap is usually 130 to 160 µm thick, with a diameter of about 9 to 10 mm (Buratto and Ferrari 1997; Farah *et al.* 1998; Whitten 2004). After that, the flap is moved a side and the laser pulses hit the stroma (Figure 1.13). The laser is programmed prior to each procedure for the ablative "cut" based on the patient's pre-operative refractive error (nearsightedness, farsightedness, and/or astigmatism). Once the laser ablation is completed, the surgeon gently replaces the corneal flap, with the help of alignment marks on the cornea made using blue dye. The flap position is verified by slit-lamp microscopy approximately 10 minutes after surgery, and the patient is discharged without a patch. The results of LASIK are often dramatic and very rapid, with most patients seeing well enough to drive a car without correction the very next day. However, the best post-operative visual acuity may not be obtained until 2 to 3 weeks, or in some cases, even a few months, after the procedure (Farah *et al.* 1998; Singerman and Coscas 1999; Bores 2001).

Figure 1.12: Steps of LASIK corneal flap creation by microkeratome (Bores 2001; Probst 2004).

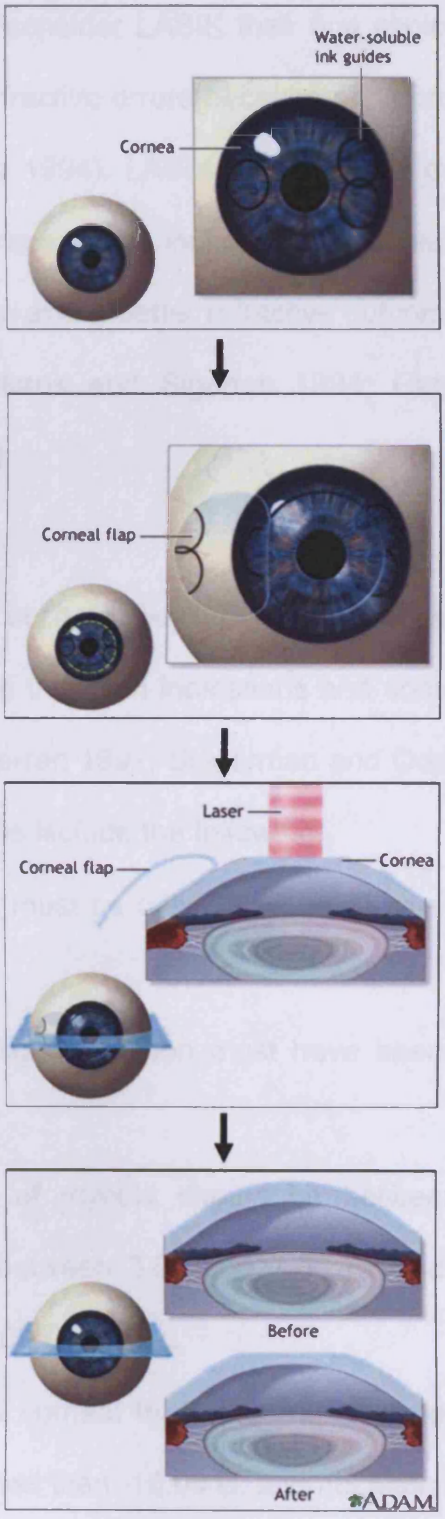

Figure 1.13: Digital drawing shows the steps of LASIK surgery. From Adam website: http://www.adam.com/index.html [Accessed: 19 March 2008].

Many surgeons consider LASIK their first choice for treating both low and high degrees of refractive errors because of its predictability and efficacy (Pallikaris and Siganos 1994). LASIK's advantages over PRK, the standard version of photorefractive surgery, include a low regression rate, minimal pain, almost no corneal haze, and a better refractive outcome with a rapid recovery of visual acuity (Pallikaris and Siganos 1994; Gimbel and Levy 1998a; Vesaluoma *et al.* 2000).

1.6.2 Indications and contraindications for LASIK surgery

The following are the main indications and contraindications for LASIK surgery (Buratto and Ferrari 1997; Singerman and Coscas 1999; Bores 2001; Probst 2004). Indications include the following:

- The patient must be over 18 years of age; there is no upper age limit.
- The cyclopligic refraction must have been stable for at least 12 months.
- The range of myopia should be between 4.00 and 16.00 D, hyperopia between 3.00 and 7.00 D, and astigmatism between 2.00 and 7.00 D.
- The central corneal thickness must be not less than 500μm for myopia of less than -10.00 D, and not less than 550 μm for myopia lying between -10.00 and -16.00D.
- The mean values of central keratometry must be greater than 39.00D (8.60 mm) and less than 47.00 D (7.18 mm).

The contraindications include:

- Monocular patient.
- Pathologies of the endothelium where the cell count is less than 1500 cells/mm^2.
- Dry eye syndrome.
- Diabetes mellitus, which could affect the wound healing process.
- Pathologies or inflammation of the eye.
- Keratoconus or forme fruste keratoconus (FFK).

1.6.3 Preoperative procedures

All patients selected for LASIK surgery must be subjected to a complete ophthalmic examination, which includes corrected visual acuity for distance and near, cyclopligic refraction, central corneal curvature, applanation tonometry, ultrasonic pachometry, and corneal topography. Ultrasonic pachometry is necessary to determine if enough corneal thickness is present to create a flap, ablate the cornea, and still leave enough tissue behind to prevent structural weakening and ectasia (Seiler *et al.* 1998). Corneal topography is useful for highlighting the shape and curvature of the cornea, as well as for identifying subclinical keratoconus or FFK, which are contraindicated for LASIK.

1.7 LASIK complications

LASIK complications can be divided into intraoperative (usually microkeratome related) and those that occur postoperatively. In addition, postoperative complications can be divided into visual acuity problems and

corneal structural changes. Intraoperative complications include an irregular or free flap, and laser beam decentration. Postoperative complications usually include a dislocated flap, corneal infection, under/overcorrection, epithelial ingrowth, diffuse lamellar keratitis, and corneal ultrastructural changes. Most studies of LASIK, with different numbers of eyes and different stages of refractive errors, have reported complication rates from 1.29 % to 11.8% (Brint *et al.* 1994; Pallikaris and Siganos 1994; Fiander and Tayfour 1995; Kremer and Dufek 1995; Salah *et al.* 1996; Gimbel *et al.* 1998b; Stulting *et al.* 1999; Melki and Azar 2001; Lin and Tsai 2005). In addition, these studies show that, with extremely skilled surgeons, complication rates can be decreased in cases of low refractive errors. In this chapter, LASIK visual outcomes and corneal ultrastructural changes will be reviewed, as they are considered the main complications.

1.7.1 LASIK visual outcomes

Usually, LASIK results in improved vision without correction. However, it does not always result in 20/20 (6/6), or even 20/40 visual acuity (Sugar *et al.* 2002a). In LASIK, the most rigid part of the stroma is intersected, thus weakening the stability of the cornea and increasing the risk of optical problems (Iskander *et al.* 2000; Muller *et al.* 2001).

Casebeer and Kezirian (1998) presented results from 911 eyes with myopia (-1.00 to -10.00 D) that underwent LASIK surgery with different excimer laser machines. They indicated that approximately 91% of eyes had 20/40 or better visual acuity 3 months postoperatively in low myopia groups

and 69% in high myopia groups. These results suggest that patients with extreme degrees of myopia generally have less favourable visual outcomes with LASIK. Farah et al. (1998) reviewed the visual outcome of LASIK surgery in many previous studies. Preoperative refraction was in the range of moderate to high myopia and the follow-up ranged from 10 days to 24 months, but was most often performed at 6 or 12 months. Postoperative results ranged from an overcorrection of +6.63 D to an undercorrection of -9.50 D, with a mean of +0.93. The studies indicate that the predictability of LASIK decreases when the preoperative myopia is high. Interestingly, the overall mean of postoperative uncorrected visual acuity of 20/20 or better has improved from 22% in old reviewed studies to 57% in recent studies, which reflects continued improvement in surgical techniques and surgeons' skills.

A report by the American Academy of Ophthalmology (Sugar *et al.* 2002a) on the efficacy and safety of LASIK concluded that the technique is effective and predictable in terms of obtaining excellent visual acuity for low to moderate myopia, but its effectiveness is less in cases of high myopia. Also, the report mentioned different side effects resulting from the use of this technique, including long-term reduced visual acuity postoperatively due to LASIK-induced corneal ultrastructural changes.

1.7.2 Effect of LASIK on corneal ultrastructure

It is important to know the effect of LASIK procedure on corneal tissues and understand the mechanism of the wound healing process after surgery, as a successful result will depend on the proper healing of the corneal surface

and maintenance of the corneal strength. However, because LASIK is a relatively new technique, the long-term effects cannot be determined satisfactorily. In addition, most previous studies that evaluate the results of LASIK discuss the clinical outcomes with little emphasis on the wound healing process and the resultant biomechanical corneal changes. In this section, the main corneal ultrastructural changes will be discussed.

1.7.2.1 Changes in corneal thickness

The main concern about LASIK surgery is the amount of integral corneal thickness that remains after flapping and ablation have been performed. A stromal bed of at least 250μm should remain after laser ablation to avoid mechanical instability (Hjortdal 1998; Seiler *et al.* 1998; Wang *et al.* 1999).

Further, a significant increase in epithelial thickness (hyperplasia) over the wound area after LASIK has been reported (Figure 1.14), despite there being no surgical alternation of the epithelial layer, while stromal thickness remains constant (Erie *et al.* 2002; Kramer *et al.* 2005; Dawson *et al.* 2005a). This change has been correlated with myopic regression, that is, an increase of 10-15 μm epithelial thickness results in a -1.0 diopter regression, and a +1.0 diopter increase in central corneal power (Chayet *et al.* 1998; Lohmann and Guell 1998; Philipp *et al.* 2003). Activated keratocytes have been found, and they are probably another reason for regression of the initial refractive effect, because the epithelial-stromal interactions i.e. chemotactic cytokines and growth factors from epithelial cells and keratocytes (Dawson *et al.* 2005a; Dawson *et al.* 2005b).

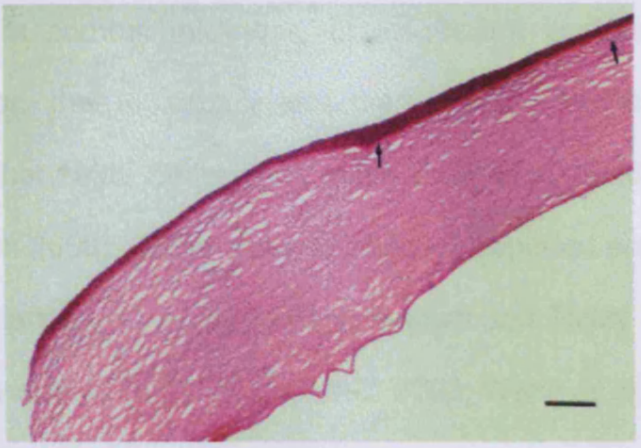

Figure 1.14: LM image shows epithelial thickening after LASIK (arrows) (Philipp *et al.* 2003).

1.7.2.2 Iatrogenic keratectasia (ectasia)

Ectasia is a thinning and abnormal bulging of the cornea after LASIK (Seiler *et al.* 1998; Amoils *et al.* 2000; Binder 2003). In fact, it is considered a very serious long-term complication and can develop from 1 week to 27 months after LASIK (Amoils *et al.* 2000; Pallikaris *et al.* 2001; Binder 2003). Although it occurs only rarely, it can cause a severe loss of vision that in some cases can be restored only by corneal transplantation (Rad *et al.* 2004).

It is believed that the corneal flap that is created during LASIK contributes minimally to the biomechanical strength of the cornea, because its attachment to the limbus and cornea has been severed. Thus, the corneal strength and shape are determined by the biomechanical properties of the residual intact corneal bed (Seiler *et al.* 1998; Randleman *et al.* 2003). The risk factors for ectasia include patients who had preoperative keratoconus, forme fruste keratoconus (FFK), high myopia, keratometry readings steeper than 46.00 dioptres (D), asymmetrical astigmatism on corneal topography,

less than 500μm corneal thickness, or insufficient postoperative residual stromal thickness, that is, usually less than 300μm (Pallikaris *et al.* 1991; Probst and Machat 1998; Seiler *et al.* 1998; Faraj *et al.* 2003; Randleman *et al.* 2003; Condon 2006). Some studies, however, reported ectasia in patients without obvious preoperative risk factors (Geggel and Talley 1999; Amoils *et al.* 2000; Pallikaris *et al.* 2001; Piccoli *et al.* 2003; Wang *et al.* 2003b; Klein *et al.* 2006).

The signs and symptoms of ectasia have many similarities with those of keratoconus, such as thinning and protrusion of the cornea, unstable topographical steepening, and a high degree of myopic astigmatism (Zadnik *et al.* 1996; Rabinowitz 1998). Therefore, it can be treated in two ways that is, non-surgical or surgical treatment, depending on its severity. In the early stages, spectacle or rigid contact lenses can be used to correct the vision while in advanced stages, corneal rings (INTACS) or corneal transplant that is, penetrating keratoplasty (PKP) or lamellar keratoplasty (LKP) are the final solutions (Seiler *et al.* 1998; Pallikaris *et al.* 2001; Chan and Boxer Wachler 2006).

1.7.2.3 Changes within the flap area

Most LASIK-related changes occur in the corneal lamellar interface wound. Histological and biomechanical studies have shown that the corneal flap in the central area of the cornea appears to be loosely connected to the underlying corneal stroma (Figure 1.15) and the wound healing process after LASIK is slow (Kato *et al.* 1999; Buhren and Kohnen 2003; May *et al.* 2004;

Kramer *et al.* 2005; Schmack *et al.* 2005). Another study found that most wounded corneas stabilise between three and six months after surgery (Chayet *et al.* 1998). However, corneal stromal wounds never heal completely, and the reason is still unknown (Maurice 1984; Dawson *et al.* 2005a).

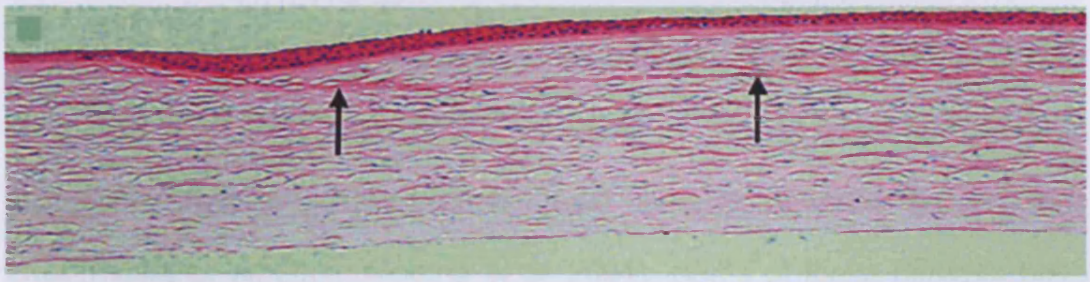

Figure 1.15: Histopathology of a 6-month-old LASIK corneal wound. The arrows indicate the lamellar wound. The stain is hematoxylin-eosin with original magnification x25 (Dawson *et al.* 2005a).

In contrast to PRK, corneal haze after LASIK is minimal (Brint *et al.* 1994; Helmy *et al.* 1996), and the regression of haze is rapid between the first and third month, whereas it continues at the same level after PRK (Pallikaris and Siganos 1994; Farah *et al.* 1998). This is because both the epithelium and Bowman's layer after LASIK are intact and, consequently, the keratocyte apoptosis area is low (Nakamura *et al.* 2001; Mohan *et al.* 2003). Keratocyte apoptosis after LASIK has been reported by some studies (Helena *et al.* 1998; Wilson 2000; Mohan *et al.* 2003). Apoptosis is located near the lamellar interface between the flap and the underlying bed, and therefore the thickness of the LASIK flap tends to determine the depth at which apoptosis occurs, that is, a thin flap will produce lower apoptosis (Helena *et al.* 1998; Wilson 2000; Mohan *et al.* 2003).

Confocal microscopy has demonstrated that the number of corneal nerve fibre bundles in the flap area decreases by 90% immediately after LASIK and returns gradually during the first year, although by one year the number remains less than half of that before LASIK (Lee *et al.* 2002). As corneal nerve fibres are sectioned by flap, corneal sensation is reduced (Kanellopoulos *et al.* 1997; Toda *et al.* 2001). This may explain the reduced blinking and relative dry eye problems that are observed postoperatively (Chuck *et al.* 2000; Rosen 2000). By using in vivo confocal and slit-lamp microscopy, high reflectivity particles have been found at the flap interface area (Pisella *et al.* 2001; Mootha *et al.* 2004). Some of these particles have been clearly identified as metallic components of the microkeratome blade (Kaufman *et al.* 1998). The other particles are thought to be cellular debris or inflammatory cells present at the interface level. The density of these particles nevertheless decreases with time (Pisella *et al.* 2001; Dawson *et al.* 2005b).

Histopathological studies on human LASIK corneas are rare in the literature because the technique is relatively new and, hence, most LASIK patients are young. The first histopathological evaluation of LASIK human corneas was in 2002 by Anderson *et al.* They found significant changes had occurred in human corneal ultrastructures after LASIK. They examined four corneas that had undergone LASIK three months and twenty months prior to death and found an absence of corneal nerves, epithelial ingrowth into the wound, activation of keratocytes in and adjacent to the wound, irregular collagen fibrils in the wound bed, and severed collagen bundles adjacent to the wound. These findings were more pronounced in three-month LASIK than

in twenty-month LASIK corneas, and the wound interface was hardly noticeable in old LASIK corneas. Some previous human results, that is, disorganised collagen fibrils and activated keratocytes, have been found in rabbit LASIK corneas (Perez-Santonja *et al.* 1998; Park and Kim 1999). May et al. (2004) found some results similar to Anderson's study. In addition, May et al. (2004) and Priglinger et al. (2006) compared in vitro and in vivo LASIK corneas and found similarities in ultrastructural results, which provide encouragement to conduct more in vitro human LASIK studies.

Recently, two large studies of human LASIK corneas showed results similar to Anderson's study. Kramer et al. (2005) and Dawson et al. (2005a) conducted histology and transmission electron microscopy on forty-eight and thirty-eight post mortem LASIK corneas respectively with different postoperative intervals (2 months to 7 years). They found a semicircular ring of haze along the wound margin of the LASIK flap (Figure 1.16), a variable amount of epithelial ingrowth into the lamellar wound, and undulations of Bowman's layer with mild epithelial hyperplasia over the wound margin, although it was never found over the paracentral flap surface. They also found a statistically significant increase in keratocytes at the LASIK wound margin, regardless of the time from LASIK to death. However, the posterior aspect of the flap had keratocyte densities similar to those of the control corneas.

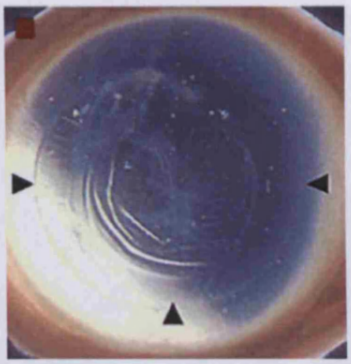

Figure 1.16: Gross photograph showing a hazy semicircular ring at the flap margin (arrowheads) and a clear central flap area. The concentric circular wrinkles are a transient artefact induced on the anterior cornea by the weight of the corneoscleral button (Dawson *et al.* 2005a).

Moreover, collagen fibrils in the extracellular matrix were variably spatially disordered compared with those within a normal corneal stroma. The collagen interfibril space was increased (with a mean of 42.0 ± 0.7nm) and varied in increment at different wound areas (Figure 1.17). In addition, the collagen diameter had decreased (with a mean of 20.6 ± 0.3nm) from normal. Finally, abnormally large, non-fibril-bound proteoglycans were found in the interface scar, whereas the residual stromal bed showed a predominance of normal size, fibril-bound proteoglycans. Most of the findings in Dawson's study were prominent in the first few months after LASIK and were rarely found in wounds older than six months, supporting findings from previous studies (Chayet *et al.* 1998; Anderson *et al.* 2002). However, Kramer's study did not find an observable correlation between postoperative intervals and the severity or type of pathologic change.

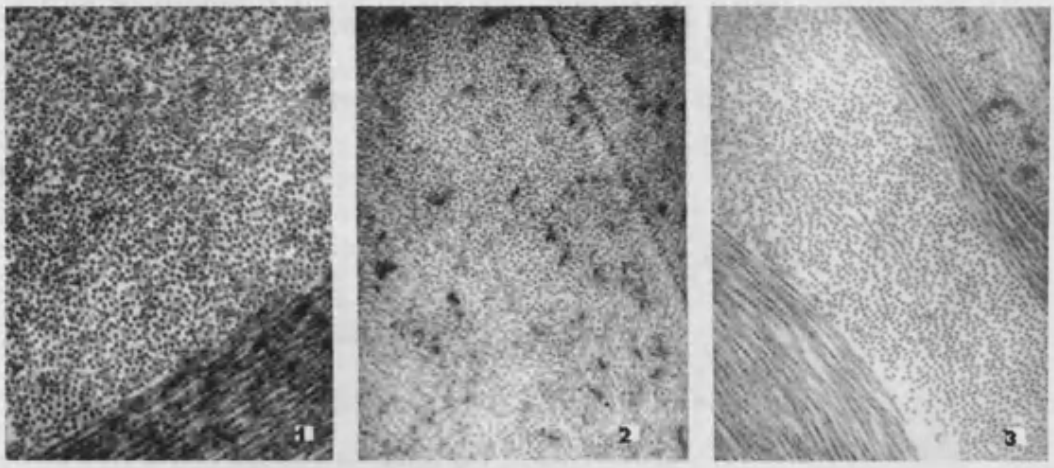

Figure 1.17: Transmission electron microscopy shows (pictures 1 to 3) increased interfibrillar spacing of corneal collagen fibrils after LASIK at different areas i.e. in the flap, adjacent to the wound, and in the residual posterior corneal stroma. The interfibrillar spacing was largest and most varied in the paracentral and central interface wound region (Kramer, 2005).

LASIK has not yet been reported to cause damage to the corneal endothelium. Kent and co-workers (1997) used fluorescent vital dyes to count endothelial cells and assess their viability after -25.0 diopter LASIK. They did not find a significant difference between treated and control corneas. Moreover, Perez-Santoja et al. (1997a and b) used specular microscopy to assess cell density, coefficient of variation in cell size, and hexagonality after LASIK and found LASIK did not cause significant damage to the endothelium. Other studies (Pallikaris and Siganos 1994; Jones *et al.* 1998; Knorz *et al.* 1998) support these findings and conclude that long-term follow-up studies are needed to confirm endothelial safety after LASIK. On the other hand, most endothelial cells are lost during ablation or within the first period of time after PRK (Isager *et al.* 1998).

In conclusion, LASIK is a major advance in the field of photorefractive surgery. However, studies on LASIK complications indicate that this technique

is not always safe and may lead to loss of vision. Therefore, more corneal ultrastructural studies are necessary to understand and avoid LASIK long-term side effects.

1.8 Femtosecond laser technology

Corneal flap creation is considered the most important part of the LASIK procedure. Although modern microkeratomes can produce high-quality corneal flaps, most beginners and even experienced LASIK surgeons occasionally create suboptimal flaps (Friedlaender 2006). Therefore, the new bladeless technology, the femtosecond laser, was introduced in order to eliminate the common complications associated with the creation of the flap using mechanical microkeratomes (Ratkay-Traub *et al.* 2001; Nordan *et al.* 2003; Binder 2004; Sarayba *et al.* 2007a).

Currently, there are two femtosecond laser systems available in the market: IntraLase Pulsion FS^{TM} (IntraLase Corp., Irvine, CA) and Femtec Femtosecond Laser (20/10 Perfect Vision, Heidelberg, Germany). Both systems are based on the same technology and are mainly used to cut LASIK flaps. Different investigators have reported good experiences and results for the IntraLase system (Ratkay-Traub *et al.* 2001; Nordan *et al.* 2003; Ratkay-Traub *et al.* 2003; Kezirian and Stonecipher 2004). Beside flap creation, femtosecond lasers can be used in a variety of corneal surgeries including lamellar keratoplasty and intrastromal incisions for Intacs ring implants, and they can also be used to trephine both donor and recipient corneas for penetrating keratoplasty in a pattern that gives good tissue alignment and less

postoperative astigmatism (Sugar 2002b; Soong *et al.* 2005; Tran *et al.* 2005; Friedlaender 2006; Buratto and Bohm 2007; Holzer *et al.* 2007; Slade 2007).

1.8.1 Femtosecond Laser Mechanism

In order to create a LASIK corneal flap, the femtosecond laser (10^{-15} seconds) delivers laser pulses of infrared wavelength (1053 nm) to produce tissue disruption at a specified and precise level within the corneal stroma (Kezirian and Stonecipher 2004; Montes-Mico *et al.* 2007). The laser pulse passes harmlessly through the outer layers of the cornea until it reaches its exact focal point (Figure 1.18A) and hits 1 μm diameter of corneal stromal tissue to create microphotodisruption or an expanding bubble of carbon dioxide and water that in turn cleaves the tissue. Thousands of laser spots are programmed to be sited next to each other in a spiral or raster pattern and create a circumferential side cut, that is, a LASIK flap (Figure 1.18B), which can be lifted with blunt dissection (Kurtz *et al.* 1997; Friedlaender 2006; Stonecipher *et al.* 2006). The laser beam is delivered through a round, flat glass plate on the end of a removable cone attached to the laser machine (Figure 1.18A) (Ratkay-Traub *et al.* 2001; Sugar 2002b; Kezirian and Stonecipher 2004; Friedlaender 2006).

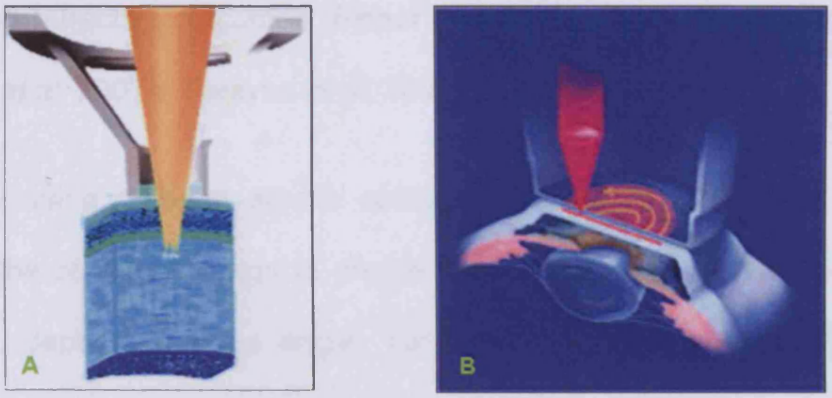

Figure 1.18 (A and B): The application of a femtosecond laser to the applanated cornea to create a LASIK flap. (Figure 1.18A from: www.ooglasertrefpunt.nl [Accessed 10 October 2007] and Figure 1.18B from (Sugar 2002b)

The femtosecond laser system was first used in 1999, with a repetition rate engine of 2 kHz. The spot and line separation was 14x14 µm and the energy setting per spot was 6µJ (Ratkay-Traub *et al.* 2001; Nordan *et al.* 2003; Sarayba *et al.* 2007a). With this engine, it would take 2 to 3 minutes to create a 9-mm diameter flap. After a series of improvements, it has been found that a higher repetition rate leads to lower surgical energy settings and closer spot/line separation being required, which consequently increases the speed of the procedure (Stonecipher *et al.* 2006). Therefore, a fast 30 kHz laser engine was commercially released in 2005 so a 9-mm flap could be created in 60 seconds using a spot/line separation of 10x10 µm with spot energy of 1.5 to 2.0 µJ (Binder 2004; Kezirian and Stonecipher 2004; Binder 2006; Sarayba *et al.* 2007b). Currently, a 60 kHz laser engine is available, with which a 9-mm flap can be created in 20 seconds using a spot/line separation of 6x6 µm and energy of 0.7 to 1.1 µJ (Sarayba *et al.* 2007a). It has been found that the use of smaller spot/line separations and lower energy levels result in smooth optical (stromal) surfaces that may improve the LASIK

visual and refractive outcomes (Eisner and Binder 2006; Friedlaender 2006; Sarayba *et al.* 2007a; Sarayba *et al.* 2007b).

By using different simple settings, the femtosecond laser machine enables the corneal surgeon to design precisely the corneal flap in terms of diameter, depth and edge angle. To accommodate the use of two laser systems, that is, femtosecond and excimer lasers, patients are treated on a bed that swings at an angle for the creation of the femtosecond laser flap and then swings under the excimer laser for completion of the LASIK procedure.

1.8.2 Femtosecond laser versus mechanical microkeratome

The femtosecond laser and the mechanical microkeratome platforms have different mechanisms of action for creating LASIK corneal flaps. The femtosecond laser requires no moving instrumentation during flap creation, which is considered a significant safety advantage, as it prevents further damage to the stromal structure and preserves epithelial layer integrity. The mechanical microkeratome, on the other hand, pivots the microkeratome head across the corneal epithelium and stroma under high pressure. Therefore, both systems have different intraoperative and postoperative results. Many different studies have been performed comparing the visual, refractive, and corneal structure outcomes of corneas whose flaps were created using a mechanical microkeratome and those whose flaps were created with the femtosecond laser. It has been found that the femtosecond laser is superior to the mechanical microkeratome, as discussed below (Kezirian and Stonecipher 2004; Durrie and Kezirian 2005; Tran *et al.* 2005; Stonecipher *et al.* 2006; Montes-Mico *et al.* 2007; Sarayba *et al.* 2007b).

Generally, femtosecond lasers are highly recommended for cases where poor flap creation may occur. These include inadequate patient cooperation; patients who have very thin corneas for the intended level of correction, where a microkeratome would potentially prepare a thicker flap; steep or flat corneas, that is, corneal curvature greater than 48D or lower than 42D, where flap complications are more likely with a microkeratome, such as a buttonhole; and corneas with anterior basement membrane dystrophy (Friedlaender 2006; Netto *et al.* 2007).

The main feature that attracts most corneal surgeons to rely on femtosecond laser technology for LASIK flap creation is the ability of the system to create a uniform, thin and accurate flap thickness, which cannot always be obtained with most mechanical microkeratomes, where unexpectedly thick flaps can occur, as can those with variable thickness, being thinner in the centre and thicker in the periphery, as shown in Figure 1.19 and Figure 1.20 (Giledi and Daya 2003; Binder 2004; Binder 2006; Friedlaender 2006; Stonecipher *et al.* 2006). This variability in thickness occurs because mechanical microkeratome flaps are highly dependent on anatomic factors, particularly corneal curvature, whereas femtosecond laser flaps are uniform, despite anatomic variability, and their dimensions accurately reflect the settings selected by the surgeon (Sugar 2002b; Nordan *et al.* 2003; Binder 2004; Binder 2006; Friedlaender 2006).

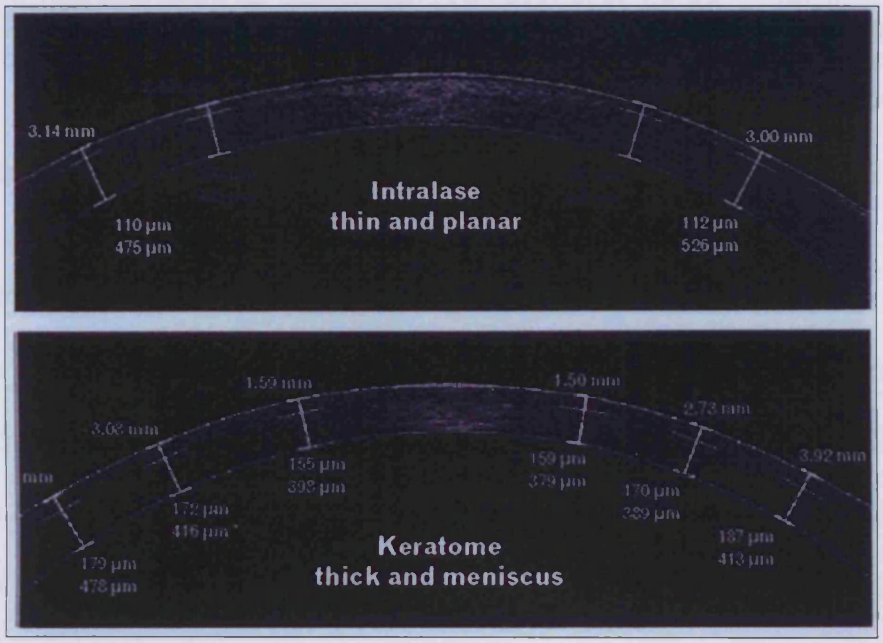

Figure 1.19: This Zeiss Visante imaging system shows the differences in LASIK flap thickness and shape between the IntraLase Femtosecond laser and the mechanical microkeratome (Stonecipher *et al.* 2006).

Figure 1.20: Schematic diagram shows the shape of LASIK corneal flap created by mechanical microkeratome (left), and by Femtosecond laser (right). The femtosecond laser flap has the same thickness throughout. From: www.lasik-center.com [Accessed 10 October 2007]

By comparing the biomechanical stability of the cornea, it has been found that femtosecond laser flaps have greater biomechanical stability than have mechanical microkeratome flaps, albeit still below the tensile strength of a normal corne (Alio *et al.* 2005; Stonecipher *et al.* 2006). This strength comes about because the femtosecond laser flap heals to be stronger than the microkeratome flap at the periphery (Schmack *et al.* 2005; Stonecipher *et al.*

2006). This feature may be considered a key safety factor for the avoidance of ectasia following LASIK (Seiler *et al.* 1998; Kezirian and Stonecipher 2004) and, therefore, more studies are needed to support this finding.

In a retrospective study of 376 eyes, Kezirian and Stonecipher (2004) made a comparison between LASIK results obtained with femtosecond lasers and with two popular mechanical microkeratomes. They found that the long-term uncorrected visual acuity was similar in all three techniques. Moreover, another study found no significant differences in the visual outcomes between the two techniques (Javaloy *et al.* 2007). However, better uncorrected visual acuity, better contrast acuity, and less flap-induced higher order aberration were found with the femtosecond laser in the immediate postoperative period up to the third postoperative month (Tanzer *et al.* 2005; Stonecipher *et al.* 2006). Surgically induced (iatrogenic) astigmatism in LASIK spherical corrections has been found significantly less often with the femtosecond laser than with the mechanical microkeratome (Kezirian and Stonecipher 2004). The explanation for this may lie in the morphology of the flap, the edge angle, and the constant flap thickness (Durrie and Kezirian 2005; Stonecipher *et al.* 2006; Sarayba *et al.* 2007a).

Morphological studies of the appearance of the stromal surface after femtosecond laser flap creation have documented the smoothness of the stromal surface, which is considered a critical factor in achieving better visual and refractive outcomes following LASIK (Porter *et al.* 2003; Sarayba *et al.* 2007a; Sarayba *et al.* 2007b). This smoothness does not appear when a modern microkeratome with a new blade is used (Figure 1.21) (Binder *et al.*

1997; Behrens *et al.* 2000; Sarayba *et al.* 2007b). The smoothness and the normal morphological appearance of the femtosecond laser flap is due to the laser pulses being closer to each other and the lower energy setting used, as explained before.

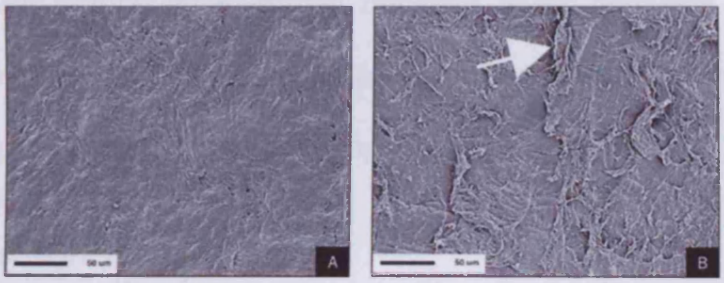

Figure 1.21: Scanning electron microscopy images of stromal bed after LASIK flap creation by: **A**) IntraLase femtosecond laser using 60 kHz engine and by: **B**) Zyoptix XP microkeratome using a fresh blade. Original magnification: x300. Raised collagen lamellae (white arrow) roughen the bed, possibly due to the shearing mechanism of the microkeratome (Sarayba *et al.* 2007a).

1.8.3 Femtosecond Laser complications

The most frustrating complication during the creation of a LASIK corneal flap using a femtosecond laser is the suction break. Loss of suction can occur with improper positioning of the suction ring on the eye (Nordan *et al.* 2003; Friedlaender 2006). However, it has been found that lower energy lasers (30 or 60 kHz) decrease the incidence of the suction break, as flap creation time will be short, that is, less than 20 seconds, whereas most suction break cases occur after 30 seconds of suction application (Principe *et al.* 2004; Sarayba *et al.* 2007a).

The main postoperative complication of femtosecond laser technology is corneal inflammation. The incidence of diffuse lamellar keratitis (DLK) was found to be significantly greater in femtosecond laser cases than in mechanical microkeratome cases (Touboul *et al.* 2005; Holzer *et al.* 2006; Javaloy *et al.* 2007). However, it has been found that reducing the laser side cut energy will reduce inflammation because fewer epithelial cells will be injured. Currently, DLK is a rare complication of use of the femtosecond laser due to the improvement in the engine speeds (Friedlaender 2006).

In summary, the femtosecond laser has significant safety benefits compared to mechanical microkeratomes for LASIK flap creation. It shows improvement in flap thickness predictability and in visual and refractive outcomes, which may be considered a better microkeratome choice for wavefront-guided LASIK or the new refractive surgery technique that is, sub-Bowman's keratomileusis (SBK) (Durrie *et al.*, 2008).

1.9 X-ray Diffraction

Diffraction is the apparent bending and spreading of waves when they meet an obstruction. X-ray diffraction (XRD) has been used extensively in the field of vision sciences to study ex vivo corneal or scleral ultrastructures. In the present context, it has allowed scientists to measure collagen fibril orientation, collagen interfibril spacing, and collagen fibril diameter through the whole tissue thickness, at specific chosen points. There are two types of XRD: conventional and synchrotron (Margaritondo 1988; Meek and Quantock 2001). Conventional XRD uses low intensity x-ray beams and requires long

exposure times, and therefore is no longer used to examine corneas. On the other hand, synchrotron XRD uses high intensity x-ray beams, which permit small spot sizes and short exposure times, that is, seconds or minutes. It allows the study of collagen fibrils within a large area and in their native condition without the need for dehydration, embedding or staining. The disadvantage of XRD is that the x-rays pass through thick tissue sections and the resulting pattern is therefore an average for the whole sample.

1.9.1 Principle of Diffraction

Generally, if parallel waves strike a barrier, these will be divided into three parts. The first part will hit the barrier, the second part will pass into, and possibly through the barrier, and the third part will hit the edge of the barrier and appear to be bent. This last part will create a new spherical wavefront, and a series of new waves will exist due to the effect of the constructive and destructive interface (Figure 1.22). This effect is called diffraction (Meek 1973) and is associated with all waves, including x-rays. In 1913, the English physicist Sir W. Bragg and his son explained the principle of x-ray diffraction.

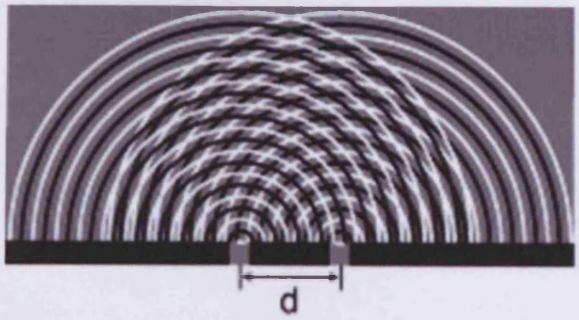

Figure 1.22: Diagram of double-slit diffraction of water waves. From website: http://www.en.wikipedia.org/wiki/Diffraction [Accessed: 20 March 2008].

Bragg's law: An x-ray that reflects from a layer of atoms or atomic structures at a given level in the tissue has travelled less distance than an x-ray that reflects from a layer deeper inside the tissue. The penetrating x-ray travels down to the internal atoms, is reflected, and travels back over the same distance before arriving back at the surface. The distance travelled depends on the separation of atoms and the angle at which the x-ray entered the tissue. This condition can be expressed by Bragg's law (Figure 1.23), where Theta (θ) is the beam angle of incidence, (d) is the distance between atoms, and the variable lambda (λ) is the wavelength of the incident X-ray beam. The lower beam must travel the extra distance (AB + BC) to continue travelling parallel and adjacent to the top beam. Also, Bragg's law shows that in a given system (fixed λ and n), the scattering angle (2θ) is inversely related to the spacing (d).

$$n\lambda = 2d \sin\theta$$

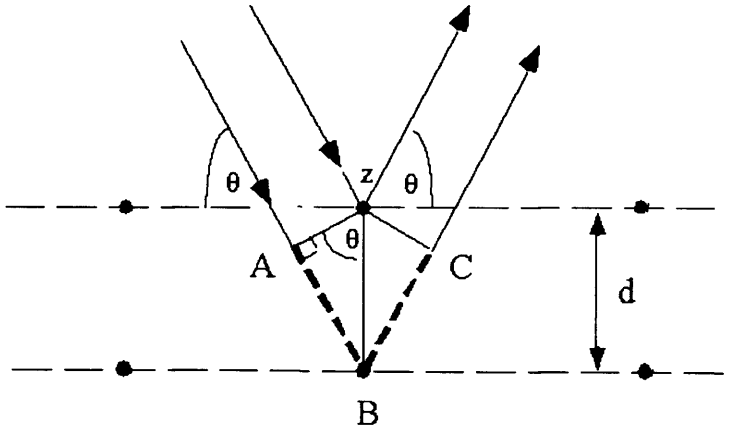

Figure 1.23: Bragg's law. From: http://www.eserc.stonybrook.edu/projectjava/bragg/ [Accessed: 20 March 2008]

In the case of corneal tissue, when the x-ray beam hits collagen molecules or fibrils, it scatters parallel and at 90° degrees from the axis of the

fibrils. This leads to two sets of so-called 'reflections': meridional and equatorial (Newton and Meek 1998a; Newton and Meek 1998b). A backstop is put in the centre to block the straight x-ray beam that is not diffracted (Figure 1.24).

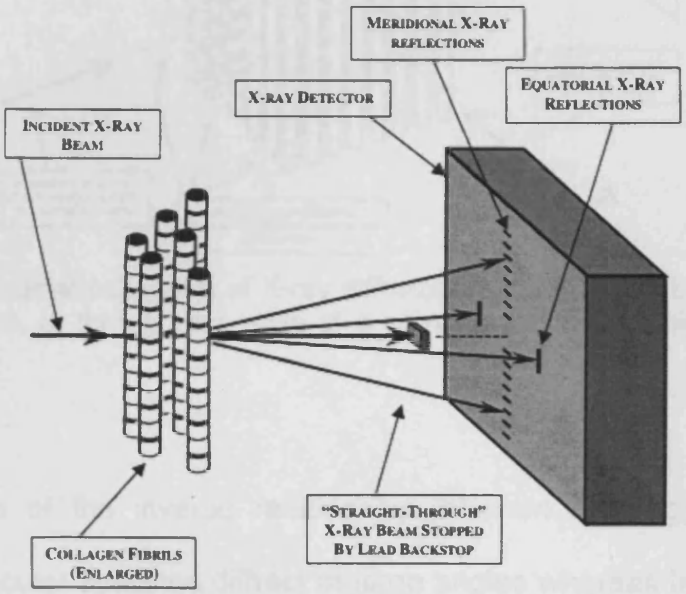

Figure 1.24: schematic diagram of the mechanism of an X-ray diffraction through collagen fibrils (Meek and Quantock 2001).

The human cornea contains huge numbers of collagen fibrils with different perpendicular directions that are in the way of the X-ray beam. Therefore, X-ray diffraction will give rise to a series of superimposed meridional and equatorial patterns, that is, a series of concentric circles, as shown in Figure 1.25.

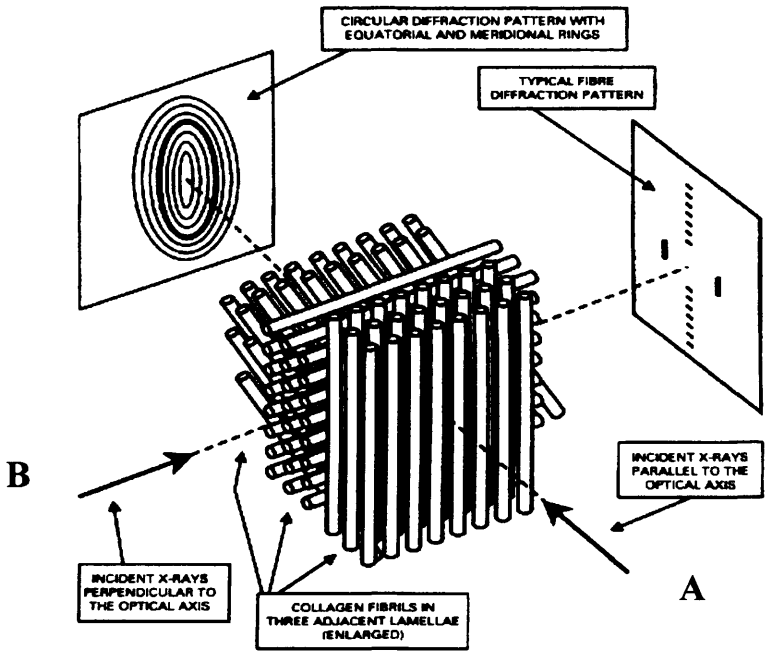

Figure 1.25: Schematic diagram of X-ray diffraction pattern, either through the front of the cornea (A), or through the edge of a corneal strip (B) (Meek and Quantock 2001).

Because of the inverse relationship inherent in Bragg's law, small atomic or molecular spacings diffract at large angles whereas large structures such as fibrils diffract at low angles. Thus, two types of patterns are produced by X-ray diffraction, that is, high and low angle patterns. High angle patterns are recorded with a specimen-detector distance of around 15 centimetres and are used in this study to measure collagen fibril orientation, whereas low angle patterns are recorded with a specimen-detector distance of around 8 metres and used to measure the collagen fibril diameter as well as interfibrillar spacing (Meek and Quantock 2001).

1.10 Microscopy

Microscopy is the technical field of using microscopes to view samples or objects. In biosciences, there are three well-known branches of

microscopy: transmission electron microscopy (TEM), scanning electron microscopy (SEM), and light microscopy (LM). In the field of optometry and ophthalmology, these techniques are considered essential to study structural changes in ocular tissues. Table 1.2 shows some of the differences between these techniques. Full details about specimen preparation for each technique can be found in Chapter 2.

Feature	TEM	SEM	LM
General use	Sections (40-150 nm)	Surface morphology	Surface morphology & sections (1-40μm)
Source of illumination	High-speed electron	High-speed electron	Visible light
Magnification range	500-500,000x	20-150,000x	10-1,000x
Lens type	Electromagnetic	Electromagnetic	Glass

Table 1.2: Comparison of selected features of transmission electron microscopy (TEM), scanning electron microscopy (SEM), and light microscopy (LM) (Flegler *et al.* 1993).

1.10.1 Transmission Electron Microscopy (TEM)

The TEM is a high-resolution imaging machine that uses a beam of highly energetic electrons to examine objects on a very fine scale. The modern TEM can achieve magnification of one million times, with a resolution of 0.1 nm (Hayat 1989; Bozzola and Russell 1999).

The TEM (Figure 1.26) consists of an evacuated metal cylinder (the column) about 2 metres high with the source of illumination, a tungsten filament (the cathode), at the top. If the filament is heated and a high voltage (the accelerating voltage) of between 40,000 to 100,000 volts is passed between it and the anode, the filament will emit electrons. These negatively charged electrons are accelerated to an anode (positively charged) placed

just below the filament, some of which pass through a tiny hole in the anode, to form an electron beam, which passes down the column. The speed at which they are accelerated to the anode depends on the amount of accelerating voltage present. The double condenser lenses focus the electron beam onto the specimen, which is clamped into the removable specimen grid. As the electron beam passes through the specimen, electrons are focused to form an image on the screen that can be captured by a camera (Meek 1973; Hayat 1989; Bozzola and Russell 1999).

Figure 1.26: Picture of JEOL 1010 transmission electron microscope. From: http://mic.nichd.nih.gov/jeol_1010_tem.htm [Accessed: 21 March 2008].

In the conventional TEM, proper sample preparation is critical to obtain good results. In the beginning, the biological specimen must be fixed (or stabilised) so that its ultrastructure is as close as possible to that in the living material when exposed to the vacuum. After that, the specimen must be dehydrated since it will be exposed to a very high vacuum when being

examined. Also, the limited penetrating power of electrons means that the specimen must be very thin or must be sliced into thin sections (50 - 100 nm) to allow electrons to pass through. Specimen sectioning (cutting) is done with an ultramicrotome.

1.10.2 Scanning electron microscopy (SEM)

SEM is another popular type of electron microscopy. Similar to TEM, SEM uses electrons to illuminate a specimen and create an enlarged image and, hence, the procedure is run under high-vacuum conditions. It has great resolving capabilities, as well as a high magnification range, but less than that of the TEM. A specimen for SEM requires extensive preparation in order to obtain image quality, on nanometre (nm) and micrometer (μm) scale, and so acquire detailed data. Unlike the TEM, the SEM image relies on surface processes rather than transmission so the microscope is able to image bulk samples, has a much greater depth of view, and can produce images that are a good representation of the three-dimensional-like structure of the sample. However, since SEM uses electrons instead of light to carry the information generated during image formation, all resultant images are black and white rather than in colour. Sample preparation for SEM includes specimen fixation, specimen dehydration, and conductive coating, the reason for the latter being to prevent the accumulation of static electric fields at the specimen due to the electron irradiation required during imaging and, also, to improve contrast (Watt 1997; Bozzola and Russell 1999; Goldstein *et al.* 2002).

1.10.3 Light microscopy (LM)

LM involves passing visible light transmitted through or reflected from a thin specimen through a single lens or multiple lenses to allow a magnified view of the specimen (Bradbury and Bracegirdle 1998). The resulting image can be detected directly by the eye, imaged on a sheet of photographic paper or captured and saved digitally. LM can magnify objects by up to 1,000 times, revealing microscopic details of the specimen. Chemical fixation, dehydration, sectioning, and staining are usually applied to the specimen before examination. Different dyes are used to stain different structures in order to enhance contrast and, hence, obtain a detailed image (Stephens and Allan 2003). The LM procedure is much easier than those of TEM or SEM. Moreover, the resultant images are in colour and can be edited through an LM computer imaging system.

1.11 Aims of the Study

The general aim of this thesis is to study the corneal structure and ultrastructure in normal and LASIK human corneas using different means, specifically, wide-angle XRD, TEM, SEM, and LM. It is firstly aimed to characterise the ultrastructure of the normal human cornea using wide-angle XRD and compare it with the corneal ultrastructure of two different sized mammalian species (camel and rabbit) in order to find out that the human cornea possesses a unique collagen fibril orientation (Chapter 3). As LASIK surgery includes partial corneal trephination and stromal ablation, the collagen fibril orientation and distribution in the human cornea will be studied after full-thickness corneal trephination (Chapter 4), and at different corneal depths

(Chapter 5) in order to gain quantitative information about the arrangement and distribution of stromal collagen in each location. Moreover, *in vitro* human LASIK will be run to mimic *in vivo* LASIK and to study the corneal structural and ultrastructural changes after LASIK surgery (Chapter 6). Finally, post-mortem LASIK corneas and post-LASIK ectatic corneal tissues will be investigated to find out the corneal structural differences between the two cases (Chapter 7) and compare them with the *in vitro* LASIK results.

Chapter 2. General Materials and Methods

2.1 Introduction

All human, camel, and rabbit corneoscleral tissues used in this study were obtained in accordance with the tenets of the declaration of Helsinki for the use of human tissue and the Association for Research in Vision and Ophthalmology (ARVO) statement for the use of animals in ophthalmic research. In order to preserve the structure, all tissues were either stored at -80°C or fixed in 4% paraformaldehyde until the time of the experiment. The pre-experiment sample preparation for each experiment will be explained in detail in the next chapters.

2.2 X-Ray Diffraction (XRD)

2.2.1 Sample preparation

All tissues were marked by a suture or surgical marker pen (Schuco International Ltd, London, UK) in the most superior part of the corneoscleral button (12 o'clock). In order to minimise tissue dehydration during X-ray exposure, the cornea was wrapped in Clingfilm™ (Superdrug Stores Plc., Croydon, UK) and placed in an airtight Perspex (databank, UK) chamber with Mylar (Dupont-Teijin, UK) windows, and sealed with grease.

2.2.2 Data collection and analysis

All experiments were performed at station 14.1 at the Synchrotron Radiation Source (SRS, Daresbury, UK), using a wide angle XRD, which has a beam of 0.1488 nm wavelength and a 0.2 mm x 0.2 mm square cross-section of the specimen. This wide angle XRD was used to map in detail collagen fibril organisation along medial-lateral and inferior-superior meridians across the sclera, limbus, and cornea (Figure 2.1). The corneoscleral button was carefully positioned at a specific location to ensure that the X-ray passed through the anterior corneal face parallel to the cornea's optical axis. A variety of exposure times, that is, 25, 30, or 45 seconds, were used based on the thickness of the cornea and the intensity of the x-ray at the time of the experiment. In addition, different step sizes were used for each experiment, that is, 0.30 mm to 1.00 mm, depending on the protocol of each experiment. A motor was used to move the whole Perspex chamber, enabling the tissue to be examined without being touched.

The resulting x-ray patterns were recorded on a Quantum 4R Charge-Couple Device (CCD) detector (ADSC, Poway, CA) located 150 mm behind the specimen (Figure 2.1). A lead backstop was positioned between the sample and the detector to stop any undeviated x-rays.

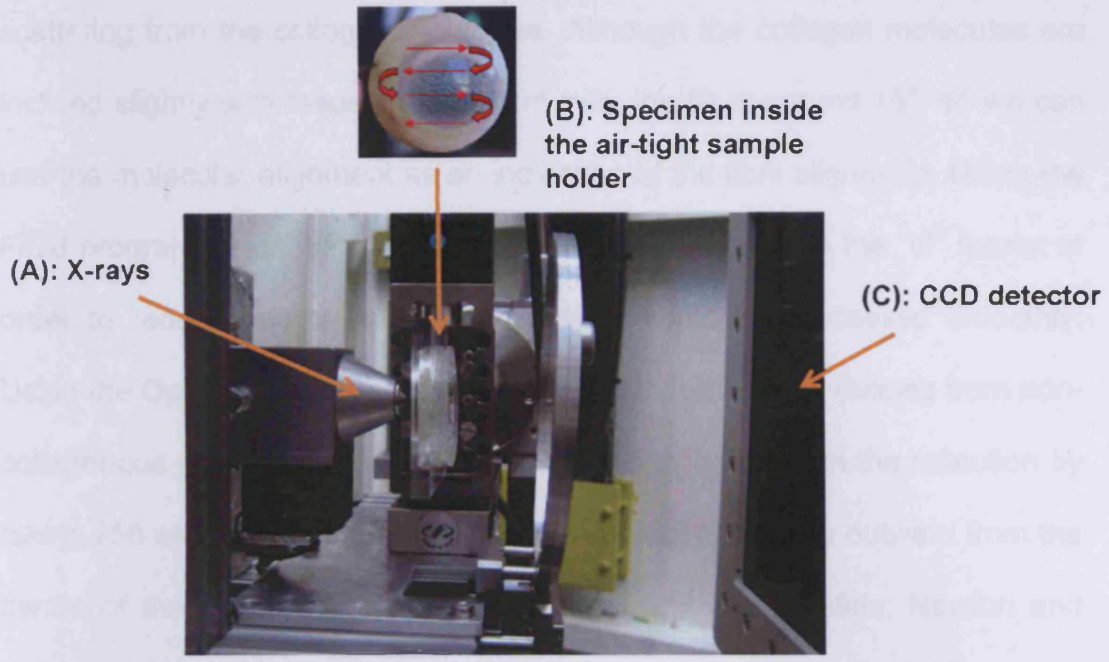

Figure 2.1: These pictures show some parts from the XRD experiment at station 14.1 (SRS, Daresbury, UK). A wide angle x-ray beam with a wavelength of 0.1488 nm (A) passed through the anterior corneal face and made raster scans across the cornea with the rim of the surrounding sclera (B). The resulting x-ray patterns were recorded on a Quantum 4R Charge-Couple Device (CCD) detector (C). (Original pictures from Dr. C. Boote)

All data were then transferred to the Structural Biophysics Laboratory at the School of Optometry and Vision Sciences (Cardiff University) for analysis. Normalised intensity profiles and maps of x-ray patterns were obtained using the following programmes:

1- Unix based image analysis software-Fit2d (ESRF, France);

2- Windows based graphics package – Optimas (Media Cybernetics, UK);

3- Windows based spreadsheets software, Excel (Microsoft, UK); and

4- Windows based statistics package - Statistica (Statsoft, UK).

Figure 2.2 shows the major steps of XRD analysis. A high angle XRD pattern from the central human cornea (Figure 2.2A) shows the backstop position in the centre and the four lateral lobes (maxima) corresponding to x-ray

scattering from the collagen molecules. Although the collagen molecules are inclined slightly with respect to the fibril axis, the tilt is around 15°, so we can use the molecular alignment as an indication of the fibril alignment. Using the Fit2d programme, all "img" XRD images were converted to the "tif" format in order to reduce image size so the images could be processed smoothly. Using the Optimas program, the radial "background" scatter (arising from non-collagenous components in the cornea) was subtracted from the reflection by taking 256 segments and fitting a power law function radially outward from the centre of the pattern in each case (Newton and Meek 1998a; Newton and Meek 1998b). Following this, the scatter was summed for each radial position and the summed scatter plotted as a function of angle (Figure 2.2B). This x-ray scatter distribution was divided into two components, as shown in Figure 2.2B: (A) isotropic scatter from collagen fibrils distributed equally in all directions, and (B) preferentially aligned fibril scatter. Using the Excel software, unwanted isotropic scatter was subtracted (Daxer and Fratzl 1997; Boote *et al.* 2004), and after shifting the data by 90° to account for the fact that the reflections (scatterings) are at right angles to the fibril axes (Figure 2.2C), the preferentially aligned fibril scatter was converted, using Excel and Statistica programs, into the polar coordinate shape as seen in Figure 2.2D (Connon and Meek 2003). Displaying Figure 2.2C in polar co-ordinates allows us to readily see the preferred fibril directions that gave rise to the X-ray reflection in Figure 2.2A. The radial size of the plot is proportional to the number of fibrils disposed in that direction

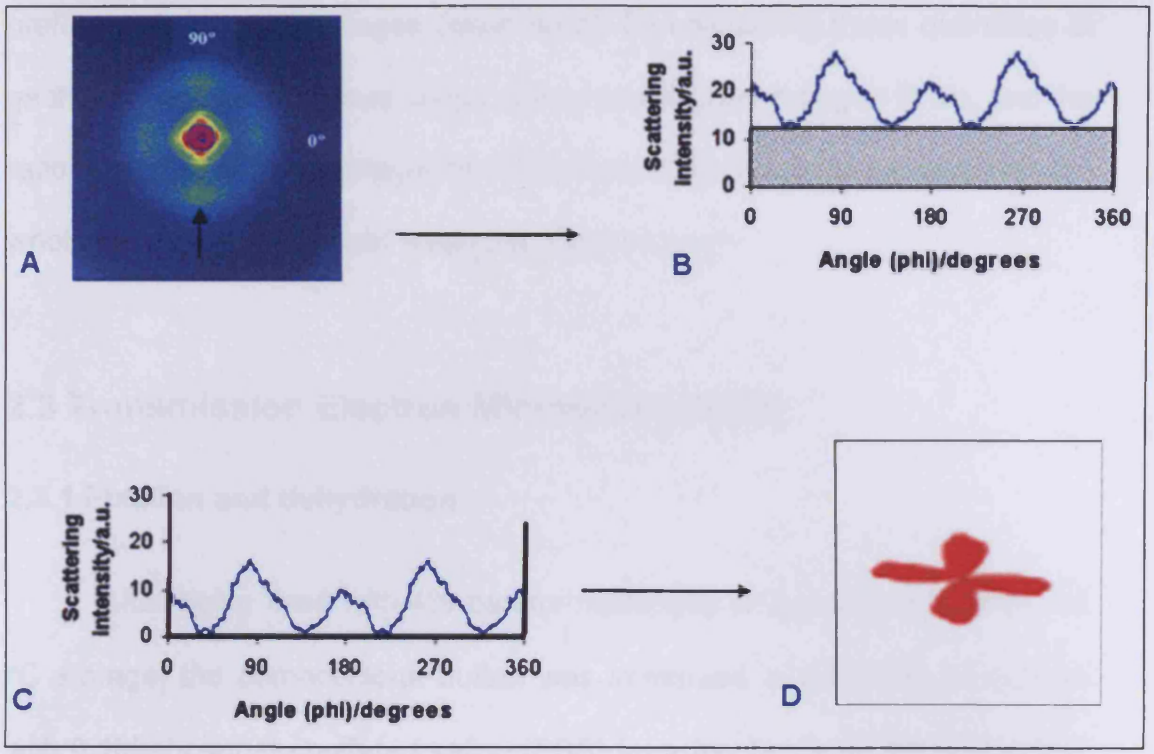

Figure 2.2: Main steps of XRD analysis. (A): Sample of a high angle XRD pattern from the central human cornea. Arrow indicates the x-ray reflection which is comprised of four lobes. (B): Distribution of scattering intensity around collagen molecule in (A) showing aligned scatter (curved lines) and isotropic scatter (shaded area). (C): Distribution of scattering intensity after the subtraction of isotropic scatter. (D): The resultant polar plot pattern (shifted by 90°).

Each X-ray pattern was analysed to produce a polar plot representing quantitatively the amount of collagen preferentially aligned in a given direction or directions, summed throughout the full thickness of the tissue at that point. A polar plot map of collagen-preferred orientation was then created in order to visualise the spatial distribution of preferentially aligned collagen fibrils over the whole tissue.

The total area under the scatter intensity graph in Figure 2.2B is proportional to the mass of collagen at that point in the tissue. This can be subdivided into the mass of isotropic collagen (shaded area) and the mass of

preferentially aligned collagen (clear area). By calculating these quantities at each point across the tissue, maps of total and aligned collagen fibrils, and the ratio of total to aligned collagen fibril distribution (termed beta values) over the whole tissue were produced using the Excel program.

2.3 Transmission Electron Microscopy (TEM)

2.3.1 Fixation and dehydration

After being fixed with 4% paraformaldehyde or being thawed from -80 °C storage, the corneoscleral button was immersed in 2.5% glutaraldehyde with 0.1M phosphate buffered saline (PBS) for a few hours for strong fixation. The tissue was then washed twice with 0.1M PBS (15 minutes each time) to remove excess glutaraldehyde, and subsequently was fixed using 1% osmium tetroxide (O_SO_4) for 2 hours. The specimen was then washed three times with distilled water (10 minutes each time) and stained for 45 minutes in a 0.5% aqueous solution of uranyl acetate. Excess uranium was then removed by briefly washing the specimen in double distilled water. The specimen was then dehydrated in graded alcohol (ethanol) ranging from 50%, 70%, and 90% for 15 minutes on each occasion, then in 100% twice for 15 minutes on each occasion. Next, several triangular-shaped sections were cut from the centre of the cornea and immersed in propylene oxide for 40 minutes. Tissues were then incubated in a mixture of propylene oxide and Epon resin (Araldite monomer CY212 10.0g, hardener DDSA 10.0g, and accelerator BDMA 0.30g) for 4 hours, then in 100% Epon resin for another 4 hours. After that, samples were incubated in 100% fresh resin overnight to allow impregnation of the

resin into the tissue. Tissue preparation was performed at room temperature on a rotator in the fume cupboard, with constant agitation to allow the whole surface of the sample to be exposed to the solution. Finally, the specimens were placed flat in labelled blocks i.e. the central cornea faced the pointed tip of the block, and polymerised in pure Epon resin at 70°C for 8 hours in order to harden the blocks and form a pyramid shape.

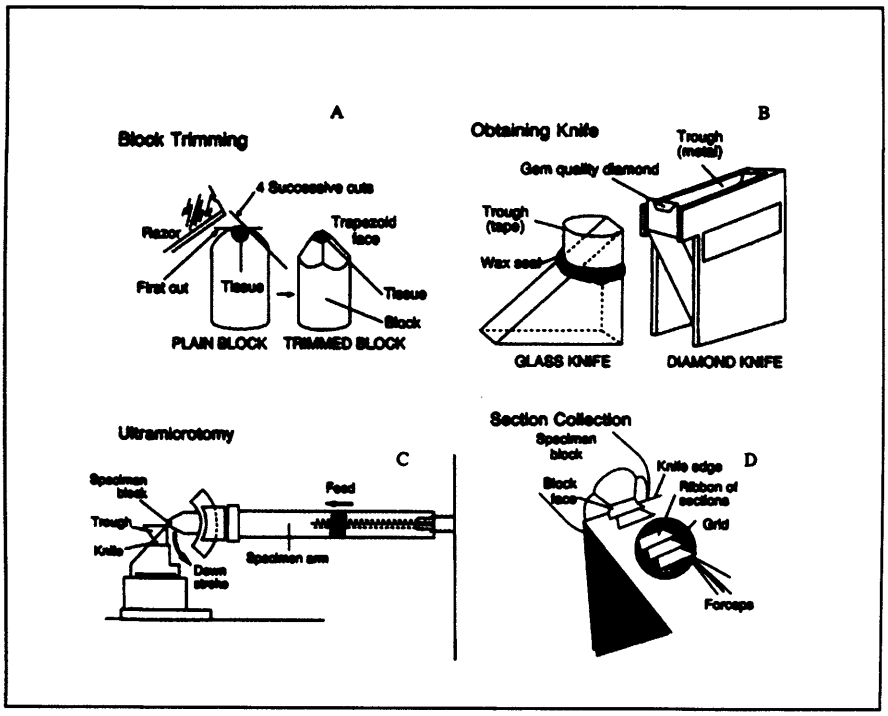

Figure 2.3: Schematic diagram of steps involved in the ultramicrotomy process (Bozzola and Russell 1992).

The blocks were then trimmed to expose the sample and to form a pyramidal cutting face (Figure 2.3A) using a razor blade. A glass knife was made using an LKB 7800 knife maker, and a plastic trough was attached to the knife using wax (Figure 2.3B) to hold the water, onto which the cut sections could drift. Thin (1 μm) and ultrathin (70-95 nm) corneal sections were cut with glass or diamond knives on a Reichart-Jung microtome

(Reichert Ultracut E, Leica, UK) (Figure 2.3C). The thin sections were then stained with toluedine blue and checked by a light microscope to make sure that the corneal sections were suitable for TEM, that is, a thin section with all corneal layers present. After appropriate ultrathin sections were obtained, chloroform was used to expand the sections in the water trough. The sections were then collected onto 300 square mesh copper 3.05mm grids (Figure 2.3D) and put in a Petri dish until the time of staining.

2.3.2 Staining and TEM examination

In order to obtain a clear visualization of the corneal ultrastructure, uranyl acetate and lead citrate were used to stain the corneal grids. These solutions were cleared of aggregates by centrifugation at 10,000 - 14,000 r/pm for 3 -5 minutes. Two methods were used to stain the grids. In the first method, the corneal grids were stained by being floated on droplets of 2.0% uranyl acetate for 5 minutes then washed briefly in distilled water to remove any excess uranyl acetate. After that, the grids were floated on lead citrate for 2 minutes and washed again briefly with distilled water. In the second method, the corneal grids were stained by being floated on droplets of 2.0% uranyl acetate and kept in an oven at 50° C for 45 minutes. After that, the grids were washed by being dipped frequently in distilled water for 2 minutes; they were then floated on droplets of lead citrate for 5 minutes then washed again by being dipped in distilled water. Finally, the corneal grids were lifted onto a Petri dish for a few minutes to dry; they were then ready for TEM examination. A JEOL 1010 TEM (JEOL Ltd., Akishima, Japan) operated at an accelerating voltage of 80Kv and a Philips EM 208 TEM (Fei Company, Eindhoven, The

Netherlands) at a voltage of 100kv were used to examine the corneal ultrastructure. Many images were taken from the epithelium, stroma, and endothelium at various magnifications (5000 to 40000).

2.4 Scanning electron microscopy (SEM)

2.4.1 Fixation and staining

Corneoscleral tissue was immersed in 2.5% glutaraldehyde in 0.1M sodium cacodylate buffer, pH 7.4, for 2 hours at room temperature then washed in 0.1M phosphate-buffered saline (PBS) to remove the fixative solution. After that, the tissue was placed in a solution of 5-10% NaOH for 2-5 days (replenished daily) in order to remove most of the cellular elements, including epithelial cells, and to allow clear visualization of the collagen lamellae (Komai and Ushiki 1991).

The tissue was then fixed using 1% osmium tetroxide (O_SO_4) in a Sorensen phosphate buffer for 2 hours. After that, the specimen was washed briefly in a phosphate buffer then washed four times with distilled water (15 minutes each time) to remove any excess osmium. A 0.5% aqueous solution of uranyl acetate was used for 60 minutes to stain the tissue to enhance visualisation.

2.4.2 Dehydration and examination

After being briefly washed in distilled water to remove any uranium, the tissue was dehydrated in graded alcohol (ethanol) ranging from 50%, 70%, and 90% for 15 minutes on each occasion, then in 100% twice. After that, the

sample was further dried by immersion 3 times in hexamethyl disilazane (HMDS) for 30 minutes; then, the tissue vial lid was removed and the vial was placed in a desiccator in the fume hood for a few days to allow the HMDS to evaporate. All the above steps were carried out in a fume hood with protective gloves. Special care was taken in handling osmium and HMDS.

Finally, the sample was mounted on an aluminium stub, using an adhesive carbon disc, and lifted on to the bench for 30 minutes to ensure full adhesion. Then, the tissue was coated with a layer of gold in a sputter coater to enhance structure visualisation. A high vacuum SEM (Philips XL 20) operated at an accelerating voltage of 25–30 kV was used to study the tissue structure at different magnifications.

2.5 Light microscopy (LM)

2.5.1 Preparation of corneal tissue for wax sectioning

Fixed human corneal tissues were dissected in appropriately small triangular shapes in order to study the corneal cross section using a light microscope. Tissues were then dehydrated in a graded series of ethanol concentrations, that is, 50%, 70%, 90%, and 100% of ethanol (30 minutes each) then in 2 changes of 100% ethanol for 1 hour each. Dehydrated tissues were then immersed in 50% chloroform for 30 min, 100% chloroform for 1 hour followed by 100% chloroform for 30 min. Each corneal tissue was then embedded in a mould containing molten wax by immersing the tip of the cutting surface (central cornea). The wax was labelled with the tissue

reference number and solidified by placing the mould on a cold plate (RA Lamb, East Sussex, UK) for 30 min. The wax blocks were then stored at 4°C until the time of sectioning.

2.5.2 Corneal tissue sectioning

The corneal wax block was trimmed and serial sections of 7μm thickness were cut using an HM330 microtome (Micron, Germany). Every 10-20 sections were floated briefly into a cold water bath then into a warm water bath (45-50°C) in order to flatten the sections and remove any wrinkles. Finally, all the sections were transferred onto microscope slides (3-5 sections in each slide) and were dried in an oven at 50°C overnight to allow the adhesion of the sections to the slides to take place.

2.5.3 Haematoxylin and eosin staining and LM examination

Haematoxylin and Eosin staining were used to stain various corneal tissue structures such as collagen, epithelial and endothelial cells as shown in the next experimental chapters. Corneal waxed sections were dewaxed by immersing the slides in two changes of xylene for 5 minutes each, and were then rehydrated through a graded series of alcohol concentrations, that is, in 100%, 90%, 70% and 50% alcohol (one minute each), then rinsed in running tap water for 1 minute to remove the alcohol. After that, the slides were immersed in a container of haematoxylin for 5 minutes then washed with water to remove any excess dye. Next, the slides were immersed in an eosin solution for 3 minutes followed by a brief water wash and a series of graded brief dehydrations by alcohol (50%, 70%, 90% and 100% alcohol). After

drying, two drops of DPX adhesive medium were applied to the slides, which were then covered by glass coverslips and allowed to dry overnight. Sections were examined by light microscope (DMRAZ, Leica Milton, UK) and images were taken by Qwin3 imaging software at different magnifications.

Chapter 3. A comparative study of collagen fibril orientation and distribution in the cornea of different mammalian species

3.1 Introduction

The mammalian stroma, which accounts for nearly 90% of the cornea, is composed of a large amount of water and collagen fibrils. Furthermore, it is believed that the strength and transparency of the cornea is due to the uniform arrangement of these fibrils within the water matrix. However, it has been found that the collagen fibril diameter and interfibrillar spacing between collagen fibrils varies among mammalian species (Meek and Leonard 1993), with the camel having the largest fibril diameter and interfibrillar spacing. In a small-angle XRD study, Meek *et al.* noted that the human cornea has a unique orthogonal collagen fibril orientation in the central area and uniaxial (tangential) orientation at the periphery (Meek *et al.* 1987). This orthogonal orientation of the human cornea was confirmed recently by wide-angle XRD, which was used to map the whole corneoscleral button (Aghamohammadzadeh *et al.* 2004). Moreover, the collagen fibril orientation of other species has also been studied and compared with the human cornea (Boote *et al.* 2004; Hayes *et al.* 2007). To the best of our knowledge, no wide-angle XRD study has been reported showing the collagen fibril orientation and distribution of rabbit (a species that is commonly used in corneal research) and camel corneas. Therefore, in this study, the collagen fibril orientation and distribution of these two different-sized mammalian species were studied using wide-angle XRD and were compared with the collagen fibril

arrangement of the human cornea. The hypothesis is that the human cornea has a unique collagen fibril orientation that cannot be found in other mammalian species.

3.2 Materials and Methods

Ten corneas with part of the sclera from different mammalian species were used in this wide-angle XRD study as follows: three human corneas, three rabbit corneas, and four camel corneas. The general XRD method was explained in chapter 2, section 2.2.

Three human (Homo sapiens sapiens) corneas with the rim of the sclera (two males and one female aged 43, 66 and 73 years old) were obtained from the UK Corneal Transplant Service, Eye Bank (Bristol, UK). These corneas were time-expired and not suitable for corneal transplant due to the loss of endothelial cells. The corneas were kept in containers of organ culture medium and stored in an incubator at 37°C for different periods (4-7 weeks). On receipt, the corneas were removed from the culture medium, wrapped individually in clingfilm, and stored frozen at -80°C prior to the XRD experiment. Each cornea was defrosted at room temperature immediately prior to XRD data collection. Because the superior part of the corneoscleral button (12 o'clock) was unknown, a few quick tests were done by XRD to align the sample and find out the correct cross shape of the collagen fibrils. XRD was collected at 0.3mm intervals for 30 or 45 seconds of exposure time.

Three rabbit (Oractologus cuniculus) corneas were obtained from two New Zealand white rabbits (2-3 kg). The rabbits were killed and the

corneoscleral buttons were extracted immediately at the Joint Services Department of the Heath Hospital (Cardiff, UK). All tissues were marked by a suture in the most superior part of the corneoscleral button (12 o'clock), wrapped individually in cling film, and then taken to Cardiff University and stored frozen at -80°C until the XRD experiment. Wide-angle XRD was collected at different settings, that is, at 0.3, 0.5, and 1.00mm step sizes and the exposure times were 30 and 45 seconds.

Four corneoscleral buttons of the one-humped camel (Camelus dromedarius) were obtained from two young camels (2-4 years old) at the slaughterhouse (Riyadh, Saudi Arabia). The camels were killed and the whole eyes were dissected immediately. After that, the corneoscleral tissues were removed, the superior part marked; the tissues were kept in 4% paraformaldehyde containers, and then brought to Cardiff University and stored until the day of the experiment. Wide-angle XRD was collected at 1mm intervals for 25 seconds exposure time.

Due to the large size of the camel corneoscleral buttons and the limited capacity of the specimen holder, each button was trephined 12mm-14mm centrally then wrapped in cling film to fit into the airtight Perspex chamber.

3.3 Results

3.3.1 Human corneas

Figure 3.1 shows the polar plot map derived from wide-angle XRD for the preferred collagen fibril orientation in the human cornea, limbus and part

of sclera. It is clear that the collagen fibrils in the central area of the cornea are shaped orthogonally, that is, in the superior-inferior and nasal-temporal directions. This result is similar to the previous XRD findings on the human cornea (Meek *et al.* 1987; Newton 2001; Aghamohammadzadeh *et al.* 2004). However, Figure 3.1 shows a small central area (black arrows) where the collagen fibril orientation is uniaxial, that is, in the superior-inferior direction only. Toward the periphery, the collagen orthogonal shape becomes more tangentially arranged and consistent with a circumcorneal annulus of fibrils at the limbus (dotted circle). Moreover, there was a much higher proportion of aligned collagen in the limbus relative to the centre of the cornea as indicated by the colour of the plots and the key factors (Figure 3.1). Again, these findings are in agreement with other previous studies (Newton and Meek 1998b; Aghamohammadzadeh *et al.* 2004).

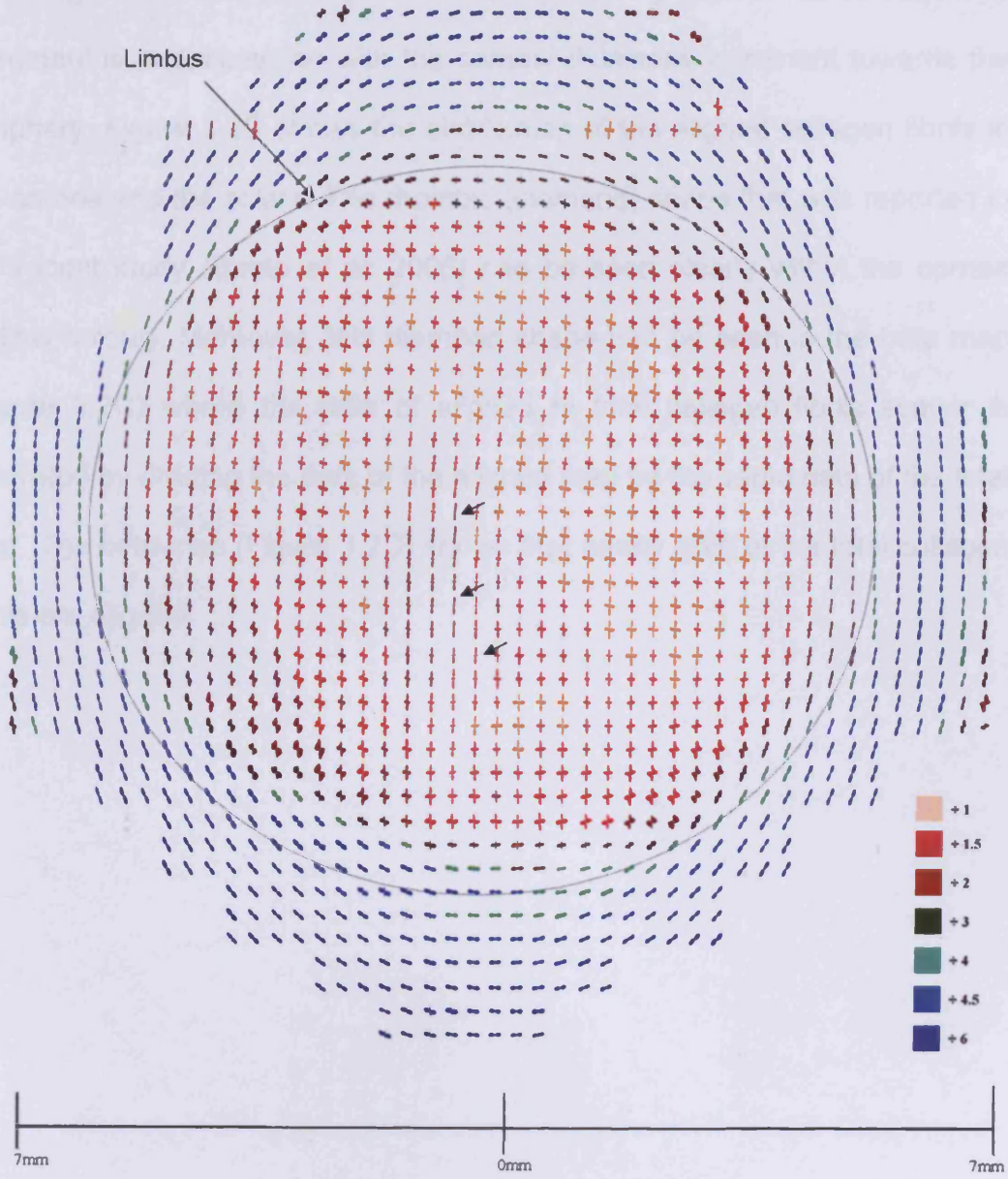

Figure 3.1: Polar plots of the preferred collagen fibril orientation in a normal human cornea with part of the sclera (Right eye) sampled at 0.3mm intervals. Plots were scaled down by factors shown on the right. Small black arrows show uniaxial orientation of collagen fibrils which may be related to a crease in the cornea.

The contour maps of total collagen, aligned collagen, and their ratio (beta values) (Figure 3.2) give us an overview of the amount and organisation of collagen fibrils in the whole corneoscleral tissue of the human eye. Figure 3.2A shows that the total collagen fibrils increase from the centre of the

cornea (yellow-brown colour) towards the periphery (brown-red colour). This increment is in conjunction with the corneal thickness increment towards the periphery. Figure 3.2B shows the distribution of the aligned collagen fibrils in the cornea and the sclera. The rhombic (diamond) shape that was reported in our recent study (Boote *et al.* 2006) can be seen clearly within the cornea (yellow colour). Moreover, this diamond shape can be seen in the beta map (Figure 3.2C) where the ratio of aligned to total collagen fibrils scatter is illustrated by dividing the data of the aligned map by the same data of the total map. The beta map (Figure 3.2C) shows that nearly 40% of the total collagen fibrils are aligned.

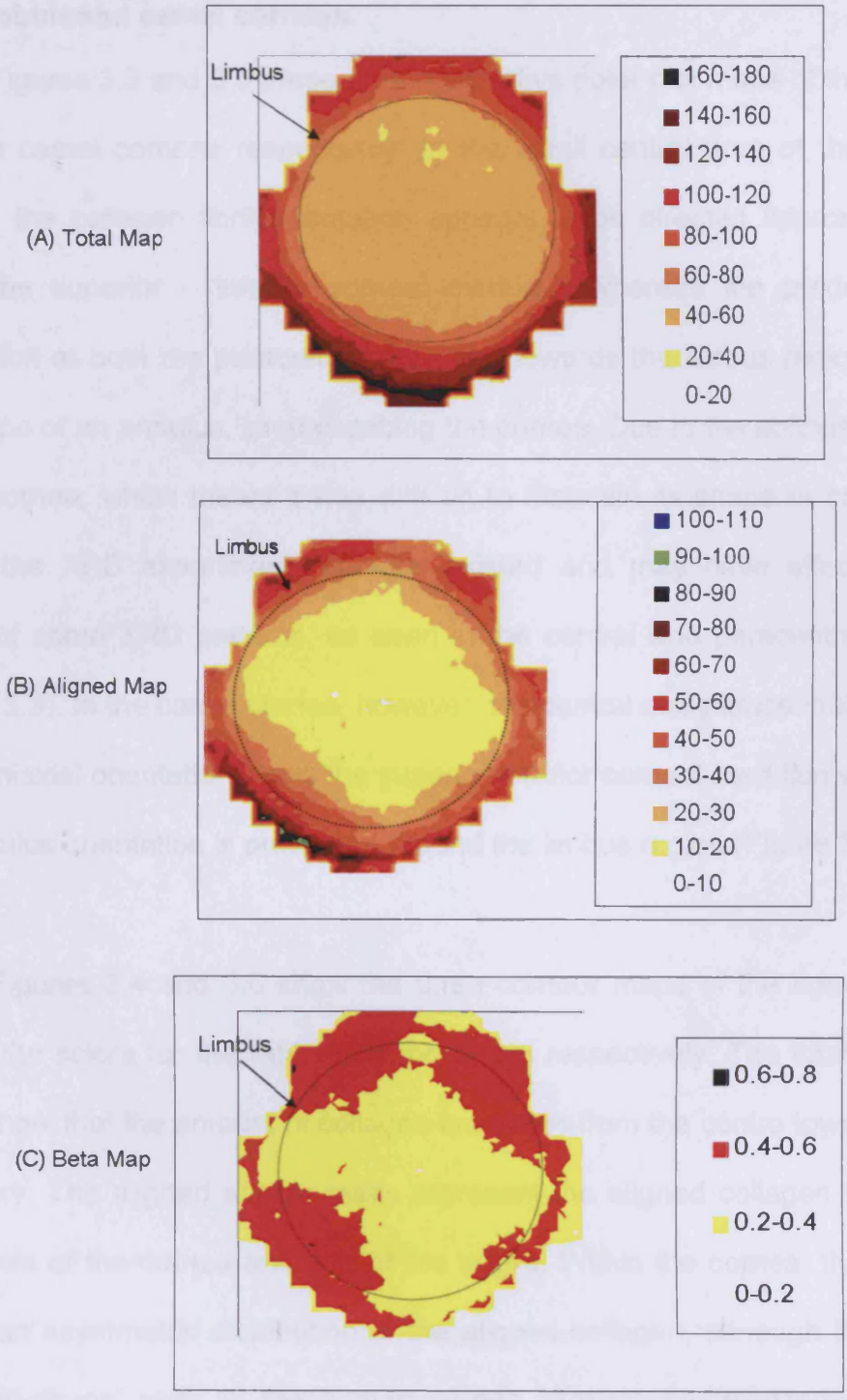

Figure 3.2: Contour maps of XRD across the human cornea with scleral rim showing the distribution of collagen (Right eye). (A) Total fibrillar collagen XRD. (B) Preferentially aligned collagen fibrils. (C) Ratio of aligned/total collagen fibrils. XRD values are in arbitrary units. Dotted circle indicates the limbus region.

3.3.2 Rabbit and camel corneas

Figures 3.3 and 3.5 present representative polar plot maps of the rabbit and the camel corneas respectively. In the small central area of the rabbit cornea, the collagen fibril orientation appears to be directed approximately along the superior – inferior corneal meridian, whereas the predominant orientation at both the paracentral area and towards the limbus region takes the shape of an annulus, circumscribing the cornea. Due to the softness of the rabbit cornea, which meant it was difficult to maintain its shape or curvature during the XRD experiment, wrinkles existed and may have affected the shape of some XRD patterns, as seen in the central and paracentral areas (Figure 3.3). In the camel cornea, however, the central and paracentral cornea show uniaxial orientation along the superior-inferior corneal meridian whereas the annulus orientation is presented around the limbus region (Figure 3.5).

Figures 3.4 and 3.6 show the three contour maps of the cornea with part of the sclera for the rabbit and the camel respectively. The total scatter maps show that the amount of collagen increases from the centre towards the periphery. The aligned scatter maps represent the aligned collagen fibrils in each area of the cornea and part of the sclera. Within the cornea, there is a hint of an asymmetric distribution of the aligned collagen, although the clear 'diamond-shape' seen in the human cornea (Aghamohammadzadeh *et al.* 2004; Boote *et al.* 2006) is not so obvious, particularly in the camel cornea. The beta maps of both animals show the proportion of collagen that is preferentially aligned. It was found that nearly 30% and 25% of the collagen

fibrils are aligned in the rabbit and the camel corneas respectively as shown in Figures 3.4C and 3.6C.

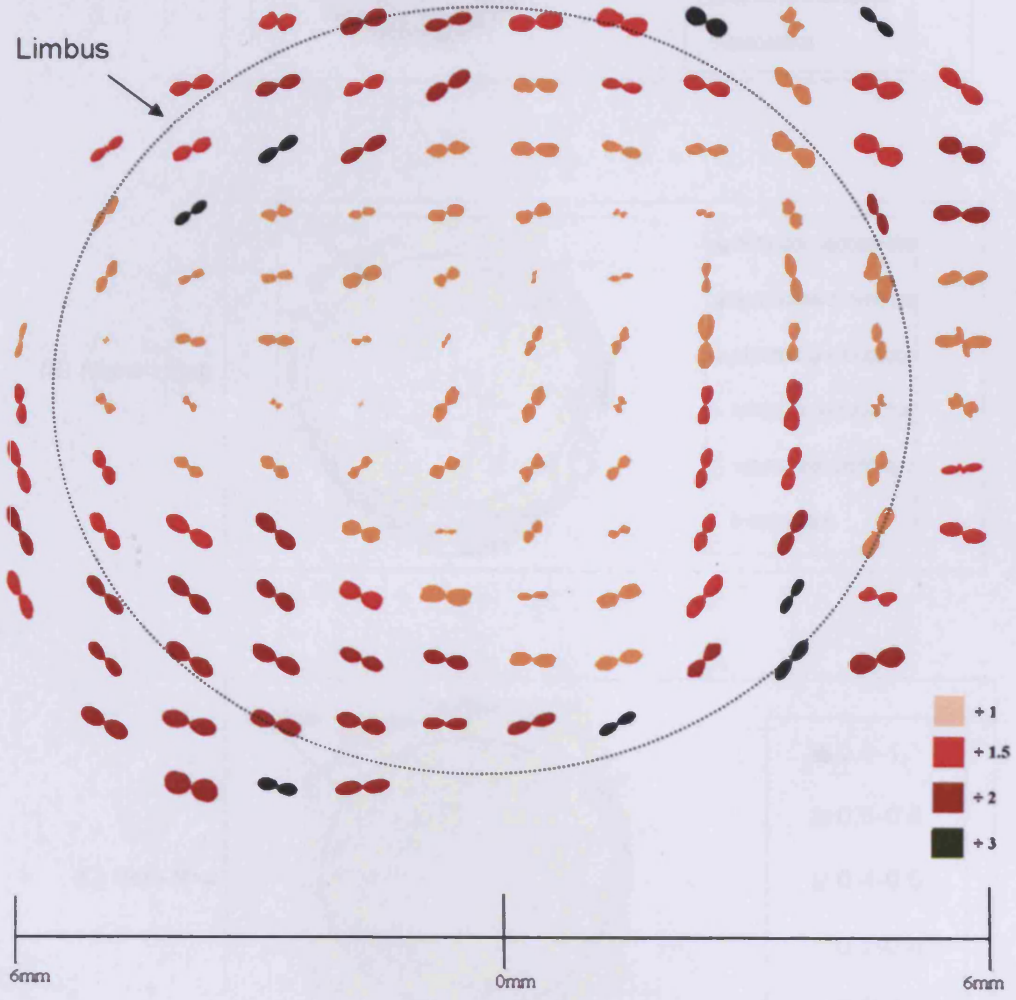

Figure 3.3: Vector plot map showing the preferred collagen fibril orientation in the rabbit cornea with part of the sclera. The dotted circle indicates the limbus border. XRD was taken at 0.5mm step size. The polar map was scaled down by the factors shown in the key.

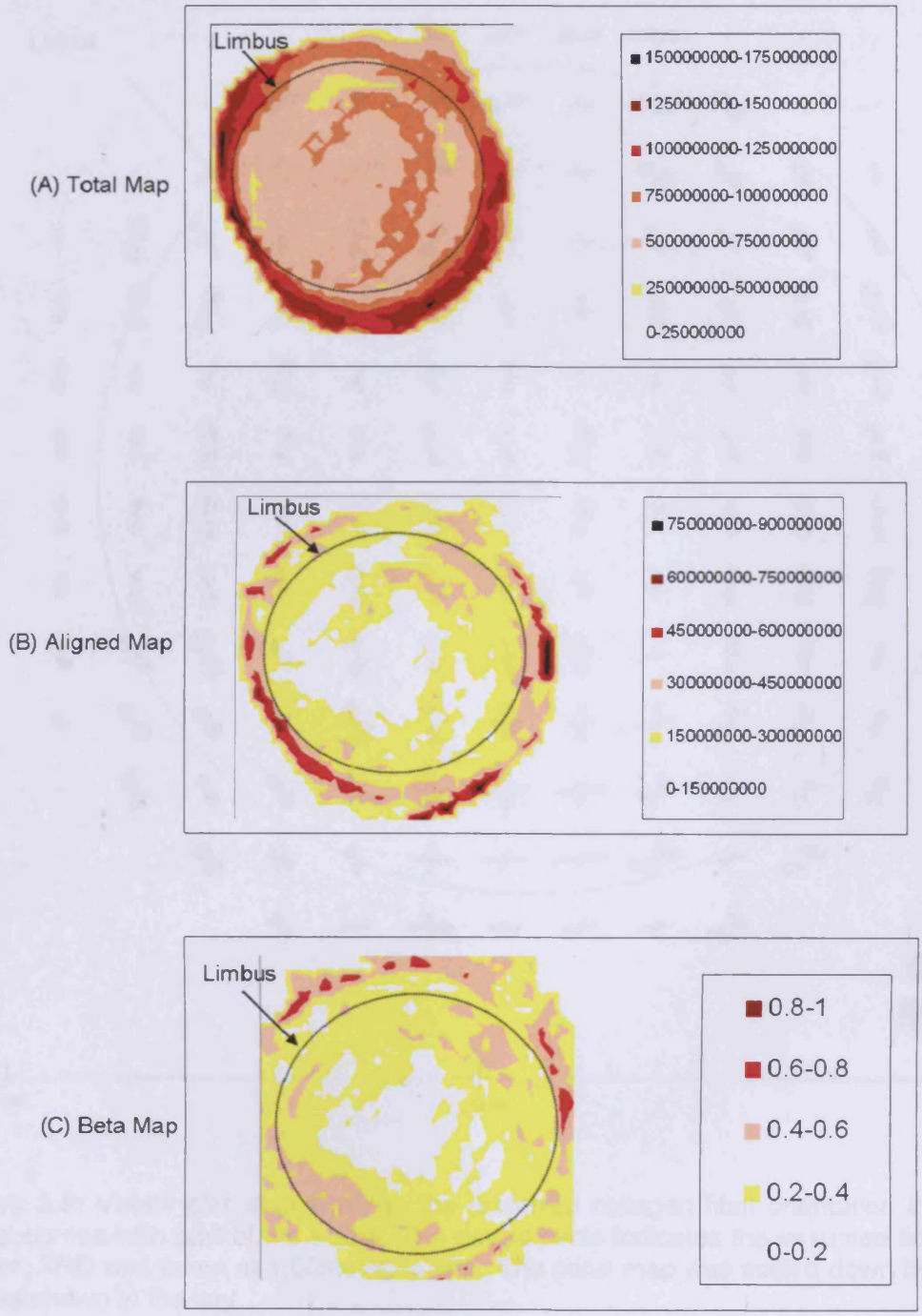

Figure 3.4: Contour maps of XRD across the rabbit cornea with part of the sclera showing the distribution of collagen. (A) Total collagen distribution. (B) Aligned collagen fibrils distribution. (C) Ratio of aligned/total collagen fibrils. XRD are in arbitrary units. Dotted circle indicates the limbus region.

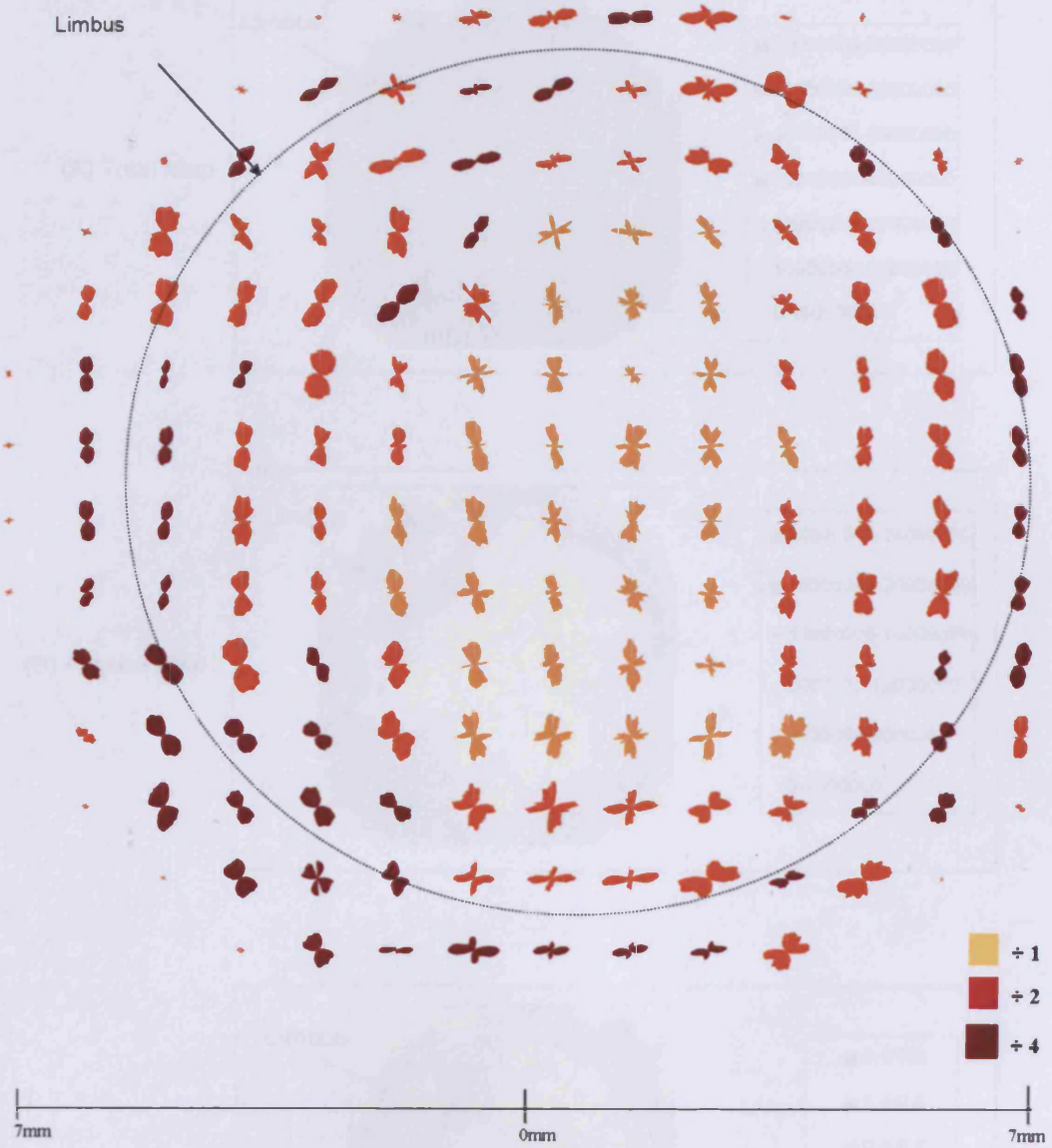

Figure 3.5: Vector plot map showing the preferred collagen fibril orientation in the camel cornea with part of the sclera. The dotted circle indicates the assumed limbus border. XRD was taken at 1.00mm step size. The polar map was scaled down by the factors shown in the key.

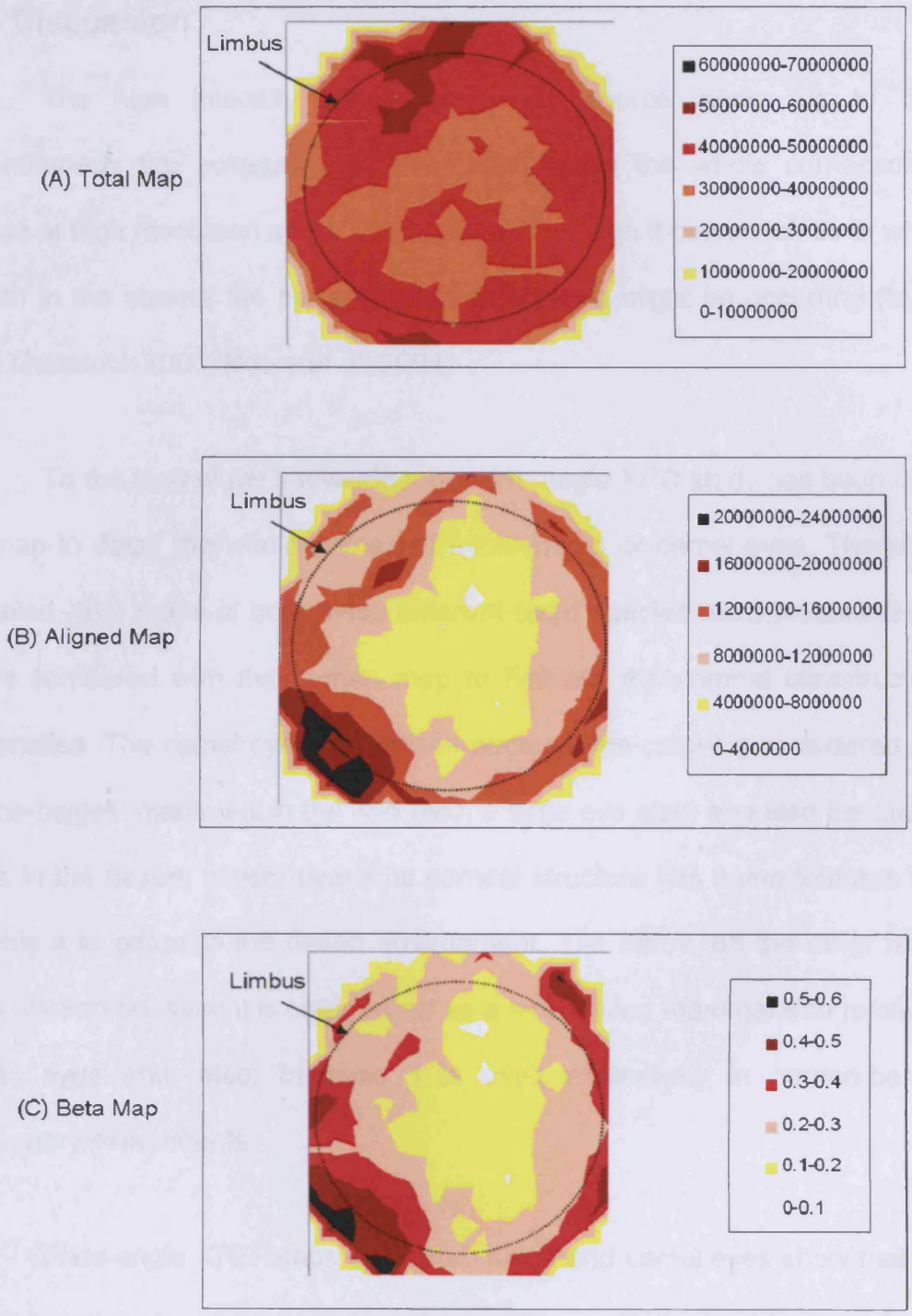

Figure 3.6: Contour maps of XRD across the camel cornea with part of the sclera showing the distribution of the collagen fibrils. (A) Total fibrils distribution. (B) Aligned fibrils distribution. (C) Ratio of aligned/total collagen fibrils distribution. XRD are in arbitrary units. The dotted circle indicates the limbus region.

3.4 Discussion

The high intensity synchrotron x-ray source allows us to map quantitatively the collagen fibril orientation within the whole corneoscleral tissue at high resolution and for a short time although it cannot tell us at which depth in the stroma the preferred fibril orientation might be occurring (Meek and Quantock 2001; Boote *et al.* 2004).

To the best of my knowledge, no wide-angle XRD study has been done to map in detail the whole cornea of either rabbit or camel eyes. Therefore, detailed XRD maps of both these different-sized species were presented and were compared with the human map to find out the corneal ultrastructural anomalies. The camel eye was chosen because the camel is considered one of the biggest mammals in the wild (with a large eye size) and also because it lives in the desert, which means its corneal structure has some features that enable it to adapt to the desert environment. The rabbit, on the other hand, was chosen because it is categorised as a small-sized mammal with relatively small eyes and, also, because it is used extensively in human-benefit laboratory experiments.

Wide-angle XRD maps of human, rabbit and camel eyes show that the relative amounts and arrangement of collagen fibrils in the central and paracentral cornea are not uniform whereas the arrangement is almost the same at and around the limbus region.

The human polar plots map (Figure 3.1) derived from the wide-angle XRD shows that the orientations of collagen fibrils in the cornea and limbus

are not uniform, that is, they show an orthogonal orientation centrally and an annulus circumscribing the cornea peripherally. This unique 'strong' orientation is due to the mechanical forces of the six voluntary extraocular muscles (4 rectus and 2 oblique muscles) of the orbit that produce eye movement and, therefore, play an important role in corneal biomechanical properties and, hence, in corneal visual function. These findings are in line with those reported in previous studies (Daxer and Fratzl 1997; Newton and Meek 1998a; Aghamohammadzadeh *et al.* 2004; Boote *et al.* 2006). Meek's group (Aghamohammadzadeh *et al.* 2004) was the first to generate a detailed map of the preferred collagen fibril orientations for a normal human cornea. I replicated the results in this study in order to compare it with other mammalian species and to use it as a control map for other experiments (see next experimental chapters).

All mammalian species have four extraocular rectus muscles with variations in length, width, and location (Prangen 1928; Prince 1960; Hayes *et al.* 2007). Therefore, the collagen arrangement of the cornea is suggested to be the same in all species. However, this is not the case, as indicated by the previous results (Boote *et al.* 2004; Hayes *et al.* 2007) and by this study's results. In our recent paper, Hayes *et al.* (2007) found a predominantly vertical collagen orientation in horse, cow, and marmoset eyes. In addition, we found a predominantly circumferential collagen orientation in pig, rabbit, and mouse eyes (Figure 3.7). In this study, I found a predominantly vertical orientation in camel eyes and a predominantly circumferential orientation in rabbit eyes. Therefore, it appears that the collagen fibril orientation relates to the body

size, and also to the eye size, of the animal species, that is, a large sized animal possesses a vertical collagen orientation whereas a small sized animal possesses a circumferential orientation.

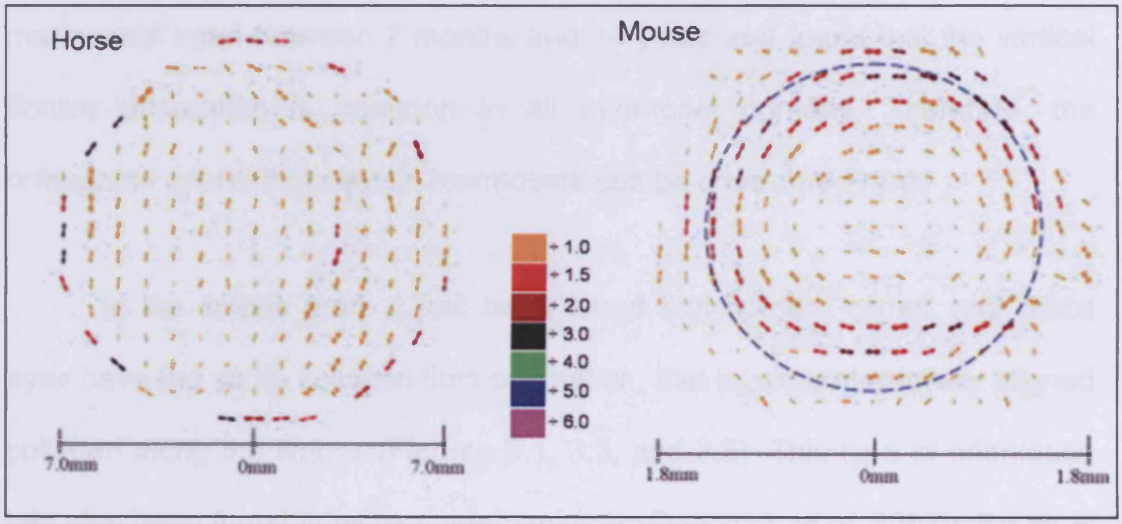

Figure 3.7: Vector plot maps showing the predominant direction of stromal collagen fibrils in horse and mouse. The dotted circle in the mouse map indicates the limbus. Vector plots are scaled down by the factors shown in the key. (Maps have been modified from Hayes *et al.* 2007).

Compared to other mammalian species, it can be said that the human cornea possesses a unique orthogonal collagen orientation that has not been reported in any animal until now. However, Hayes (2007) found that a few marmoset corneas have orthogonal collagen orientation similar to the human cornea (4 out of 20 marmoset corneas examined) whereas the majority possess a vertical collagen orientation. It is thought that this similarity in orthogonal orientation is due to the closeness of the extraocular rectus muscles of both marmosets and humans to the limbus compared to other species (Prangen 1928; Hayes *et al.* 2007). However, in this paper, the authors did not mention the age of the marmosets and it can be concluded

that this orthogonal orientation was found in marmoset corneas during the early stages of development such as the temporary orthogonal orientation that was found in chick corneas during the later stages of embryogenesis (Quantock *et al.* 2003a). Boote *et al.* (2004) examined ten eyes of common marmosets aged between 7 months and 14 years and found that the vertical fibrillar orientation is common in all marmoset corneas. Therefore, the orthogonal orientation seen in marmosets can be considered rare.

In the limbus area, it has been found that human, camel, and rabbit eyes have the same collagen fibril orientation, that is, circumferentially aligned collagen along the limbus (Figures 3.1, 3.3, and 3.5). This type of orientation has also been found in all examined animals (Quantock *et al.* 2003b; Boote *et al.* 2004; Hayes *et al.* 2007). It is thought that this annulus orientation is important in maintaining the curvature of the cornea as it is located at the border of different curvature tissues, that is, corneal and scleral (Maurice 1984; Aghamohammadzadeh *et al.* 2004).

In all examined corneas, the amount of collagen fibrils increases from the centre towards the periphery, as shown in all vector plot maps (Figures 3.1, 3.3, and 3.5) and total maps (Figures 3.2A, 3.4A, and 3.6A), that is, map colours become darker towards the periphery as indicated by the key factors and the arbitrary units (Figures 3.1, 3.3, and 3.5). This result has also been found in all examined mammalian species (Aghamohammadzadeh *et al.* 2004; Boote *et al.* 2004; Hayes *et al.* 2007) and it is due to the increment in the corneal thickness from the centre towards the periphery and the resultant

increment in the amount of collagen lamellae in the same direction, that is, from 500 μm centrally to 700μm peripherally for the human cornea (Maurice 1984; Kaufman *et al.* 1988; Fatt and Weissman 1992), from 350 μm centrally to 450 μm peripherally for the rabbit cornea (Prince 1964; Schulz *et al.* 2003) and from 760 μm centrally to more than 930 μm peripherally for the camel cornea (Osuobeni and Hamidzada 1999). The human maps were clear and easy to explain due to the stiffness of both the sclera and the cornea, which preserved the button curvature during the XRD experiment. On the other hand, the rabbit maps were not clear due to the softness of the rabbit cornea, which led to wrinkles being present that were not found in the rigid human cornea. In addition, it was hard to interpret the camel maps due to the large oval shape of the corneoscleral button, which made it difficult to maintain the corneal curvature during tissue fixation and transportation.

Aligned maps (Figures 3.2B, 3.4B, and 3.6B) show that collagen fibrils tend to make a rhombus (diamond) shape. This shape is clear in the human map whereas it is not so obvious in either the rabbit or the camel maps. In addition, Boote *et al.* (2004) did not find this shape in marmoset corneas, which, again, suggests that the human cornea possesses a unique corneal ultrastructure. This diamond shape is thought to arise from a population of 'anchoring lamellae' that enter and leave the cornea without crossing the centre, and play an important role in maintaining corneal curvature and strength (Aghamohammadzadeh *et al.* 2004; Boote *et al.* 2006).

Finally, the beta map, which is the ratio of the aligned to the total collagens, of the human cornea (Figure 3.2C) shows that the lowest proportion of aligned collagen fibrils is concentrated more at an oblique direction (at 4 to 5 and 10 to 11 o'clock) in the case of the right eye and, thus, has been used to differentiate between right eyes and left eyes (at 1 to 2 and 7 to 8 o'clock) as reported in our recent paper (Boote *et al.* 2006). However, this proportion of aligned collagen fibrils did not appear clearly in the beta maps of either the rabbit or the camel corneas (Figures 3.4C, and 3.6C). Furthermore, it was not clear in the marmoset cornea (Boote *et al.* 2004), which supports the conclusion that the human cornea possesses a unique fibrillar orientation.

In conclusion, the orthogonal arrangement of corneal collagen is a unique feature of the human cornea. On the other hand, small-sized animals possess a circumferential collagen orientation whereas large-sized animals possess a vertical collagen orientation. These findings show that the collagenous architecture of animal corneas are different from those of human corneas, and such findings may encourage scientists to concentrate their ophthalmic researches on human corneas rather than on animals in order to improve corneal surgery techniques such as LASIK. In addition, it is recommended that more wide-angle XRD studies be run to cover most types of mammalian species and to find out the predominant collagen orientation in each size class.

Chapter 4. Study of corneal collagen fibril organisation after full-thickness trephination

4.1 Introduction

As mentioned earlier, the human cornea possesses a unique collagen fibril orientation that plays an important role in the biomechanical stability of the cornea. Any damage to this orientation, such as incisions into corneal tissue, may change the corneal curvature and, hence, lead to degradation of its optical properties. For example, high and irregular astigmatism is a significant problem after penetrating keratoplasty (Perlman 1981; Radner *et al.* 1999). This astigmatism is most probably a result of imprecise trephination or differences in the size and undercut between the donor button and the recipient cornea (Bourne *et al.* 1982; Heidemann *et al.* 1985; Radner *et al.* 1999). Suturing technique is also another factor that induce post-keratoplasty astigmatism (Musch *et al.* 1989; Karabatsas *et al.* 1998; Javadi *et al.* 2006). Corneal trephination techniques produce distinct morphological differences, that is, disordered collagen fibrils at the cut edges of the donor buttons and their recipient beds (Radner *et al.* 1999). XRD and TEM have been used widely to study the collagen fibril arrangement in normal and trephined or wounded rabbit corneas at different wound healing periods (Rawe *et al.* 1994; Kaji *et al.* 1998; Connon and Meek 2003; Connon and Meek 2004). Radner *et al.* (1999) used TEM, SEM, and LM to compare the human corneal ultrastructure appearance of cut edges after using two different trephination techniques, that is, epithelial and endothelial sides punching methods. No

wide-angle XRD study has been done to find out the collagen fibril orientation and distribution after full-thickness trephination and before the start of the wound healing process. Therefore, in this study, wide-angle XRD was used to study the collagen arrangement at 9mm, 6mm, and 4mm full-thickness human corneal trephination. Moreover, a 4mm trephination with 45° rotation was also done to examine the collagen fibril orientation at a different angle. It is hoped that the results of this study will help to interpret the changes found in the corneal refractive properties after corneal surgery such as penetrating keratoplasty or LASIK.

4.2 Materials and Methods

Three time-expired healthy adult human corneas with part of the sclera, as mentioned in section 3.2, were obtained from the UK Corneal Transplant Service, Eye Bank (Bristol, UK). On receipt, the corneas were removed from the culture medium containers, wrapped individually in cling film, and stored frozen at -80°C. On the day of the experiment, each cornea was defrosted at room temperature immediately prior to XRD data collection. Different sized trephines with Taflon block (Altomed, UK) were then used to create a full thickness trephination from the endothelial side for all corneas, as shown in Figures 4.1 and 4.2. After that, the first cornea with part of the sclera (14mm) was mapped twice, that is, before and after a 9 mm trephination. Because the allocated time to run the experiment at station 14.1 was limited, the size of the second and the third corneas was trephined to 9mm to remove unnecessary tissue of the sclera and the limbus (Figure 4.1) and, hence, reduce the time required for XRD to finish each experiment. After that, the

second 9mm cornea was mapped twice, that is, before and after a 6mm full-thickness trephination. The third 9mm cornea was mapped twice, that is, after 4mm full-thickness trephination and after the 4mm trephined area was rotated 30° - 45°. In all the experiments, the trephined portion was replaced in its original position with the help of a surgical marking pen that was used to draw a vertical line along the cornea in order to confirm the correct repositioning of the trephined button (Figure 4.1). The marking pen was also used as a guide in the 4mm rotation experiment. Wide-angle XRD was collected at 0.3mm intervals for 30 and 45 seconds exposure time.

Figure 4.1: Steps of human corneoscleral trephination. (1) Cornea with part of the sclera was placed in upside down position on the Teflon block and 9mm trephine was pressed fully to cut the cornea 1-2 mm away from the limbus. (2) The 9 mm corneal button after full-thickness trephination (black arrow). (3) Another cornea (9mm) after 6mm trephination. The purple marking pen was used to draw a vertical line along the cornea to help in the realignment of the trephined portion.

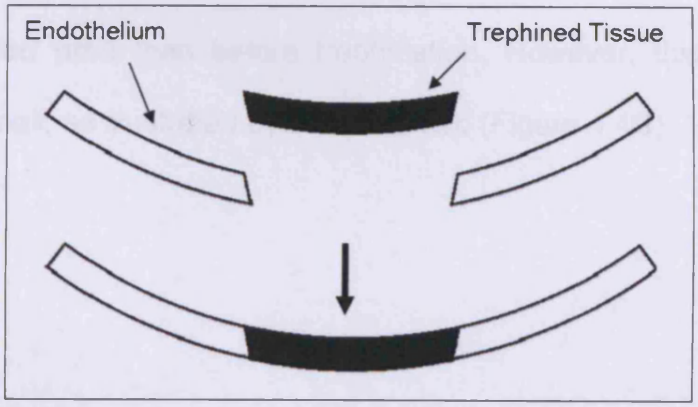

Figure 4.2: Schematic diagram of the trephination technique used in this study, that is, from the endothelial side with the posterior punch technique. The trephined button was then replaced in its original position (Jacobsen and Hojgaard-Olsen 2006).

4.3 Results

No changes in the collagen fibril orientation or distribution were detected in the XRD map after the 9mm full-thickness corneal trephination. On the other hand, a slight alteration in the collagen fibril orientation and distribution was seen in the 6mm trephination, which became more obvious in the 4mm trephination.

Figure 4.3 shows the collagen fibril arrangement in the 6mm trephination where the fibrils were converted from the orthogonal shape to a circumferential arrangement along the trephine wound in the area of 7 to 9 o'clock only. The amount of collagen was also increased in that area, as indicated by the factors key (brown colour). In the remaining trephined areas, however, no obvious change in the fibril orientation could be detected when compared with the control map (see Figure 3.1 in chapter 3 for the control map). Moreover, total and aligned collagen maps (Figure 4.4 A and B) show the alteration in the same area, that is, between 7 and 9 o'clock. The total map indicates that the amount of collagen fibrils increases in the area of trephine whereas the aligned map indicates that these fibrils are more aligned in the wounded area than before trephination. However, this alignment is considered small, as illustrated by the beta map (Figure 4.4C).

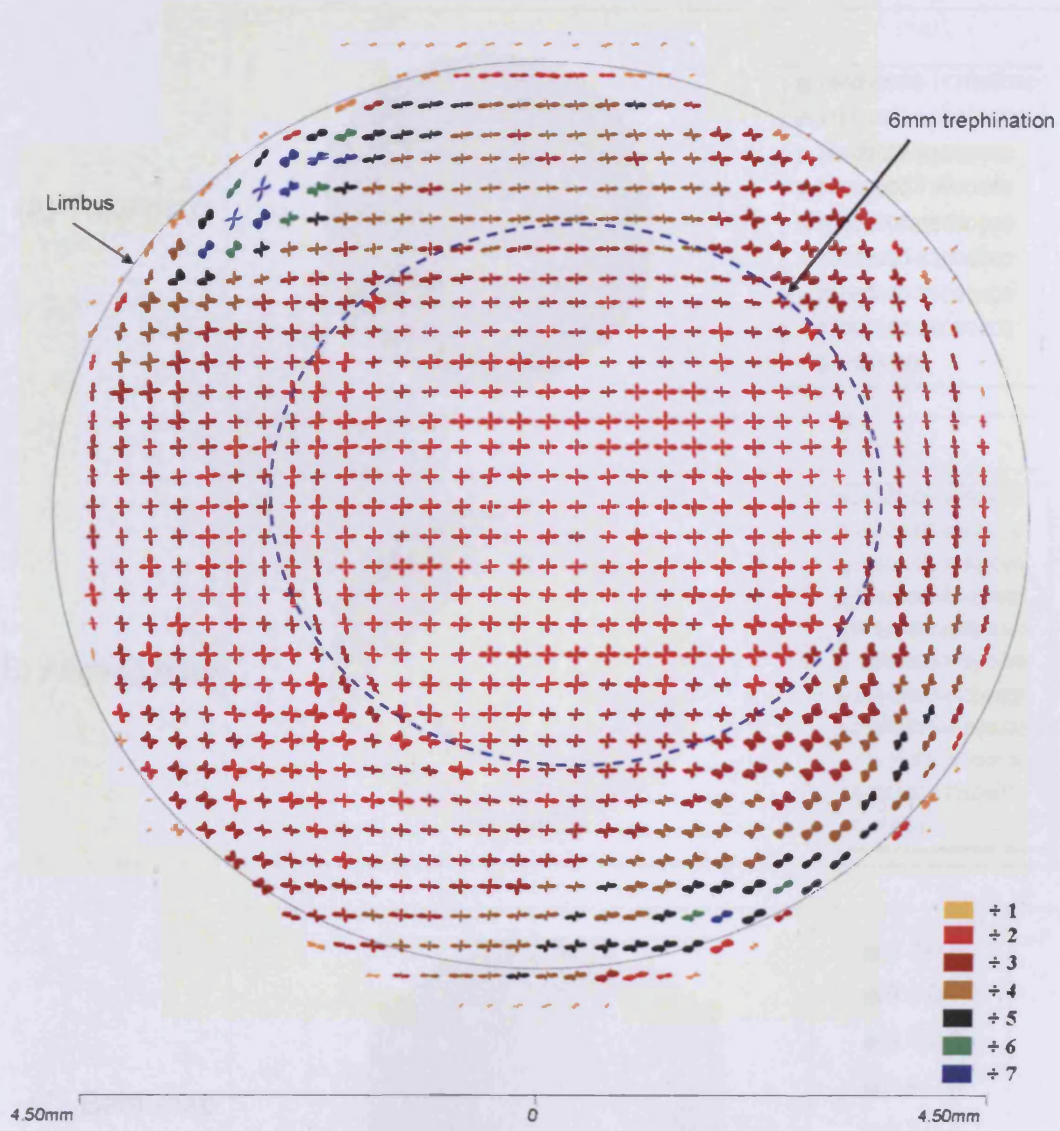

Figure 4.3: Polar plot XRD map of 9mm human cornea after 6mm full-thickness trephination. The cornea was sampled at 0.3mm intervals. Plots were scaled down by the factors shown in the key.

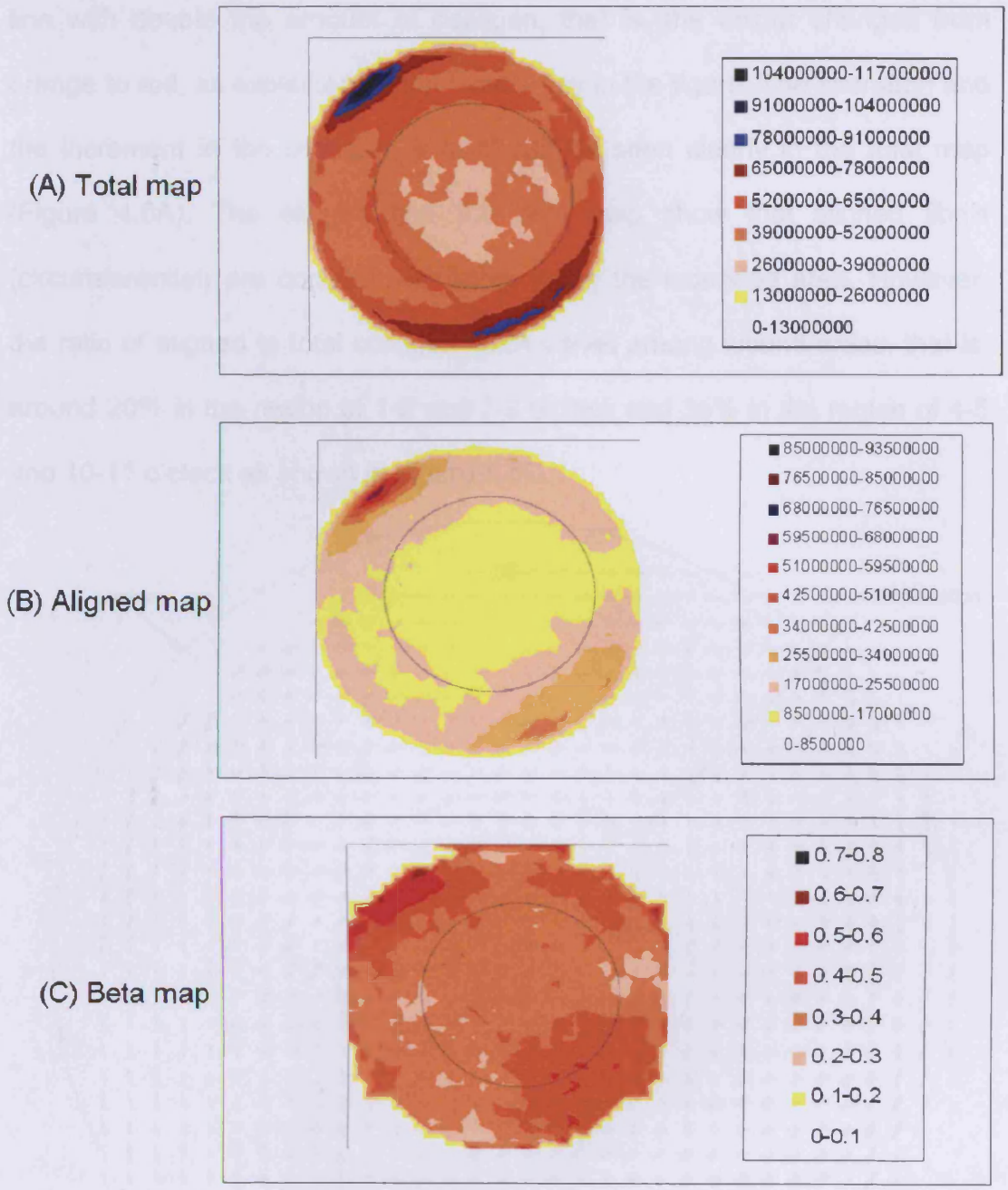

Figure 4.4: Distribution of collagen in 9mm cornea after 6mm full-thickness trephination. Scatter is expressed in arbitrary units. Dotted circle indicates trephination.

Figure 4.5 shows the XRD map of the 4mm full-thickness trephination. The alteration in the collagen fibril orientation along the trephined area is clear. As in the 6mm trephination, the fibrils take the annulus shape along the trephine

line with double the amount of collagen, that is, the colour changes from orange to red, as explained by the factors key in the figure. The alteration and the increment in the collagen amount can be seen clearly in the total map (Figure 4.6A). The aligned and the beta map show that aligned fibrils (circumferential) are concentrated more along the wounded area. However, the ratio of aligned to total collagen fibrils varies among wound areas, that is, around 20% in the region of 1-2 and 7-8 o'clock and 35% in the region of 4-5 and 10-11 o'clock as shown in Figure 4.6C.

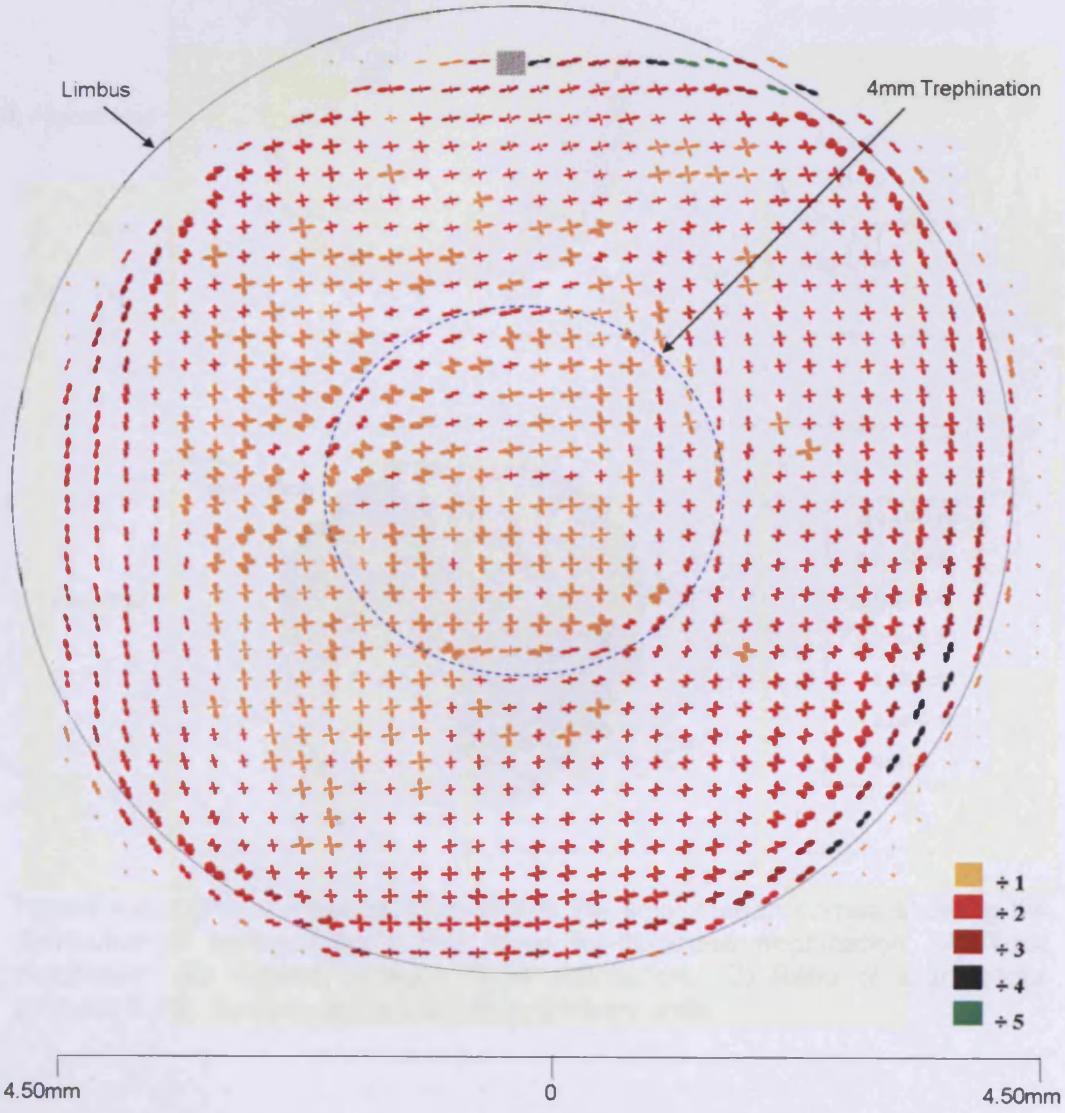

Figure 4.5: XRD map of preferred collagen fibril orientation of 9mm human cornea after 4mm full-thickness trephination. Polar plots are shown at 0.3mm intervals. Scaled-down factors are shown in the key.

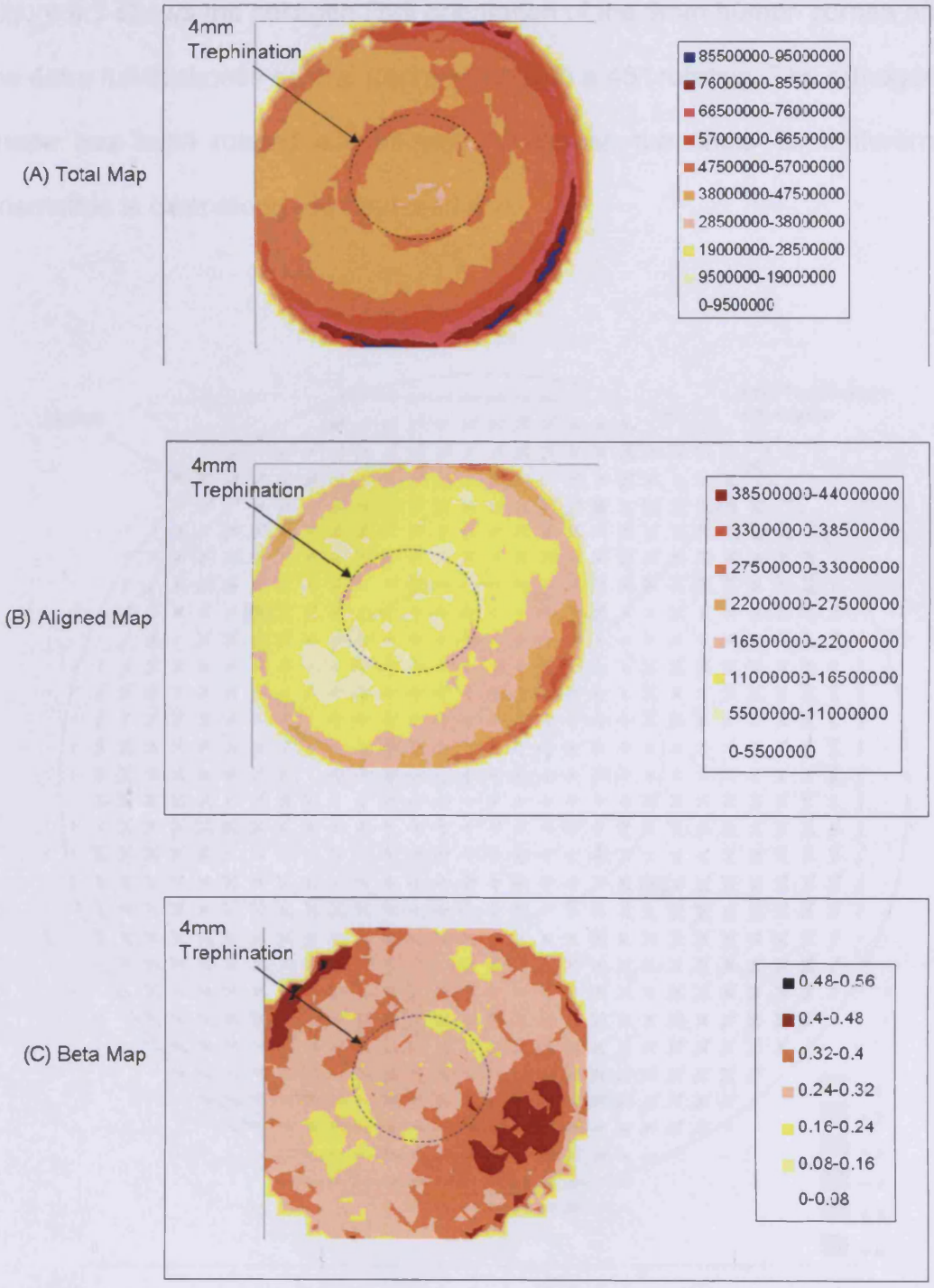

Figure 4.6: Contour maps of XRD across the 9mm human cornea showing the distribution of collagen fibrils after 4mm full-thickness trephination. (A) Total distribution. (B) Aligned collagen fibrils distribution. (C) Ratio of aligned/total collagen fibrils. Scatters are explained in arbitrary units.

Figure 4.7 shows the collagen fibril orientation of the 9mm human cornea after the 4mm full-thickness central trephination with a 45° rotation. The orthogonal shape has been rotated 45° as well. Moreover, the fibrils' circumferential orientation is clear along the trephined line.

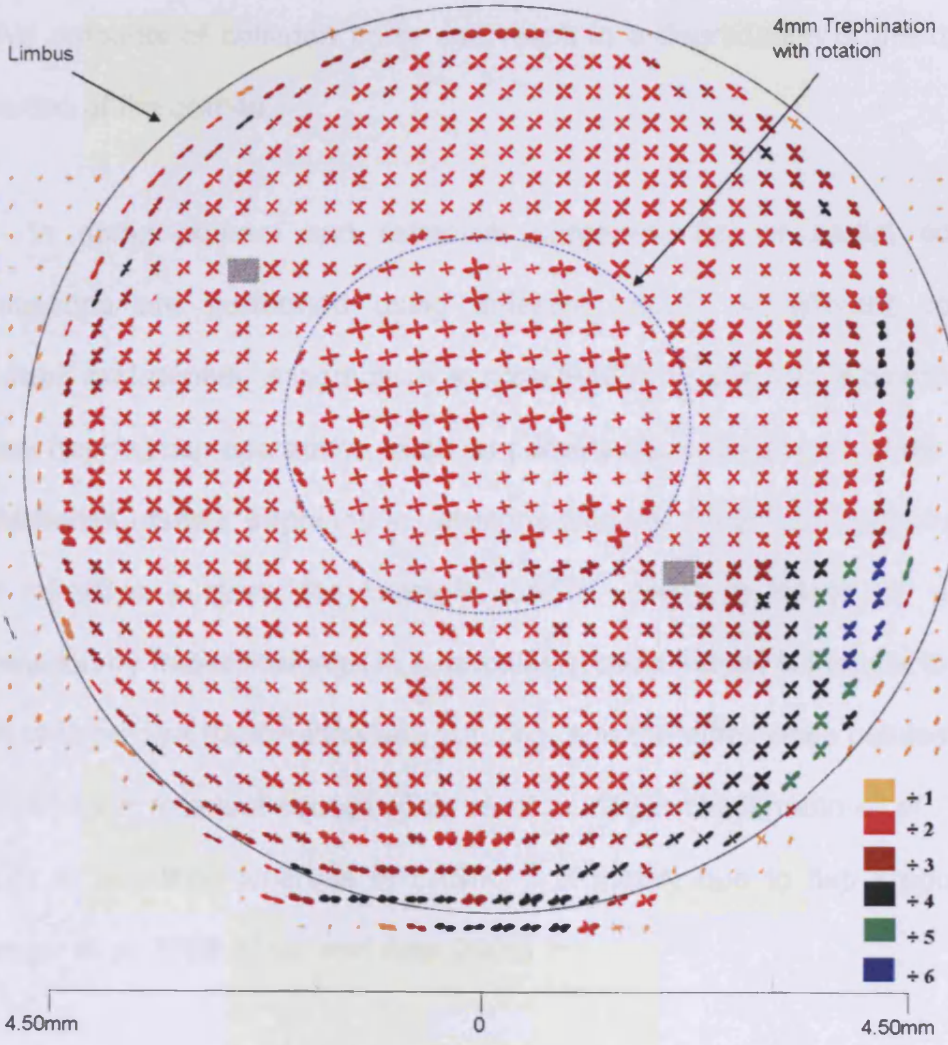

Figure 4.7: Polar plot XRD map showing the orientation of collagen fibrils of 9mm human cornea after 4mm full-thickness trephination with ≈ 45° rotation. Cornea was sampled at 0.3mm intervals and larger plots were scaled down by the factors shown in the key. The corneal tissue beyond the central 4mm appeared oblique because tissue alignment (cross shape) for XRD was done to the central area. The two small grey rectangle shapes in the map correspond to missing data at that area.

4.4 Discussion

Transparency is believed to be dependant upon the spatial organisation of the collagen fibrils in the cornea, which, with other properties such as fibril diameter uniformity produce destructive interference of scattered incident light (Maurice 1957; Benedek 1971; Scott 1985; Rawe *et al.* 1994; Meek and Fullwood 2001); thus, any alteration in the structure or in the relative amounts of collagen fibrils can result in a degradation of the optical properties of the cornea.

In some corneal and refractive surgeries, full or partial corneal trephinations are performed using different means at different corneal diameters and depths. Astigmatism is considered a significant problem after corneal trephination operations, such as penetrating keratoplasty, which uses full thickness corneal trephination, whereas it is not a common complication after refractive surgery, for example, LASIK, which is based on partial trephination by microkeratome. In keratoplasty, astigmatism is thought to be a result of imprecise trephination and suturing, and the differences between the donor and the recipient cornea (Bourne *et al.* 1982; Heidemann *et al.* 1985; Radner *et al.* 1999) whereas in LASIK, it is mainly due to flap irregularity (Iskander *et al.* 2000; Melki and Azar 2001).

As mentioned previously, both XRD and TEM have been used widely to determine the collagen arrangement in normal and wounded corneas. However, in the literature, no XRD study has been conducted to find out the immediate effect of corneal trephination on the collagen arrangement at different diameters, which is considered a key effect before starting the wound

healing process. Therefore, the orientation and distribution of collagen fibrils in full-thickness trephined human corneas were described by analysing synchrotron wide-angle XRD patterns both qualitatively and quantitatively.

In this study, human corneas were trephined in the same way as donor corneal grafts, that is, from the endothelial side with the posterior punch technique (Tanne 1993). The trephined button was immediately returned to its original position, which is believed to produce a minimum of side effects on the corneal structure because both donor and recipient tissue are from the same cornea and, also, the cut design is similar to that that has been reported to cause less morphological distortion (Radner *et al.* 1999). Therefore, what is presented here is the minimum effect of trephination on collagen fibrils that can worsen in some trephination surgeries. After trephination, and after repositioning the trephined button to its original corneal place, the whole corneal button was exposed immediately to wide-angle XRD, which means that there was no time for tissue to heal or to be reorganised.

No alteration in the collagen fibril orientation or distribution was found in the 9mm trephined cornea when compared with a normal cornea. On the other hand, X-ray patterns of 4mm trephined cornea indicate that the amount (density) of collagen fibrils increases and they are aligned preferentially around wound edges (Figures 4.5 and 4.6). This high density of collagen was less noticeable in the 6mm trephined cornea (Figure 4.3 and 4.4). Connon and Meek (2003) found the same result during the healing of 2mm full-thickness trephined wounds in rabbits. Rawe *et al.* (1994) found that, in vivo, the arrangement of collagen fibrils is disordered in the early stages of scar

tissue healing. In our study, we cannot assume that this increment in collagen mass is due to the synthesis of collagen as reported previously because we ran XRD immediately after trephination and there was no time for wound healing. Instead, we can say that the increase in collagen mass near the edge of the trephination is due to the effect of the trephine blade on the collagen arrangement, that is, the stress force of the blade causes collagen fibrils to accumulate upon each other or is the cause of slippage at both sides. However, more high resolution, wide-angle XRD studies are needed to give more detail of the affected area as the current resolution (minimum step size) for XRD at SRS, Daresbury is 0.25mm intervals.

There are two possible reasons for the varied results between 9mm and 4mm trephination. Firstly, due to the known increment in corneal thickness from the centre towards the periphery, the amount of collagen lamellae increases. This could make the increment in the collagen mass due to trephination unnoticeable. Secondly, the collagen fibril orientation at the periphery takes the shape of circular or tangential patterns that are similar to the shape or orientation of the collagen fibrils seen in the trephined (wounded) area. Consequently, the alteration in the collagen fibrils will be unremarkable. The invisible change in 9mm trephination allows us to conclude that the high degree of astigmatism seen in PKP after 7- 8 mm trephination would be reduced if surgeons were to use 9mm trephination with perfect suturing. However, it has been found that a large corneal graft is not recommended as it may induce graft rejection due to the closeness to the limbal area (Williams *et al.* 1992; Price *et al.* 1996). The small diameter trephination, that is, less

than 7mm, will lead to a noticeable distortion in vision because it happens close to the central cornea that overlies the pupil, which is responsible for refracting and focusing the light on the fovea. In addition, the corneal central and paracentral areas possess smaller amounts of collagen fibrils that are oriented orthogonally, and any small alteration caused by the trephine will be noticeable and characterized as astigmatism. Further experiments, however, are needed to support this assumption.

When the 4mm trephined button was rotated 45° and repositioned in relation to the whole cornea, the orthogonal shape rotated as well and became distinctive from the rest of the cornea (Figure 4.7). This may indicate that during a corneal graft, the trephined button should be placed in the recipient cornea with the corrected position (orientation) in order to avoid the differences in the collagen fibril orientation that may lead to optical or biomechanical problems. This finding is in agreement with the recently reported study by Boote *et al.* (2006), which found that the collagen fibril orientation and distribution in left and right corneas are structurally distinct and should be taken into account during a corneal graft.

In conclusion, despite advances in ophthalmic surgical techniques, postoperative biomechanical complications, such as astigmatism, remain a major problem. It has been found that collagen fibril disorder after full-thickness trephination is more obvious when a small diameter trephine is used, as the collagen fibrils tend to take a circular shape along the trephined edges instead of an orthogonal shape, which may explain the corneal

biomechanical instability with the resultant astigmatism. Furthermore, the difference in the collagen fibril orientation that may occur between the donor and the recipient corneas may also cause this biomechanical instability. More corneal trephination experiments with high resolution wide-angle XRD are needed to extend our knowledge in this field.

Chapter 5. X-Ray diffraction of the human cornea at different depths

5.1 Introduction

Corneal transparency depends on the unique architecture of the stroma, which accounts for 90% of the corneal thickness. In humans, the central stroma is made of ~200 stacked lamellae that lie parallel to the corneal surface (Maurice 1957). These lamellae do not generally have the same orientation as each other; the change in orientation between lamellae may be any angle between 0 and 180° (Maurice 1969; Newton and Meek 1998b). Within a single lamella, collagen fibrils of a uniform diameter are laid down parallel to one another and to the corneal surface. They are embedded in a hydrated matrix rich in proteoglycans, salts, and keratocytes (Quantock *et al.* 2001; Meek *et al.* 2003). This stromal integrated arrangement produces a destructive interference of light scattered in all directions other than the forward direction, leading to tissue transparency and, also, gives the cornea its shape and strength (Farrell and McCally 2000; Aghamohammadzadeh *et al.* 2004).

The literature includes many human studies that have been done to find out the collagen fibril orientation within the cornea (Kokott 1938; Meek *et al.* 1987; Komai and Ushiki 1991; Daxer and Fratzl 1997; Aghamohammadzadeh *et al.* 2004). The main outcomes of these studies indicate that, in the human cornea, there is a preferred fibril orientation in the

inferior-superior and nasal-temporal directions, mainly in the posterior stroma (Meek *et al.* 1987; see also Chapter 3 herein). This preferred orientation occurs at the centre of the cornea and is maintained to within 2mm of the limbus, where a gradual change to a tangential disposition occurs. However, the collagen fibril orientation and distribution at different depths of the human cornea are still not well investigated. Therefore, in the present study, the new femtosecond laser technology was used to cut the human corneas into different depth layers and wide-angle XRD was used to study the collagen fibril orientation and distribution at each layer and is thus the first step towards a full three-dimensional reconstruction of corneal lamellae preferred orientations. The results of this study should help us interpret the biomechanical reasons for some refractive problems, such as post-LASIK astigmatism or ectasia.

5.2 Materials and Methods

Seven human corneas with rim of sclera were used in this study. Three of them were obtained from Bristol eye bank; they were not suitable for corneal transplant and were immersed into culture medium bottles and kept in a 37° C incubator. The remaining four corneas were obtained from the National Disease Research Interchange (NDRI, Philadelphia, USA). They were dissected from two pairs of donor globes and were kept frozen in dry ice until arrival at Cardiff University. Due to the processes of freezing, thawing and storing in the culture medium, some of the corneas had become swollen. By using Pachette2™ Ultrasonic Pachymeter (DGH Technology, USA), the measured corneal thickness of the seven corneas ranged from 570 μm to

1040μm. All the corneas were then kept in 4% paraformaldehyde until the time of experiment.

On the day of the experiment, each cornea was placed in a sterile Barron artificial anterior chamber (Katena Products Inc.,NJ, USA) as shown in Figure 5.1, which was initially designed to safely facilitate the positioning, securing and inflating of the donor cornea during corneal transplant and lamellar surgery procedures, and, in this study, to retain corneal shape and curvature during the experiment by means of pumping a balanced salt solution (BSS) underneath the cornea via the two tube ports with lockers, as shown in Figure 5.2.

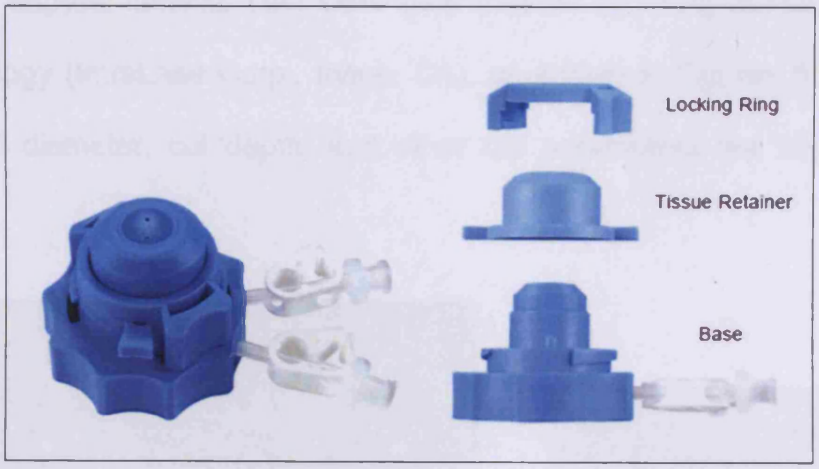

Figure 5.1: The Barron Artificial Anterior Chamber has three pieces: base with tissue pedestal, tissue retainer and locking ring. The base has two ports with silicon tubing, which is used to inject liquids or air to pressurize the cornea and maintain corneal curvature during trephination (Pictures reproduced and modified from www.katena.com).

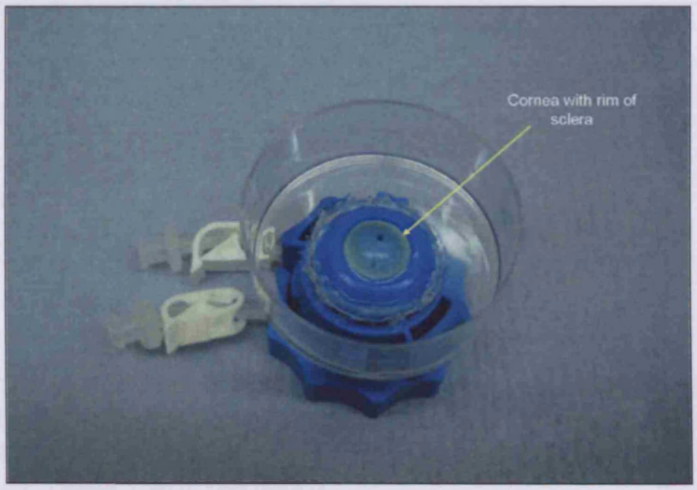

Figure 5.2: The Barron Artificial Anterior Chamber after modification. This figure shows the human cornea (yellow arrow) placed over the tissue retainer while the scleral annulus is located over the ridge; and clamped by the locking ring. A small diameter Petri dish was trephined centrally and attached firmly to the Barron chamber by silicon glue in order to work as a liquid reservoir to keep the cornea hydrated.

Three corneal lamellar cuts were then created by using femtosecond laser technology (IntraLase Corp., Irvine, CA), as shown in Figures 5.3, 5.4, and 5.5. Cut diameter, cut depth, and other cut parameters are shown in Table 5.1.

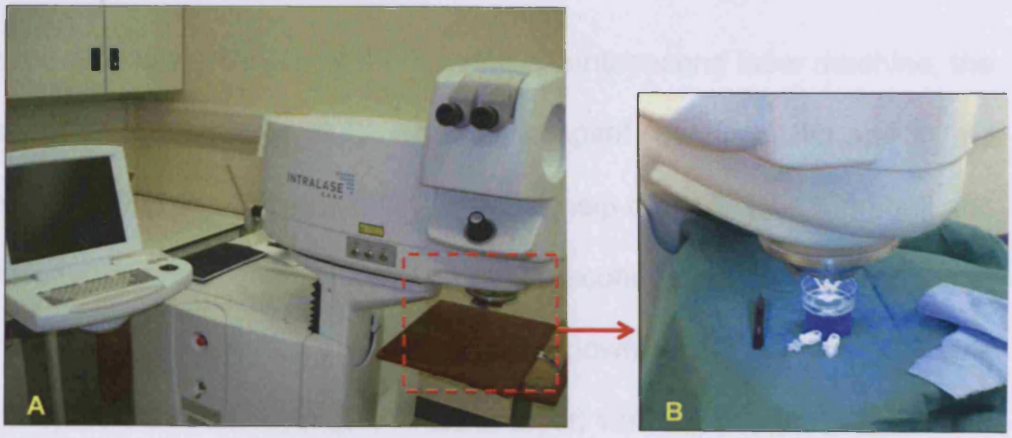

Figure 5.3: (A) Intralase femtosecond laser system. (B) The position of the Barron chamber with the human cornea during corneal flap creation. Note the patient interface (cone shape) that is attached to the laser machine and used to flatten the cornea and through which the laser beam passes.

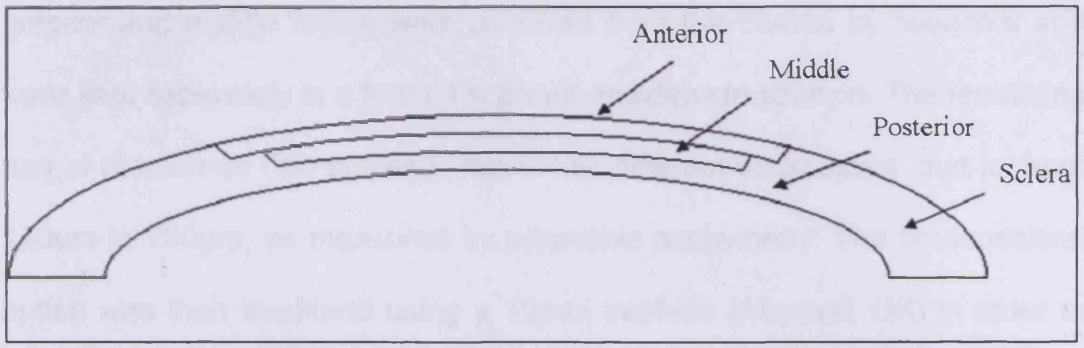

Figure 5.4: Corneal schematic diagram showing the way the cornea was cut into three layers. The thickness of the anterior, middle and posterior layers was varied for different corneas.

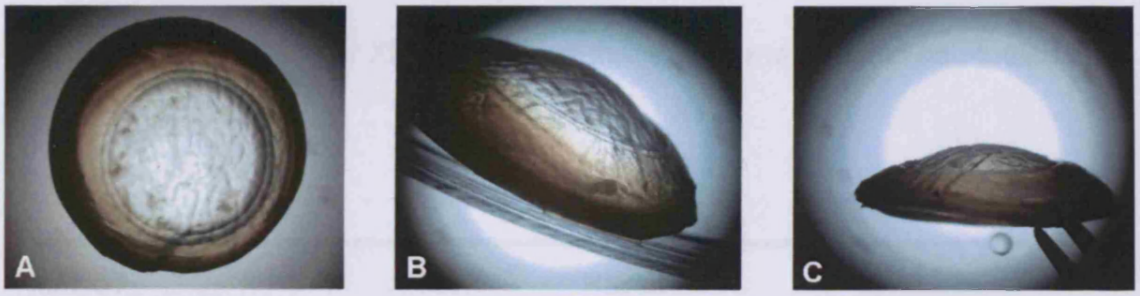

Figure 5.5: Microscopic pictures from different angles for the corneoscleral button after femtosecond laser cut. (A) shows the cut round edges of the anterior and middle layers. (B) and (C) show the preserved corneal curvature after using Barron artificial corneal holder.

Due to the limited availability of the IntraLase femtosecond laser machine, the experiment was conducted at St. Thomas hospital (London, UK) and at the Centre for Sight (East Grinstead, UK) with the help of Prof. John Marshall and Mr. Sheraz Daya research groups. The femtosecond laser cut was in a raster pattern without a hinge for all corneas, as shown in the parameters table (Table 5.1). The first cut layer (the anterior layer) was 8.5 mm in diameter with a thickness of 120, 140, 160, 200, 250 or 300 μm based on each cornea's experimental protocol. The second middle layer was 7.5mm in diameter with a thickness ranging from 120μm to 300μm, similar to the anterior layer. The

anterior and middle layers were removed from the cornea by tweezers and were kept separately in a fresh 4% paraformaldehyde solution. The remaining part of the cornea (the posterior layer) had different thicknesses, that is, from 150μm to 750μm, as measured by ultrasonic pachymetry. The corneoscleral button was then trephined using a 12mm trephine (Altomed, UK) in order to remove unwanted extra scleral tissue, and was put in 4% paraformaldehyde until the time of XRD. All the corneas were taken to the SRS (Daresbury, UK) for XRD to map the collagen fibril orientations in each layer. The most superior part of all corneal layers were marked with a razor in order to align the specimen properly for XRD so that all three layer maps could be studied in relation to each other.

Method	Raster
Diameter	7.5mm to 8.5mm
Depth	120μm to 300μm
Hinge	No
Hinge Angle	No
Cut Energy	0.80 μJ
Side Cut Angle	70°
Pocket Start Depth	220 μm
Spot/Line Separation	4x4 μm

Table 5.1: Parameters of IntraLase femtosecond laser machine. Different depths and diameters were used to cut the cornea.

5.3 Results

Table 5.2 shows the thickness of each corneal layer that was cut by the femtosecond laser. From the seven corneas, two corneas have been excluded due to tissue tearing during the experiment.

Cornea / Layer (μm)	C1	C2	C3	OD	OS
Anterior	120 (12%)	140 (14%)	160 (28%)	250 (36%)	200 (33%)
Middle	120 (12%)	140 (14%)	160 (28%)	250 (36%)	200 (33%)
Posterior (remaining)	800 (76%)	710 (72%)	250 (44%)	200 (28%)	200 (33%)
Total Thickness	1040	990	570	700	600

Table 5.2 : The thickness (in micrometres) of the anterior and middle layer that were cut by femtosecond laser. Numbers in brackets represent the percentage of the total corneal thickness. The posterior (remaining) layer thickness was measured by ultrasonic pachymeter. Note that the three layers in C3, OD and OS corneas have comparable thicknesses in each layer.

All polar plot maps show that the middle and posterior parts of the human cornea demonstrated a preferentially orthogonal arrangement of collagen fibrils, directed along the superior-inferior and nasal-temporal meridians whereas the anterior cornea (33% of total corneal thickness) showed irregular collagen fibril orientation.

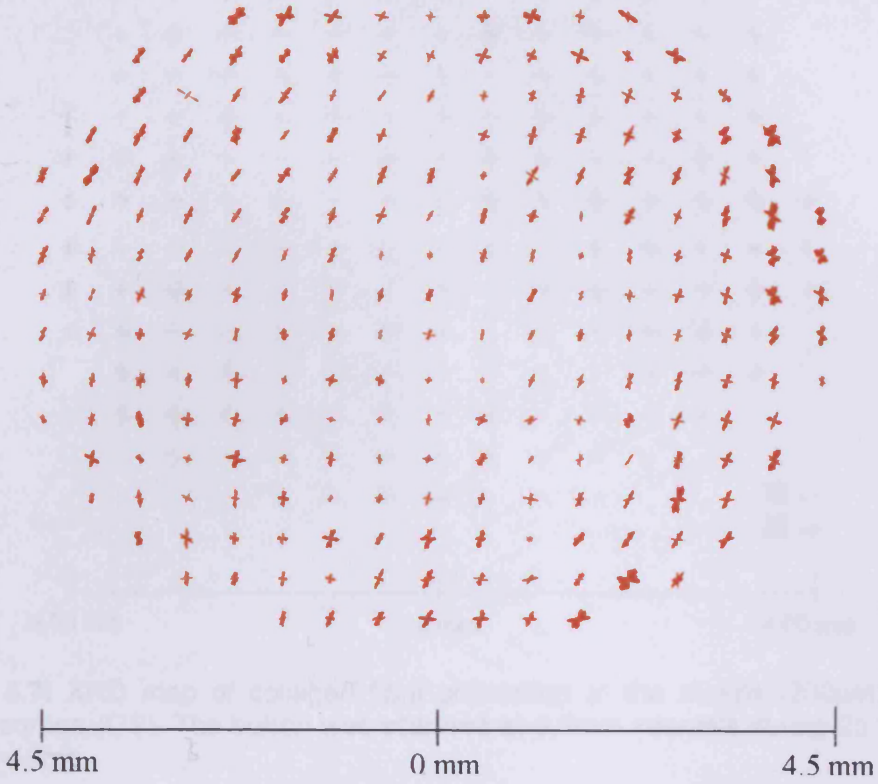

Figure 5.6: XRD map of collagen fibril orientation at the anterior 200μm normal human cornea (OS). The tissue diameter is ~9mm with 0.5mm XRD step size and 25 seconds exposure time.

Figure 5.6 shows the orientation of collagen fibrils in the anterior one third of the cornea. No consistent preferred orientation can be detected in this anterior region except, perhaps, towards the periphery.

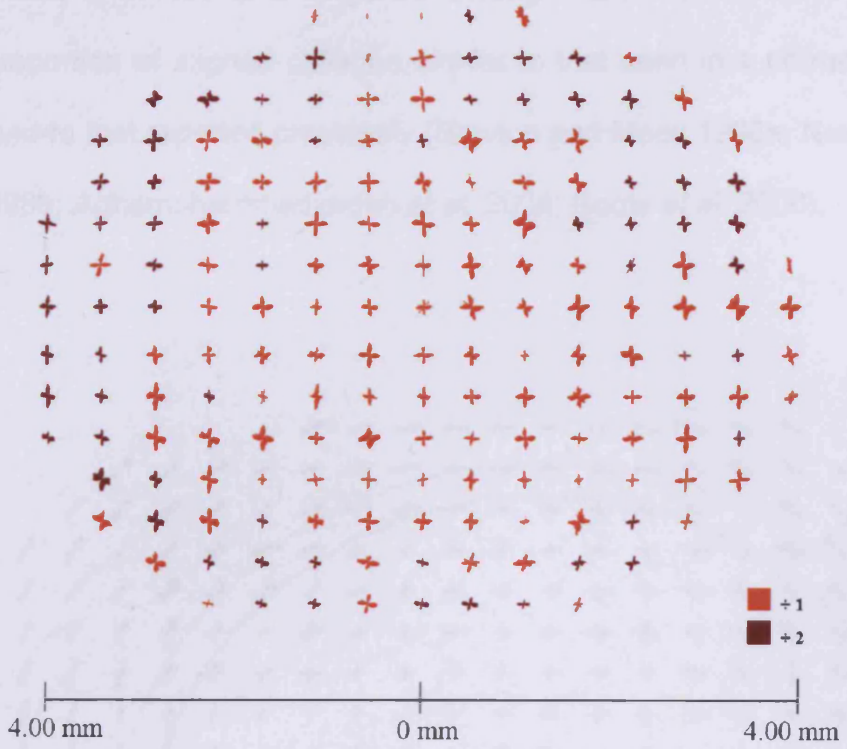

Figure 5.7: XRD map of collagen fibril orientation at the middle (200µm) normal human cornea (OS). The button was scanned at 0.5mm intervals during 25 seconds exposure time.

Figure 5.7 shows the collagen fibril orientation in the middle of the cornea, that is, the second 200 µm cut. Collagen fibrils appear well oriented orthogonally all over the 8mm corneal tissue with an increase in the number of lamellae towards the periphery, as indicated by the scaled-down factors (brown colour). Figure 5.8 shows the collagen fibril orientation in the remaining corneal tissue with part of sclera. The collagen fibrils appear well ordered all over the cornea including the remaining 200µm centrally. The collagen arrangement in the central 8-9 mm is similar to that found in the centre of a normal human cornea (see Figure 3.1 in Chapter 3) and is consistent with previous XRD work (Meek *et al.* 1987; Daxer and Fratzl 1997; Aghamohammadzadeh *et al.* 2004; Boote *et al.* 2005; Boote *et al.* 2006). The orthogonal orientation of the central

corneal fibrils is shifted to a tangential arrangement near the limbus with a higher proportion of aligned collagen similar to that seen in a normal human cornea and to that reported previously (Newton and Meek 1998a; Newton and Meek 1998b; Aghamohammadzadeh *et al.* 2004; Boote *et al.* 2006).

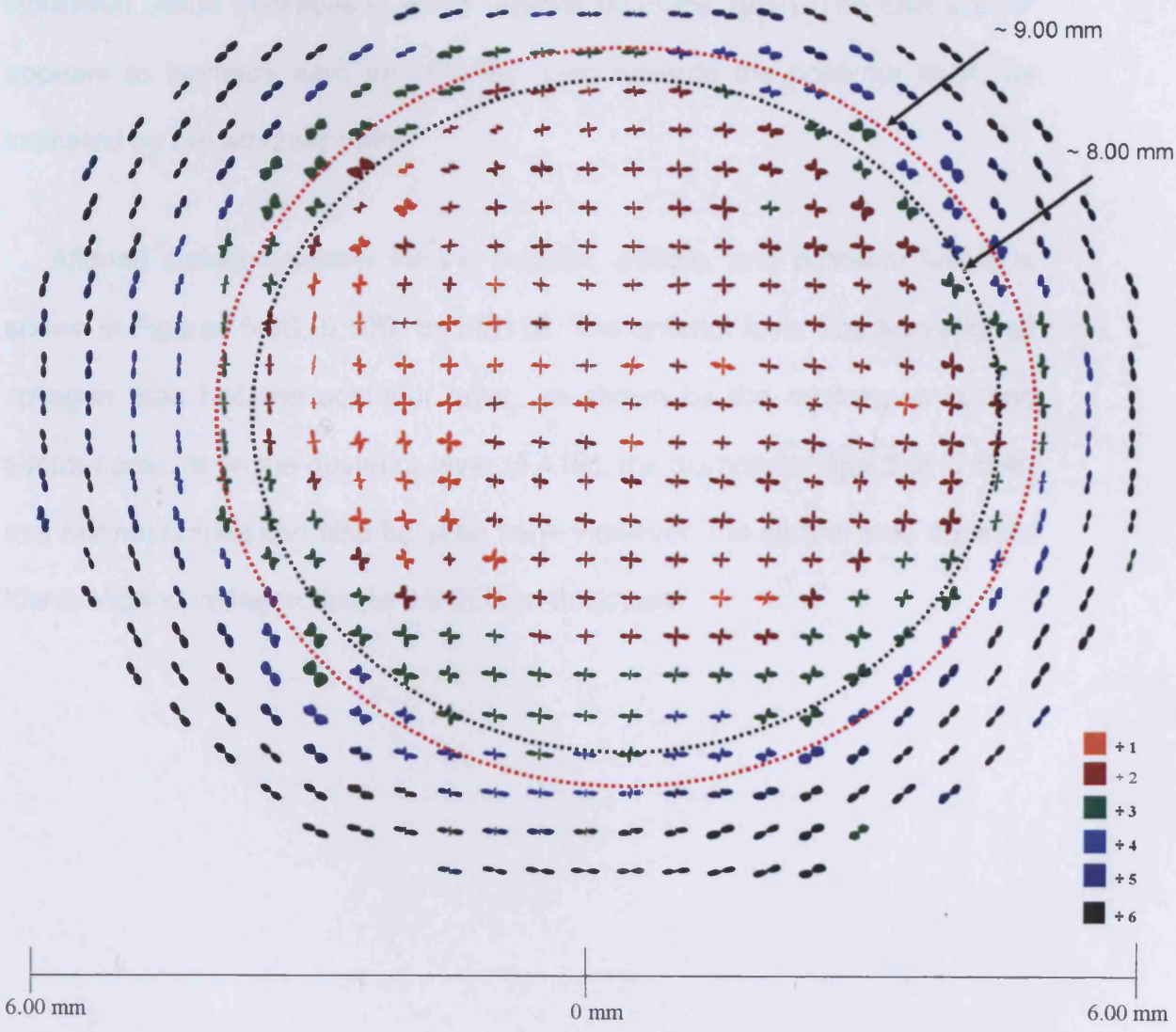

Figure 5.8: XRD map of collagen fibril orientation of the whole 12mm corneoscleral button (OS). 400µm out of 600µm of the central 8-9mm area has been removed (dotted circles). So, the remaining posterior central thickness was 200µm. XRD exposure time was 25 seconds with 0.5mm step size.

Figures 5.9, 5.10, and 5.11 show the distribution of collagen fibrils in the anterior, middle, and posterior (remaining) corneal layers. Figures 5.9A and 5.10A indicate that the total scatter from fibrillar collagen remains fairly constant in the central 3-4mm (red-brown contour) and increases towards the periphery (dark colour contours). In the posterior total map (Figure 5.11A), the increase in scattering is clear from the centre towards the periphery due to the increased tissue thickness in these regions (Maurice 1957). The total scatter appears to increase from the anterior layer towards the posterior layer, as indicated by the arbitrary units.

Aligned collagen scatter for the anterior, middle, and posterior layers is shown in Figures 5.9B, 5.10B, and 5.11B. The anterior layer has less aligned collagen than has the posterior layer, as shown by the arbitrary units and contour colours. In the posterior layer (5.11B), the diamond shape that is seen in a normal cornea can also be seen here. However, the central area appears low in aligned collagen due to the 200μm thickness.

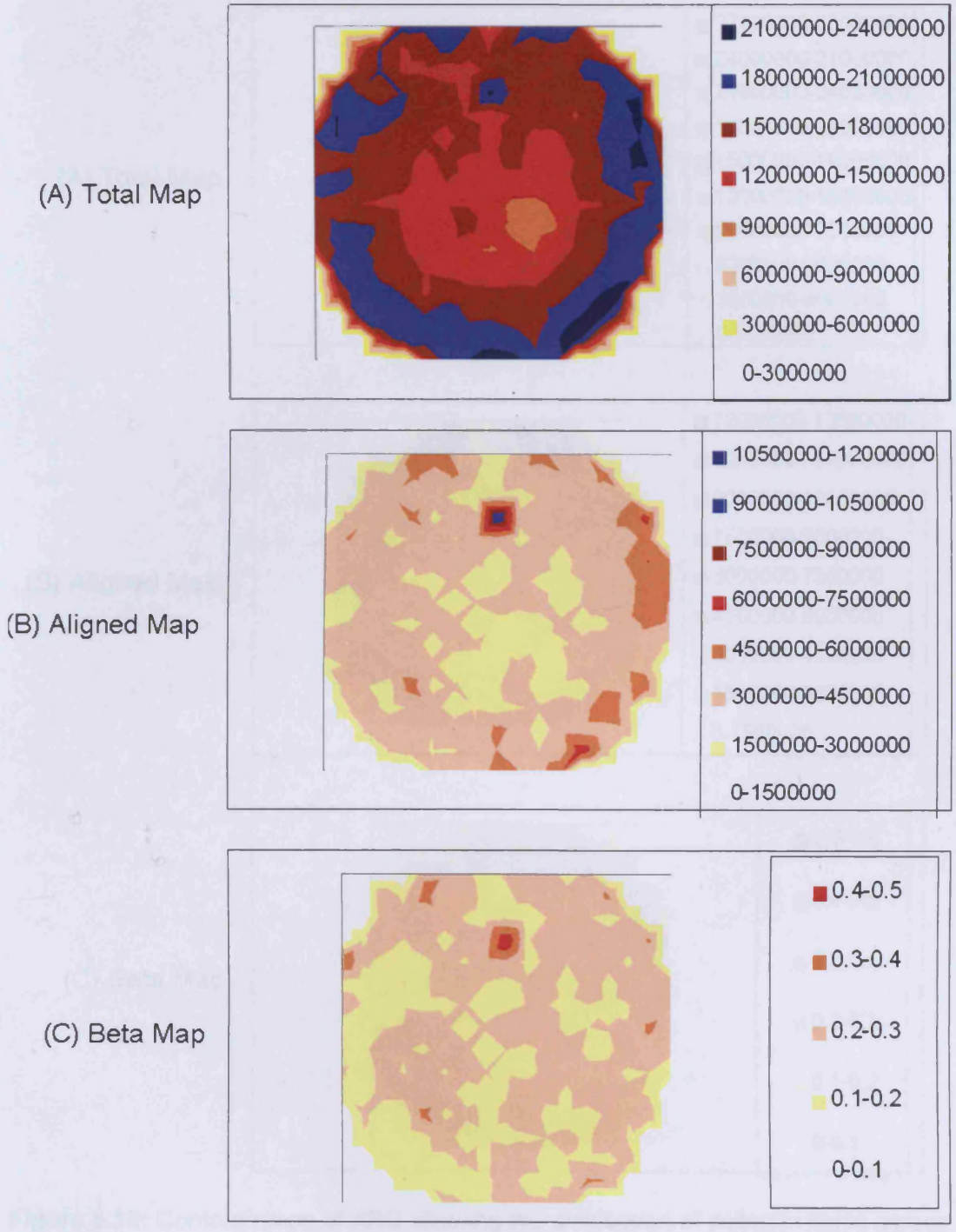

Figure 5.9: Contour maps of XRD showing the distribution of collagen fibrils across the 200μm anterior cornea. (A) Total fibrillar collagen scatter, (B) Scatter from only preferentially aligned collagen fibrils, (C) Ratio of aligned/total scatter. Scatter is in arbitrary units.

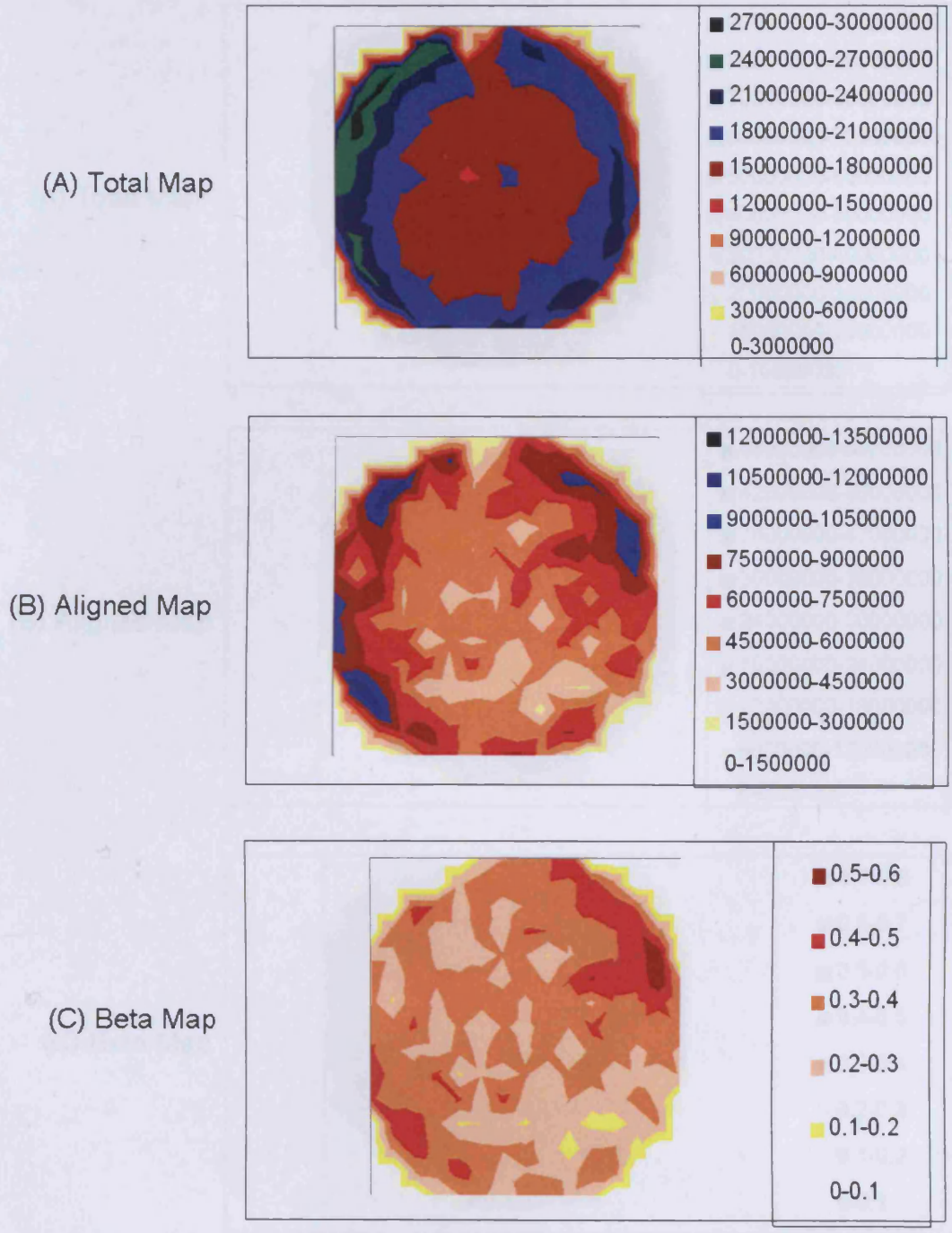

Figure 5.10: Contour maps of XRD showing the distribution of collagen fibrils across the 200μm of the middle of the cornea. (A) Total fibrillar collagen scatter, (B) Scatter from only preferentially aligned collagen fibrils, (C) Ratio of aligned/total scatter. Scatter in arbitrary units.

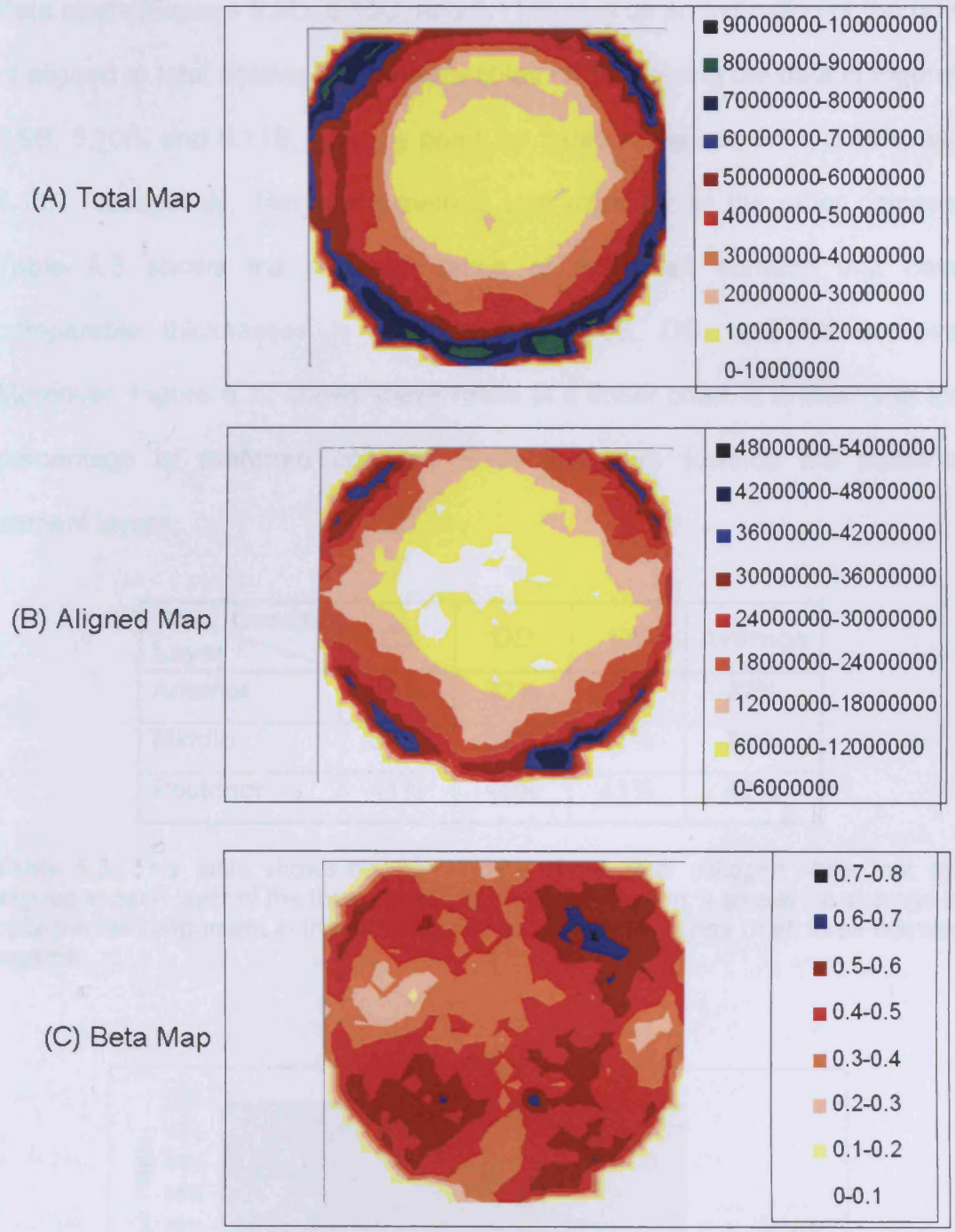

Figure 5.11: Contour maps of XRD showing the distribution of collagen fibrils across the remaining posterior (central) 200μm of cornea with scleral rim. (A) Total fibrillar collagen scatter, (B) Scatter from only preferentially aligned collagen fibrils, (C) Ratio of aligned/total scatter. Scatter in arbitrary units.

Beta maps (Figures 5.9C, 5.10C, and 5.11C) give us an indication of the ratio of aligned to total scatter. These were obtained by dividing the data in Figures 5.9B, 5.10B, and 5.11B, point by point, by those in Figures 5.9A, 5.10A, and 5.11A respectively. The same method was used for all the other corneas. Table 5.3 shows the resultant ratios of the three corneas that have comparable thicknesses in each layer i.e. C3, OD, and OS corneas. Moreover, Figure 5.12 shows these ratios in a linear chart. It is clear that the percentage of preferred collagen fibrils increases towards the posterior corneal layers.

Cornea / Layer	C3	OD	OS	**Average**
Anterior	24%	22%	21%	**22%**
Middle	30%	32%	31%	**31%**
Posterior	41%	45%	41%	**42%**

Table 5.3: This table shows the percentage of the total collagen fibrils that are aligned in each layer of the three human corneas. In addition, it shows the average of collagen fibril alignment in the anterior, middle and poster layers of all three corneas together.

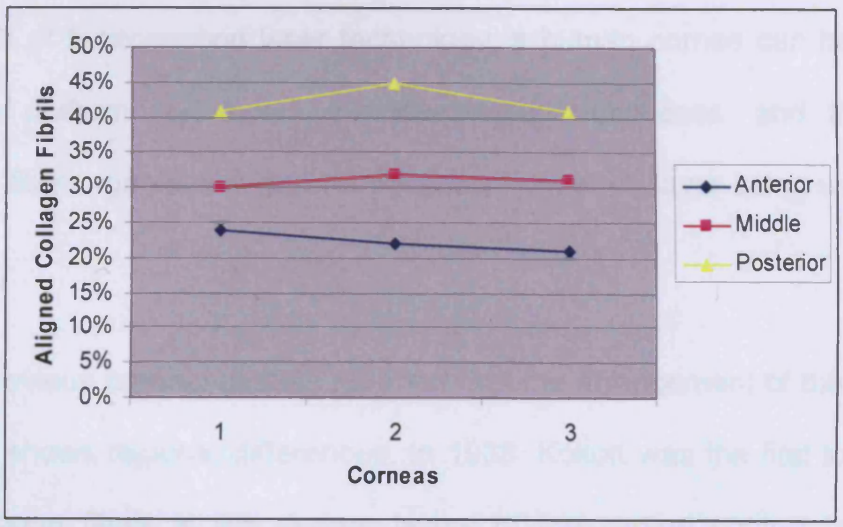

Figure 5.12: This line chart shows the percentage of the total collagen fibrils that are aligned in each layer of the three human corneas (1:C3, 2:OD, and 3:OS).

5.4 Discussion

By using a femtosecond laser and wide-angle XRD, for the first time, a whole map for the collagen fibril orientation and distribution at different human corneal depths has been shown. The results indicate that the collagen fibrils are well ordered in the posterior two thirds of the corneal thickness whereas the first third reveals a distorted collagen arrangement.

Most results of previous wide-angle XRD studies were acquired from the orientation of all the collagen fibrils in the path of the x-ray beam, that is, the resulting pattern is an average for the thickness of the whole cornea (Meek and Quantock 2001; Meek *et al.* 2005). On the other hand, electron microscopy has provided much information on the arrangement of the collagen fibrils at different corneal depths, but it has not been so successful in determining larger scale orientation (Komai and Ushiki 1991); furthermore, it has shown considerable variation among studies. This variation has been attributed to methodological factors, mainly tissue preparation (Freund *et al.* 1995; Daxer *et al.* 1998; Meek and Fullwood 2001). Recently, with the revolution of femtosecond laser technology, a human cornea can be cut into separate uniform layers with predetermined thicknesses, and the gross collagen fibril organisation can be obtained from each layer using wide-angle XRD.

Previous corneal studies reported that the arrangement of the collagen lamellae shows regional differences. In 1938, Kokott was the first to suggest that collagen fibrils in the deeper layers of the central cornea take on a

preferential orientation along the superior-inferior and nasal-temporal corneal meridians (Komai and Ushiki 1991). XRD studies later confirmed this, and indicated that the preferred orientation is more prevalent in the posterior half of the cornea (Meek *et al.* 1987). Further quantitative analysis by low-angle XRD has indicated that, in total, around two thirds of the fibrils of the stroma tend to lie within the 45° sectors of the superior-inferior and nasal-temporal directions (Daxer and Fratzl 1997). Recently, Boote *et al.* (2005) found that, on average, one third of the collagen fibrils tend to lie within a 45° sector, and these oriented fibrils have the same quantity along the superior-inferior and nasal-temporal meridians. Away from the centre of the cornea, Newton and Meek (1998 a and b) discovered that this arrangement no longer predominates at the periphery, and fibrils tend to take the shape of a circumferential annulus at the limbus. TEM and SEM studies showed that collagen lamellae in the anterior one third of the stroma are much narrower and more irregularly interwoven than are those in the deeper two thirds (Hogan *et al.* 1971; Davson 1984; Klyse and Beuerman 1989; Komai and Ushiki 1991).

The results herein are in agreement with the previous studies and show that the collagen fibril orientation in the first third of corneal thickness, that is, 200μm out of 600 μm is irregular whereas the remaining deeper layers show an orthogonal orientation. Due to the limitation of a femtosecond laser to a maximum of 9mm diameter cut, it was difficult to show the collagen fibril orientation around the limbus regions. Table 5.2 shows that cuts of different thickness have been used with each cornea in order to find out the starting

point for the preferred orthogonal fibril orientation, which in turn has been found to be after the first third of corneal total thickness. The irregular fibril orientation was more pronounced in the central 4mm area (Figure 5.6). Beyond that, collagen fibrils tend to take the orthogonal shape towards the periphery. This change is believed to be due to the increment in the number of lamellae, although the thickness was constant. This conclusion is supported by the change in the colour of plots (orange to brown) seen in figure 5.7 which means increasing in the number of fibrils within the same layer (200μm).

In addition to polar plots, contour maps (Figures 5.9, 5.10, and 5.11) support the finding that the anterior one third of corneal thickness has less aligned collagen than have the other two thirds. The diamond shape that is seen in a normal cornea (Aghamohammadzadeh *et al.* 2004; Boote *et al.* 2006) can also be seen in the posterior 12mm corneoscleral layer, with fewer aligned fibrils centrally due to the 200 μm thickness. The percentage of aligned fibrils in each layer, which is derived from beta map of each layer, shows an increase in fibril alignment from the anterior towards the posterior layer (Table 5.3 and Figure 5.12). Again, this gives more ultrastructural details to the previous studies' findings that the posterior cornea has a greater number of well-ordered lamellae than has the anterior. The results herein cover a large area of the cornea, that is, 8-9mm diameter, whereas the previous studies' results are limited to small corneal areas.

Current popular refractive surgeries involve the ablation of corneal lamellae. To date, these techniques have been improved and developed using a fairly experimental approach and complex assumptions. Therefore,

the outcomes of refractive surgery may differ from the expected ones, largely because of the lack of information available on the organisation of collagen fibrils in the cornea (Fullwood 2004). Currently, finite element models are being developed to simulate the biomechanical response of the cornea and predict the result of refractive surgery in terms of shape and astigmatism. It is believed that the quantitative information presented herein is essential for an understanding of the biomechanical properties of the cornea and may add crucial details about the collagen fibril organisation to the ongoing work of the computational finite element models (Pinsky *et al.* 2005; Lanchares *et al.* 2008) and hence, help in the geometric interpretation of the corneal and surgical data. For example, the biomechanical changes that caused by flap cutting and laser ablation in LASIK surgery can be predicted preoperatively.

Chapter 6. Human *in vitro* LASIK by femtosecond laser technology

6.1 Introduction

Since its introduction by Pallikaris in 1989, LASIK has become the most popular method of performing refractive surgery in the world (Rosen 2000). The popularity and, thus, the importance of this procedure have elicited considerable interest in the corneal histological and ultrastructural changes after LASIK, that is, changes that are associated with the creation of an anterior corneal flap. Studies performed on LASIK have shown that LASIK is characterised by a weak healing response along the flap surface. The weakness is more obvious along the central and paracentral flap interface with the stromal bed where scar formation is almost nonexistent (Perez-Santonja *et al.* 1998; Kramer *et al.* 2005; Schmack *et al.* 2005; Dawson *et al.* 2005a). As a result, the tensile strength of the flapped cornea continues to be weaker than that of the normal cornea and could result in the separation of the flap from the remaining cornea months or even years after surgery (Schmack *et al.* 2005; Maguen *et al.* 2007; Ramirez *et al.* 2007).

Wound healing following LASIK has been extensively studied in animal models (Perez-Santonja *et al.* 1998; Kato *et al.* 1999; Miyamoto *et al.* 2003; Mohan *et al.* 2003). On the other hand, as most LASIK patients are relatively young, only a few human histopathologic studies have been done. Most of these studies are primarily case reports from corneal button specimens obtained after PKP for post-LASIK complications (Geggel and Talley 1999;

Salchow *et al.* 1999; Wright *et al.* 2000; Maguen *et al.* 2007) or from eyes of blind people on whom LASIK was performed just prior to enucleation (Latvala *et al.* 1996). The first pathologic evaluation of healthy human corneas after successful LASIK was reported by Anderson *et al.* in 2002, and was on four corneas from two patients. The study demonstrated the presence of epithelial ingrowth into the wound, transient activation of keratocytes in and adjacent to the wound, and disorganised collagen fibrils in the wound area. Recently, a few studies have been published on post-mortem human corneas that had undergone LASIK (Mootha *et al.* 2004; Dawson *et al.* 2005a; Dawson *et al.* 2005b; Priglinger *et al.* 2006). The histological and immunohistochemical findings presented by most of these studies regarding corneas after LASIK were in agreement with Anderson's findings.

To understand the biomechanical instability of the cornea after LASIK, it is essential to investigate the ultrastructural changes in stromal collagen fibrils because collagen is considered the main architecture component of the corneal stroma and any alteration to its structure will lead to biomechanical and refractive problems that will affect corneal transparency (Maurice 1957). Therefore, an *in vitro* LASIK using femtosecond laser technology has been conducted on donor human corneas to simulate the in vivo situation of LASIK and, hence, study the collagen fibril orientation and other ultrastructural changes by means of XRD, SEM, and TEM. The results of this study may help to explain differences in the biomechanical behaviour caused by ablation depth and the duration of healing.

6.2 Materials and Methods

Fourteen time-expired human donor corneas with scleral rim were obtained from Bristol eye bank. The mean age of the corneas was 82 years ± 4.8 (SD) (range 75 to 87 years old). Each cornea was kept in a container of organ culture medium in a standard incubator at 37°C for a maximum of 6 weeks before the experiment. As a result of long-term storage, most of the corneas were swollen. Therefore, the corneas were placed in a flask containing minimum essential medium (MEM) (Sigma, UK) and 5% dextran (Sigma, UK) for a period of up to 12 hours to obtain the required corneal thickness, that is, within the range of 550μm to 650 μm measured by using Pachette2™ Ultrasonic Pachymeter (DGH Technology, USA).

With the help of Prof. John Marshall and Mr. David O'brant, *In vitro* LASIK was carried out at St. Thomas hospital in London on twelve corneas. The remaining two corneas were used as controls. The twelve corneas were divided equally into three groups of corneas i.e. as if -3.00 D, -6.00 D, and -9.00 D of refractive errors (4 corneas in each group). As described in Chapter 5, each corneoscleral button was secured in sterile Barron Artificial Anterior Chamber (Katena Products Inc., NJ, USA). A LASIK corneal flap was then created by using femtosecond laser technology (IntraLase Corp., Irvine, CA). Flap diameter, flap depth, and other flap parameters were constant for all treated corneas as shown in Table 6.1.

Method	Raster
Diameter	8.5mm
Depth	160 µm
Hinge	Superior
Hinge Angle	50°
Cut Energy	0.80 µJ
Side Cut Angle	70°
Pocket Start Depth	220 µm
Spot/Line Separation	4x4 µm

Table 6.1: Parameters of LASIK flap creation by IntraLase femtosecond laser machine.

After creating a LASIK flap for all the corneas, a spatula (or toothed forceps) was used to peel back the flap, then *In vitro* LASIK was carried out using Schwind ESIRIS excimer laser system (Schwind, Kleinostheim, Germany) with a 6mm ablation zone and 35 µm to 110µm ablation depth depending on the refractive errors. After LASIK, all Barron chambers with the attached corneoscleral buttons were kept in a sterile incubator at 37° C for two different culture periods: one week and three weeks. During culture, tissue culture medium (MEM, Gibco, UK) was introduced into the Petri dish every eight hours to keep the specimen in a humid environment. Medium change was undertaken every 24 hours and the corneas were examined regularly by microscope for contamination or corneal pathology.

At the end of each culture period, the corneoscleral buttons were removed from the Barron artificial chamber and immersed in 4% paraformaldehyde with 0.1M phosphate buffer for tissue fixation, and were then sent to Cardiff University for ultrastructural investigation. Each corneoscleral button was then trephined by 12 or 14mm trephines (Altomed, UK) in order to remove unwanted extra scleral tissue. X-ray diffraction, scanning electron microscopy and transmission electron microscopy were used to reveal any ultrastructural changes after LASIK in each refractive error group and were compared with the control corneas.

6.3 Results

At the end of each culture period, the corneas were examined by microscope for contamination or corneal pathology. No defect was found in any of the corneas. The LASIK flap margin was perceivable in all the corneas regardless of the surgical ablation depth or the time spent in culture after surgery. Moreover, during SEM and TEM preparation, the corneal flap in the central area of the cornea appeared to be loosely connected to the underlying stroma.

6.3.1 X-ray Diffraction (XRD)

Wide-angle XRD of *in vitro* LASIK human corneas with different ablation depths and different culture periods revealed that the preferred collagen fibril orientation is similar to that found in normal human corneas. The orthogonal (four maxima in the inferior-superior and nasal-temporal directions)

collagen fibril orientation presents clearly in the central area (Figures 6.1 and 6.2). Further, these directions start to change near the limbus and become a circum-corneal annulus and continue with the same orientation towards the scleral area. In particular, no changes in fibril orientation were seen within the flap area or along the flap edge. Figure 6.1 presents the XRD map of a -9.00D LASIK cornea that has been cultured for one week only. The area of the LASIK flap illustrates the normal appearance of the collagen fibril orientation. This orientation has also been found in LASIK corneas with low refractive errors (less ablation) and a long healing (culture) period as illustrated in Figure 6.2.

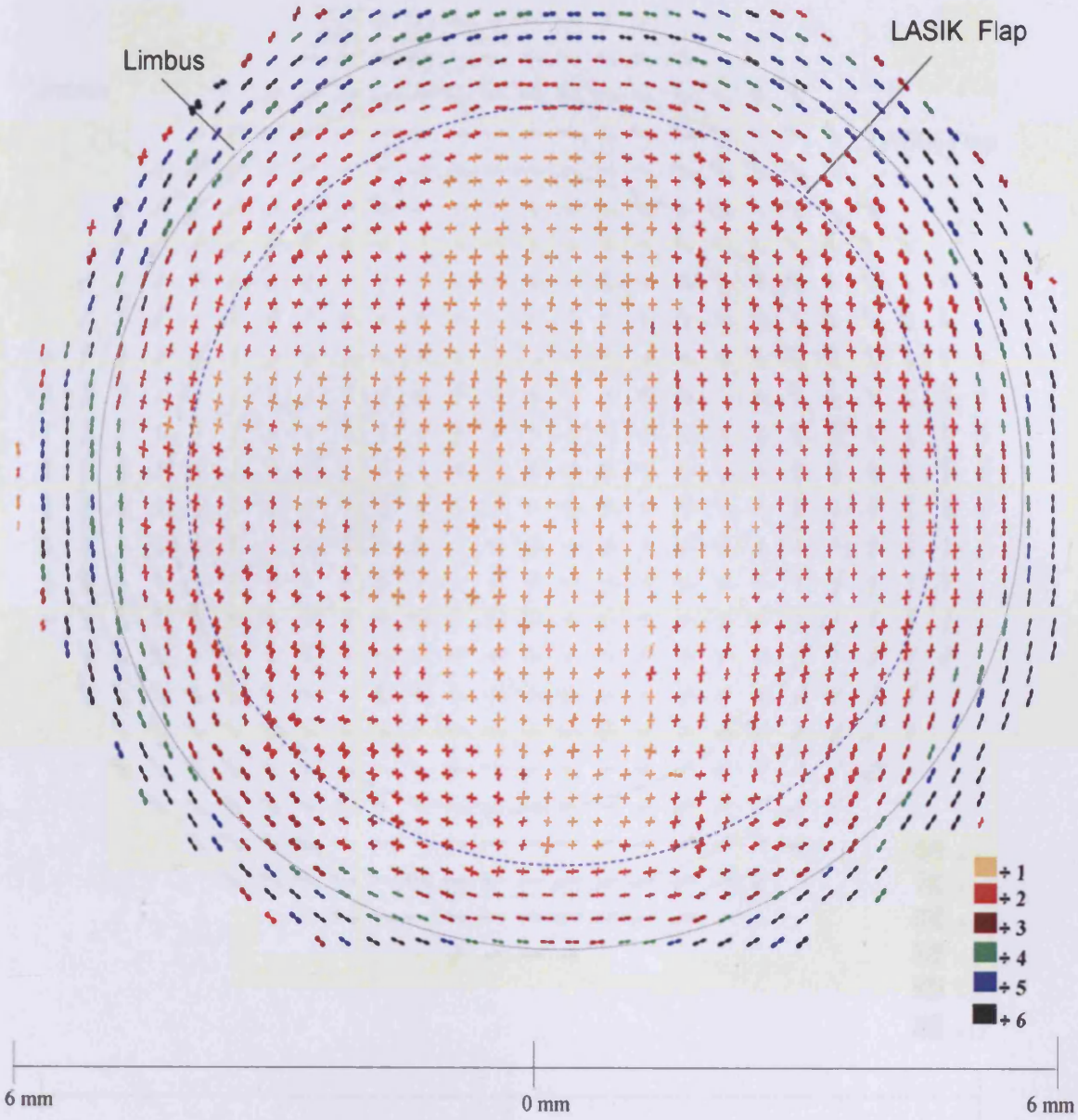

Figure 6.1: XRD map of a human cornea after -9.00D *in vitro* LASIK. The cornea had been cultured for one week. The cornea was sampled at 0.3mm intervals and the plots were scaled down by the factors showed in the right.

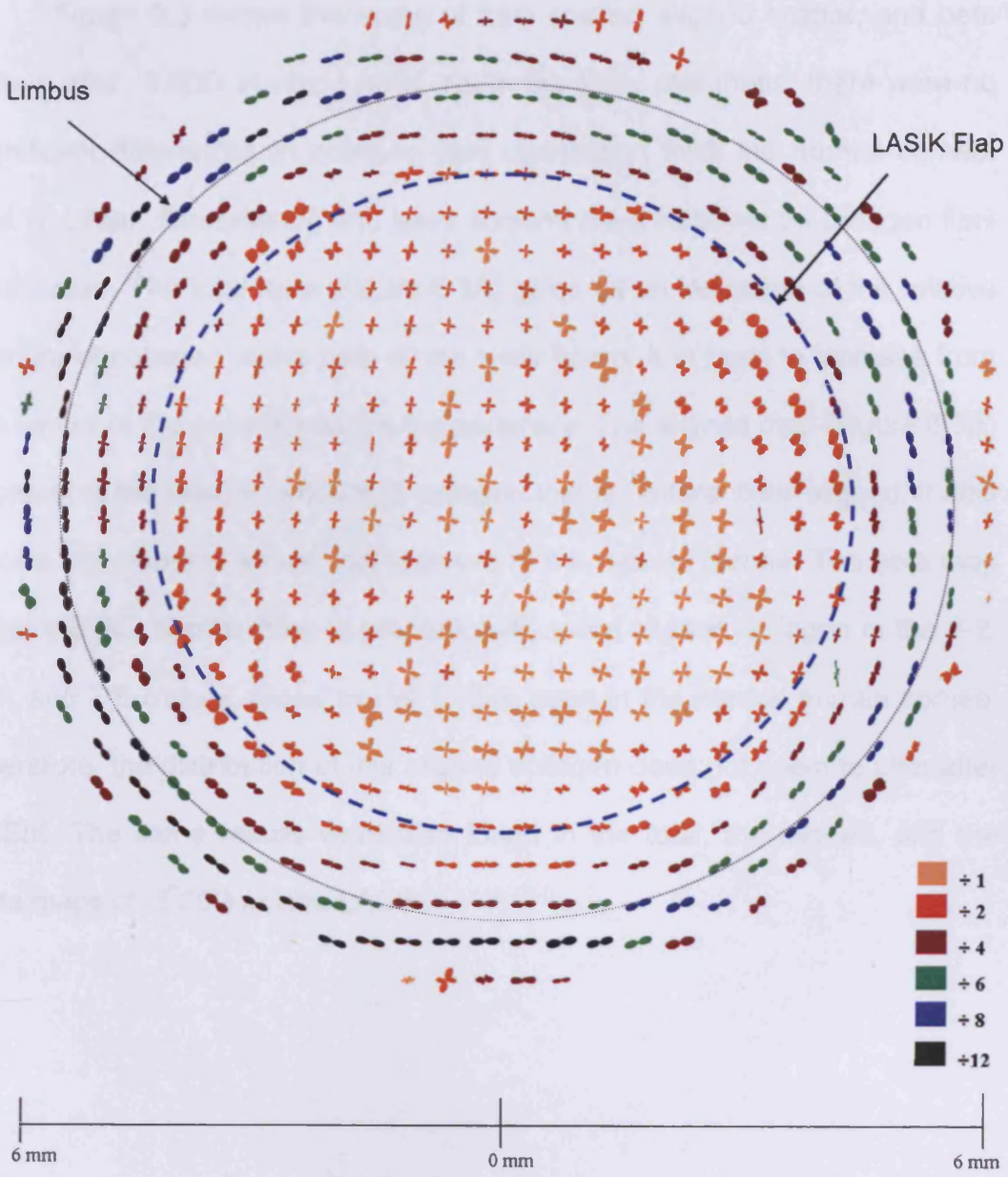

Figure 6.2: XRD map of a human cornea after -3.00D *in vitro* LASIK. The cornea had been cultured for 3 weeks. The cornea was sampled at 0.5mm intervals and the plots were scaled down by the factors showed in the right.

Figure 6.3 shows the maps of total scatter, aligned scatter, and beta values after -9.00D *in vitro* LASIK. As in the polar plot maps, there were no significant differences in collagen fibril distribution from the normal cornea, that is, LASIK flap creation and laser ablation have no effect on collagen fibril distribution. The total map (Figure 6.3A) gives us an indication of the relative amount of collagen in the path of the x-ray beam. It is seen to increase from the centre of the cornea towards the periphery. The aligned map (Figure 6.3B) represents the relative amount of collagen that is preferentially aligned. It also shows the diamond shape that appears in the normal cornea. The beta map (Figure 6.3C) shows there is proportionally more aligned collagen in the 1-2, 4-5, and 7-8 o'clock zones similar to that seen in the normal human cornea. Therefore, the distribution of this aligned collagen does not seem to alter after LASIK. The same results were also found in the total, the aligned, and the beta maps of -3.00D *in vitro* LASIK.

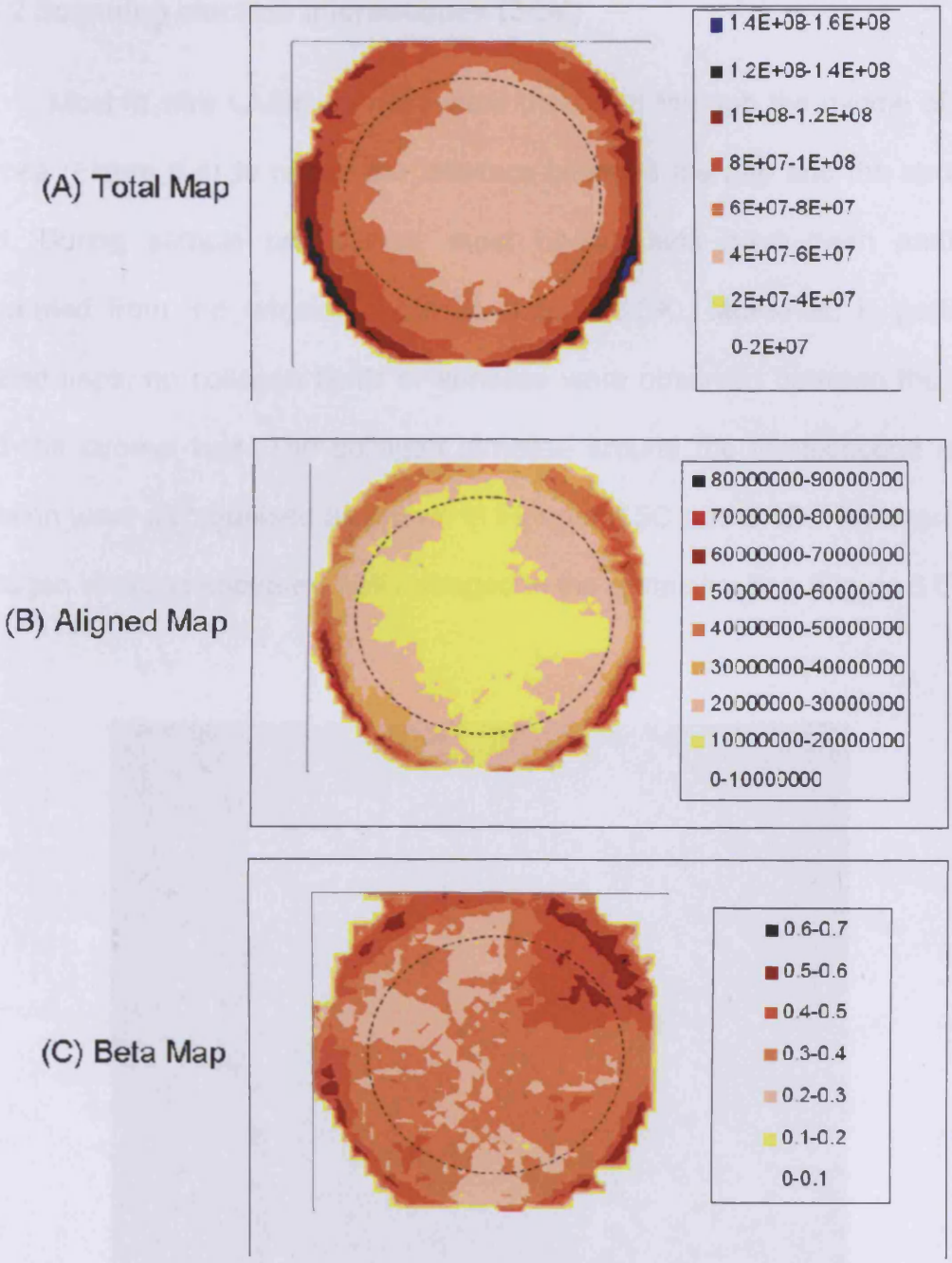

Figure 6.3: Contour maps of XRD from -9.00D *in vitro* LASIK cornea after one week in culture. Dotted circles indicate LASIK flap. Scales are in arbitrary units.

6.3.2 Scanning electron microscopes (SEM)

Most *in vitro* LASIK corneas were dissected through the middle of the cornea (Figure 6.4) to reveal the interface between the flap and the stromal bed. During sample preparation, most LASIK flaps have been partially separated from the remaining cornea (Figure 6.5A). Moreover, in partially healed flaps, no collagen fibrils or lamellae were observed between the flap and the stromal bed. The collagen lamellae around the femtosecond laser incision were disorganised as shown in Figures 6.5C and 6.5D. However, the collagen lamellae appeared well arranged in the remaining flap (Figure 6.6).

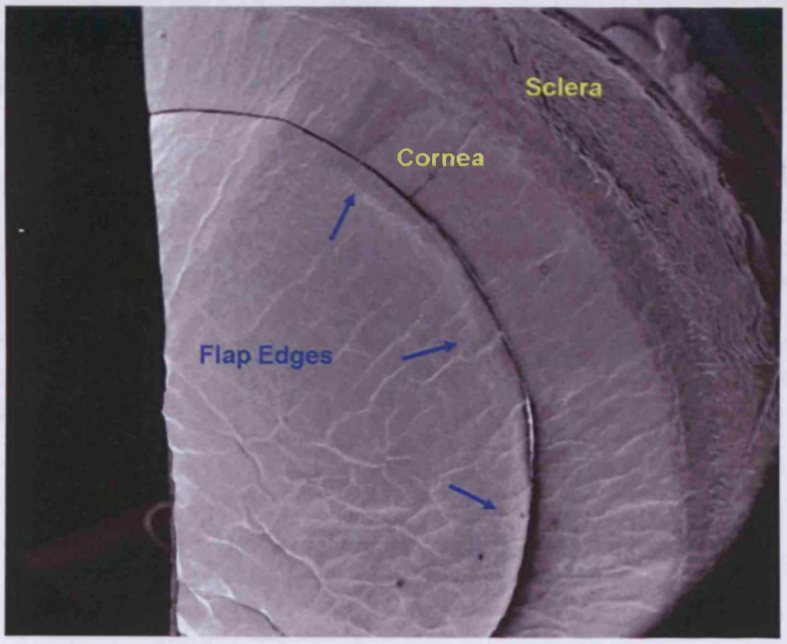

Figure 6.4: SEM image of *in vitro* LASIK cornea after dissection into two halves. This half shows the opposite side to the hinge. The flap edge is clear with apparent separation from the remaining cornea. (Original magnification x 70).

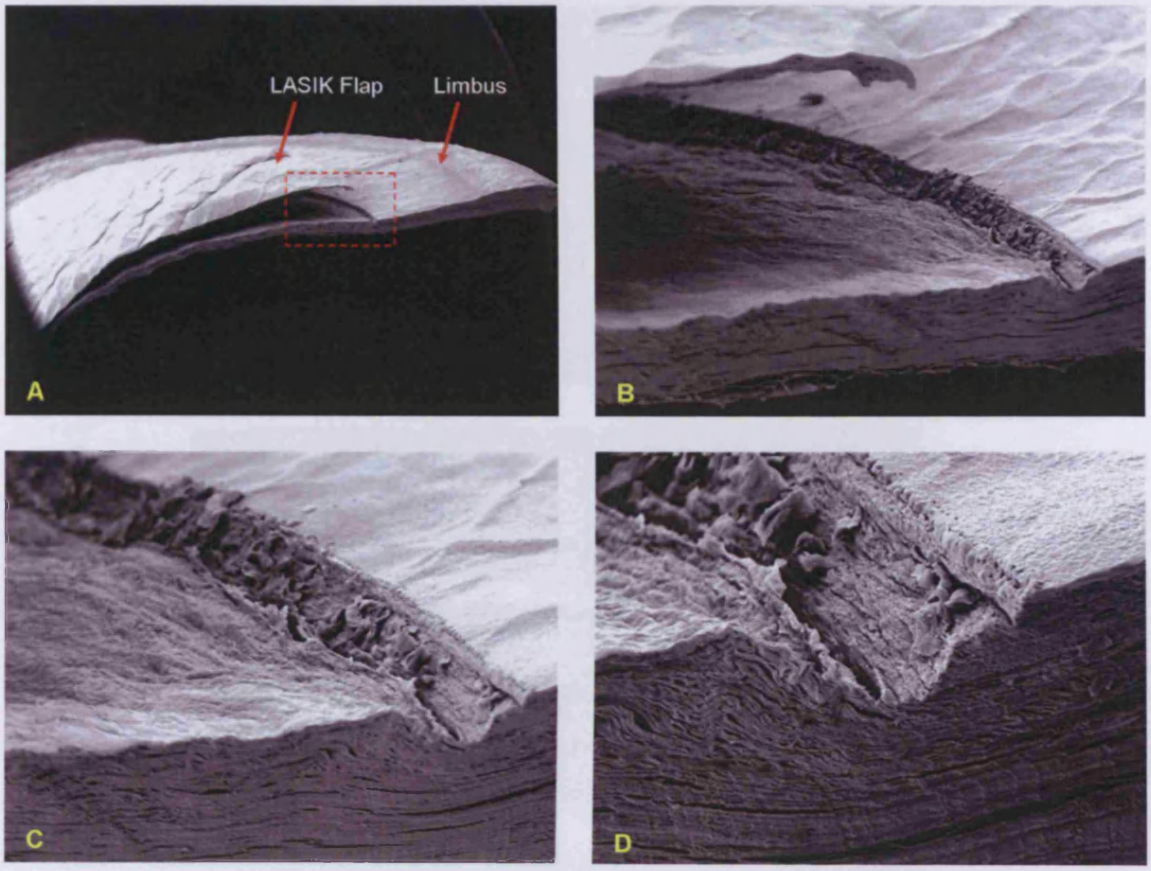

Figure 6.5: SEM images with different magnifications showing a cross section of a human cornea after -6.00 D *in vitro* LASIK and one week culture period. A: Part of the LASIK flap opposites to hinge location showing partial flap detachment from the remaining stromal bed. B, C, and D are magnified images of the red rectangle area. B and C show the flap edge and the smoothness of the stromal surface after femtosecond laser. D: more details of the starting area for flap creation by femtosecond laser showing a deep cut (ablation) and disorganised collagen lamellae around the wound surface. (Original magnification of A, B, C, and D are x50, x140, x200, and x250 respectively).

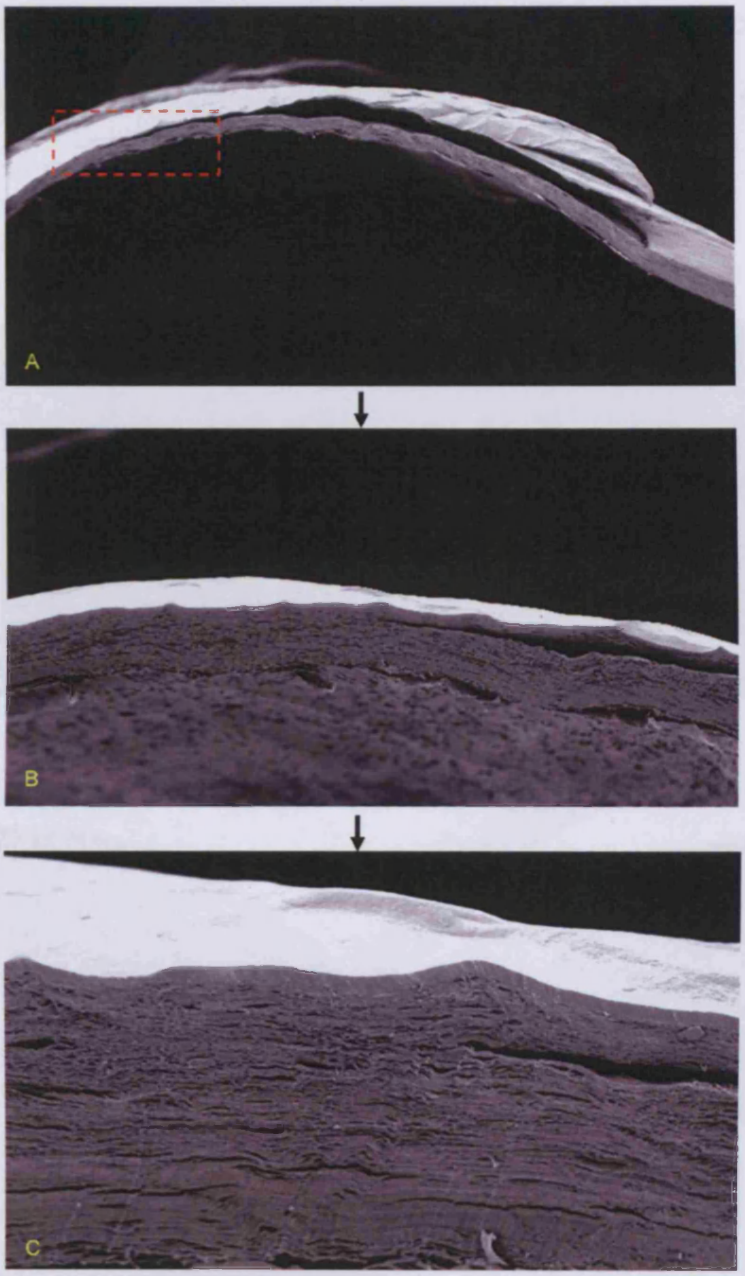

Figure 6.6: SEM images of cross section at the hinge area. A: shows the beginning of the LASIK flap where the flap starts its separation from the stromal bed. B and C are magnified images to the red rectangle hinge area in A. (Original magnification of A, B, and C are x70, x150, and x230 respectively).

NaOH removed all cellular components and kept the collagen lamellae intact. Therefore, the flap edge appears free from cellular components (Figure 6.7), which increases the chance of flap separation from the remaining cornea

and may explain the biomechanical weakness of a LASIK cornea. After femtosecond laser, the corneal stromal bed was smooth and without clear irregularities or raised collagen lamellae (Figures 6.8).

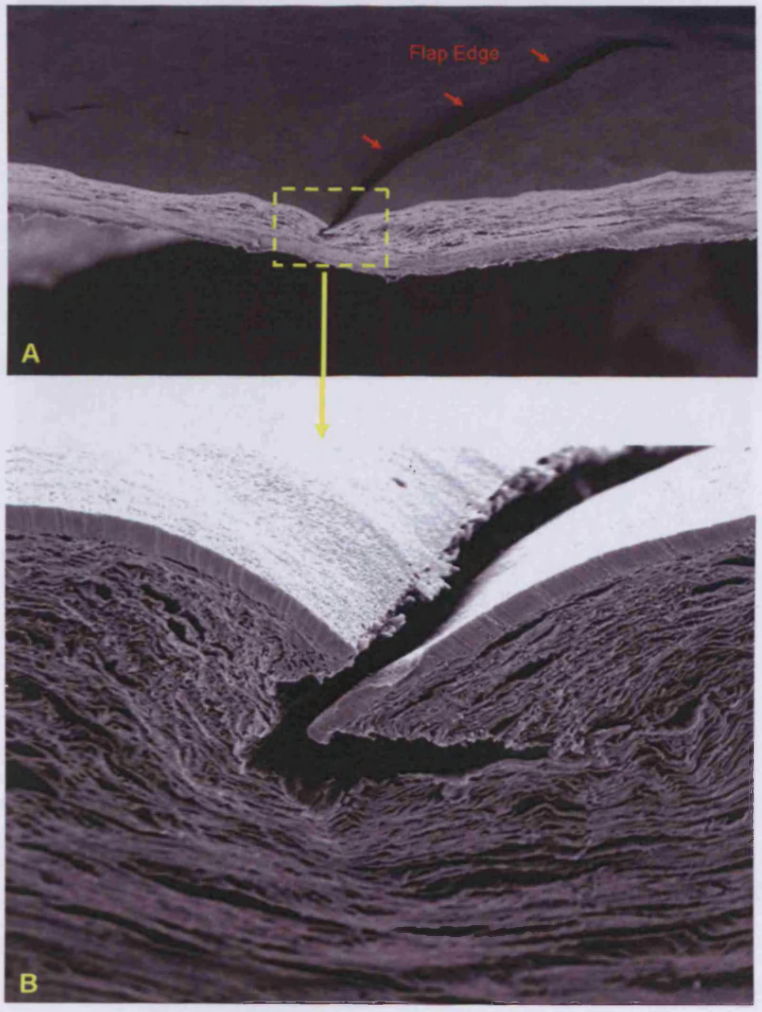

Figure 6.7: SEM images of LASIK cornea showing the flap edge. Due to the effect of NaOH, the edge appears as empty space surrounded by disorganised collagen lamellae. The remaining flap surface appears to have adhered to the stromal bed. (Original magnifications for A and B are x170 and x350 respectively).

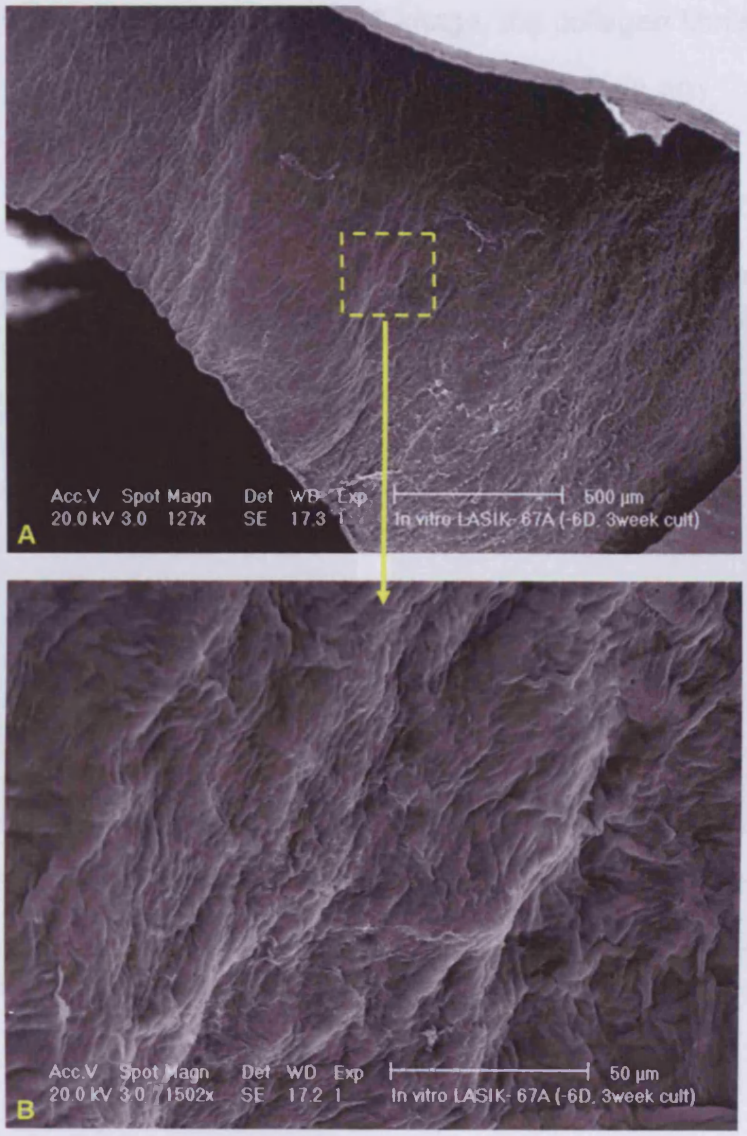

Figure 6.8: SEM images show the smoothness of the stromal bed after femtosecond laser and -6.00D ablation. (Original magnification for A and B are x130 and x1500 respectively.)

6.3.3 Transmission electron microscopy (TEM)

TEM showed that the collagen fibril lamellae close to the incision had a wavy appearance (Figure 6.9A). There was no correlation of the extent of collagen lamellar disarray in the wound with the length of postoperative culture period. However, the collagen fibrils in the middle of the flap (Figure 6.10) as well as in the remaining stroma remained intact and kept their

orientation. In a high-magnification TEM image, the collagen fibrils were tightly packed, with apparent equal interfibrillar distance (Figure 6.9B).

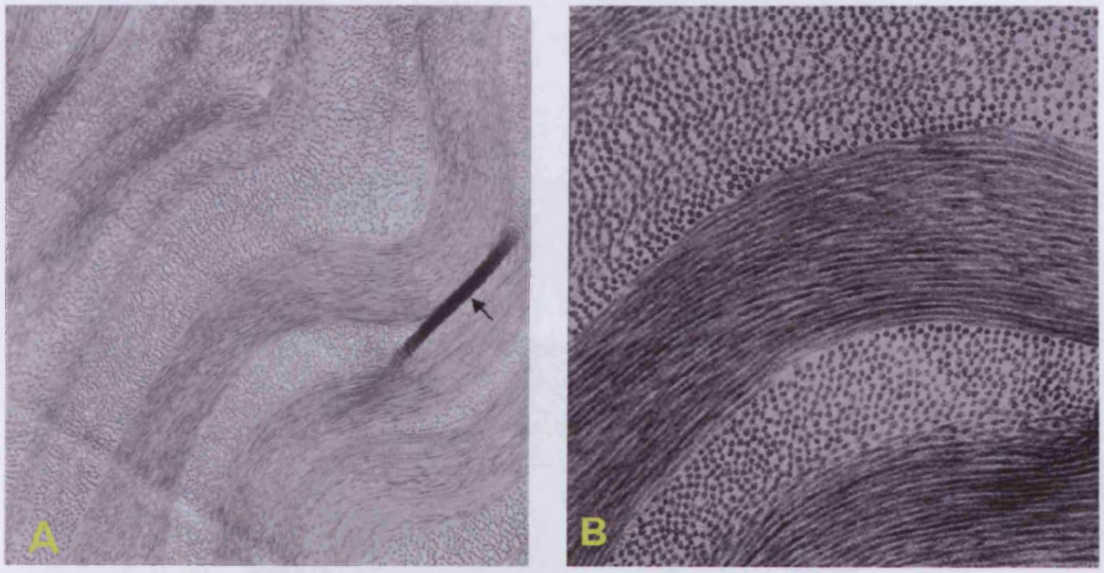

Figure 6.9: TEM images of collagen fibril arrangement close to the flap edge of *in vitro* LASIK. Note the even interfibrillar spacing although the collagen lamellae appear wavy. The black line (black arrow in A) indicates artefact during film processing (original magnification for A and B are x16,000 and 32,000 respectively).

Figure 6.10: TEM image of *in vitro* LASIK cornea shows the even distribution of collagen lamellae in the middle of the flap after one week in culture. Black arrows indicate artefacts due to sample preparation (original magnification x10,000).

In most corneas, the gap between the flap and the stromal bed was clear, that is, no fibrils were found connecting the two sides of the incision. Keratocytes were present in or adjacent to the wound and appeared to be activated as shown in figure 6.11. The corneal endothelium was intact in all examined corneas.

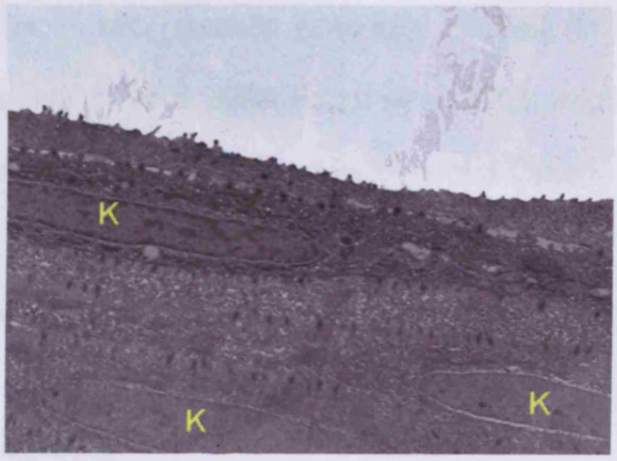

Figure 6.11: TEM image of *in vitro* LASIK cornea after one week in culture shows the presence of keratocytes (K) in the stromal bed close to the flap-bed interface (original magnification x5000).

6.4 Discussion

LASIK surgery includes corneal flap creation, stromal ablation, and repositioning of the flap without sutures. This technique leads to a minimal corneal wound healing response that happens mainly at the cellular level around the flap edges making the anterior corneal tissue (lamellae) ineffective biomechanically, thus leading to optical problems, such as ectasia (Perez-Santonja *et al.* 1998; Seiler *et al.* 1998; Park and Kim 1999; Lombardo and Katz 2001; Anderson *et al.* 2002).

In this study, different means have been used to find out the ultrastructural changes after LASIK surgery. The *in vitro* LASIK model was chosen due to the difficulty in obtaining 12 post-mortem LASIK corneas at one time; most LASIK patients are still young, as the first LASIK procedure started in 1991 (Pallikaris *et al.* 1991; Kymionis *et al.* 2007). In addition, it has been found that the wound healing reactions of *in vitro* cultured LASIK-treated corneas parallel the in vivo situation described clinically in humans or in the rabbit animal model (May *et al.* 2004; Rajan *et al.* 2005; Priglinger *et al.* 2006). The new flap creation technology (femtosecond laser) has been used because, firstly, it was difficult to create corneal flap by the mechanical microkeratome while the cornea is attached to the artificial chamber and secondly, it was an opportunity to show the effect of this new technology on corneal structure by SEM.

Wide-angle XRD results (Figures 6.1 - 6.3) indicate that the collagen fibril orientation and distribution after LASIK, with different ablation depths and up to three weeks of culture, are similar to the orientation and distribution found in the normal cornea. This normal appearance in XRD needs to be confirmed by more studies for a number of reasons. Firstly, the changes in collagen fibrils, if they occur, will have happened in the anterior stroma where the flap takes place and, as mentioned earlier, XRD measures the arrangement of the collagen fibrils through the whole corneal thickness which may not reveal the change in collagen fibril orientation along the 70-100 μm flap thickness (the remaining flap thickness is the free-collagen fibrils epithelial layer). Secondly, the XRD resolution used in this study (0.3 mm step size)

was not small enough to identify any difference in the collagen fibrils at the flap area, that is, at station 14.1 in Daresbury, the XRD step size cannot be decreased to less than 0.25 mm. Thirdly, at the area of 9mm corneal diameter, the collagen fibrils take the shape of an annulus surrounding the cornea and, as mentioned in Chapter 4, 6mm and 4mm trephinations change the shape of the fibrils from orthogonal to annulus. Accordingly, the changed shape of the collagen fibrils at the flap edges will be undetectable. Therefore, it is recommended to conduct more XRD experiments with a high step size resolution and/or conduct XRD on the flap tissue alone in order to understand the ultrastructural changes after LASIK.

The SEM results (Figures 6.4 – 6.9) show the structure of both the LASIK flap and the stromal bed. After applying NaOH, which removes cellular components and leaves the collagen lamellae intact (Ohtani 1987; Komai and Ushiki 1991), the flap-bed interface became more obvious and the disruptive effect of the femtosecond laser on the collagen lamellae around the flap edges could be seen clearly at high magnification (Figures 6.5D and 6.7B). The femtosecond laser ablated more collagen tissue at the starting point of the flap (Figure 6.5D), which may be considered a disadvantage of this technology, as it weakens the flap edges, that is, the strongest part in the flap during wound healing process (Schmack *et al.* 2005). Figure 6.6 shows the starting point of the LASIK flap from the hinge side. Collagen lamellae separation started at a small angle and increased towards the other side of the flap. No bridging fibrils or lamellae between the bed and the flap could be detected, which leaves the flap weak and, thus, explains the easy separation

or dislocation of the flap from the bed months or years after surgery (Durrie and Aziz 1999; Nilforoushan *et al.* 2005). The lamellae in both sides were well ordered and parallel to the corneal surface in spite of the effect of dehydration and shrinkage on the corneal tissue, which was clear in some excluded samples. These clear images give an overview of the corneal biomechanical insults caused by the LASIK flap and which seem difficult to heal or to compromise and, in some cases, may lead to ectasia (Amoils *et al.* 2000). At high magnification (Figures 6.5 and 6.8), the stromal surface appears smooth and without the irregularities or multiple lamellae elevations that are seen with mechanical microkeratome (Kaji *et al.* 1998; Sarayba *et al.* 2007a; Sarayba *et al.* 2007b). This finding is in agreement with the previous studies that concluded that the femtosecond laser is superior to the mechanical microkeratome (Kezirian and Stonecipher 2004; Tran *et al.* 2005; Stonecipher *et al.* 2006). Full details about femtosecond laser versus mechanical microkeratome can be found in Chapter 1, section 1.8.2.

On TEM, the collagen lamellae arrangement appeared wavy around the flap edge whereas it is considered well ordered in the middle of the flap as well as in the remaining stroma. This difference in the arrangement is probably a result of the flap creation technique. The femtosecond laser creates two kinds of wounds: an incision at the flap margin (starting point) that disrupts a large amount of collagen lamellae (Figure 6.5D) and reacts with scar tissue formation, and an intrastromal lamellar wound in the central area that shows only mild collagen lamellae disruption and a minimum reaction with scar tissue formation, for example, activated-like keratocytes as shown in Figure 6.11. On the other hand, interfibrillar distances appear normal on both

sides of the wound (Figures 6.9 and 6.10), which may explain the perfect visual acuity results obtained immediately after LASIK surgery. On examination of post-mortem LASIK corneas, Rumelt *et al.* (2001) found the same TEM results whereas Anderson *et al.* (2002) and Kramer *et al.* (2005) found disorganised collagen fibrils and increased interfibrillar spacing in the wound area. This disparity might be related to the tissue condition before the TEM process, for example, a swollen cornea, or different chemical methods that have been used to prepare the sample for TEM.

SEM and TEM findings may support the previous histologic and immunohistochemical studies of corneas after LASIK (Wachtlin *et al.* 1999; Philipp *et al.* 2003; Priglinger *et al.* 2006) that reported the lack of pronounced morphologic changes in the central area of the LASIK interface and the minimal wound healing at the flap edges. However, in this study, the maximum cultural period was three weeks. Therefore, more studies with longer cultural periods are recommended to support the hypothesis of the reduced wound healing reactions after performing this surgical procedure.

In summary, this study aimed to show the early effect of LASIK surgery with femtosecond laser technology on corneal ultrastructure. XRD showed that collagen fibril organisation was not affected by the LASIK procedure whereas SEM and TEM gave us an overview of the flap-bed interface shape and collagen lamellae distribution that in some instances is parallel to XRD findings. Further similar studies are recommended to expand our knowledge about the LASIK procedure effect on corneal tissue.

Chapter 7. Ultrastructural features of post-mortem and ectatic LASIK corneas.

7.1 Introduction

LASIK surgery has many postoperative complications (see chapter 1, section 1.7), and ectasia is considered one of the most serious long-term postoperative complications. Although it occurs only rarely, it can cause a severe loss of vision that in some cases can be restored only by corneal transplantation (Pallikaris *et al.* 2001; Rad *et al.* 2004). In the literature, huge numbers of publications evaluate the results of LASIK surgery. However, most of them discuss the clinical outcomes with little emphasis on ultrastructural changes. Also, most studies that concentrate on ultrastructural changes are based on animal models (see, for example, Amm, Wetzel *et al.* 1996; Park and Kim 1999; (Miyamoto *et al.* 2003). As shown in Chapter 3, also as reported in the literature, one must realise that the architecture and biological properties of animal corneas can be quite different from those of humans (Amm *et al.* 1996; Park and Kim 1999; Dawson *et al.* 2005a).

Recently, a few papers have been published studying ultrastructural changes in healthy human post-mortem LASIK corneas (see section 6.1 for more details). Furthermore, a small number of case reports have been presented showing the histopathologic and the ultrastructural changes in ectatic corneas (Jabbur *et al.* 2001; Ou *et al.* 2002; Spadea *et al.* 2002; Seitz *et al.* 2003; Kim *et al.* 2006; Maguen *et al.* 2007). Therefore, in this chapter, the corneal ultrastructural features of two healthy post-LASIK corneas and

three post-LASIK ectatic corneas are presented and compared. The corneas are presented as case reports because each cornea has different clinical data. It is hoped that the results of this study may help to clarify the structural basis of the biomechanical changes that induce ectasia after LASIK, which are still not fully understood.

7.2 Materials and methods

Five LASIK corneas were used in this study (Table 7.1). Two post-mortem healthy LASIK corneas were obtained from Dr. Henry Edelhauser, (Emory Hospital, NE, USA). The third cornea was obtained from Dr. Jose Velarde (Instituto Cántabro de Oftalmología, Santander, Spain) from a patient who had undergone penetrating keratoplasty (PKP) after a diagnosis of post-LASIK ectasia. The remaining two corneas were obtained from King Khaled Eye Specialist Hospital (KKESH, Riyadh, Saudi Arabia) from two patients who had had PKP performed after post-LASIK ectasia. One normal donor cornea from the Bristol Eye Bank (Bristol, UK) was used as a control. All the corneas were stored in 4% paraformaldehyde and were sent to Cardiff University for ultrastructural investigation. On arrival, wide-angle XRD, SEM, TEM, and LM were carried out for the corneal buttons, as shown in Table 7.1. More details about each case are shown in the next pages. In addition, the general methods for preparing the tissues for XRD, SEM, TEM, and LM were explained in Chapter 2.

Case/ Eye	Age/ Sex	Surgery/ Date	Diagnosis	Sample Source	Procedure
1/ R	55/ M	LASIK, 2000	Post-mortem	USA	SEM, TEM, LM
2/ L	55/ M	LASIK, 2000	Post-mortem	USA	SEM, TEM, LM
3/ R	30/ M	LASIK, 2001	Ectasia	Spain	XRD, SEM, TEM, LM
4/ R	35/ M	LASIK, 1995	Ectasia	SA	TEM, LM
5/ L	26/ M	LASIK, 2003	Ectasia	SA	TEM, LM

Table 7.1: Clinical data of the LASIK corneas, source of corneas, and type of investigation run for each cornea. (USA) United States of America. (SA) Saudi Arabia.

7.3 Case reports

7.3.1 Cases 1 and 2

Two healthy post-LASIK corneoscleral buttons of a 55-year-old male donor were received from the eye bank by Dr. Henry Edelhauser (Emory Hospital, NE, USA). The donor had had LASIK surgery in both eyes 5-6 years before death. Unfortunately, no other ocular history details, such as refractive errors and corneal topography map, were available from the eye bank. The corneas were stored in Optisol solution then were fixed in 4% Paraformaldehyde prior to shipment. On receipt, the corneas were dissected into two halves; one half was used for SEM and the other half was used for TEM and LM investigations. In this case, the concentration of NaOH during the SEM process was reduced from 10% for 5 days to 5% for 2 days in order to keep some of the cellular components.

7.3.1.1 Case 1 and case 2 results

Five years after LASIK surgery, the LASIK flap edges can be seen clearly in SEM images (Figures 7.1 and 7.2). The flap was attached firmly to the stromal bed except at the edges where there were tissue gaps. The disarrayed collagen lamellae around the flap edge and along the flap-bed interface can be detected at higher magnifications (Figures 7.1C and 7.2C). At one side (Figure 7.2), the flap edge shows chatter marks of what is believed to be the effect of the microkeratome blade. These chatter marks can be seen clearly at a higher magnification (Figure 7.3A). Due to the effect of NaOH, the flap edges appear empty of cellular components (10-20μm wide hollow space) and no connection is noticeable between the flap margin and the adjacent corneal tissue except some bridging fibres (Figure 7.3B).

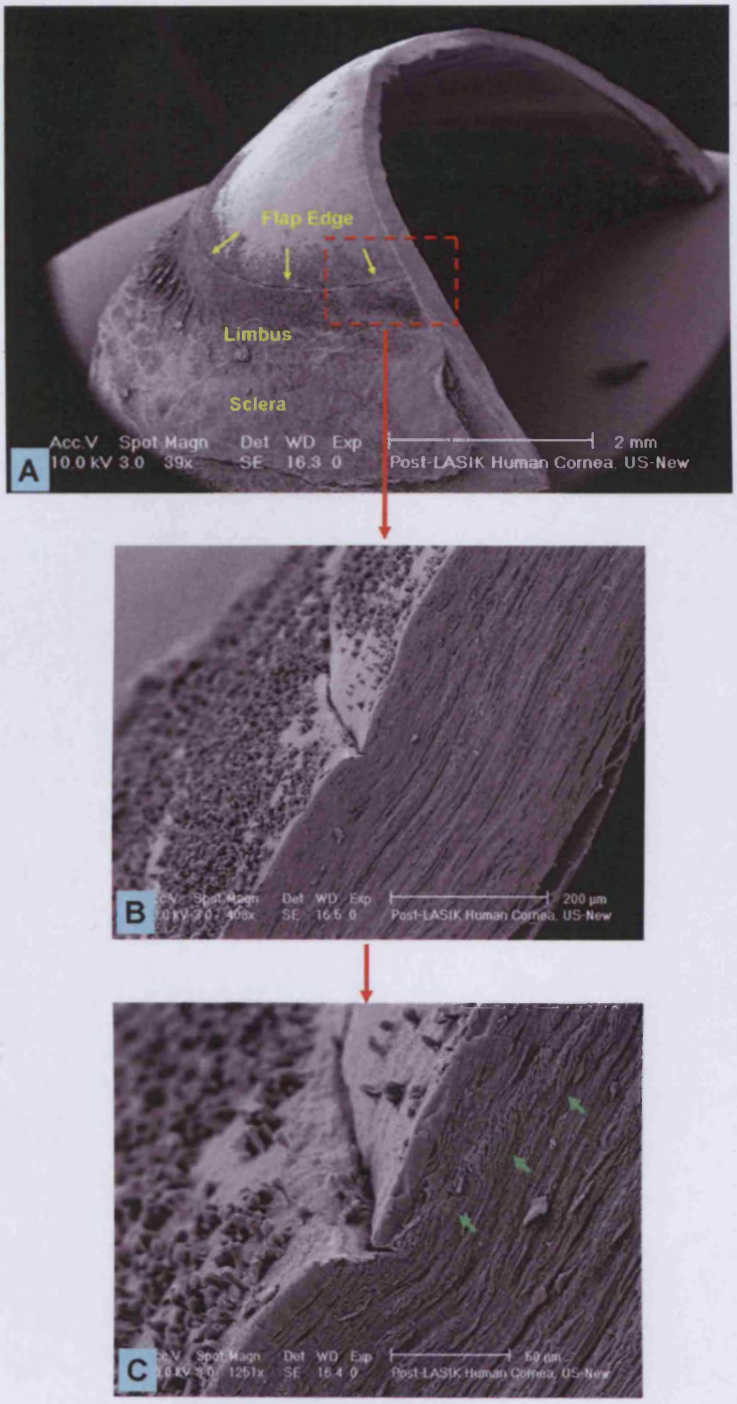

Figure 7.1: SEM images show a cross section of a post-mortem LASIK cornea (rgiht). The flap edge (yellow arrows in A) can be seen clearly. At higher magnifications, the flap edge appears separated from the adjacent corneal tissue (B). In addition, the flap-bed interface (green arrows in C) shows disarray in the collagen lamellae. The black particles on epithelial and limbal surfaces are believed to be basal epithelial cells. (Original magnifications for A, B, and C are x40, x400, and x1250 respectively).

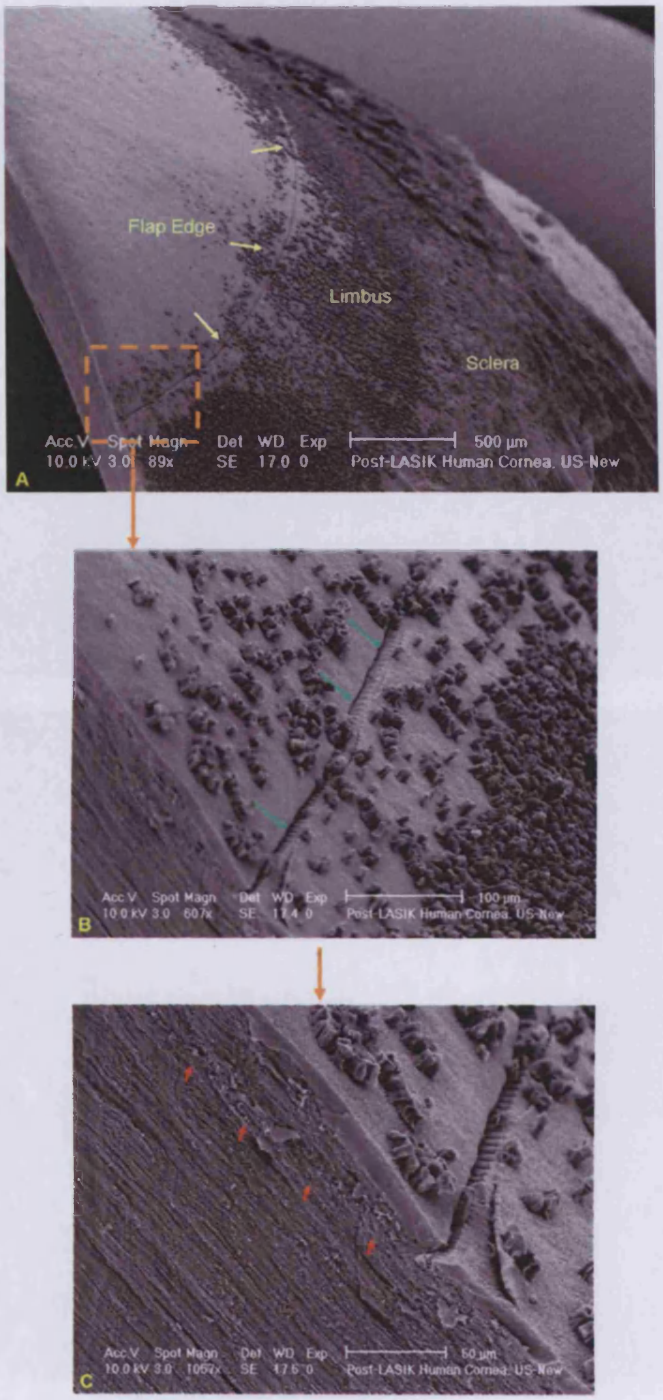

Figure 7.2: SEM images of post-mortem LASIK cornea (right) show the flap edge at different magnifications. (A) General view of the flap edge. (B) and (C) show the incision point of the microkeratome (green arrows) and the flap-bed interface where collagen lamellae appear disorganised (red arrows). The scattered black particles on the cornea are believed to be basal epithelial cells. Original magnifications for A, B, and C are x90, x600, and x1050 respectively.

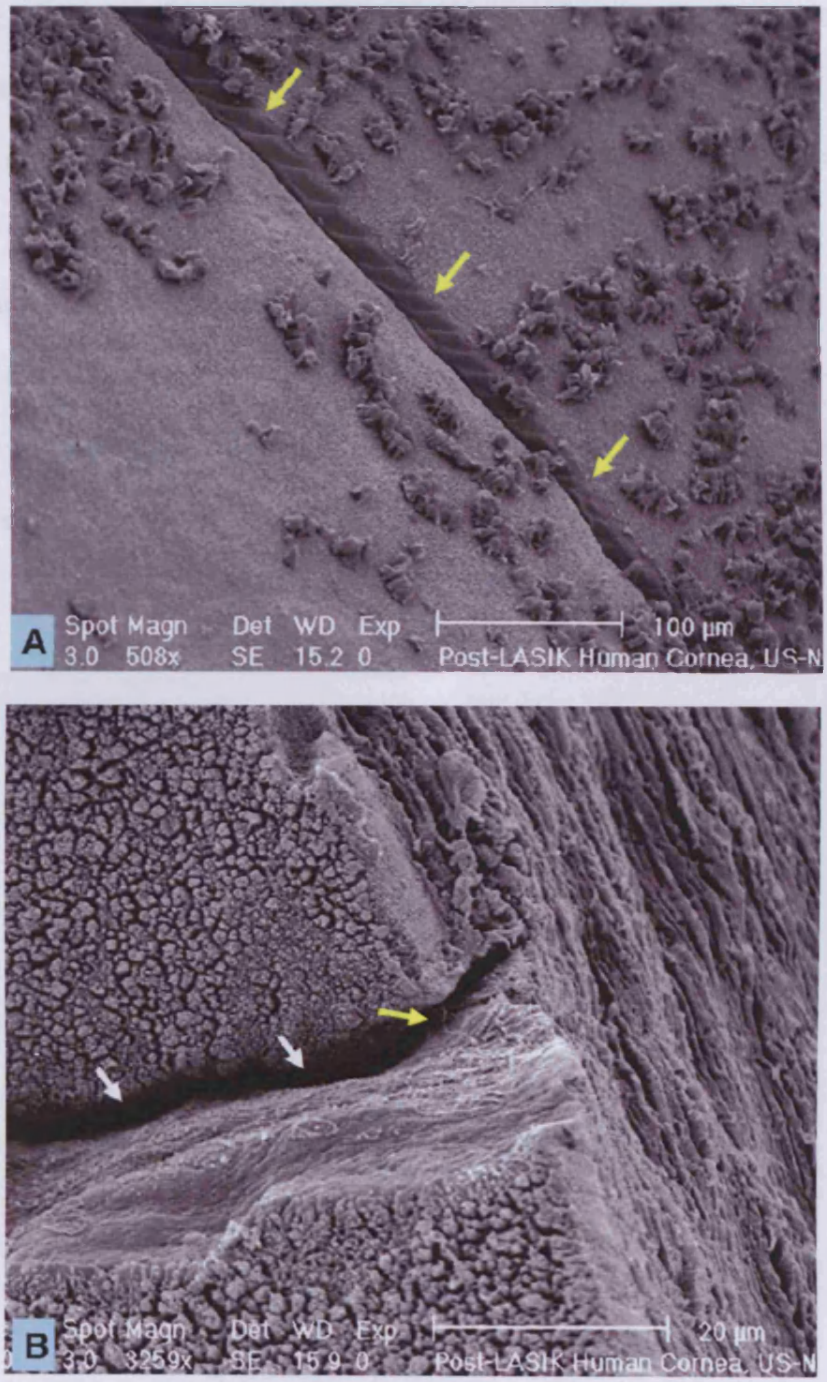

Figure 7.3: SEM images of post-mortem LASIK cornea. (A) shows the microkeratome head incision (yellow arrows) from a different angle. (B) shows vertical view of the flap edge where it appears empty from scar formation components (white arrows) and only a few bridging fibres connecting the flap to the stromal bed (yellow arrow). Original magnification is x500 (A) and x3250 (B).

TEM images (Figure 7.4) show that the collagen lamellae on both sides of the flap-bed interface are parallel to the corneal surface. However, they take the shape of waved lamellae instead of straight lamellae. The flap-bed interface measures 1-2 μm and appears free from collagen fibrils or bridging components. At higher magnifications, Figure 7.5 shows the interfibrillar spacing in two regions, that is, in the middle of the flap and in the middle of the remaining stroma. It appears that both locations have normal interfibrillar spacing when compared with normal cornea.

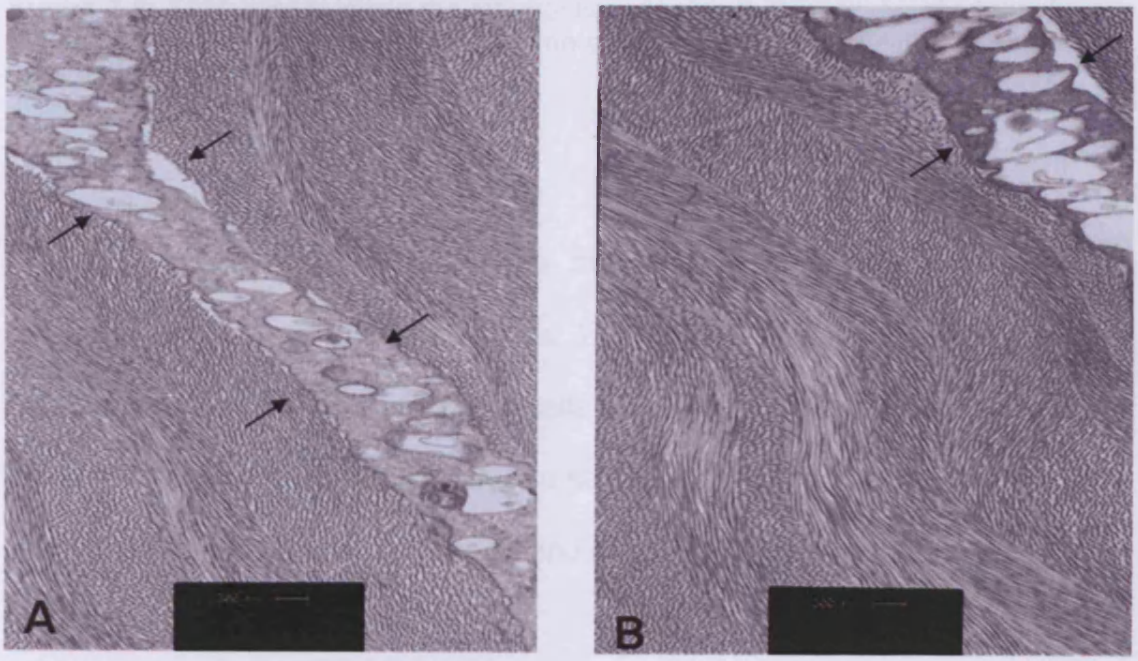

Figure 7.4: TEM images of the flap-bed interface after LASIK. Collagen lamellae appear parallel with corneal surface but are waved rather than straight. Collagen interfibrillar distances appear normal. Note the gap with what is believed to be scar tissue formation between the flap and the stromal bed (black arrows). Original magnification is x16,000 for A and B.

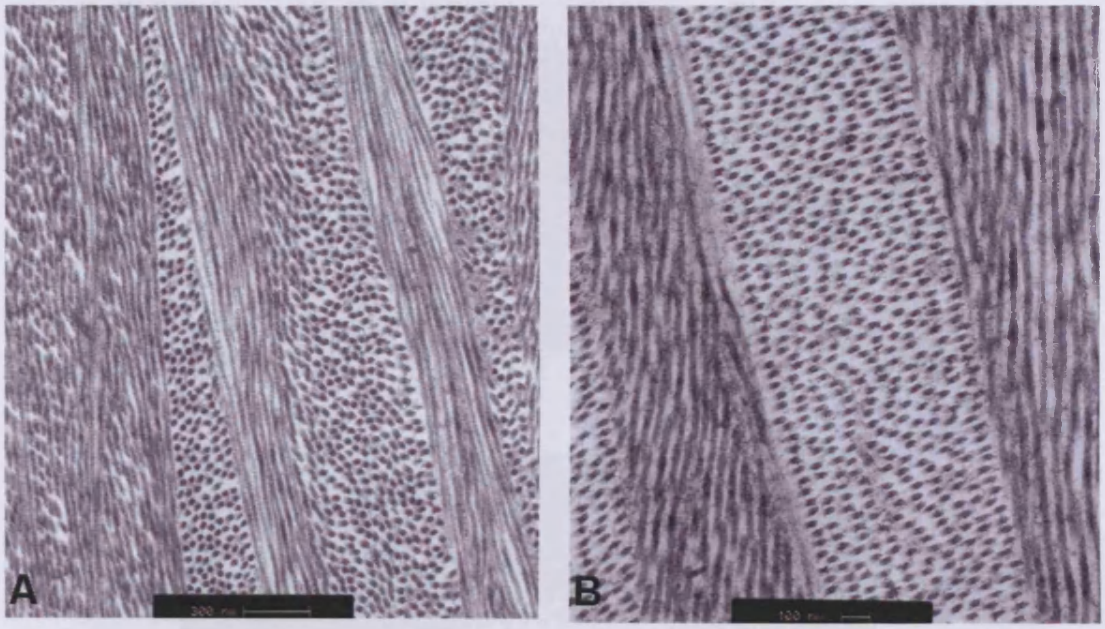

Figure 7.5: TEM images show the interfibrillar spacing in the middle of LASIK flap (A) and in the middle of the remaining stroma (B). Original magnification is x32,000 for A and x40,000 for B.

LM images (Figure 7.6) show that the flap-bed interface can be detected with different LM light colours. The epithelial layer appears intact in the middle of the flap although some cells are missing because of the sample preparation process. In addition, due to sample dissection, the flap edges did not appear on LM images. Bowman's and endothelial layers appear intact.

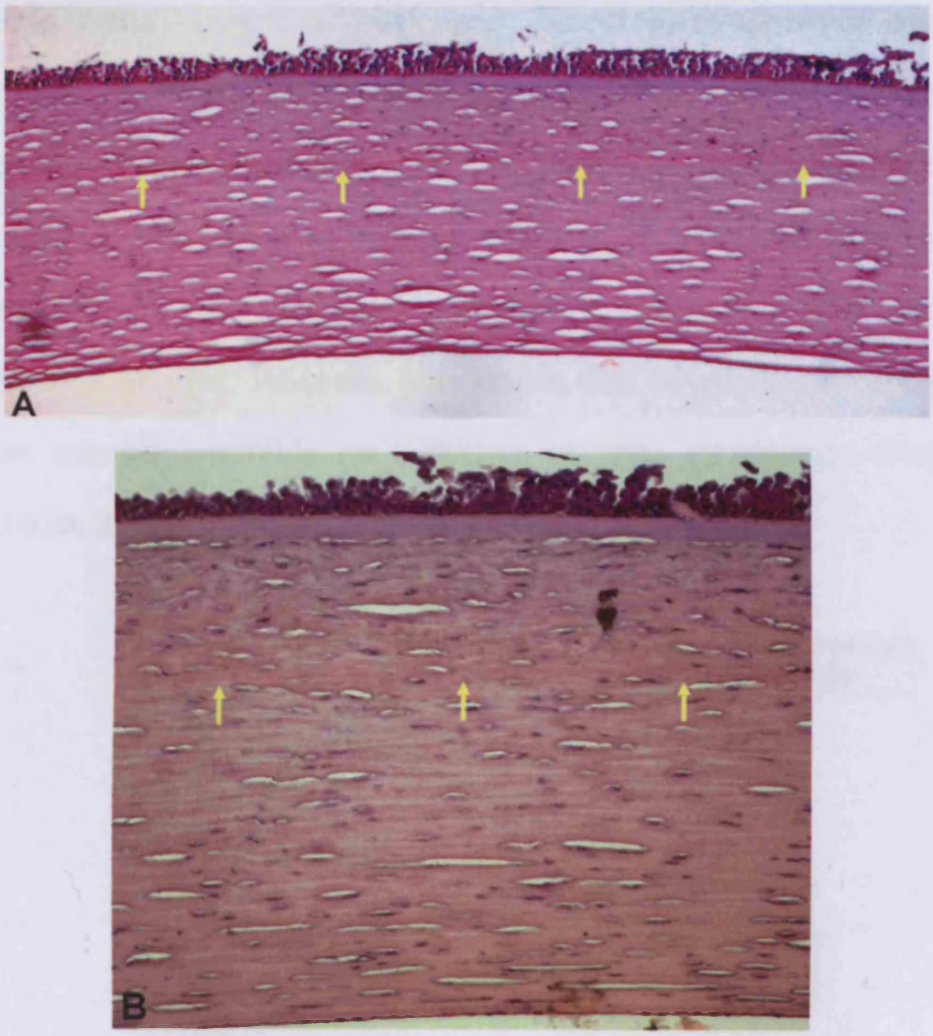

Figure 7.6: LM images of post-mortem LASIK cornea with different LM light colours. The flap-bed scar can be seen (yellow arrows). Also, some of the epithelial cells appear disorganised. Bowman's layer looks intact. Original magnification is x5 (A) and x10 (B).

7.3.2 Case 3

A 30-year-old man, according to the clinical data supplied by his previous surgeon, had a preoperative refraction of -2.00 -0.00 × 0° in the right eye and -2.00 -0.75 x 60° in the left eye. The best-corrected visual acuity (BCVA) was 20/20 for both eyes. The pre-LASIK central corneal pachymetry was 532μm and 526μm in the right and left eyes respectively. IOP was

12mmHg in both eyes. The family history was negative for ocular disorders, particularly for keratoconus. Preoperative corneal topography showed steepening of up to 48 D and 1.64 D of asymmetric astigmatism. However, only a single, incomplete topographic image was supplied from his previous surgeon (Figure 7.7), which indicates that the patient may have had early keratoconus or FFK. However, it is known that placido-based topographic images can be unreliable as indicators of early keratoconus (Belin and Khachikian 2007).

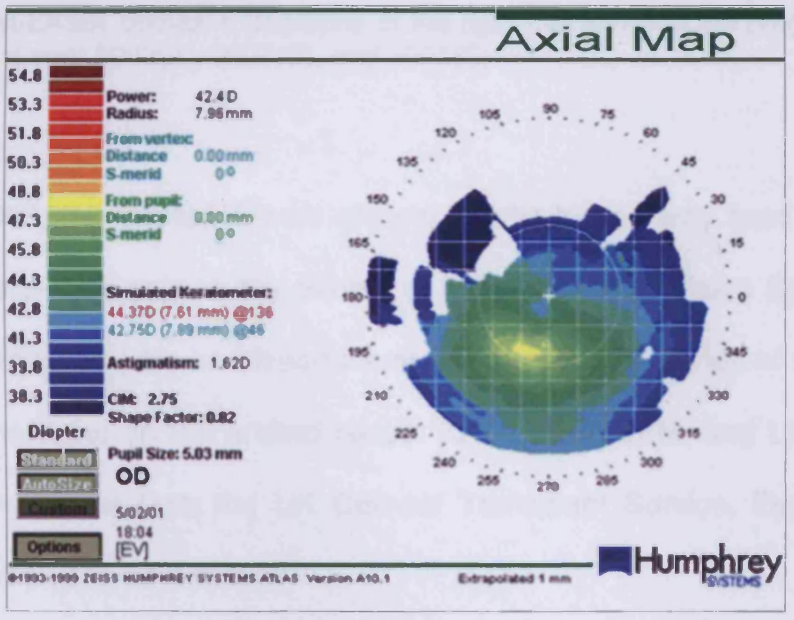

Figure 7.7: Corneal topography of the right eye before LASIK surgery. It shows corneal steeping up to 48 D in the inferior-central quadrant.

LASIK was performed by his surgeon in both eyes in 2001. The surgery and postoperative period were uneventful. The post-LASIK central corneal pachymetry was 506μm and 515μm in the right and left eyes respectively. Since 2002, the patient's BCVA had become worse in the right eye, and an inferior steepening developed rapidly in the topographic images, suggesting a

corneal ectasia (Figure 7.8). In 2005, a slit-lamp examination showed clinical signs of ectasia in the right eye, that is, corneal thinning and protrusion, and after the wearing of rigid contact lenses failed to correct the condition, PKP was performed on the right eye.

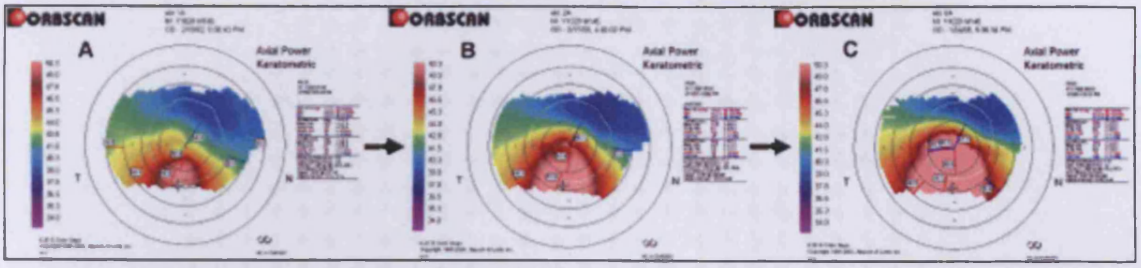

Figure 7.8: Post-LASIK corneal topography of the right eye showing the progress of inferior ectasia at year 2002(A), 2003(B), and 2005(C).

After PKP, the grafted 8 mm corneal ectatic button was fixed in 4% buffered formalin then sent to the School of Optometry and Vision Sciences (Cardiff University, UK) for an ultrastructure investigation. A series of studies were then carried out on the grafted tissue: XRD, TEM, SEM, and LM. One normal human cornea from the UK Corneal Transplant Service, Eye Bank (Bristol, UK) was used as a control.

7.3.2.1 Case 3 results

Figure 7.9 shows a polar plot map from the whole ectatic tissue. The cross-shaped polar plots in normal corneas indicate the preferred orientation of the collagen in the vertical and horizontal directions throughout the central region (see figure 3.1 in chapter 1). This arrangement is not changed in the ectatic button though the inferior part of the map (the central area of ectasia)

shows a slight reduction in intensity as illustrated by the orange coloured patterns. This indicates that there is some loss of collagen in this region.

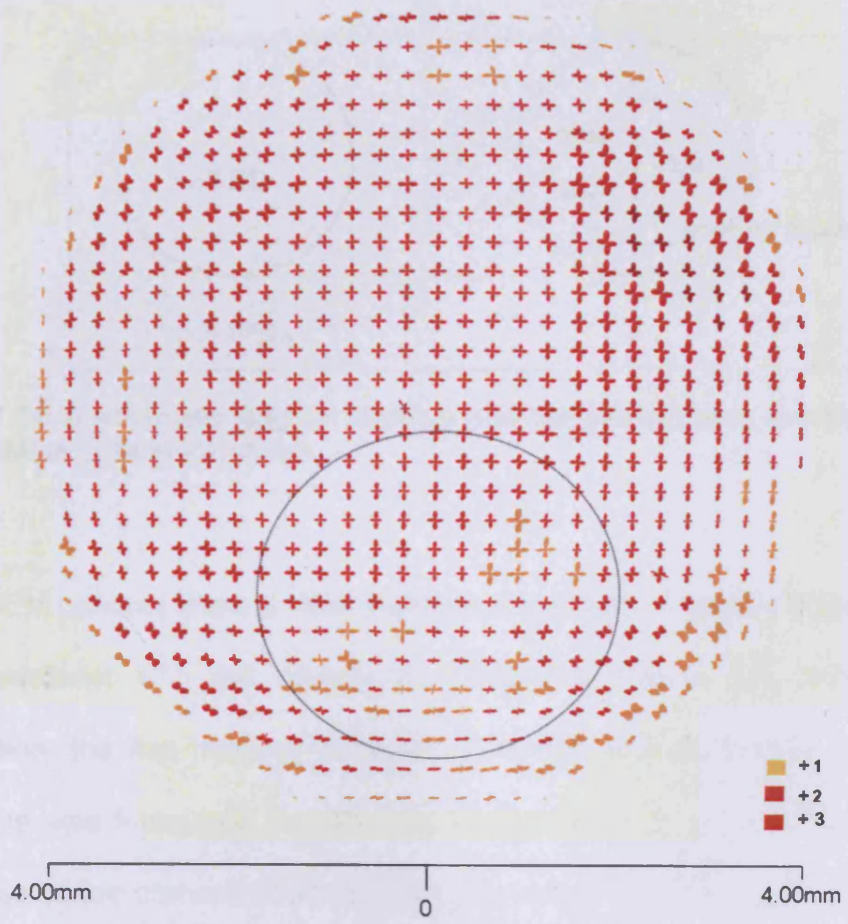

Figure 7.9: XRD map of 8mm ectatic human cornea. The dotted circle indicates the central area of ectasia.

After XRD, the 8mm corneal button was bisected centrally with a razor blade, with half to be used for SEM and the other half for both TEM and LM (Figure 7.10).

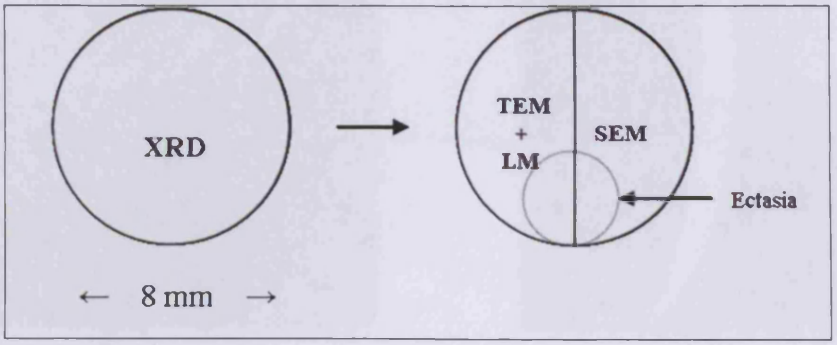

Figure 7.10: A schematic diagram showing how the ectatic tissue was bisected for SEM, TEM, and LM examinations.

SEM pictures show a clear thinning at the area of ectasia (Figure 7.11), which coincides with the corneal topography in Figure 7.8. During SEM preparation, the flap became detached from the residual stromal bed when the tissue was immersed in 10% NaOH (Figure 7.12), which indicates the weakness of the corneal wound healing. By using the SEM scale bar, it was calculated that the thickness of the inferior ectatic area was 230μm, the thickness of the central partially affected area was 280μm, and the thickness of the superior normal area, that is, at 12 o'clock, was 340μm. There was tissue shrinkage due to NaOH and the dehydration processes. On the other hand, the thickness of the corneal flap was constant all over the tissue, that is, 80 μm (Figure 7.12) (after removal of the epithelium layer by NaOH and dehydration).

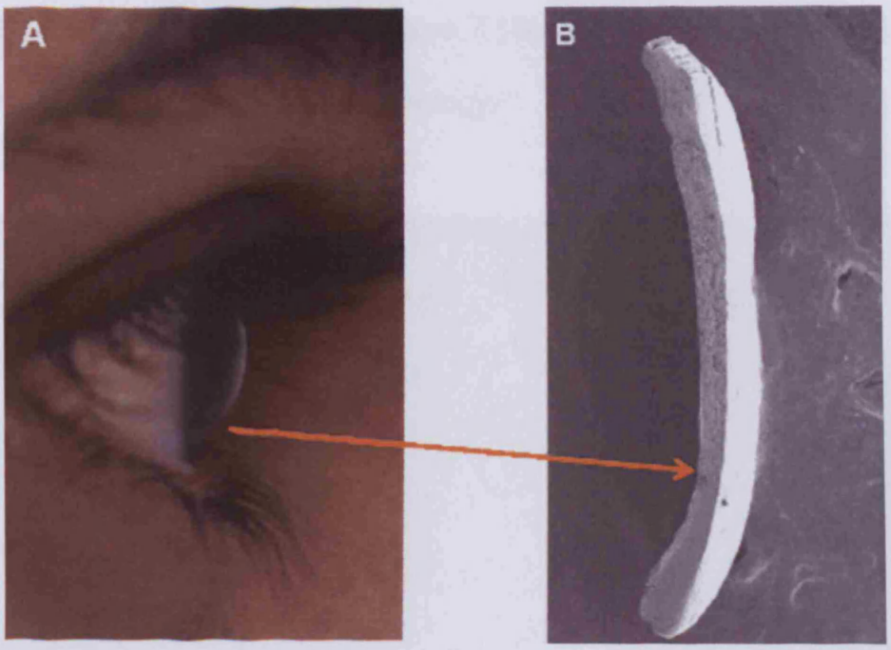

Figure 7.11: (B) is an SEM picture showing a cross section of the cornea with inferior ectasia (arrow head). A normal eye is shown in (A) for illustration purpose only.

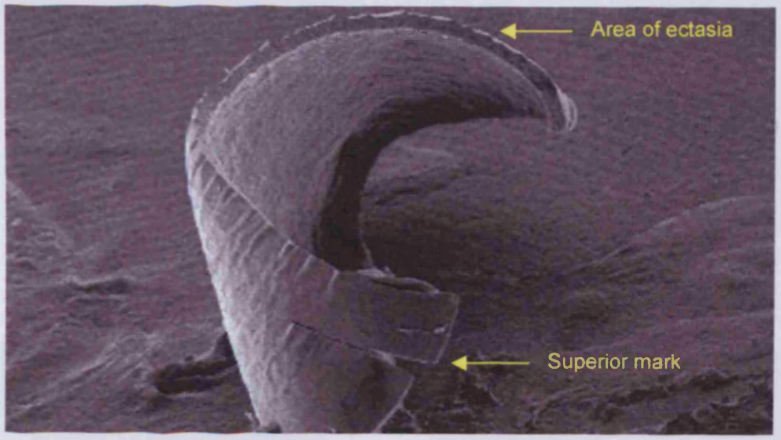

Figure 7.12: SEM picture of LASIK corneal flap only; detached from the remaining cornea after immersion in 10% NaOH.

TEM results show a normal collagen lamellae arrangement on both sides of the flap-bed interface (Figure 7.13). The fibril diameter and interfibrillar spacing appear normal at the area of ectasia (Figure 7.14). By using LM, the interface between the flap and the residual stromal bed can be

detected at different magnifications (Figure 7.15). Moreover, the epithelial and endothelial layers show a normal morphology.

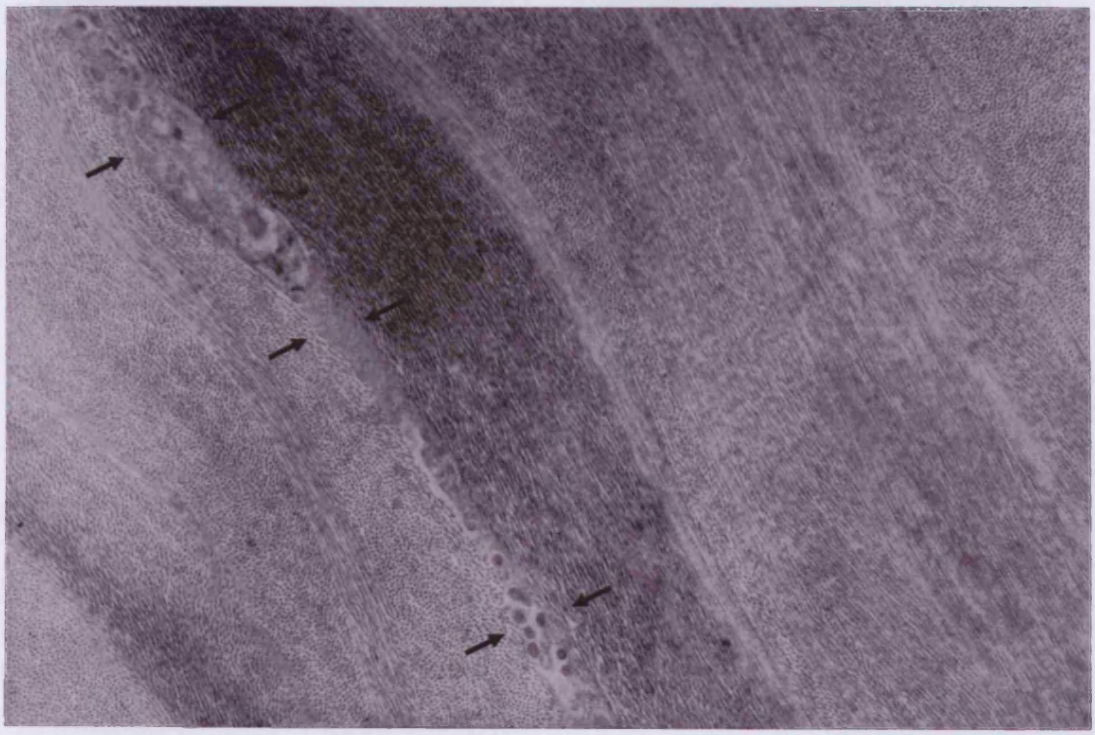

Figure 7.13: TEM image shows general view of the flap-bed interface (black arrows). Collagen lamellae appear parallel to each other and to the corneal surface. In addition, collagen fibrils are well distributed. Original magnification x6000.

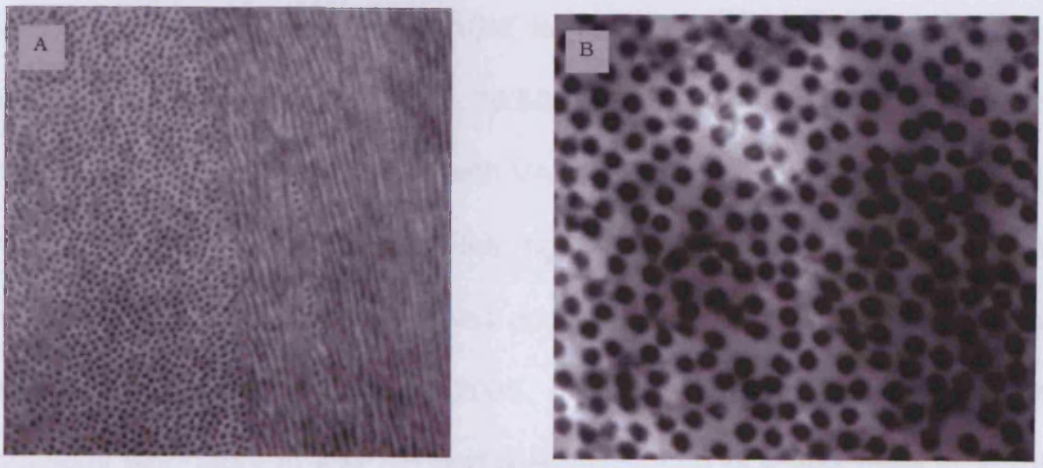

Figure 7.14: TEM pictures of ectatic corneal stroma showing collagen fibril distribution (A) and interfibrillar spacing (B) at different magnifications; (A) x8,000 and (B) x40,000.

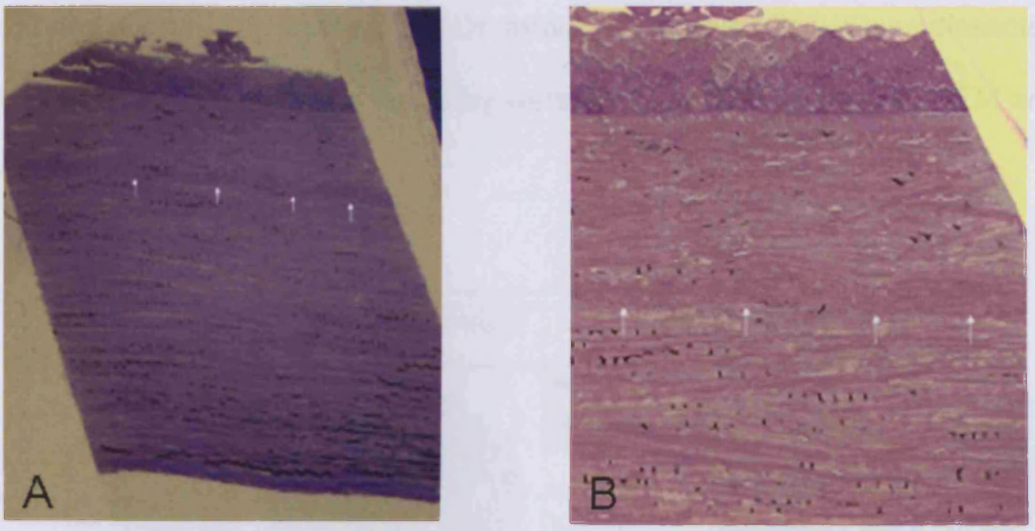

Figure 7.15: LM cross sections of post-LASIK ectatic cornea. Flap border can be seen within the stroma (white arrows). In addition, both epithelial and endothelial layers appear intact. Original magnifications: x10 (A) and x20 (B).

7.3.3 Case 4

A 35-year-old man reported to KKESH (Riyadh, Saudi Arabia) in March 2005 with complaints of reduced VA and dry eyes during the previous 6 years. The patient stated that he had had LASIK surgery in both eyes when he was 25 years old (10 years previously). No pre-LASIK details were provided from the medical centre that ran the LASIK for him. On examination, it was found that the subjective refraction was - 10.50 - 6.00 X 20 with VA of 20/80 for the right eye and - 4.75 - 3.25 X 145 with VA of 20/30 for the left eye. The patient was found to have ectasia in the right eye (Figure 7.16) and myopic astigmatism in the left eye, and was advised to have PKP for the right eye. PKP was performed in January 2006. The grafted button was sent to the pathology laboratory at KKESH and a small portion of it was fixed in a 10% buffered formalin that was then sent to the School of Optometry and Vision

Sciences (Cardiff University, UK). On arrival, the corneal tissue was dissected into small triangular shapes and they were processed to be used in TEM and LM investigations.

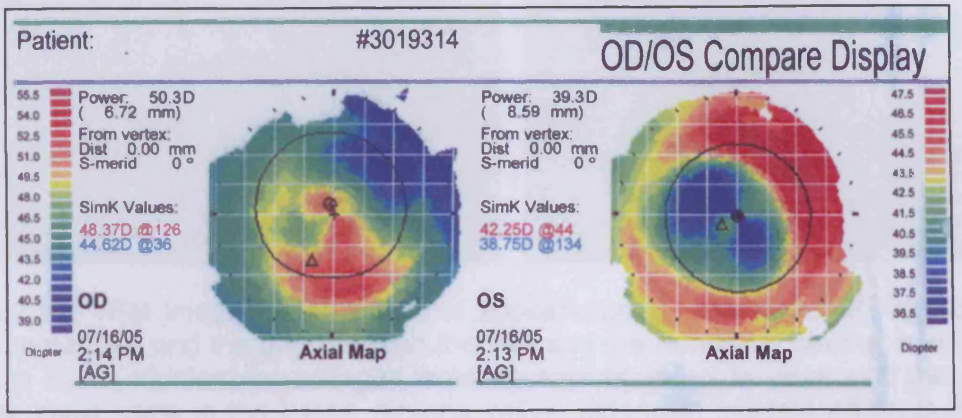

Figure 7.16: Corneal topography of both eyes after LASIK showing inferior steepening on the right eye.

7.3.3.1 Case 4 results

Ten years after LASIK surgery, the flap-bed interface can be detected (Figure 7.17B and 7.19). Figure 7.17A shows a keratocyte within the stroma and close to the flap-bed interface. Both the keratocyte and the surrounding collagen lamellae appear well organised and parallel to the corneal surface. The flap-bed gap can be seen clearly at a higher magnification (Figure 7.17B). There was scar formation along the flap-bed interface. It is believed that due to the weak wound healing, the flap-bed gap occurred after TEM sample preparation. Collagen fibrils in the middle of stroma and within the flap area were well ordered with apparent equal interfibrillar spacing (Figures 7.18 A and B).

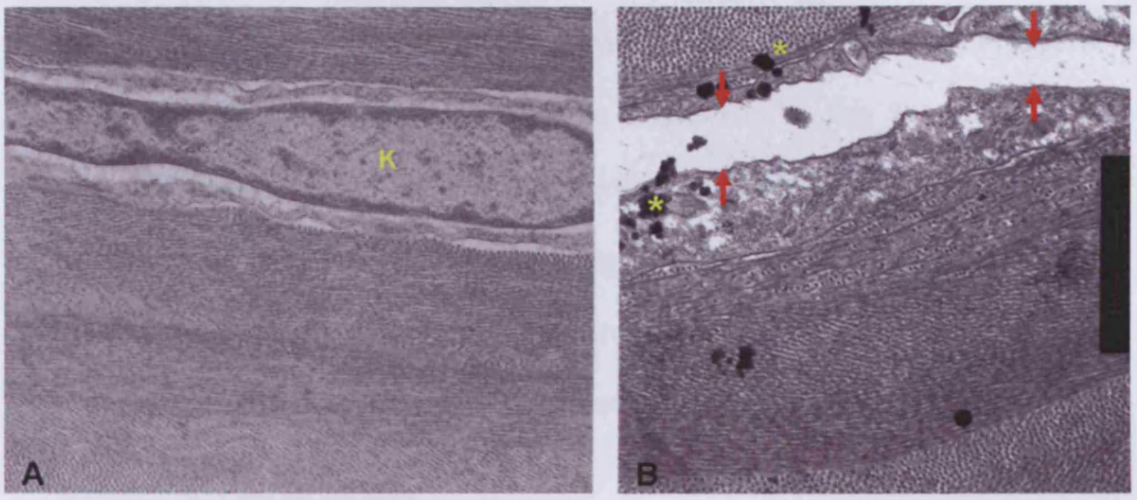

Figure 7.17: TEM images show a normal appearance of keratocytes (K) in ectatic LASIK cornea (A) and the gap between the flap and the remaining stromal bed (red arrows in B). In addition, the collagen lamellae appear well ordered around the gap (B). The black spots in the image (around yellow asterisks) indicate artefacts from TEM film processing. Original magnifications are x16,000 (A) and x20,000 (B).

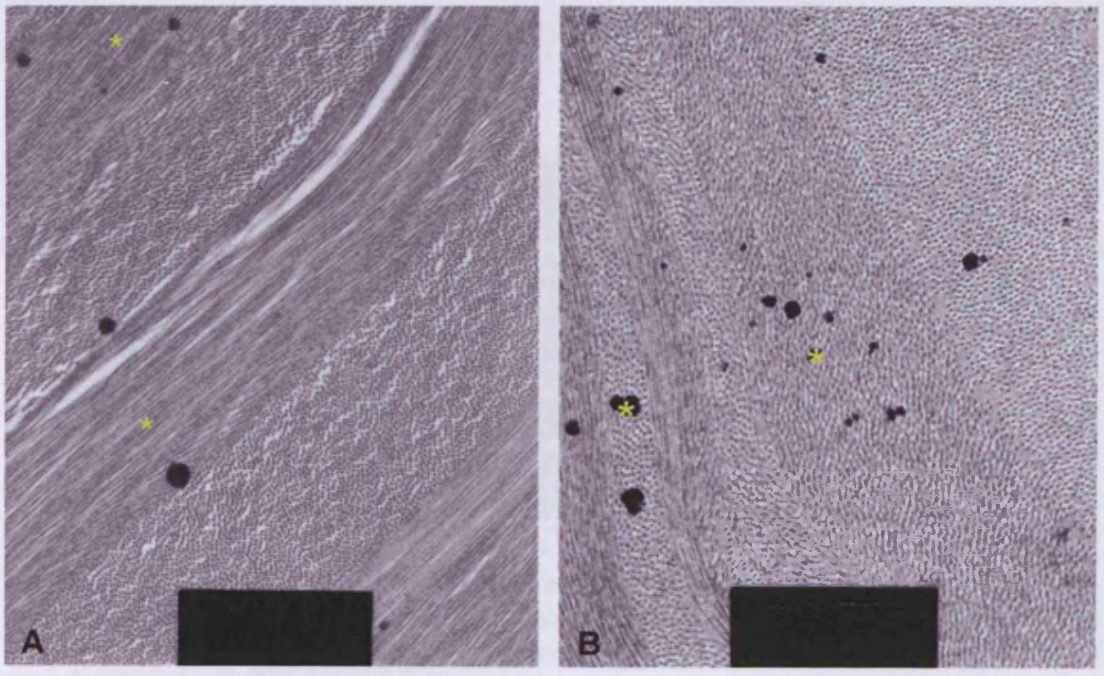

Figure 7.18: TEM images show the collagen fibril distribution in the stroma (A) and in the flap area (B). The collagen lamellae arrangement in the flap area appears slightly waved (B). The black spots in the images (around yellow asterisks) indicate artefacts from TEM film processing. Original magnifications are x16,000 (A) and x20,000 (B).

The flap incision point (flap edge) caused distortion to the surrounding corneal tissues, that is, the epithelium, Bowman's, and anterior stromal layers (Figure 7.19). The epithelial layer shows thickening at the flap edge, but appears normal along the central flap surface. In addition, Bowman's layer shows adjacent folding into the overlying corneal epithelium. The stromal lamellae show alteration in their structure along the flap border with the remaining stroma (Figure 7.19B). The endothelial layer appears intact.

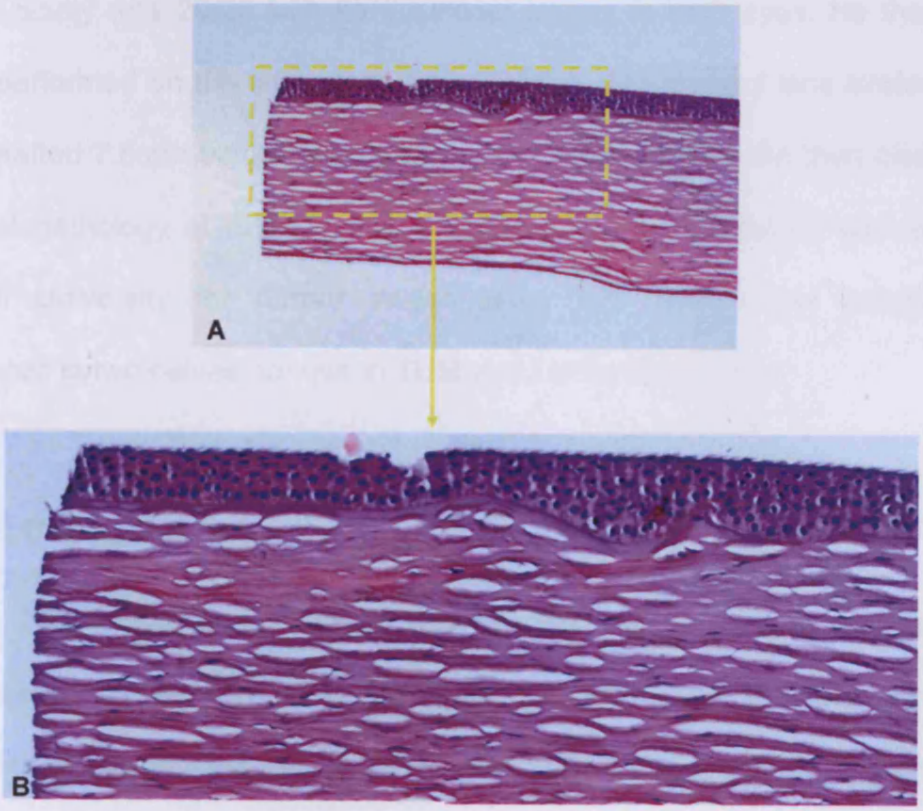

Figure 7.19: LM images show the flap incision point and flap-bed interface. The epithelial thickness is increased and disordered at the flap edge. The collagen lamellae structure is misshapen along the flap-bed interface. Original magnifications are x5 (A) and x10 (B).

7.3.4 Case 5

A 26-year-old male attended KKESH (Riyadh, Saudi Arabia) with a complaint of reduced vision. The patient's ocular history stated that in 1999 he was diagnosed as having myopic astigmatism in both eyes with visual acuity of 20/60 in the right eye and 20/200 in the left eye, and was fitted with hard contact lenses. There was no history of keratoconus in his family. In January 2003, the patient had LASIK surgery in both eyes. Six months after LASIK, the patient was diagnosed as having post-LASIK ectasia in both eyes and his visual acuity was 20/25 with hard contact lenses in both eyes. He then had PKP performed on the left eye in June 2006 due to contact lens intolerance. The grafted 7.5mm button was fixed in 10% buffered formalin then dissected for histopathology at KKESH and a small portion of the button was sent to Cardiff University for further investigation. On receipt, the button was dissected in two halves, for use in TEM and LM investigations.

7.3.4.1 Case 5 results

TEM images show that the collagen lamellae run in a straight fashion and parallel to the corneal surface (Figure 7.20A). The fibril diameter and interfibrillar spacing appear within normal limits (Figure 7.20B). Figure 7.21 shows the LASIK flap-bed interface with what is believed to be scar tissue formation. The collagen lamellae around the space seem to be well organised.

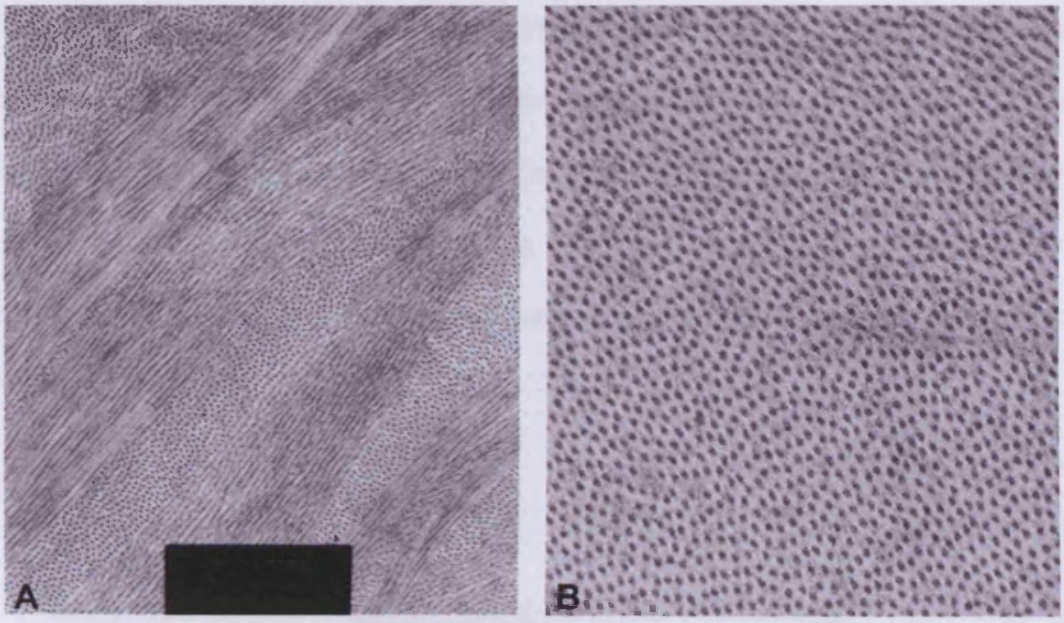

Figure 7.20: TEM images of ectatic cornea after LASIK. (A) Collagen lamellae appear well ordered in the mid of stroma. With higher magnification, interfibrillar spacing appears uniform. (B) Original magnifications are x16,000 (A) and x32,000(B).

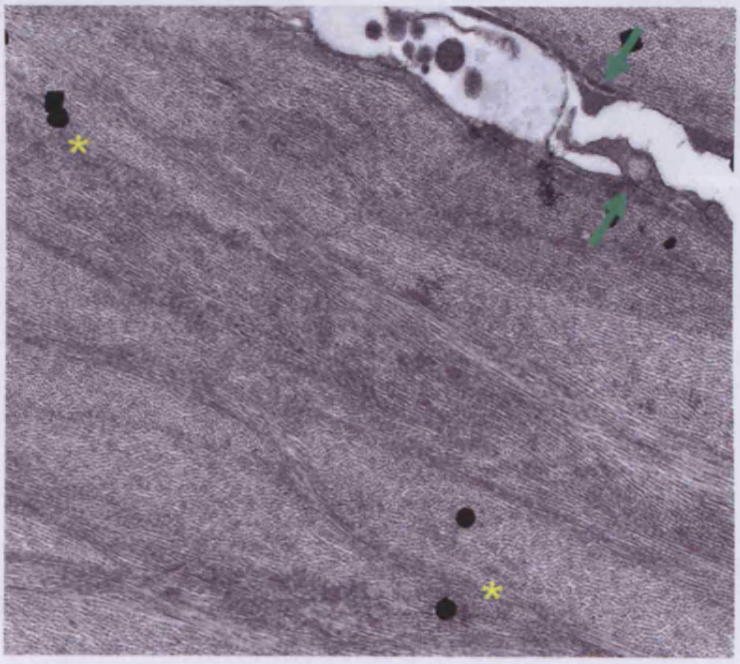

Figure 7.21: TEM image of ectatic cornea after LASIK. Note the flap-bed gap seen between the green arrows with what is believed to be scar tissue formation. Collagen lamellae are ordered and parallel to the corneal surface. Black spots on the image (yellow asterisks) are TEM film processing artefacts. Original magnification x7,000.

LM shows that the corneal epithelium is variable in thickness with a decrease centrally (Figure 7.22A). Bowman's layer is intact along the whole central corneal tissue with a single definite break (gap) with the epithelial layer (Figure 7.22B). The stroma shows a faint separation line at the flap-bed interface indicating the LASIK flap within the anterior part of the stroma (yellow arrows in Figure 7.22).

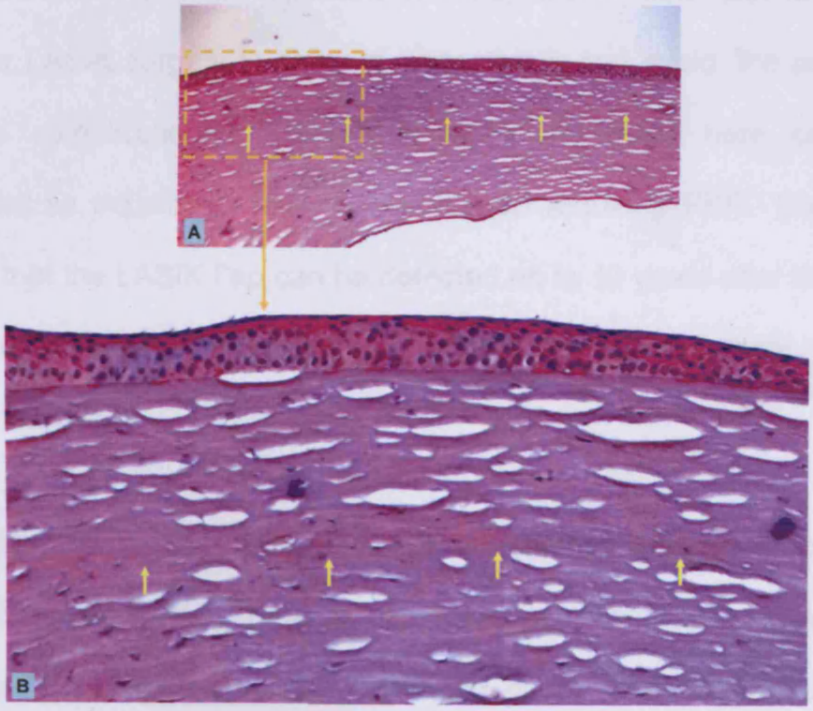

Figure 7.22: LM images of ectatic cornea after LASIK. Yellow arrows indicate the flap-bed border. Collagen lamellae appear slightly changed. Original magnifications are x5 (A) and x10 (B).

7.4 Discussion

Generally, the results of LASIK surgery are excellent and pain-free, with most patients seeing well enough to work or drive without correction the very next day. However, after only one decade of using this procedure, it was

noted that a serious long term complication could arise: ectasia (Seiler *et al.* 1998). It was thought that this side effect happens in some cases of preoperative high myopia, preoperative thin cornea, or preoperative keratoconus, but many studies have reported ectasia in all stages of myopia, in normal corneal thickness (more than 500 μm), or in corneas without keratoconus or forme fruste keratoconus (FFK) (Geggel and Talley 1999; Amoils *et al.* 2000; Joo and Kim 2000; Binder 2003; Klein *et al.* 2006; Condon *et al.* 2007). Therefore, it is important to study the corneal ultrastructural changes after LASIK surgery in order to understand, and avoid, the possible postoperative complications. The LASIK study presented here contains normal as well as ectatic corneas that ended up requiring PKP. The main result shows that the LASIK flap can be detected up to 10 years after surgery, which explains the weakness of the flap and the possibility of ectasia months or years after surgery.

In LASIK, the part of the cornea that is essential to maintain corneal curvature and strength (Park D *et al.* 1995; Muller *et al.* 2001; Klein *et al.* 2006) is sliced off (flapped) to allow the laser beam to ablate the stromal tissue directly and change the shape of the cornea in order to correct the refractive errors. This created flap has been found to contribute minimally to the biomechanical strength of the cornea (Roberts 2000; Philipp *et al.* 2003; Chan and Boxer Wachler 2006), and the residual stromal thickness alone will determine the strength and stability of the cornea which, with time, may become weak and distorted, thus leading to ectasia (Seiler *et al.* 1998; Muller *et al.* 2001; Pallikaris *et al.* 2001; Randleman *et al.* 2003). The factors that are

believed to accelerate the incidence of ectasia after LASIK include intraocular pressure, ocular muscle action and eye rubbing habits (Geggel and Talley 1999; Piccoli *et al.* 2003; Klein *et al.* 2006).

In case 3, the preoperative corneal topography showed steepening of up to 47 D and 1.64 D of asymmetric astigmatism. Only a single, incomplete topographic image was supplied from the patient's previous surgeon (Figure 7.7), which indicates that the patient may have had early keratoconus or FFK. However, it is known that placido-based topographic images can be unreliable as indicators of early keratoconus (Belin and Khachikian 2007). In cases 4 and 5, no preoperative corneal topography or clinical data were provided. Therefore, it was difficult to assume that the patients had had early keratoconus or FFK. In the previous three ectatic cases, ectasia happened in one eye only although LASIK had been performed on both eyes. This may indicate that the patients had had early keratoconus in the affected eye and that LASIK had accelerated the progress of the disease until it became ectasia.

SEM results of normal and ectatic LASIK corneas revealed that the superficial flap edges and the flap-bed interface can be detected easily regardless of the time after the surgery, that is, flap borders have been detected four and five years after the LASIK procedure. In a detailed ultrastructural study of 38 post-mortem LASIK corneas, Dawson *et al.* (Dawson *et al.* 2005a) found two types of wound healing scar associated with the LASIK corneal flap: a hyper-cellular fibrotic scar at the flap wound margin and a hypo-cellular primitive scar at the remaining paracentral and central

areas of lamellar wound. The margin scar works as an adhesive to hold the corneal flap (Dawson *et al.* 2005a). Results from this study confirm that corneal wound healing after LASIK happens superficially (epithelium cell healing only) and the collagen lamellae do not bond with each other again after LASIK. Cases 1 and 2 (Figures 7.1, 7.2, and 7.3) show that the flap edges appear empty, and are separated from the adjunct corneal tissue by 10-20μm (Figure 7.3). This gap occurred after removal of the cellular components, and the collagen lamellae were kept intact by NaOH. In addition, when the ectatic tissue (case 3) was put in NaOH, the LASIK-flap separated from the remaining cornea, indicating that after four years, the flap still does not contribute to the biomechanical integrity of the cornea. This separation did not happen in the normal LASIK cornea (cases 1 and 2) because the trephined ectatic button (8mm) was within the flap area (9mm) and, hence, became separated from the flap hinge or the flap edges, that is, free flap.

In the ectatic button (case 3), SEM results revealed a thinning at the inferior part of the cornea (Figure 7.11), which is usually, but not always, (Faraj *et al.* 2003) seen in both keratoconus and ectasia. (Jonsson and Behndig 2005) found that the thinnest point of the cornea is located in the inferotemporal quadrant. Moreover, Smolek (1993) reported regional differences in the interlamellar strength being lowest in the inferior position, which may explain the presence of ectasia (protrusion) at that region of the cornea. On the other hand, the thickness of the flap was constant at all regions of the cornea, that is, 80 μm at the apex of the ectasia, at the central,

and at superior part of the flap, which means that the factors that lead to thinning do not affect the flap tissue due to the lack of connection.

By using the wide-angle XRD technique, it has been found that the collagen fibril orientation in the 8mm ectatic corneal button (Figure 7.9) is similar to that found in a normal cornea (Figure 3.1) or to the normal collagen fibril arrangement found in corneas after *in vitro* LASIK (Figures 6.1 or 6.2), that is, superior-inferior and nasal-temporal directions (Meek *et al.* 1987; Aghamohammadzadeh *et al.* 2004). However, the XRD map shows a reduction in collagen fibril intensity (collagen fibril number) at the presumed apex of the ectasia (dotted circle in Figure 7.9). These findings may indicate that in ectasia, the preferred collagen fibril orientation does not alter and the thinning that happens at the area of ectasia is due to a loss of collagen lamellae or to intra- or inter-lamella creeping (slippage) as a result of long term biomechanical resistance to the IOP. In keratoconus, both low-angle XRD (Daxer and Fratzl 1997) and wide-angle XRD (Meek *et al.* 2005) concluded that the corneal deformation and protrusion are due to slippage between the collagen fibrils. This conclusion can be applied to the case presented herein, as ectasia has many similar features to keratoconus and, also, collagen lamellae in the presumed central region of ectasia appear to be displaced as indicated by the colour of the polar plots (Figure 7.9). This conclusion could only be confirmed, and so support the finding that LASIK weakens the biomechanical strength of the cornea and predisposes ectasia, if we were to measure the collagen contents and run XRD on the whole

corneoscleral ectatic button, which cannot be done at present because of the difficulty of obtaining ectatic corneoscleral tissue.

TEM results of normal LASIK corneas (Figure 7.4) show that the collagen lamellae around the flap-bed interface are well arranged and parallel to the corneal surface, but appear in a waved shape. This waved shape was also found in the corneas after *in vitro* LASIK (TEM results in Chapter 6). On the other hand, this waved shape was not so obvious in the ectatic corneas (Figures 7.13, 7.18, and 7.20). These varied outcomes were also found in other TEM studies (Jabbur *et al.* 2001; Rumelt *et al.* 2001; Kim *et al.* 2006). There is no clear explanation for the findings of this study but it could be that the instability of the corneal biomechanics after LASIK led to irregularities in the corneal layers. In addition, the results of TEM depend critically on the procedure adopted, the resin employed (Meek and Fullwood 2001), and the area examined, for example, TEM uses high magnification of small areas that may hide other tissue areas from view. The collagen fibril diameter and interfibrillar spacing of both normal and ectatic LASIK corneas (Figures 7.5, 7.14, 7.18, and 7.20) appear similar to those in normal human cornea. The well-ordered collagen lamellae and the normal distribution of collagen fibrils indicate that the reduced vision in ectatic patients is not a result of any disarrangement of the collagen fibrils, which is known to affect corneal transparency, but, instead, is a result of a corneal biomechanics insult due to the flap creation. TEM results support the XRD findings that collagen fibril structures do not change in ectasia.

With LM, the flap-bed interface can be seen clearly in all five cases (Figures 7.6, 7.15, 7.19, and 7.22), which means that the LASIK flap does not heal completely for up to 10 years postoperatively. On the other hand, the epithelial layer structures appear normal, which may indicate that the corneal wound healing happens at the cellular level only. At the microkeratome incision (Figure 7.19), the epithelial layer was thickened, Bowman's layer was folded, and the collagen lamellae arrangement was irregular. These typical changes at the flap edge have been reported in many LASIK studies (Philipp *et al.* 2003; Kramer *et al.* 2005; Dawson *et al.* 2005a; Kim *et al.* 2006; Priglinger *et al.* 2006; Maguen *et al.* 2007). Moreover, case 4 indicates that these changes can be seen up to 10 years post-LASIK. The flap edges of other cases could not be seen in LM because, firstly, the flap edges of the normal LASIK corneas were dissected and were used for SEM and TEM techniques, and secondly, the 8mm PKP trephination inside the 9mm LASIK flap for the other two ectatic corneas did not allow the flap edges to be included in the trephined button.

In summary, this study presents the structural and ultrastructural changes in normal and ectatic corneas after LASIK surgery. It shows that the LASIK flap, undoubtedly, is biomechanically ineffective and does not integrate with the remaining bed of the cornea. Furthermore, the collagen fibril organisation does not change after LASIK, but the number of collagen fibrils appears to be reduced at the area of ectasia if present. More studies, however, are needed to understand the human corneal biomechanics after LASIK and, also, to discover other refractive techniques to correct the

refractive errors without the need for flap creation, which is apparently considered the main cause for ectasia.

Chapter 8. General discussion and conclusion

The aim of this thesis was to study the corneal structure, in particular collagen fibril organisation, in normal and LASIK human corneas. In the beginning (Chapter 3), it was shown that the human cornea possesses a central unique collagen fibril orientation that was not found in large animals, such as camels, or in small animals, such as rabbits, which are frequently used as models for corneal research. However, towards the limbus, the corneas of humans, camels, and rabbits as well as previously reported animals (Quantock *et al.* 2003a; Boote *et al.* 2004; Hayes *et al.* 2007) have the same collagen fibril orientation, that is, an annulus circumscribing the cornea. This common orientation is believed to add strength to the curvature of the cornea where two ocular tissues with different radii of curvature meet, that is, the transparent cornea and the opaque sclera. By looking at this study's results as well as at previous XRD animal results, I can conclude, for the first time, that the large animals possess a vertical collagen orientation whereas the small animals possess a circumferential orientation.

Then, I investigated in greater depth the human corneal ultrastructure to understand the effect of trephination on collagen fibril orientation and distribution, trying to mimic PKP and/or LASIK procedures. The results (Chapter 4) indicate that the central corneal trephination (at 4 mm diameter) will clearly change the collagen fibril orientation or distribution around the trephine-wound edges (Figures 4.5 and 4.6). This change will be less as we move toward the limbus. These results may encourage ophthalmic surgeons,

where possible, to use a large graft diameter for PKP in order to avoid postoperative complications such as astigmatism. However, caution should be taken to avoid graft rejection. These results may also give a good explanation for the low post-LASIK astigmatism rate found in the literature. In addition, Figure 4.7 indicates that the trephined button should be implanted in the same orientation in the recipient cornea to avoid optical or biomechanical problems. This was fully explained in our recent paper (Boote *et al.* 2006), which also concludes that the left and right eyes are structurally different.

After that, I concentrated on studying the LASIK surgery, as it is considered the most frequently performed photorefractive procedure in the world. Corneal structure and ultrastructure was studied after *in vitro* and *in vivo* LASIK (Chapters 6 and 7). Before that, and as LASIK surgery includes flap creation and laser ablation, it was considered important to study the collagen fibril organisation at different corneal depths in order to understand the precise effect of the LASIK technique on collagen lamellae and, also, to expand our knowledge of what has been discovered previously on collagen fibril arrangement (see Chapter 5). By using femtosecond laser technology and wide-angle XRD, it was found that the first third (33%) of the corneal thickness has a distorted collagen fibril orientation whereas the orientation becomes clearly orthogonal towards the posterior cornea (endothelium side). By understanding these details, it can be concluded that the LASIK flap creation and laser stromal ablation occur usually in the irregular collagen fibril layers These layers have been found to be the strongest part of the cornea and essential for maintaining corneal curvature and strength (Park *et al.* 1995;

Muller *et al.* 2001; Klein *et al.* 2006). Therefore, these combined findings allow us to understand in a defined way the reason behind the presence of high astigmatism or ectasia in some LASIK patients. Furthermore, the results presented herein may add valuable information to the ongoing work of the computational finite element models (Pinsky *et al.* 2005; Lanchares *et al.* 2008).

In vitro LASIK was then conducted on donor human corneas to simulate the *in vivo* situation of LASIK and to study the collagen fibril orientation and other changes to the corneal structure by means of XRD, SEM, and TEM. Wide-angle XRD results (Figures 6.1 - 6.3) indicate that the collagen fibril orientation and distribution after LASIK are similar to those for the normal cornea. The results in Chapter 5 show this normal orientation was expected because the flap creation and the laser ablation usually occur in the first third of corneal thickness that already has an isotropic collagen fibril orientation (Figure 5.6). Also, as XRD measures the whole corneal thickness at once, the LASIK-effect cannot be easily detected. The normal collagen fibril orientation was also found in the post-LASIK ectatic cornea (Chapter 7, Figure 7.9). However, the map shows a reduction in the thickness at the presumed apex of the ectasia, which is believed to be due to a loss of collagen lamellae or to intra- or inter-lamella slippage as a result of long term biomechanical resistance to the IOP and the resultant corneal protrusion.

TEM, SEM, and LM of normal and ectatic LASIK corneas (Chapters 6 and 7) showed that the flap-bed interface can be detected easily regardless of the time after the surgery, that is, flap borders have been detected up to 10

years after the LASIK procedure (Chapter 7, case 4). Moreover, applying NaOH on LASIK corneas confirms that corneal wound healing happens superficially (epithelium cell healing only) and the collagen lamellae do not bond with each other again after LASIK, as no bridging fibrils or lamellae between the bed and the flap could be detected, which leaves the flap weak and, thus, explains the easy separation or dislocation of the flap from the bed months or years after surgery. Also, the results give an overview of the corneal biomechanical insults caused by the LASIK flap, which seem difficult to avoid and, in some cases, may lead to ectasia.

Interestingly, the collagen fibril diameter and interfibrillar spacing of both normal and ectatic LASIK corneas appear similar to those in normal human corneas, which may explain the perfect visual acuity results obtained immediately after LASIK surgery and, also, indicate that the reduced vision in ectatic patients is not a result of any disarrangement of the collagen fibrils, which is known to affect corneal transparency, but, instead, is a result of a corneal biomechanics insult due to the flap creation.

In conclusion, the results of this thesis indicate that animal corneas have a collagen fibril orientation different from that found in the human cornea and, therefore, they cannot be used as research models for human-benefit experiments. Also, although LASIK surgery has many advantages over other photorefractive procedures, the resultant corneal biomechanical insult makes it an undesirable procedure and, hence, alternative procedures that provide

the best visual outcomes while at the same time protecting the integrity of the cornea should be investigated.

.....

References

Aghamohammadzadeh H, Newton RH and Meek KM (2004) X-ray scattering used to map the preferred collagen orientation in the human cornea and limbus. *Structure (Camb)* 12(2): 249-256.

Alio J, Ortiz D and Pinero D (2005). Flap biomechanics with the femtosecond and mechanical microkeratomes. Data presented at the Meeting of the European Society of Cataract and Refractive Surgeons. September; Lisbon, Portugal.

Ambrosio R, Jr. and Wilson S (2003) LASIK vs LASEK vs PRK: advantages and indications. *Semin Ophthalmol* 18(1): 2-10.

Amm M, Wetzel W, Winter M, Uthoff D and Duncker GI (1996) Histopathological comparison of photorefractive keratectomy and laser in situ keratomileusis in rabbits. *J Refract Surg* 12(7): 758-766.

Amoils SP, Deist MB, Gous P and Amoils PM (2000) Iatrogenic keratectasia after laser in situ keratomileusis for less than -4.0 to -7.0 diopters of myopia. *Journal of Cataract & Refractive Surgery* 26(7): 967-977.

Anderson NJ, Edelhauser HF, Sharara N, Thompson KP, Rubinfeld RS, Devaney DM, L'Hernault N and Grossniklaus HE (2002) Histologic and ultrastructural findings in human corneas after successful laser in situ keratomileusis. *Arch Ophthalmol* 120(3): 288-293.

Behrens A, Seitz B, Langenbucher A, Kus MM, Rummelt C and Kuchle M (2000) Evaluation of corneal flap dimensions and cut quality using the Automated Corneal Shaper microkeratome. *J Refract Surg* 16(1): 83-89.

Belin MW and Khachikian SS (2007) Keratoconus: it is hard to define, but. *Am J Ophthalmol* 143(3): 500-503.

Benedek GB (1971) The theory of transparancy of the eye. *Appl. Optics.* 10: 459-473.

Benedetto DA, Shah DO and Kaufman HE (1975) The instilled fluid dynamics and surface chemistry of polymers in the preocular tear film. *Invest Ophthalmol* 14(12): 887-902.

Bennett A and Rabbetts R (1998). The schematic eye. Clinical Visual Optics, Butterworth-Heinemann: 207-228.

Binder PS (2003) Ectasia after laser in situ keratomileusis. *J Cataract Refract Surg* 29(12): 2419-2429.

Binder PS (2004) Flap dimensions created with the IntraLase FS laser. *J Cataract Refract Surg* 30(1): 26-32.

Binder PS (2006) One thousand consecutive IntraLase laser in situ keratomileusis flaps. *J Cataract Refract Surg* 32(6): 962-969.

Binder PS, Moore M, Lambert RW and Seagrist DM (1997) Comparison of two microkeratome systems. *J Refract Surg* 13(2): 142-153.

Boote C, Dennis S, Huang Y, Quantock AJ and Meek KM (2005) Lamellar orientation in human cornea in relation to mechanical properties. *J Struct Biol* 149(1): 1-6.

Boote C, Dennis S and Meek K (2004) Spatial mapping of collagen fibril organisation in primate cornea - an X-ray diffraction investigation. *Journal of Structural Biology* 146(3): 359-367.

Boote C, Hayes S, Abahussin M and Meek KM (2006) Mapping collagen organization in the human cornea: left and right eyes are structurally distinct. *Invest Ophthalmol Vis Sci* 47(3): 901-908.

Bores LD (2001) *Refractive eye surgery*2ed Ed.UK, Blackwell Science, Inc.

Bourne WM, Davison JA and O'Fallon WM (1982) The effects of oversize donor buttons on postoperative intraocular pressure and corneal curvature in aphakic penetrating keratoplasty. *Ophthalmology* 89(3): 242-246.

Bozzola J and Russell L (1992) *Electron microscopy, principles and techniques for biologists*Boston, Jones and Bartlett Publishers.

Bozzola J and Russell L (1999) *Electron microscopy, principles and techniques for biologists*2nd ed.Sudbury, USA, Jones and Bartlett Publishers.

Bradbury S and Bracegirdle B (1998) *Introduction to Light Microscopy* 2nd ed.Oxford, UK, BIOS Scientific Publishers.

Brint SF, Ostrick DM, Fisher C, Slade SG, Maloney RK, Epstein R, Stulting RD and Thompson KP (1994) Six-month results of the multicenter phase I study of excimer laser myopic keratomileusis. *J Cataract Refract Surg* 20(6): 610-615.

Buhren J and Kohnen T (2003) Stromal haze after laser in situ keratomileusis: clinical and confocal microscopy findings. *J Cataract Refract Surg* 29(9): 1718-1726.

Buratto L and Bohm E (2007) The use of the femtosecond laser in penetrating keratoplasty. *Am J Ophthalmol* 143(5): 737-742.

Buratto L and Ferrari M (1997) Indications, techniques, results, limits, and complications of laser in situ keratomileusis. *Curr Opin Ophthalmol* 8(4): 59-66.

Burgeson RE (1988) New collagens, new concepts. *Annu Rev Cell Biol* 4: 551-577.

Chan CC and Boxer Wachler BS (2006) Corneal ectasia and refractive surgery. *Int Ophthalmol Clin* 46(3): 13-25.

Chan D, Lamande SR, McQuillan DJ and Bateman JF (1997) In vitro expression analysis of collagen biosynthesis and assembly. *J Biochem Biophys Methods* 36(1): 11-29.

Chapman JA, Tzaphlidou M, Meek KM and Kadler KE (1990) The collagen fibril--a model system for studying the staining and fixation of a protein. *Electron Microsc Rev* 3(1): 143-182.

Chayet AS, Assil KK, Montes M, Espinosa-Lagana M, Castellanos A and Tsioulias G (1998) Regression and its mechanisms after laser in situ keratomileusis in moderate and high myopia. *Ophthalmology* 105(7): 1194-1199.

Chuck RS, Quiros PA, Perez AC and McDonnell PJ (2000) Corneal sensation after laser in situ keratomileusis. *J Cataract Refract Surg* 26(3): 337-339.

Collin SP and Collin HB (2000) A comparative SEM study of the vertebrate corneal epithelium. *Cornea* 19(2): 218-230.

Condon PI (2006) 2005 ESCRS Ridley Medal Lecture: will keratectasia be a major complication for LASIK in the long term? *J Cataract Refract Surg* 32(12): 2124-2132.

Condon PI, O'Keefe M and Binder PS (2007) Long-term results of laser in situ keratomileusis for high myopia: risk for ectasia. *J Cataract Refract Surg* 33(4): 583-590.

Connon CJ and Meek KM (2003) Organization of corneal collagen fibrils during the healing of trephined wounds in rabbits. *Wound Repair Regen* 11(1): 71-78.

Connon CJ and Meek KM (2004) The structure and swelling of corneal scar tissue in penetrating full-thickness wounds. *Cornea* 23(2): 165-171.

Davson H (1984) *The eye*.Vol 1B. 3rd ed.New York, Academic Press.

Dawson D, Kramer T, Grossniklaus H, Waring G and Edelhauser H (2005a) Histologic, ultrstructure, and immunofluorescent evaluation of human laser-assisted in situ keratomileusis corneal wounds. *Arch Ophthalmol* 123: 741-756.

Dawson DG, Holley GP, Geroski DH, Waring GO, 3rd, Grossniklaus HE and Edelhauser HF (2005b) Ex vivo confocal microscopy of human LASIK corneas with histologic and ultrastructural correlation. *Ophthalmology* 112(4): 634-644.

Daxer A and Fratzl P (1997) Collagen fibril orientation in the human corneal stroma and its implication in keratoconus. *Invest Ophthalmol Vis Sci* 38(1): 121-129.

Daxer A, Misof K, Grabner B, Ettl A and Fratzl P (1998) Collagen fibrils in the human corneal stroma: structure and aging. *Investigative Ophthalmology & Visual Science* 39(3): 644-648.

Doane KJ, Yang G and Birk DE (1992) Corneal cell-matrix interactions: type VI collagen promotes adhesion and spreading of corneal fibroblasts. *Exp Cell Res* 200(2): 490-499.

Duke-Elder S and Wybar. aKC (1961) *System of ophthalmology. Vol.2, The anatomy of the visual system*.2 London, Henry Kimpton.

Durrie DS and Aziz AA (1999) Lift-flap retreatment after laser in situ keratomileusis. *J Refract Surg* 15(2): 150-153.

Durrie DS and Kezirian GM (2005) Femtosecond laser versus mechanical keratome flaps in wavefront-guided laser in situ keratomileusis: prospective contralateral eye study. *J Cataract Refract Surg* 31(1): 120-126.

Edelhauser H (1994). Physiology. The cornea, Scientific foundations and clinical practice. G. Smolin and R. Thoft. Boston, Brown and Company: 25-46.

Efron N (2001) *The cornea, its examination in contact lens practice*Oxford, Butterworth-Heinemann.

Ehlers N (1965) The thickness of the precorneal tear film. *Acta Ophthalmol* 81: 92-100.

Eisner RA and Binder PS (2006) Technique for measuring laser in situ keratomileusis flap thickness using the IntraLase laser. *J Cataract Refract Surg* 32(4): 556-558.

Erie JC, Patel SV, McLaren JW, Ramirez M, Hodge DO, Maguire LJ and Bourne WM (2002) Effect of myopic laser in situ keratomileusis on epithelial and stromal thickness: a confocal microscopy study. *Ophthalmology* 109(8): 1447-1452.

Farah SG, Azar DT, Gurdal C and Wong J (1998) Laser in situ keratomileusis: literature review of a developing technique. *J Cataract Refract Surg* 24(7): 989-1006.

Faraj HG, Gatinel D, Chastang PJ and Hoang-Xuan T (2003) Corneal ectasia after LASIK. *J Cataract Refract Surg* 29(1): 220.

Farrell R and McCally R (2000). Corneal transparency. In Principles and practice of ophthalmology. D. Albert and F. Jakobiec. Philadelphia, Saunders company: 629-643.

Fatt I and Weissman BA (1992) *Physiology of the eye: an introduction to the vegetative functions*2ndLondon, Butterworth-Heinemann.

Fiander DC and Tayfour F (1995) Excimer laser in situ keratomileusis in 124 myopic eyes. *J Refract Surg* 11(3 Suppl): S234-238.

Flegler S, Heckman J and Klomparens K (1993) *Scanning and electron microscopy, An introduction*Oxford, UK, Oxford univesity press.

Forrester J, Dick A, McMenamin P and Roberts F (2002) *The eye: basic sciences in practice*2edEdinburgh, WB Saunders.

Fratzl P and Daxer A (1993) Structural transformation of collagen fibrils in corneal stroma during drying. An x-ray scattering study. *Biophysical Journal* 64(4): 1210-1214.

Freund DE, McCally RL, Farrell RA, Cristol SM, L'Hernault NL and Edelhauser HF (1995) Ultrastructure in anterior and posterior stroma of perfused human and rabbit corneas. Relation to transparency. *Invest Ophthalmol Vis Sci* 36(8): 1508-1523.

Friedlaender MH (2006) LASIK surgery using the IntraLase femtosecond laser. *Int Ophthalmol Clin* 46(3): 145-153.

Friend J and Hassell JR (1994). Biochemistry of the cornea. The cornea, Scientific foundations and clinical practice. G. Smolin and R. Thoft. Boston, Brown and Company: 47-68.

Fullwood NJ and Meek KM (1993) A synchroton X-ray study of the changes occurring in the corneal stroma during processing for electron microscopy. *J Microsc* 169 (Pt 1): 53-60.

Gallagher JT (1989) The extended family of proteoglycans: social residents of the pericellular zone. *Curr Opin Cell Biol* 1(6): 1201-1218.

Geggel HS and Talley AR (1999) Delayed onset keratectasia following laser in situ keratomileusis. *J Cataract Refract Surg* 25(4): 582-586.

Giledi O and Daya SM (2003) Unexpected flap thickness in laser in situ keratomileusis. *J Cataract Refract Surg* 29(9): 1825-1826.

Gimbel HV and Levy SG (1998a) Indications, results, and complications of LASIK. *Curr Opin Ophthalmol* 9(4): 3-8.

Gimbel HV, Penno EE, van Westenbrugge JA, Ferensowicz M and Furlong MT (1998b) Incidence and management of intraoperative and early postoperative complications in 1000 consecutive laser in situ keratomileusis cases. *Ophthalmology* 105(10): 1839-1847; discussion 1847-1838.

Gipson I (1994). Anatomy of the conjunctiva, cornea and limbus. The cornea, Scientific foundations and clinical practice. G. Smolin and R. Thoft. Boston, Brown and Company: 3-24.

Goes RM, Laicine EM, Porcionatto MA, Bonciani Nader H and Haddad A (1999) Glycosaminoglycans in components of the rabbit eye: synthesis and characterization. *Curr Eye Res* 19(2): 146-153.

Goldman JN and Benedek GB (1967) The relationship between morphology and transparency in the nonswelling corneal stroma of the shark. *Invest Ophthalmol* 6(6): 574-600.

Goldstein J, Newbury D, Joy D, Lyman C, Echlin P and al E (2002) *Scanning Electron Microscopy and X-ray Microanalysis*3rd ed., Kluwer Academic / Plenum Publishers.

Goodfellow JM, Elliott GF and Woolgar AE (1978) X-ray diffraction studies of the corneal stroma. *J Mol Biol* 119(2): 237-252.

Hamada R, Giraud JP, Graf B and Pouliquen Y (1972) [Analytical and statistical study of the lamellae, keratocytes and collagen fibrils of the central region of the normal human cornea. (Light and electron microscopy)]. *Arch Ophtalmol Rev Gen Ophtalmol* 32(8): 563-570.

Hassell JR, Kimura JH and Hascall VC (1986) Proteoglycan core protein families. *Annu Rev Biochem* 55: 539-567.

Hayat M (1989) *Principles and techniques of electron microscopy, biological applications*3rdLondon, The Macmillan Press Ltd.

Hayes S, Boote C, Lewis J, Sheppard J, Abahussin M, Quantock AJ, Purslow C, Votruba M and Meek KM (2007) Comparative study of fibrillar collagen arrangement in the corneas of primates and other mammals. *Anat Rec (Hoboken)* 290(12): 1542-1550.

Heidemann DG, Sugar A, Meyer RF and Musch DC (1985) Oversized donor grafts in penetrating keratoplasty. A randomized trial. *Arch Ophthalmol* 103(12): 1807-1811.

Helena MC, Baerveldt F, Kim WJ and Wilson SE (1998) Keratocyte apoptosis after corneal surgery. *Invest Ophthalmol Vis Sci* 39(2): 276-283.

Helmy SA, Salah A, Badawy TT and Sidky AN (1996) Photorefractive keratectomy and laser in situ keratomileusis for myopia between 6.00 and 10.00 diopters. *J Refract Surg* 12(3): 417-421.

Hjortdal JO (1998) On the biomechanical properties of the cornea with particular reference to refractive surgery. *Acta Ophthalmol Scand Suppl*(225): 1-23.

Hogan M, Alvarado J and Weddel J (1971) *Histology of the human eye*Philadelphia, WB Saunders.

Holly FJ (1973) Formation and rupture of the tear film. *Experimental Eye Research* 15(5): 515-525.

Holzer MP, Rabsilber TM and Auffarth GU (2006) Femtosecond laser-assisted corneal flap cuts: morphology, accuracy, and histopathology. *Invest Ophthalmol Vis Sci* 47(7): 2828-2831.

Holzer MP, Rabsilber TM and Auffarth GU (2007) Penetrating keratoplasty using femtosecond laser. *Am J Ophthalmol* 143(3): 524-526.

Ihanamaki T, Pelliniemi LJ and Vuorio E (2004) Collagens and collagen-related matrix components in the human and mouse eye. *Prog Retin Eye Res* 23(4): 403-434.

Isager P, Guo S, Hjortdal JO and Ehlers N (1998) Endothelial cell loss after photorefractive keratectomy for myopia. *Acta Ophthalmol Scand* 76(3): 304-307.

Iskander NG, Peters NT, Penno EA and Gimbel HV (2000) Postoperative complications in laser in situ keratomileusis. *Current Opinion in Ophthalmology* 11(4): 273-279.

Jabbur NS, Stark WJ and Green WR (2001) Corneal ectasia after laser-assisted in situ keratomileusis. *Arch Ophthalmol* 119(11): 1714-1716.

Jacobsen IE, Jensen OA and Prause JU (1984) Structure and composition of Bowman's membrane. Study by frozen resin cracking. *Acta Ophthalmol (Copenh)* 62(1): 39-53.

Jacobsen N and Hojgaard-Olsen K (2006) Promising results using the Hanna Corneal Trephine System in penetrating keratoplasty. *Cornea* 25(4): 371-376.

Javadi MA, Naderi M, Zare M, Jenaban A, Rabei HM and Anissian A (2006) Comparison of the effect of three suturing techniques on postkeratoplasty astigmatism in keratoconus. *Cornea* 25(9): 1029-1033.

Javaloy J, Vidal MT, Abdelrahman AM, Artola A and Alio JL (2007) Confocal microscopy comparison of intralase femtosecond laser and Moria M2 microkeratome in LASIK. *J Refract Surg* 23(2): 178-187.

Johnson ME and Murphy PJ (2004) Changes in the tear film and ocular surface from dry eye syndrome. *Prog Retin Eye Res* 23(4): 449-474.

Jones SS, Azar RG, Cristol SM, Geroski DH, Waring GO, 3rd, Stulting RD, Thompson KP and Edelhauser HF (1998) Effects of laser in situ keratomileusis (LASIK) on the corneal endothelium. *Am J Ophthalmol* 125(4): 465-471.

Jonsson M and Behndig A (2005) Pachymetric evaluation prior to laser in situ keratomileusis. *J Cataract Refract Surg* 31(4): 701-706.

Joo CK and Kim TG (2000) Corneal ectasia detected after laser in situ keratomileusis for correction of less than -12 diopters of myopia. *J Cataract Refract Surg* 26(2): 292-295.

Kaji Y, Obata H, Usui T, Soya K, Machinami R, Tsuru T and Yamashita H (1998) Three-dimensional organization of collagen fibrils during corneal stromal wound healing after excimer laser keratectomy. *J Cataract Refract Surg* 24(11): 1441-1446.

Kanellopoulos A, Pallikaris I, Donnenfeld E, Detorakis S, Koufala K and Perry aH (1997) Comparison of corneal sensation following photorefractive keratectomy and laser in situ keratomileusis. *J Cataract Refract Surg* 23: 34-38.

Karabatsas CH, Cook SD, Figueiredo FC, Diamond JP and Easty DL (1998) Combined interrupted and continuous versus single continuous adjustable suturing in penetrating keratoplasty: a prospective, randomized study of induced astigmatism during the first postoperative year. *Ophthalmology* 105(11): 1991-1998.

Kato T, Nakayasu K, Hosoda Y, Watanabe Y and Kanai A (1999) Corneal wound healing following laser in situ keratomileusis (LASIK): a histopathological study in rabbits. *Br J Ophthalmol* 83(11): 1302-1305.

Kaufman H, Barron B, McDonald M and Waltman S (1988) *The cornea*London, Churchill Livingstone.

Kaufman SC, Maitchouk DY, Chiou AG and Beuerman RW (1998) Interface inflammation after laser in situ keratomileusis. Sands of the Sahara syndrome. *J Cataract Refract Surg* 24(12): 1589-1593.

Keene DR, Lunstrum GP, Morris NP, Stoddard DW and Burgeson RE (1991) Two type XII-like collagens localize to the surface of banded collagen fibrils. *J Cell Biol* 113(4): 971-978.

Kezirian GM and Stonecipher KG (2004) Comparison of the IntraLase femtosecond laser and mechanical keratomes for laser in situ keratomileusis. *J Cataract Refract Surg* 30(4): 804-811.

Kim H, Song IK and Joo CK (2006) Keratectasia after laser in situ keratomileusis. Clinicopathological case report. *Ophthalmologica* 220(1): 58-64.

Klein SR, Epstein RJ, Randleman JB and Stulting RD (2006) Corneal ectasia after laser in situ keratomileusis in patients without apparent preoperative risk factors. *Cornea* 25(4): 388-403.

Klyse S and Beuerman aR (1989). Structure and function of the cornea. The cornea. H. K. e. al. New York, Churchill Living stone: 3-28.

Knorz MC, Wiesinger B, Liermann A, Seiberth V and Liesenhoff H (1998) Laser in situ keratomileusis for moderate and high myopia and myopic astigmatism. *Ophthalmology* 105(5): 932-940.

Kokott W (1938) Ubermechanisch-funktionelle strikturen des auges. Albrecht von Graefes. *archives of ophthalmology* 138: 424-485.

Komai Y and Ushiki T (1991) The three-dimensional organization of collagen fibrils in the human cornea and sclera. *Invest Ophthalmol Vis Sci* 32(8): 2244-2258.

Korb DR (2002) *The tear film: structure, function and clinical examination*Oxford, Butterworth-Heinemann.

Kramer TR, Chuckpaiwong V, Dawson DG, L'Hernault N, Grossniklaus HE and Edelhauser HF (2005) Pathologic findings in postmortem corneas after successful laser in situ keratomileusis. *Cornea* 24(1): 92-102.

Kremer FB and Dufek M (1995) Excimer laser in situ keratomileusis. *J Refract Surg* 11(3 Suppl): S244-247.

Kurtz RM, Liu X, Elner VM, Squier JA, Du D and Mourou GA (1997) Photodisruption in the human cornea as a function of laser pulse width. *J Refract Surg* 13(7): 653-658.

Kymionis GD, Tsiklis N, Pallikaris AI, Bouzoukis DI and Pallikaris IG (2007) Fifteen-year follow-up after LASIK: case report. *J Refract Surg* 23(9): 937-940.

Lamonde SR and Bateman JF (1997) Procollagen folding and assembly: the role of endoplasmic reticulum enzymes and molecular chaperones. *Cell Develop Biol* 10: 455-464.

Lanchares E, Calvo B, Cristobal JA and Doblare M (2008) Finite element simulation of arcuates for astigmatism correction. *J Biomech* 41(4): 797-805.

Latvala T, Barraquer-Coll C, Tervo K and Tervo T (1996) Corneal wound healing and nerve morphology after excimer laser in situ keratomileusis in human eyes. *J Refract Surg* 12(6): 677-683.

Lee BH, McLaren JW, Erie JC, Hodge DO and Bourne WM (2002) Reinnervation in the cornea after LASIK. *Invest Ophthalmol Vis Sci* 43(12): 3660-3664.

Lee JB, Kim JS, Choe C-M, Seong GJ and Kim EK (2001) Comparison of Two Procedures: Photorefractive Keratectomy Versus Laser In Situ Keratomileusis for Low to Moderate Myopia. *Japanese Journal of Ophthalmology* 45(5): 487-491.

Li HF, Petroll WM, Moller-Pedersen T, Maurer JK, Cavanagh HD and Jester JV (1997) Epithelial and corneal thickness measurements by in vivo confocal microscopy through focusing (CMTF). *Curr Eye Res* 16(3): 214-221.

Li W, Vergnes JP, Cornuet PK and Hassell JR (1992) cDNA clone to chick corneal chondroitin/dermatan sulfate proteoglycan reveals identity to decorin. *Arch Biochem Biophys* 296(1): 190-197.

Lin JM and Tsai YY (2005) Laser in situ keratomileusis for different degrees of myopia. *Acta Ophthalmol Scand* 83(1): 40-45.

Lohmann CP and Guell JL (1998) Regression after LASIK for the treatment of myopia: the role of the corneal epithelium. *Semin Ophthalmol* 13(2): 79-82.

Lombardo AJ and Katz HR (2001) Late partial dislocation of a laser in situ keratomileusis flap. *J Cataract Refract Surg* 27(7): 1108-1110.

Maguen E, Maguen B, Regev L and Ljubimov AV (2007) Immunohistochemical evaluation of two corneal buttons with post-LASIK keratectasia. *Cornea* 26(8): 983-991.

Margaritondo G (1988) *Introduction to synchrotron radiation*, Oxford University Press.

Maurice D (1969). The cornea and sclera. *in* The eye. H. Davson. London, Academic press. 1: 489-600.

Maurice DM (1957) The structure and transparency of the cornea. *J Physiol* 136(2): 263-286.

Maurice DM (1984). The corena and sclera. The eye. H. Davson. London, Academic Press, INC. 1b.

Maurice DM and Riley MV (1970). The cornea. Biochemistry of the eye. C. N. Graymore. New York, Academic.

May C-A, Priglinger SG, Neubauer AS, Alge CS, Ludwig K, Kampik A and Welge-Lu[beta]en U (2004) Laser in situ keratomileusis in human corneas: new organ culture model. *Journal of Cataract & Refractive Surgery* 30(1): 186-193.

Meek G (1973) *Practical electron microscopy for biologists*London, John Wiley & Sons ltd.

Meek KM, Blamires T, Elliott GF, Gyi TJ and Nave C (1987) The organisation of collagen fibrils in the human corneal stroma: a synchrotron X-ray diffraction study. *Curr Eye Res* 6(7): 841-846.

Meek KM, Elliott GF and Nave C (1986) A synchrotron X-ray diffraction study of bovine cornea stained with cupromeronic blue. *Coll Relat Res* 6(2): 203-218.

Meek KM, Elliott GF, Sayers Z, Whitburn SB and Koch MH (1981) Interpretation of the meridional x-ray diffraction pattern from collagen fibrils in corneal stroma. *J Mol Biol* 149(3): 477-488.

Meek KM and Fullwood NJ (2001) Corneal and scleral collagens--a microscopist's perspective. *Micron* 32(3): 261-272.

Meek KM, Fullwood NJ, Cooke PH, Elliott GF, Maurice DM, Quantock AJ, Wall RS and Worthington CR (1991) Synchrotron x-ray diffraction studies of the cornea, with implications for stromal hydration. *Biophys J* 60(2): 467-474.

Meek KM and Leonard DW (1993) Ultrastructure of the corneal stroma: a comparative study. *Biophys J* 64(1): 273-280.

Meek KM, Leonard DW, Connon CJ, Dennis S and Khan S (2003) Transparency, swelling and scarring in the corneal stroma. *Eye* 17(8): 927-936.

Meek KM and Quantock AJ (2001) The use of X-ray scattering techniques to determine corneal ultrastructure. *Prog Retin Eye Res* 20(1): 95-137.

Meek KM, Tuft SJ, Huang Y, Gill PS, Hayes S, Newton RH and Bron AJ (2005) Changes in collagen orientation and distribution in keratoconus corneas. *Invest Ophthalmol Vis Sci* 46(6): 1948-1956.

Melki SA and Azar DT (2001) LASIK complications: etiology, management, and prevention. *Surv Ophthalmol* 46(2): 95-116.

Michelacci YM (2003) Collagens and proteoglycans of the corneal extracellular matrix. *Braz J Med Biol Res* 36(8): 1037-1046.

Miyamoto T, Saika S, Yamanaka A, Kawashima Y, Suzuki Y and Ohnishi Y (2003) Wound healing in rabbit corneas after photorefractive keratectomy and laser in situ keratomileusis. *J Cataract Refract Surg* 29(1): 153-158.

Mohan RR, Hutcheon AEK, Choi R, Hong J, Lee J, Mohan RR, Ambrosio J, Renato, Zieske JD and Wilson SE (2003) Apoptosis, necrosis, proliferation, and myofibroblast generation in the stroma following LASIK and PRK. *Experimental Eye Research* 76(1): 71-87.

Moller-Pedersen T and Ehlers N (1995) A three-dimensional study of the human corneal keratocyte density. *Curr Eye Res* 14(6): 459-464.

Moller-Pedersen T, Ledet T and Ehlers N (1994) The keratocyte density of human donor corneas. *Curr Eye Res* 13(2): 163-169.

Montes-Mico R, Rodriguez-Galietero A and Alio JL (2007) Femtosecond laser versus mechanical keratome LASIK for myopia. *Ophthalmology* 114(1): 62-68.

Mootha VV, Dawson D, Kumar A, Gleiser J, Qualls C and Albert DM (2004) Slitlamp, specular, and light microscopic findings of human donor corneas after laser-assisted in situ keratomileusis. *Arch Ophthalmol* 122(5): 686-692.

Muller LJ, Pels E, Schurmans LRHM and Vrensen GFJM (2004) A new three-dimensional model of the organization of proteoglycans and collagen fibrils in the human corneal stroma. *Experimental Eye Research* 78(3): 493-501.

Muller LJ, Pels E and Vrensen GF (2001) The specific architecture of the anterior stroma accounts for maintenance of corneal curvature. *Br J Ophthalmol* 85(4): 437-443.

Muller LJ, Pels L and Vrensen GF (1995) Novel aspects of the ultrastructural organization of human corneal keratocytes. *Invest Ophthalmol Vis Sci* 36(13): 2557-2567.

Musch DC, Meyer RF, Sugar A and Soong HK (1989) Corneal astigmatism after penetrating keratoplasty. The role of suture technique. *Ophthalmology* 96(5): 698-703.

Myllyharju J and Kivirikko KI (2001) Collagens and collagen-related diseases. *Ann Med* 33(1): 7-21.

Nakamura K, Kurosaka D, Bissen-Miyajima H and Tsubota K (2001) Intact corneal epithelium is essential for the prevention of stromal haze after laser assisted in situ keratomileusis. *Br J Ophthalmol* 85(2): 209-213.

Netto MV, Mohan RR, Medeiros FW, Dupps WJ, Jr., Sinha S, Krueger RR, Stapleton WM, Rayborn M, Suto C and Wilson SE (2007) Femtosecond laser and microkeratome corneal flaps: comparison of stromal wound healing and inflammation. *J Refract Surg* 23(7): 667-676.

Newsome DA, Foidart JM, Hassell JR, Krachmer JH, Rodrigues MM and Katz SI (1981) Detection of specific collagen types in normal and keratoconus corneas. *Invest Ophthalmol Vis Sci* 20(6): 738-750.

Newsome DA, Gross J and Hassell JR (1982) Human corneal stroma contains three distinct collagens. *Invest Ophthalmol Vis Sci* 22(3): 376-381.

Newton RH (2001) mapping the orientation of the collagen fibrils. *ARVO abstract 1517.*

Newton RH and Meek KM (1998a) Circumcorneal annulus of collagen fibrils in the human limbus. *Invest Ophthalmol Vis Sci* 39(7): 1125-1134.

Newton RH and Meek KM (1998b) The integration of the corneal and limbal fibrils in the human eye. *Biophysical Journal* 75(5): 2508-2512.

Nilforoushan MR, Speaker MG and Latkany R (2005) Traumatic flap dislocation 4 years after laser in situ keratomileusis. *J Cataract Refract Surg* 31(8): 1664-1665.

Nordan LT, Slade SG, Baker RN, Suarez C, Juhasz T and Kurtz R (2003) Femtosecond laser flap creation for laser in situ keratomileusis: six-month follow-up of initial U.S. clinical series. *J Refract Surg* 19(1): 8-14.

Ohtani O (1987) Three-dimensional organization of the connective tissue fibers of the human pancreas: a scanning electron microscopic study of NaOH treated-tissues. *Arch Histol Jpn* 50(5): 557-566.

Osuobeni EP and Hamidzada WA (1999) Ultrasonographic determination of the dimensions of ocular components in enucleated eyes of the one-humped camel (Camelus dromedarius). *Research in Veterinary Science* 67(2): 125.

Ou RJ, Shaw EL and Glasgow BJ (2002) Keratectasia after laser in situ keratomileusis (LASIK): evaluation of the calculated residual stromal bed thickness. *Am J Ophthalmol* 134(5): 771-773.

Oyster CW (1999) *The human eye: structure and function*, Sinauer Associates.

Pallikaris IG, Kymionis GD and Astyrakakis NI (2001) Corneal ectasia induced by laser in situ keratomileusis. *J Cataract Refract Surg* 27(11): 1796-1802.

Pallikaris IG, Papatzanaki ME, Siganos DS and Tsilimbaris MK (1991) A corneal flap technique for laser in situ keratomileusis. Human studies. *Arch Ophthalmol* 109(12): 1699-1702.

Pallikaris IG, Papatzanaki ME, Stathi EZ, Frenschock O and Georgiadis A (1990) Laser in situ keratomileusis. *Lasers Surg Med* 10(5): 463-468.

Pallikaris IG and Siganos DS (1994) Excimer laser in situ keratomileusis and photorefractive keratectomy for correction of high myopia. *J Refract Corneal Surg* 10(5): 498-510.

Park CK and Kim JH (1999) Comparison of wound healing after photorefractive keratectomy and laser in situ keratomileusis in rabbits. *J Cataract Refract Surg* 25(6): 842-850.

Park D, Perez E and D. M (1995) Corneal lamellar strength as determined by thickness, position, and fibril orientation. *Invest Ophthalmol Vis Sci.* 36((suppl)): 39.

Park D, Perez E and Miller D (1995) Corneal lamellar strength as determined by thickness, position, and fibril orientation. *Invest Ophthalmol Vis Sci.* 36((suppl)): 39.

Perez-Santonja JJ, Linna TU, Tervo KM, Sakla HF, Alio y Sanz JL and Tervo TM (1998) Corneal wound healing after laser in situ keratomileusis in rabbits. *J Refract Surg* 14(6): 602-609.

Perlman EM (1981) An analysis and interpretation of refractive errors after penetrating keratoplasty. *Ophthalmology* 88(1): 39-45.

Petroll WM, Boettcher K, Barry P, Cavanagh HD and Jester JV (1995) Quantitative assessment of anteroposterior keratocyte density in the normal rabbit cornea. *Cornea* 14(1): 3-9.

Philipp WE, Speicher L and Gottinger W (2003) Histological and immunohistochemical findings after laser in situ keratomileusis in human corneas. *J Cataract Refract Surg* 29(4): 808-820.

Piccoli PM, Gomes AA and Piccoli FV (2003) Corneal ectasia detected 32 months after LASIK for correction of myopia and asymmetric astigmatism. *J Cataract Refract Surg* 29(6): 1222-1225.

Pinsky PM, van der Heide D and Chernyak D (2005) Computational modeling of mechanical anisotropy in the cornea and sclera. *J Cataract Refract Surg* 31(1): 136-145.

Pisella P-J, Auzerie O, Bokobza Y, Debbasch C and Baudouin C (2001) Evaluation of corneal stromal changes in vivo after laser in situ keratomileusis with confocal microscopy. *Ophthalmology* 108(10): 1744-1750.

Polack FM (1961) Morphology of the cornea. I. Study with silver stains. *Am J Ophthalmol* 51: 1051-1056.

Porter J, MacRae S, Yoon G, Roberts C, Cox IG and Williams DR (2003) Separate effects of the microkeratome incision and laser ablation on the eye's wave aberration. *American Journal of Ophthalmology* 136(2): 327-337.

Prangen AD (1928) A Study of the Comparative Anatomy of the Extra-ocular Muscles. *Trans Am Ophthalmol Soc* 26: 353-380.

Price FW, Jr., Whitson WE, Johns S and Gonzales JS (1996) Risk factors for corneal graft failure. *J Refract Surg* 12(1): 134-143; discussion 143-137.

Priglinger SG, May CA, Alge CS, Wolf A, Neubauer AS, Haritoglou C, Kampik A and Welge-Lussen U (2006) Immunohistochemical findings after LASIK confirm in vitro LASIK model. *Cornea* 25(3): 331-335.

Prince J (1960) *Anatomy and histology of the eye and orbit in domestic animals.*Springfield, IL, Charles C Thomas.

Prince JH (1964). The cornea. The rabbit in eye research, Thomas books. J. H. Prince, Springfield.

Principe AH, Lin DY, Small KW and Aldave AJ (2004) Macular hemorrhage after laser in situ keratomileusis (LASIK) with femtosecond laser flap creation. *Am J Ophthalmol* 138(4): 657-659.

Probst L (2004). Comparison of excimer lasers. LASIK: advances, contraversies, and custom. L. Probst. New Jersy, SLACK Incorporated: Chap 6.

Probst LE and Machat JJ (1998) Mathematics of laser in situ keratomileusis for high myopia. *J Cataract Refract Surg* 24(2): 190-195.

Prydal JI, Artal P, Woon H and Campbell FW (1992) Study of human precorneal tear film thickness and structure using laser interferometry. *Invest Ophthalmol Vis Sci* 33(6): 2006-2011.

Quantock AJ, Boote C, Siegler V and Meek KM (2003a) Collagen organization in the secondary chick cornea during development. *Invest Ophthalmol Vis Sci* 44(1): 130-136.

Quantock AJ, Dennis S, Adachi W, Kinoshita S, Boote C, Meek KM, Matsushima Y and Tachibana M (2003b) Annulus of collagen fibrils in mouse cornea and structural matrix alterations in a murine-specific keratopathy. *Investigative Ophthalmology & Visual Science* 44(5): 1906-1911.

Quantock AJ, Meek KM and Chakravarti S (2001) An X-ray diffraction investigation of corneal structure in lumican-deficient mice. *Investigative Ophthalmology & Visual Science* 42(8): 1750-1756.

Rabinowitz YS (1998) Keratoconus. *Surv Ophthalmol* 42(4): 297-319.

Rad AS, Jabbarvand M and Saifi N (2004) Progressive keratectasia after laser in situ keratomileusis. *J Refract Surg* 20(5 Suppl): S718-722.

Rada JA, Cornuet PK and Hassell JR (1993) Regulation of corneal collagen fibrillogenesis in vitro by corneal proteoglycan (lumican and decorin) core proteins. *Exp Eye Res* 56(6): 635-648.

Radner W and Mallinger R (2002) Interlacing of collagen lamellae in the midstroma of the human cornea. *Cornea* 21(6): 598-601.

Radner W, Skorpik C, Loewe R, Mudrich C, Radner G and Mallinger R (1999) Effect of trephination technique on the ultrastructure of corneal transplants: guided trephine system v posterior punch technique. *Br J Ophthalmol* 83(10): 1172-1177.

Radner W, Zehetmayer M, Aufreiter R and Mallinger R (1998) Interlacing and cross-angle distribution of collagen lamellae in the human cornea.[see comment]. *Cornea* 17(5): 537-543.

Rajan MS, Watters W, Patmore A and Marshall J (2005) In vitro human corneal model to investigate stromal epithelial interactions following refractive surgery. *J Cataract Refract Surg* 31(9): 1789-1801.

Ramirez M, Quiroz-Mercado H, Hernandez-Quintela E and Naranjo-Tackman R (2007) Traumatic flap dislocation 4 years after LASIK due to air bag injury. *J Refract Surg* 23(7): 729-730.

Randleman JB, Loft ES, Banning CS, Lynn MJ and Stulting RD (2007) Outcomes of wavefront-optimized surface ablation. *Ophthalmology* 114(5): 983-988.

Randleman JB, Russell B, Ward MA, Thompson KP and Stulting RD (2003) Risk factors and prognosis for corneal ectasia after LASIK. *Ophthalmology* 110(2): 267-275.

Ratkay-Traub I, Ferincz IE, Juhasz T, Kurtz RM and Krueger RR (2003) First clinical results with the femtosecond neodynium-glass laser in refractive surgery. *J Refract Surg* 19(2): 94-103.

Ratkay-Traub I, Juhasz T, Horvath C, Suarez C, Kiss K, Ferincz I and Kurtz R (2001) Ultra-short pulse (femtosecond) laser surgery: initial use in LASIK flap creation. *Ophthalmol Clin North Am* 14(2): 347-355, viii-ix.

Rawe IM, Meek KM, Leonard DW, Takahashi T and Cintron C (1994) Structure of corneal scar tissue: an X-ray diffraction study. *Biophys J* 67(4): 1743-1748.

Roberts C (2000) The cornea is not a piece of plastic. *J Refract Surg* 16(4): 407-413.

Rosen ES (2000) LASIK mania. *J Cataract Refract Surg* 26(3): 303-304.

Rumelt S, Cohen I, Skandarani P, Delarea Y, Shaul YB and Rehany U (2001) Ultrastructure of the lamellar corneal wound after laser in situ keratomileusis in human eye. *Journal of Cataract & Refractive Surgery* 27(8): 1323-1327.

Salah T, Waring GO, 3rd, el Maghraby A, Moadel K and Grimm SB (1996) Excimer laser in situ keratomileusis under a corneal flap for myopia of 2 to 20 diopters. *Am J Ophthalmol* 121(2): 143-155.

Salchow DJ, Zirm ME, Pfaller K and Stiedorf C (1999) Histology after lamellar keratoplasty and corneal excimer laser ablation. *J Refract Surg* 15(5): 590-593.

Sarayba MA, Ignacio TS, Binder PS and Tran DB (2007b) Comparative study of stromal bed quality by using mechanical, IntraLase femtosecond laser 15- and 30-kHz microkeratomes. *Cornea* 26(4): 446-451.

Sarayba MA, Ignacio TS, Tran DB and Binder PS (2007a) A 60 kHz IntraLase femtosecond laser creates a smoother LASIK stromal bed surface compared to a Zyoptix XP mechanical microkeratome in human donor eyes. *J Refract Surg* 23(4): 331-337.

Sato K, Yomogida K, Wada T, Yorihuzi T, Nishimune Y, Hosokawa N and Nagata K (2002) Type XXVI collagen, a new member of the collagen family, is specifically expressed in the testis and ovary. *J Biol Chem* 277(40): 37678-37684.

Saude T (1993) *Ocular anatomy and physiology*, Blackwell Science Ltd.

Schmack I, Dawson DG, McCarey BE, Waring GO, 3rd, Grossniklaus HE and Edelhauser HF (2005) Cohesive tensile strength of human LASIK wounds with histologic, ultrastructural, and clinical correlations. *J Refract Surg* 21(5): 433-445.

Schulz D, Iliev ME, Frueh BE and Goldblum D (2003) In vivo pachymetry in normal eyes of rats, mice and rabbits with the optical low coherence reflectometer. *Vision Res* 43(6): 723-728.

Scott JE (1985) Proteoglycan histochemistry--a valuable tool for connective tissue biochemists. *Coll Relat Res* 5(6): 541-575.

Scott JE (1988) Proteoglycan-fibrillar collagen interactions. *Biochem J* 252(2): 313-323.

Scott JE (1995) Extracellular matrix, supramolecular organisation and shape. *J Anat* 187 (Pt 2): 259-269.

Scott JE and Bosworth TR (1990) A comparative biochemical and ultrastructural study of proteoglycan-collagen interactions in corneal stroma. Functional and metabolic implications. *Biochem J* 270(2): 491-497.

Scott JE and Haigh M (1988) Identification of specific binding sites for keratan sulphate proteoglycans and chondroitin-dermatan sulphate proteoglycans on collagen fibrils in cornea by the use of cupromeronic blue in 'critical-electrolyte-concentration' techniques. *Biochem J* 253(2): 607-610.

Scott JE and Thomlinson AM (1998) The structure of interfibrillar proteoglycan bridges (shape modules') in extracellular matrix of fibrous connective tissues and their stability in various chemical environments. *J Anat* 192 (Pt 3): 391-405.

Seiler T, Koufala K and Richter G (1998) Iatrogenic keratectasia after laser in situ keratomileusis. *J Refract Surg* 14(3): 312-317.

Seitz B, Rozsival P, Feuermannova A, Langenbucher A and Naumann GO (2003) Penetrating keratoplasty for iatrogenic keratoconus after repeat myopic laser in situ keratomileusis: histologic findings and literature review. *J Cataract Refract Surg* 29(11): 2217-2224.

Sher N, Demarchi J and Lindstrom R (1993). Human application. Corneal surgery: theory, technique, and tissue. F. Brightbill. St. Louis, Mosby: Chap 41.

Singerman L and Coscas aG (1999) *Current techniques in ophthalmic laser surgery*3rd, BH.

Slade SG (2007) Applications for the femtosecond laser in corneal surgery. *Curr Opin Ophthalmol* 18(4): 338-341.

Smolin G and Thoft R (1994) *The cornea*3rdBoston, Little Brown and Company.

Soong HK, Mian S, Abbasi O and Juhasz T (2005) Femtosecond laser-assisted posterior lamellar keratoplasty: initial studies of surgical technique in eye bank eyes. *Ophthalmology* 112(1): 44-49.

Spadea L, Palmieri G, Mosca L, Fasciani R and Balestrazzi E (2002) Latrogenic keratectasia following laser in situ keratomileusis. *J Refract Surg* 18(4): 475-480.

Stephens DJ and Allan VJ (2003) Light microscopy techniques for live cell imaging. *Science* 300(5616): 82-86.

Stonecipher K, Ignacio TS and Stonecipher M (2006) Advances in refractive surgery: microkeratome and femtosecond laser flap creation in relation to safety, efficacy, predictability, and biomechanical stability. *Curr Opin Ophthalmol* 17(4): 368-372.

Stulting RD, Carr JD, Thompson KP, Waring GO, 3rd, Wiley WM and Walker JG (1999) Complications of laser in situ keratomileusis for the correction of myopia. *Ophthalmology* 106(1): 13-20.

Sugar A (2002b) Ultrafast (femtosecond) laser refractive surgery. *Curr Opin Ophthalmol* 13(4): 246-249.

Sugar A, Rapuano CJ, Culbertson WW, Huang D, Varley GA, Agapitos PJ, de Luise VP and Koch DD (2002a) Laser in situ keratomileusis for myopia and astigmatism: safety and efficacy: a report by the American Academy of Ophthalmology. *Ophthalmology* 109(1): 175-187.

Taneri S, Zieske JD and Azar DT (2004) Evolution, techniques, clinical outcomes, and pathophysiology of LASEK: review of the literature. *Surv Ophthalmol* 49(6): 576-602.

Tanne E (1993). Corneal trephines and cutting blocks. In. Corneal surgery. F. Brightbill. St Louis, Mosby: 193-198.

Tanzer D, Schallhorn S and Berown M (2005). Comparison of femtosecond vs mechanical microkeratome in wavefront guided LASIK. Data presented at the ASCRS Symposium. April; Washington DC.

Teng CC (1962) Fine structure of the human cornea: epithelium and stroma. *Am J Ophthalmol* 54: 969-1002.

Toda I, Asano-Kato N, Komai-Hori Y and Tsubota K (2001) Dry eye after laser in situ keratomileusis. *Am J Ophthalmol* 132(1): 1-7.

Touboul D, Salin F, Mortemousque B, Chabassier P, Mottay E, Leger F and Colin J (2005) [Advantages and disadvantages of the femtosecond laser microkeratome]. *J Fr Ophtalmol* 28(5): 535-546.

Tran DB, Sarayba MA, Bor Z, Garufis C, Duh YJ, Soltes CR, Juhasz T and Kurtz RM (2005) Randomized prospective clinical study comparing induced aberrations with IntraLase and Hansatome flap creation in fellow eyes: potential impact on wavefront-guided laser in situ keratomileusis. *J Cataract Refract Surg* 31(1): 97-105.

Trokel SL, Srinivasan R and Braren B (1983) Excimer laser surgery of the cornea. *Am J Ophthalmol* 96(6): 710-715.

Ueda A, Nishida T, Otori T and Fujita H (1987) Electron-microscopic studies on the presence of gap junctions between corneal fibroblasts in rabbits. *Cell Tissue Res* 249(2): 473-475.

Vesaluoma M, Perez-Santonja J, Petroll WM, Linna T, Alio J and Tervo T (2000) Corneal stromal changes induced by myopic LASIK. *Invest Ophthalmol Vis Sci* 41(2): 369-376.

Wachtlin J, Langenbeck K, Schrunder S, Zhang EP and Hoffmann F (1999) Immunohistology of corneal wound healing after photorefractive keratectomy and laser in situ keratomileusis. wachtlin@ukbf.fu-berlin.de. *J Refract Surg* 15(4): 451-458.

Wang J, Fonn D, Simpson TL and Jones L (2003a) Precorneal and pre- and postlens tear film thickness measured indirectly with optical coherence tomography. *Invest Ophthalmol Vis Sci* 44(6): 2524-2528.

Wang JC, Hufnagel TJ and Buxton DF (2003b) Bilateral keratectasia after unilateral laser in situ keratomileusis: a retrospective diagnosis of ectatic corneal disorder. *J Cataract Refract Surg* 29(10): 2015-2018.

Wang Z, Chen J and Yang B (1999) Posterior corneal surface topographic changes after laser in situ keratomileusis are related to residual corneal bed thickness. *Ophthalmology* 106(2): 406-409; discussion 409-410.

Waring G and Seiler T (1993). Laser corneal surgery: fundamentals and background. Corneal surgery: theory, technique, and tissue. F. Brightbill. St. Louis, Mosby: Chap 40.

Watt I (1997) *The Principles and Practice of Electron Microscopy*2nd ed.Cambridge, Cambridge University Press.

Whitten M (2004). The pearls of my LASIK technique. LASIK: advances, contraversies, and custom. L. Probst. New Jersy, SLACK Incorporated: Chap 8.

Wigham CG, Guggenheim JA and Hodson SA (1994) Sodium movement into and out of corneal endothelium. *Pflugers Arch* 428(5-6): 577-582.

Williams KA, Roder D, Esterman A, Muehlberg SM and Coster DJ (1992) Factors predictive of corneal graft survival. Report from the Australian Corneal Graft Registry. *Ophthalmology* 99(3): 403-414.

Wilson SE (2000) Role of apoptosis in wound healing in the cornea. *Cornea* 19(3 Suppl): S7-12.

Wright JD, Jr., Neubaur CC and Stevens G, Jr. (2000) Epithelial ingrowth in a corneal graft treated by laser in situ keratomileusis: light and electron microscopy. *J Cataract Refract Surg* 26(1): 49-55.

Zadnik K, Barr JT, Gordon MO and Edrington TB (1996) Biomicroscopic signs and disease severity in keratoconus. Collaborative Longitudinal Evaluation of Keratoconus (CLEK) Study Group. *Cornea* 15(2): 139-146.

Zieske JD (2001) Extracellular matrix and wound healing. *Curr Opin Ophthalmol* 12(4): 237-241.

Zimmermann DR, Trueb B, Winterhalter KH, Witmer R and Fischer RW (1986) Type VI collagen is a major component of the human cornea. *FEBS Lett* 197(1-2): 55-58.

.....

Publications and presentations

1. **Abahussin M**. Collagen fibril orientation in the cornea. Speaking of Science, Cardiff Universiy, April 2005. Talk.

2. **Abahussin M**, Velarde J, Meek KM, and Cotero J. Ectasia after LASIK; Case Report. EVER 2006. Vilamoura, Portugal. Poster and Talk.

3. Boote C, Hayes S, **Abahussin M** and Meek KM (2006) Mapping collagen organization in the human cornea: left and right eyes are structurally distinct. *Invest Ophthalmol Vis Sci* 47(3): 901-908.

4. Hayes S, Boote C, Lewis J, Sheppard J, **Abahussin M**, Quantock AJ, Purslow C, Votruba M and Meek KM (2007) Comparative study of fibrillar collagen arrangement in the corneas of primates and other mammals. *Anat Rec (Hoboken)* 290(12): 1542-1550.

5. **Abahussin M**, Velarde J, Hayes S, Boote C, Cotero JN, and Meek KM (2007) Ultrastructural Features of Ectasia after LASIK; Case Report. *J Cataract Refract Surg*. Submitted.

Mapping Collagen Organization in the Human Cornea: Left and Right Eyes Are Structurally Distinct

Craig Boote, Sally Hayes, Mohammad Abahussin, and Keith M. Meek

Purpose. Aspects of the biomechanics and surface topography of fellow human corneas are known to exhibit midline symmetry, but the structural basis of these observations is poorly understood. The mechanical performance of the cornea is strongly influenced by the organization of stromal collagen fibrils. The present study was designed to examine and compare the organization of collagen fibrils in the corneal stroma of left and right eyes.

Methods. Wide-angle x-ray scattering was used to map in detail the orientation and distribution of fibrillar collagen across the cornea, limbus, and adjacent sclera of three normal human eyes, including a fellow pair, and the central 9-mm corneal region of a further four eyes.

Results. Fibrillar collagen in the human cornea and limbus is arranged anisotropically, and in a highly specific manner. Left and right corneas are structurally distinct. In general, the mass distribution of preferentially aligned fibrils in the cornea appears to exhibit a degree of midline symmetry between left and right eyes.

Conclusions. Structural information, such as that presented herein, will enable a better understanding of corneal biomechanics and shape. Midline symmetry in the distribution of aligned, mechanically reinforcing collagen fibrils between left and right eyes may relate to the biomechanical and topographical enantiomorphism reported in the literature. (*Invest Ophthalmol Vis Sci.* 2006;47:901-908) DOI:10.1167/iovs.05-0893

The cornea, together with the surrounding sclera, forms the protective outer tunic of the eye, maintaining the eyeball's shape under the action of the intraocular pressure and external physical trauma. In terrestrial vertebrates, the cornea also acts as the main refracting component, providing ~70% of the total light focusing. Correct corneal curvature and transparency depend on the unique architecture of the corneal stroma, which accounts for the bulk of the tissue's thickness. In humans the stroma is composed, centrally, of ~200 stacked lamellae that lie parallel to the corneal surface.[1] Each lamella contains uniformly narrow, regularly spaced collagen fibrils embedded in a hydrated matrix rich in proteoglycans, glycoproteins, other soluble proteins, inorganic salts, and keratocyte cells. Fibrils within a lamella run approximately parallel, but subtend large angles with those in adjacent lamellae.[2]

From the Structural Biophysics Group, School of Optometry and Vision Sciences, Cardiff University, Cardiff, Wales, United Kingdom.

Supported by Medical Research Council Grant G0001033 CCLRC Beam-time Programme Grant.

Submitted for publication July 12, 2005; revised October 6, 2005; accepted December 22, 2005.

Disclosure: **C. Boote**, None; **S. Hayes**, None; **M. Abahussin**, None; **K.M. Meek**, None

The publication costs of this article were defrayed in part by page charge payment. This article must therefore be marked "*advertisement*" in accordance with 18 U.S.C. §1734 solely to indicate this fact.

Corresponding author: Keith M. Meek, Structural Biophysics Group, School of Optometry and Vision Sciences, Cardiff University, Redwood Building, King Edward VII Avenue, Cardiff CF10 3NB, UK; meekkm@cf.ac.uk.

Although corneal shape varies between individuals, it is well established that the surface topography of fellow normal human corneas exhibits a degree of nonsuperimposable midline symmetry.[3-5] The structural origin of this is unknown, but it is suspected that the precise organization of stromal collagen has a role to play in determining corneal shape through a direct impact on tissue biomechanics.[6,7] It has been well documented that the mechanical properties of the cornea vary across the tissue.[8-11] Interlamellar cohesive strength profiles have been shown to vary anisotropically in a similar manner across fellow normal corneas,[9] indicating that corresponding anisotropic reinforcing structures might exist between left and right eyes. It has been suggested[9] that such an intrinsic structural feature may predispose fellow corneas to the kind of enantiomorphic ectasia reported in keratoconus.[12] Moreover, certain regional differences in the cornea's mechanical properties[9,11] can be understood in terms of collagen fibril orientation models published in the literature.[13,14] In general, a compelling argument may be made for the anisotropic biomechanical performance of the cornea being related to regional variations in stromal collagen organization. Computational models of corneal biomechanics are now beginning to incorporate fibril orientation data,[15] with the purpose being to simulate more effectively the tissue's response to surgery. However any variational trends in collagen organization between left and right eyes, as might be expected from topographical and biomechanical considerations, remain uncharacterized, despite the potential importance of this information to our understanding of corneal mechanics and shape.

X-ray scattering has become established as a powerful research tool for examining corneal microstructure (for a review, see Ref. 16). Scattering methods have revealed a preferential orientation of collagen fibrils in the central cornea in the superior-inferior and nasal-temporal directions.[6,13,17] It has been suggested that these exist to take up the stress exerted on the cornea by the ocular motor muscles, thereby helping to preserve corneal shape.[6,17] Similar methods have also determined that, toward the corneal periphery, this arrangement alters to coalesce with an annulus of fibrils that circumscribe the cornea.[18,19] This annulus may help to maintain corneal curvature by mechanically reinforcing the limbus, the corneoscleral interface where the differing curvatures of the two tissues creates heightened circumferential tension.[20] Recently, the technique has been used to map for the first time collagen organization across a whole cornea.[14] The present study extends our knowledge by comparing the collagen organization between left and right eyes and includes structural maps of fellow corneas from a single individual.

Methods

Tissue Preparation

A pair of eyeballs (donor 1) was obtained from Manchester Eye Hospital (Manchester, UK). The eyes were removed from the donor within 2 to 3 hours of death, snap frozen using liquid nitrogen and stored frozen at −80°C until the time of the experiment. On removal, a scleral suture was added to mark the superior globe position. Immediately before data collection the eyes were thawed and the corneas excised.

leaving 2 to 3 mm of scleral rim attached. In addition, two right eyeballs (donors 2 and 3) were provided by the Great Wall Hospital (Beijing, China). These eyes were removed (again retaining 2 to 3 mm of scleral rim) within 2 to 3 hours of death, sutured and stored in 10% formalin solution until the time of data collection. (Previous x-ray experiments have revealed no significant difference between the two storage methods, in terms of the resultant wide-angle scattering data; Hayes S, personal communication, 2004.) One further right eye (donor 4) and two left eyes (donors 5 and 6) were obtained from the Bristol Eye Bank (Bristol, UK) and were harvested and prepared in an identical fashion with the eyes of donor 1. None of the six donors had any history of ocular surgery. The tenets of the Declaration of Helsinki were adhered to throughout.

Data Collection

Wide-angle x-ray-scattering data were collected on station 14.1 at the UK Synchrotron Radiation Source (Daresbury, UK), by using a 0.1488-nm wavelength x-ray beam with a square 0.2 × 0.2 mm cross-section at the specimen. Specimens were wrapped in cling film and mounted inside airtight Perspex (Databank, UK) cells, to prevent tissue dehydration. X-rays were passed through the anterior face of the cornea-sclera parallel to the cornea's optical axis, and the resultant scattering data collected on a charge-coupled (CCD) x-ray detector (ADSC, Poway, CA) placed 15 cm behind the specimen (Fig. 1A). Scattering patterns were collected at 0.5 × 0.5-mm (donor 1) and 0.4 × 0.4-mm (donor 2) intervals across the whole tissue, with the x-ray exposure times per data point being 45 (donor 1) and 75 (donor 2) seconds. The specimens were moved horizontally and vertically within the sample plane between exposures by means of a motorized translation stage (Newport, Newbury, UK) interfaced with the x-ray camera shutter. In addition, the central 9-mm corneal region of the four remaining eyes was examined at a resolution of 0.4 (donors 3 and 5), 0.3 (donor 4), and 0.25 (donor 6) mm. Exposure times were 75 (donor 3), 45 (donors 4 and 5), and 30 (donor 6) seconds.

Data Analysis

Wide-angle scattering patterns from cornea and sclera arise from interference between x-rays scattered by the regularly spaced collagen molecules making up the fibrils.[16] Collagen molecules scatter x-rays in a plane normal to their long axis and, because these molecules lie nearly parallel to the fibril axis, the distribution of scattered intensity may be analyzed to yield information about the orientation of the collagen fibrils. A typical scattering pattern from the central cornea is shown in Figure 1A. It is characterized by four lobes of heightened intensity (red) arising from the predominantly orthogonal arrangement of fibrils in this part of the tissue. For each pattern the angular distribution of normalized x-ray scatter intensity was obtained (Fig. 1B) using methods described previously.[18] The scatter was divided into two components: (1) isotropic scatter from fibrils distributed equally in all directions and (2) aligned scatter from only those fibrils that are preferentially aligned (Fig. 1B). The aligned scatter was then plotted as polar vectors, introducing a 90° phase shift to account for the fact that collagen molecules scatter x-rays normally to their long axis. In the resultant graph (Fig. 1C), the radial extent of the plot in any direction is proportional to the relative number of fibrils preferentially aligned in that direction. The polar plots were combined to produce a map showing the preferred orientation of fibrils over the tissue.

From the scattering patterns we were also able to compute for each sampled point in the tissue a single-intensity value giving a measure of the relative scatter from fibrillar collagen at that point. Total scatter from all fibrillar collagen was computed for each pattern by integrating the area under the angular distribution graphs (Fig. 1B). The data were then assimilated into a contour plot, as described previously,[14] producing for each specimen a map showing the distribution of fibrillar collagen over the tissue. Corresponding maps were produced for only preferentially aligned fibrils by integrating the area under the aligned scatter component of the distribution graph (Fig. 1B).

Results

Collagen Fibril Orientation

By using high-intensity Synchrotron x-rays we obtained maps of collagen fibril orientation across a fellow pair of corneas (donor 1) with approximately 2 mm of surrounding scleral tissue. Wide-angle x-ray-scattering patterns were collected at

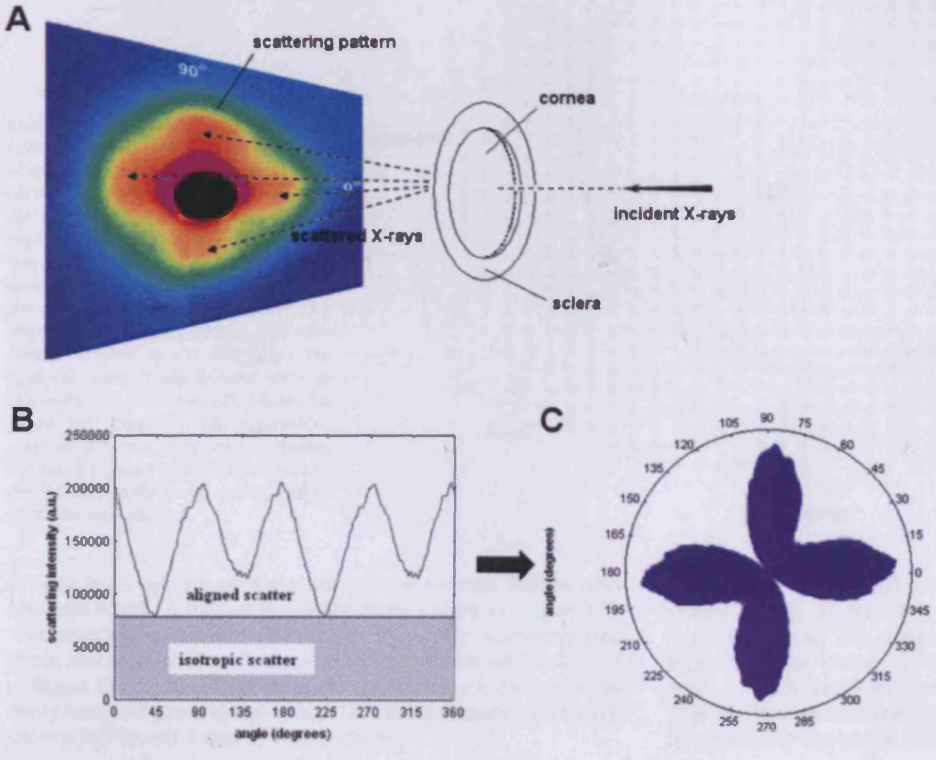

FIGURE 1. Wide-angle x-ray scattering from the cornea-sclera. (**A**) X-rays scattered by fibrillar collagen form a scattering pattern on a detector behind the specimen. (**B**) The angular distribution of scattered x-ray intensity is measured. (**C**) Scatter from preferentially aligned fibrils is converted into polar vectors. The radial extent of the resulting plot in a particular direction represents the relative number of collagen fibrils preferentially aligned in that direction.

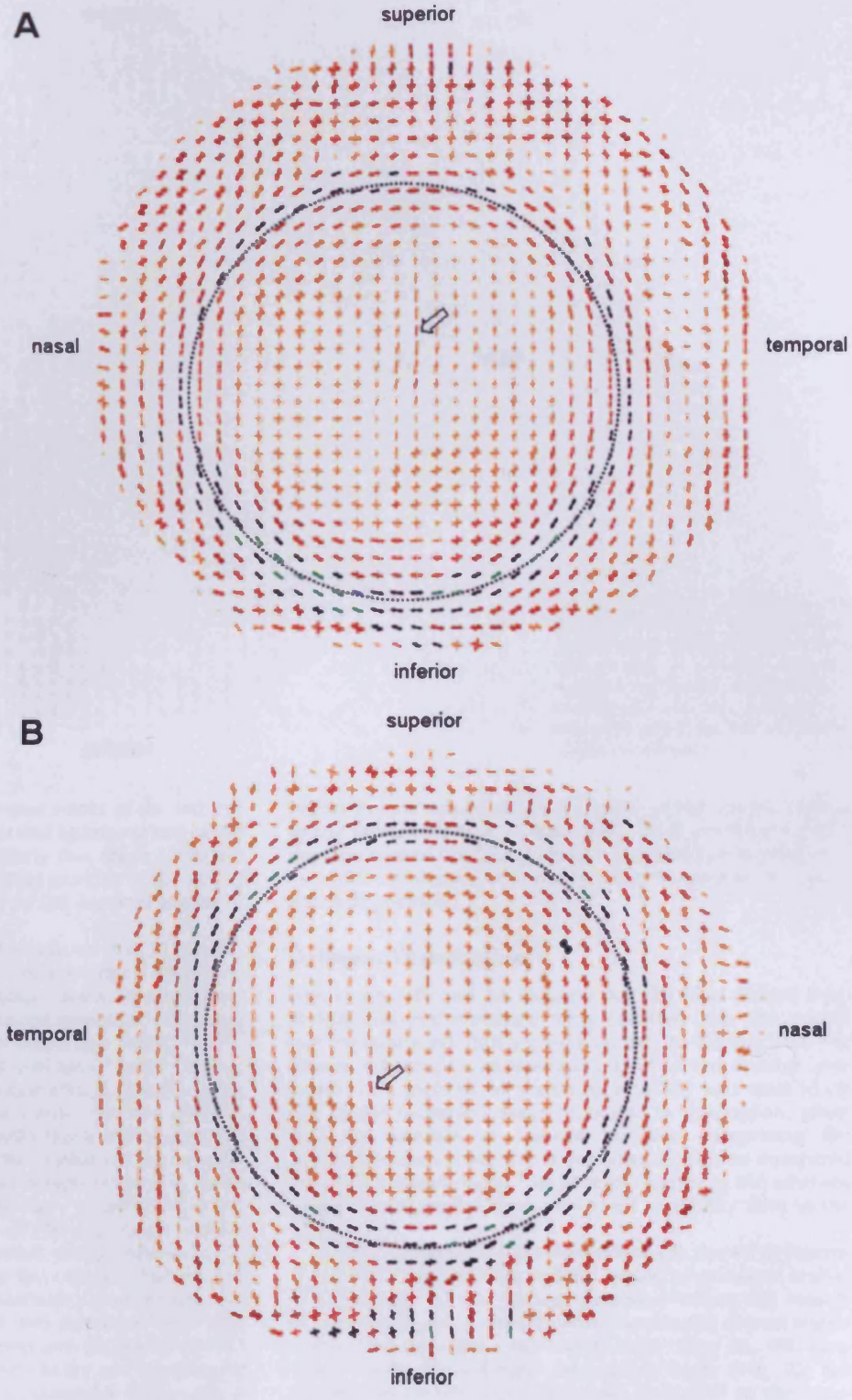

FIGURE 2. Preferred orientation of collagen fibrils in human cornea and sclera. (**A**) Left eye of donor 1, sampled at 0.5-mm intervals. *Dotted circle*: the limbus. Each sampled point is represented by a polar plot, in which the radial extent of the plot in any direction is proportional to the relative number of fibrils preferentially aligned in that direction. It was necessary to scale down the larger peripheral plots. Scale factors: *orange* (1), *red* (1.5), *dark red* (2), *black* (3), *green* (4), *blue* (5). (**B**) Equivalent map of donor's right eye. *Arrows*: localized regions in both eyes where the normal orthogonal arrangement of fibrils was altered.

0.5-mm intervals across the whole of the cornea, limbus, and adjacent sclera. A further specimen from a right eye (donor 2) was mapped at 0.4-mm resolution. From the scattering patterns, we were able to determine the preferred orientation of collagen fibrils, averaged through the specimen thickness, at every sampled point in the tissue. Data from donors 1 and 2 are shown in Figures 2 and 3, respectively.

Reference to the fibril orientation map for the right eye of donor 2 (Fig. 3) revealed an interesting feature of collagen organization in the sclera. The polar plots toward the periphery of the tissue clearly showed localized scleral fibrils with a preferred orientation directed radially toward the four cardinal points (designated superior, inferior, nasal, and temporal) of the globe. This feature was also noticeable to a

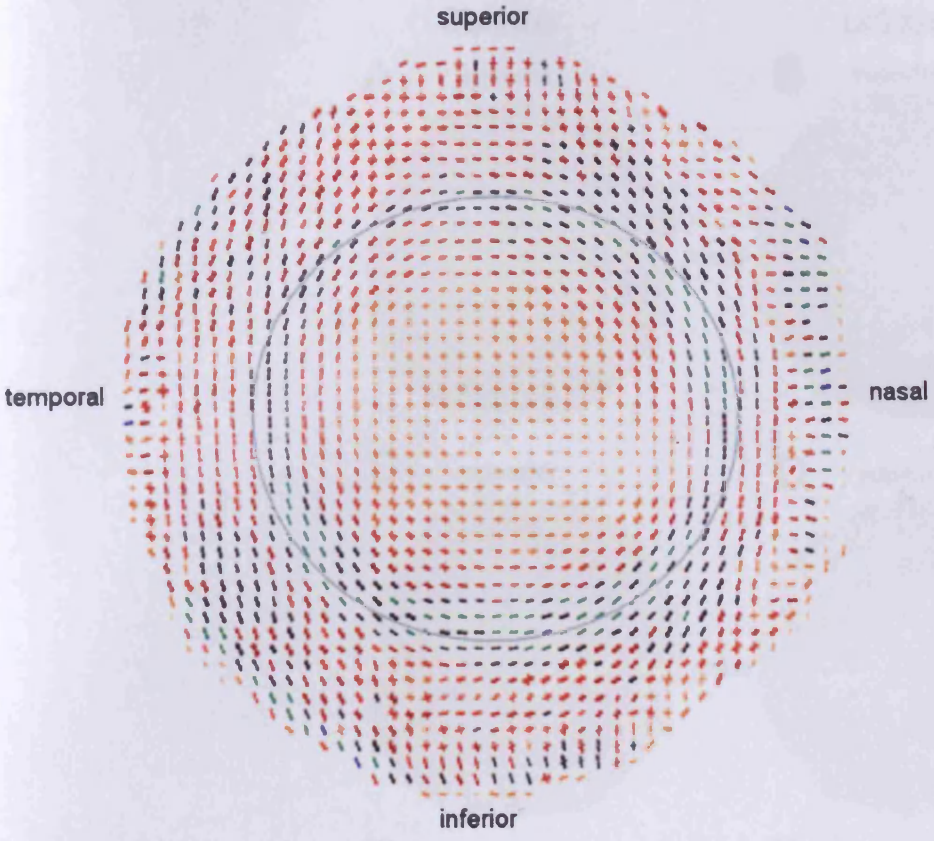

FIGURE 3. Map of preferred collagen fibril orientation across the right cornea-sclera of donor 2. Polar plots are shown at 0.4-mm intervals. Scaled-down factors are as follows: *orange* (1), *red* (1.5), *dark red* (2), *black* (3), *green* (4), *blue* (5). *Dotted circle*: the limbus.

lesser degree in the nasal and superior sclera of the left eye of donor 1 (Fig. 2A) and in the nasal and inferior sclera of the right eye (Fig. 2B). We believe it likely that these fibrils are used to anchor the sclera to the rectus muscles of the ocular motor system, which are situated at the cardinal points of the globe.[21]

The polar plots in Figures 2 and 3 indicate that, in general, the central cornea of donors 1 and 2 demonstrated a preferentially orthogonal arrangement of collagen fibrils, directed along the superior–inferior and nasal–temporal meridians. This result is consistent with previous x-ray-scattering work.[6,13,14,17] There were, however, areas in both corneas of donor 1 where the orientation was locally more uniaxial (Fig. 2, arrows), being biased in favor of superior–inferior fibrils. The two observations may be reconciled if we consider that a recent study has shown that, although on average the central cornea is populated by superior–inferior and nasal–temporal fibrils in equal proportion, individual corneas may show a significant imbalance.[6] A further important feature of the maps is the relative size of the polar plots in the peripheral oblique regions of the cornea. The left eye of donor 1 (Fig. 2A) clearly featured larger plots in the peripheral regions of the superior–nasal and inferior–temporal quadrants than in the two remaining quadrants. These larger plots extended 2 to 3 mm into the cornea relative to the center of the limbus (dotted circle) and qualitatively point to proportionally more aligned collagen in these parts of the tissue. This feature was also present in the donor's right eye (Fig. 2B) and in donor 2 (Fig. 3).

The orientation of the central corneal fibrils is clearly seen to shift toward the corneal periphery gradually (Figs. 2, 3), in favor of a more tangential arrangement. At the limbus (dotted circle) the plots are consistent with a circumcorneal annulus of fibrils, similar to that reported previously.[14,18,19] Note also from the color of the plots that there was a much higher proportion of aligned collagen in the limbus relative to the corneal center. In agreement with previous work,[18] the structure of the limbal annulus appeared asymmetrical—its width and degree of fibril alignment varying with circumferential position.

Collagen Distribution

Figures 4A, 4B, and 5A indicate that the total scatter from fibrillar collagen remained fairly constant over the cornea (yellow contours) until approximately 1 to 1.5 mm from the limbus, whereupon an increase was observed (orange contours). This increase in scattering intensity was most likely due to the increased tissue thickness in this region, given that the number of stacked lamellae comprising the stroma increases more than twofold at the limbus compared with the corneal center.[1] In general, scatter in the adjacent sclera demonstrated far more spatial variability than in the cornea.

Aligned collagen scatter from donor 1 is shown in Figures 4C and 4D. The contours define a region of minimum scatter in the central cornea (yellow contours) which was loosely rhombic in shape, compared with the circular central region in the corresponding total scatter maps (Figs. 4A, 4B). Consistent with the collagen orientation maps (Fig. 2), the scatter was clearly elevated (orange contours) in the superior–nasal and inferior–temporal quadrants of the peripheral cornea of both eyes, causing the central rhombic region to appear skewed. This additional scatter has been proposed to arise from fibrils originating in the sclera and passing through the oblique peripheral cornea on a curved path.[14,22] These so-called "anchoring" fibrils may help flatten the peripheral cornea.[14] Strikingly, the resultant shape of the central aligned scatter contours in the right (Fig. 4C)

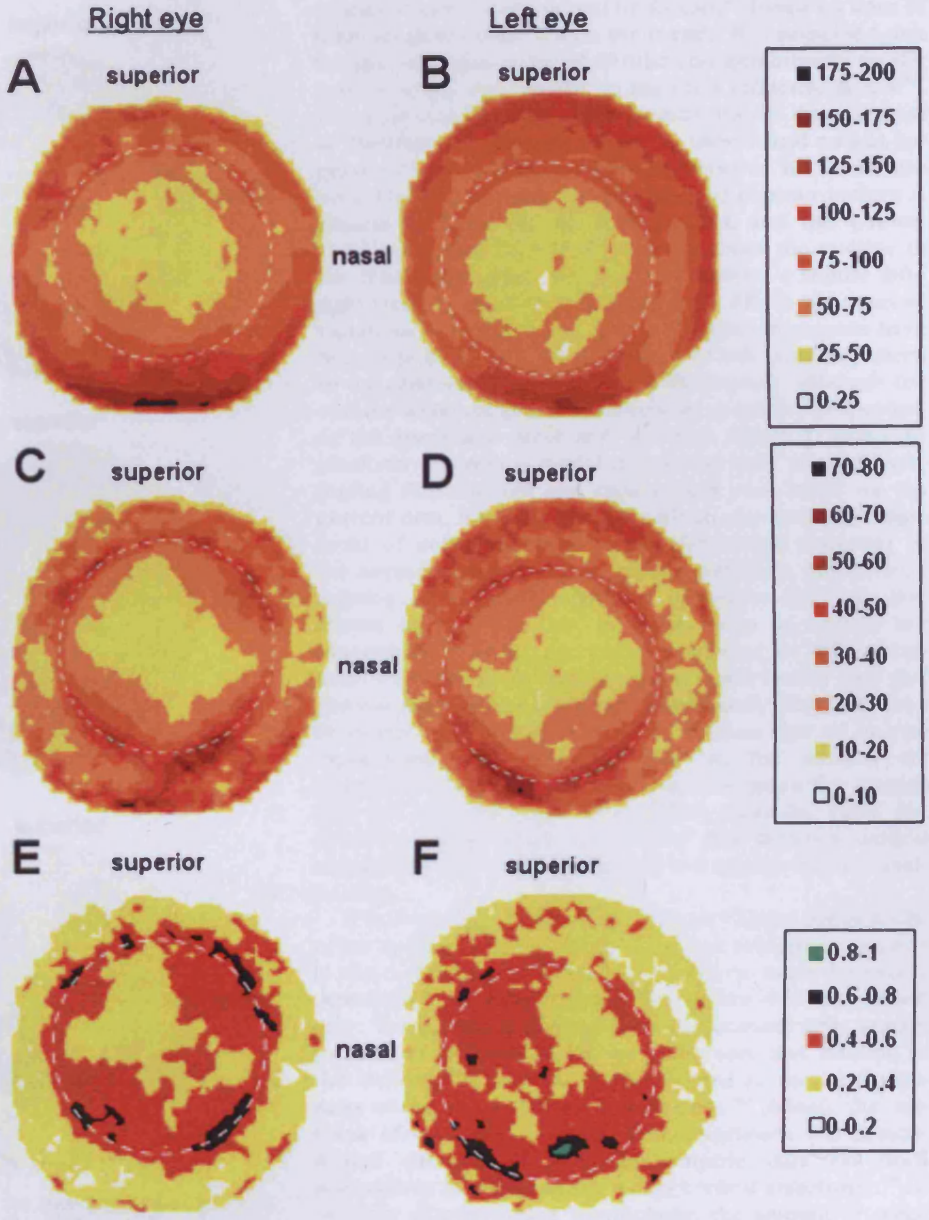

FIGURE 4. Contour maps showing the distribution of collagen in human cornea and sclera. (**A**, **B**) Total fibrillar collagen x-ray scatter from right and left eyes, respectively, of donor 1. (**C**, **D**) Scatter from only preferentially aligned collagen fibrils. (**E**, **F**) Ratio of aligned/total scatter. Scatter in arbitrary units. *Dotted circle*: the limbus.

and left (Fig. 4D) eyes exhibited a high degree of midline mirror symmetry. At the limbus (dotted line) there was a clear annulus of increased scatter intensity, which was elevated in the oblique regions compared with the cardinal points. It is further notable that maximum scatter occurred in the inferior–nasal region of the limbus in both eyes, and that overall limbal scatter is greater on the nasal side. As in the cornea, the distribution of aligned scatter around the limbus appears roughly mirrored in the fellow pair about the central body axis. Contour maps showing the ratio of aligned to total scatter are shown in Figures 4E and 4F. These were obtained by dividing the data in Figures 4C and 4D, point for point, by those in Figures 4A and 4B respectively. The maps confirm that the apparent elevations in aligned scatter we have discussed do indeed represent genuinely higher levels of preferentially aligned collagen, as opposed to simply increases in the total amount of collagen due to, for example, variations in tissue thickness. Figures 5B and 5C show that all aforementioned features of the aligned collagen distribution in the right eye of donor 1 were conserved in the right eye of donor 2. The finer sampling resolution used in the case of donor 2 (0.4 mm instead of 0.5 mm) was manifest in the improved definition of the maps in Figure 5.

To explore further the interesting observations pertaining to the distribution of aligned collagen mass, we examined the central 9-mm region of four additional corneas (two right and two left). Figure 6 shows that, although significant variation was evident between individual eyes, the characteristic distorted rhombic pattern of the aligned scatter contours was conserved. In this respect, left and right eyes may be considered structurally distinct, in that it is possible to tell a right cornea from a left by inspection of the distribution of aligned collagen alone. Notwithstanding more subtle variations between individuals, this gross structural feature appears to be an intrinsic property of the cornea.

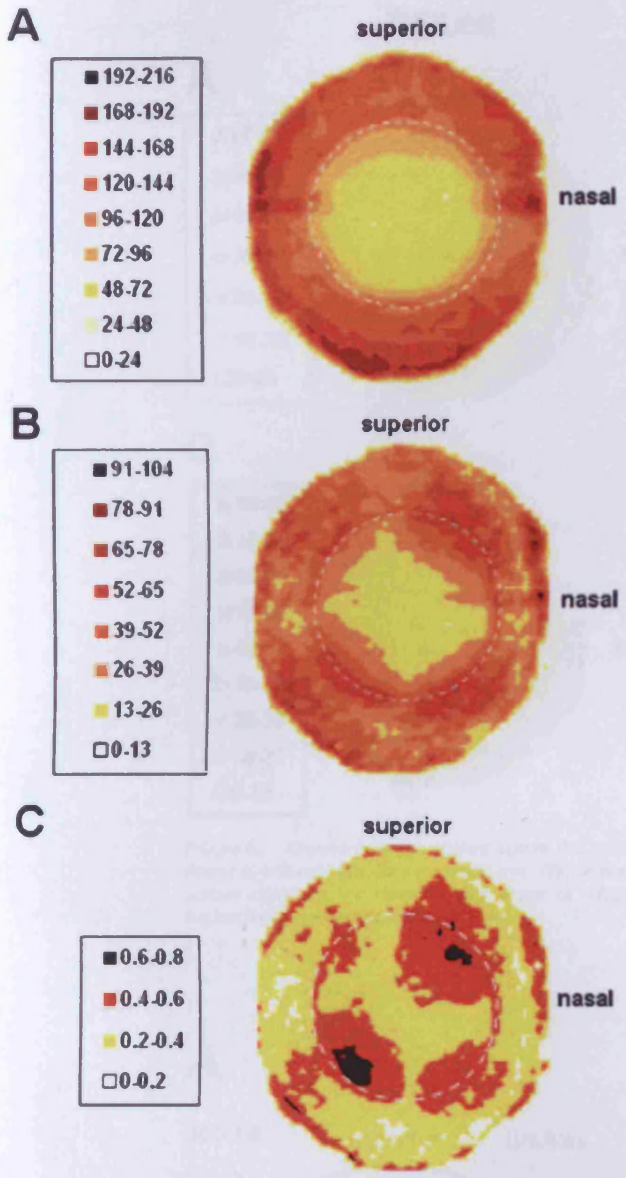

FIGURE 5. Distribution of collagen in the right cornea and sclera of donor 2. (**A**) Contour map of total fibrillar collagen x-ray scatter. (**B**) Contour map of scatter from only preferentially aligned collagen. (**C**) Ratio of aligned to total scatter. Scatter is expressed in arbitrary units. *Dotted circle*: the limbus.

DISCUSSION

A major role of collagen fibrils in connective tissues is to provide tensile reinforcement, and knowledge of fibril orientation and distribution within a tissue is necessary for a proper understanding of the tissue's mechanical properties.[23,24] In the human eye, exactly how the arrangement of the corneal lamellae is related to mechanical performance remains to be established. In this article, we have demonstrated a population of collagen fibrils in the sclera at the four cardinal points outside the cornea that are directed toward the extraocular muscles, and it may reasonably be supposed that this collagen has a mechanical function related to eye movement. The result is consistent with the scheme originally envisioned by Kokott,[25] based on lines of force measurements. Within the cornea, it is suspected that the precise organization of fibrillar collagen impacts on the tissue's shape, and thereby on the eye's refractive status.[6,7] The most striking result of the present study is that the mass of preferentially aligned collagen in the corneal stroma appears to be distributed differently between left and right eyes. The characteristic rhombus-shaped contour pattern is present in every eye we have studied, and this pattern exhibited a high degree of symmetry about the midline in the fellow pair (Figs. 4C, 4D), and showed a similar left-right trend in all other specimens (Figs. 5B, 6). Of interest, variations in birefringence data across human corneas have been reported[26] that demonstrate a broadly similar pattern to the observed aligned collagen distribution, although the authors were not able to comment on symmetry properties, as the specimens were not oriented. Figure 7 shows an idealized theoretical model of preferentially aligned, reinforcing fibrils in left and right human eyes based on the current data. It is possible that such an anisotropic arrangement of collagen relates to the differential flattening of the normal cornea along its various meridians. Moreover, a scheme of inherent structural symmetry such as that shown in Figure 7 may in theory help to explain the topographical enantiomorphism exhibited by fellow corneas. With this in mind, however, it is relevant to note that corneal shape is known to vary significantly from individual to individual.[3,27] Further, it is unfortunate that no in vivo topographic data were available on the corneas we examined, and no direct comparison between the current data and corneal shape is therefore possible. Thus, the definitive establishment of a causal link between corneal topography and collagen organization awaits further investigation.

It is instructive to consider potential clinical implications of the current results. Intrinsic structural anisotropy, such as in the distribution of reinforcing collagen, could become a determinant of corneal shape during keratorefractive surgery. The extent of postoperative astigmatism after certain procedures depends on the size, direction, and location of the incision,[28,29] and this may be related to the inhomogeneity of the stroma's fibril arrangement.[30] Indeed, the outcome of computer-simulated tunnel incisions has demonstrated the benefit of using empiric data on fibril orientations to mechanically model corneal anisotropy.[15] In the case of penetrating keratoplasty, the amount of surgically induced refractive error is determined by many factors, including trephination technique,[31,32] suture type,[33,34] and postoperative management.[35,36] It is possible that collagen organization could also have a bearing on the clinical outcome, particularly given empiric evidence that graft alignment appears to affect the magnitude of astigmatism after transplant (Rapuano CJ, et al. *IOVS* 1995;36:ARVO Abstract 653). In addition, the results of the present study might also be relevant to LASIK surgery. Specifically, the data suggest that, during flap creation, the extent of collagen fibril disruption may depend on the direction of the microkeratome pass. However, it must be borne in mind that the current data represent an average through the full-thickness tissue. The fibril model as it stands requires extension to include structural changes with stromal depth before a conclusive argument could be made. Nevertheless, the present study may prove an integral step toward providing a fundamental structural platform on which to interpret the cornea's mechanical response to surgery.

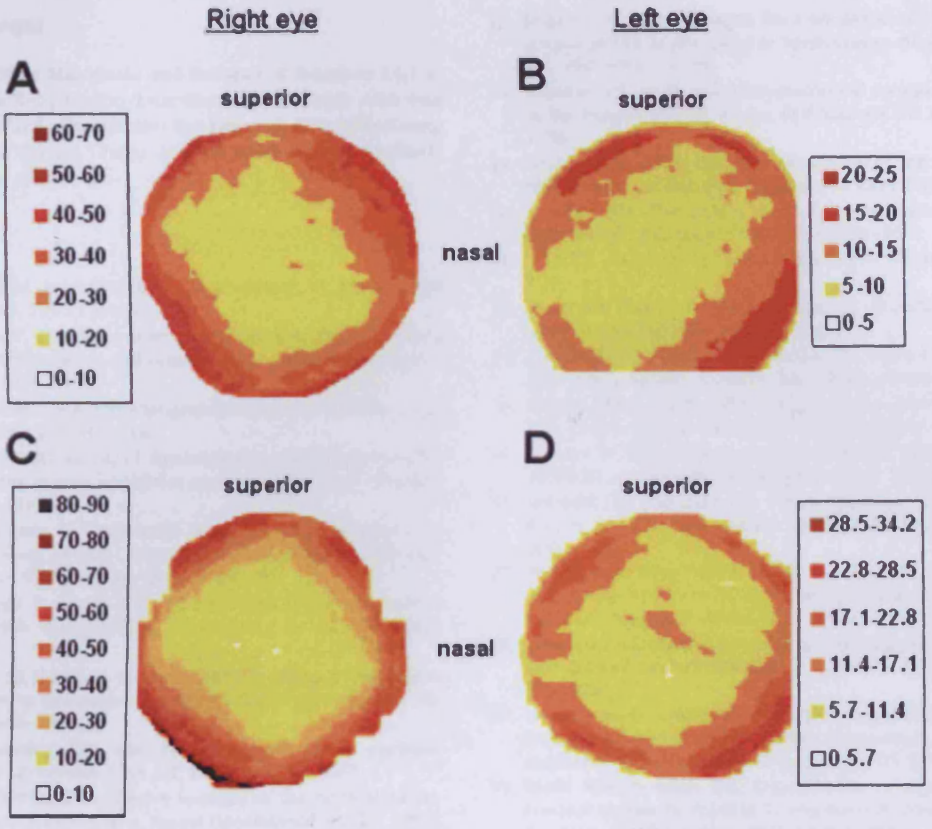

FIGURE 6. Aligned collagen scatter across the central 9-mm corneal region of (**A**) donor 3, right eye; (**B**) donor 6, left eye; (**C**) donor 4, right eye; (**D**) donor 5, left eye. Note the distorted rhombic pattern of the scatter contours, the characteristic shape of which distinguishes (**A**, **C**) right from left (**B**, **D**) corneas. Scatter is expressed in arbitrary units.

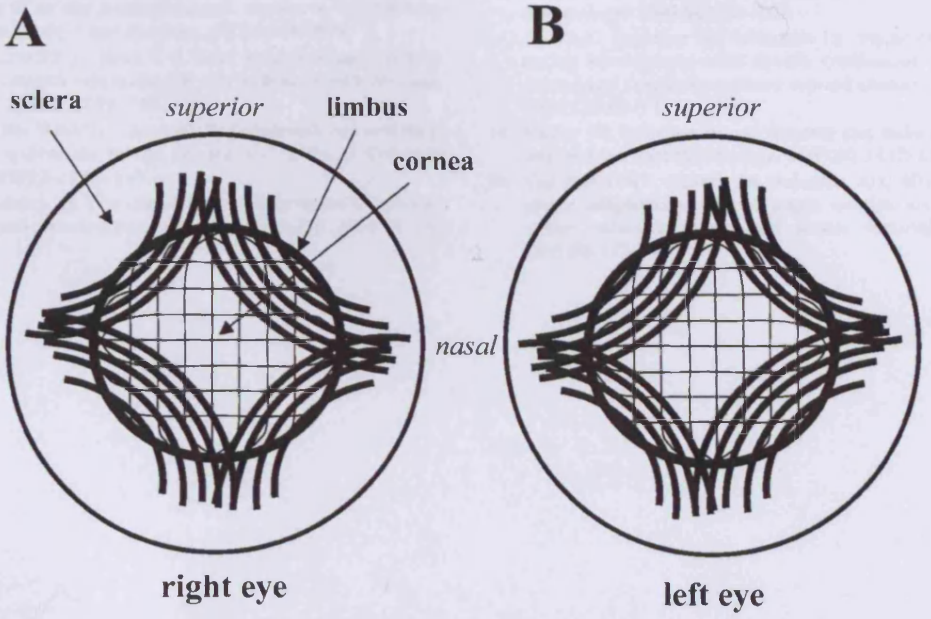

FIGURE 7. Idealized theoretical model showing the directions of preferentially aligned, reinforcing collagen fibrils in the cornea, limbus, and adjacent sclera of human eyes. The fibril arrangements in (**A**) right and (**B**) left eyes are distinct, being symmetrical about the body midline.

Acknowledgments

The authors thank Mike Macdonald and the staff of Beamline 14.1 at the UK Synchrotron X-ray Source (Daresbury, UK) for help with data collection, and Tom Kelly (Manchester Eye Hospital, UK), Yifei Huang (Great Wall Hospital, Beijing, China), and Val Smith (Bristol Eye Bank, UK) for provision of specimens.

References

1. Maurice DM. The structure and transparency of the corneal stroma. *J Physiol.* 1957;136:263-286.
2. Komai Y, Ushiki T. The three-dimensional organization of collagen fibrils in the human cornea and sclera. *Invest Ophthalmol Vis Sci.* 1999;32:2244-2258.
3. Dingeldein SA, Klyce SD. The topography of normal corneas. *Arch Ophthalmol.* 1989;107:512-518.
4. Smolek MK, Klyce SD, Sarver EJ. Inattention to nonsuperimposable midline symmetry causes wavefront analysis error. *Arch Ophthalmol.* 2002;120:439-447.
5. Serrao S, Lombardo G, Lombardo M. Differences in nasal and temporal responses of the cornea after photorefractive keratectomy. *J Cataract Refract Surg.* 2005;31:30-38.
6. Boote C, Dennis S, Meek KM. Lamellar orientation in human cornea in relation to mechanical properties. *J Struct Biol.* 2005; 149:1-6.
7. Meek KM, Tuft SJ, Huang Y, et al. Changes in collagen orientation and distribution in keratoconus corneas. *Invest Ophthalmol Vis Sci.* 2005;46:1948-1956.
8. Smolek MK. Interlamellar adhesive strength in human eyebank corneas. *Invest Ophthalmol Vis Sci.* 1990;31:1087-1095.
9. Smolek MK. Interlamellar cohesive strength in the vertical meridian of human eye bank corneas. *Invest Ophthalmol Vis Sci.* 1993; 34:2962-2969.
10. Hjordtal JO. Regional elastic performance of the human cornea. *J Biomechanics.* 1996;29:931-942.
11. Shin TJ, Vito RP, Johnson LW, McCarey BE. The distribution of strain in the human cornea. *J Biomechanics.* 1997;30:497-503.
12. Wilson SE, Lin DTC, Klyce SD. Corneal topography of keratoconus. *Cornea.* 1991;10:2-8.
13. Meek KM, Blamires T, Elliott GF, Gyi TJ, Nave C. The organisation of collagen fibrils in the human corneal stroma: a synchrotron X-ray diffraction study. *Curr Eye Res.* 1987;6:841-846.
14. Aghamohammadzadeh H, Meek KM. X-ray scattering used to map the preferred collagen orientation in the human cornea and limbus. *Structure.* 2004;12:249-256.
15. Pinsky PM, van der Heide D, Chernyak D. Computational modeling of mechanical anisotropy in the cornea and sclera. *J Cataract Refract Surg.* 2005;31:136-145.
16. Meek KM, Quantock AJ. The use of X-ray scattering techniques to determine corneal ultrastructure. *Prog Retin Eye Res.* 2001;20:95-137.
17. Daxer A, Fratzl P. Collagen fibril orientation in the human corneal stroma and its implications in keratoconus. *Invest Ophthalmol Vis Sci.* 1997;38:121-129.
18. Newton RH, Meek KM. Circum-corneal annulus of collagen fibrils in the human limbus. *Invest Ophthalmol Vis Sci.* 1998;39:1125-1134.
19. Newton RH, Meek KM. The integration of the corneal and limbal fibrils in the human eye. *Biophys J.* 1998;75:2508-2512.
20. Maurice DM. The cornea and sclera. In: Davson H, ed. *The Eye.* Orlando, FL: Academic Press; 1969:489-600.
21. Wolff E. *Anatomy of the Eye and Orbit.* 9th ed. London: Arnold; 1997.
22. Meek KM, Boote C. The organization of collagen in the corneal stroma. *Exp Eye Res.* 2003;78:503-512.
23. Hukins DWL. Collagen orientation. In Hukins DWL, ed. *Connective Tissue Matrix.* London: Macmillan; 1984:210-240.
24. Hukins DWL, Aspden RM. Composition and properties of connective tissues. *Trends Biochem Sci.* 1985;10:260-264.
25. Kokott W. Über mechanisch-funkionelle Strukturen des Auges. *Albrecht von Graefes Arch Ophthalmol.* 1938;138:424-485.
26. Jaronski JW, Kasprzak HT. Linear birefringence measurements of the *in vitro* human cornea. *Ophthalmic Physiol.* 2003;23:361-369.
27. Bogan SJ, Waring GO III, Ibrahim O, Drews C, Curtis L. Classification of normal corneal topography based on computer-assisted videokeratography. *Arch Ophthalmol.* 1990;108:945-949.
28. Kohnen T. Corneal shape changes and astigmatic aspects of scleral and corneal tunnel incisions. *J Cataract Refract Surg.* 1987;23: 301-302.
29. Wirbelauer C, Anders N, Pham DT, Wollensak J. Effect of incision location on preoperative oblique astigmatism after scleral tunnel incision. *J Cataract Refract Surg.* 1997;23:365-371.
30. Meek KM, Newton RH. Organization of collagen fibrils in the corneal stroma in relation to mechanical properties and surgical practice. *J Refract Surg.* 1999;15:695-699.
31. Girard LJ, Eguez I, Esnaola N, Barnett L, Maghraby A. Effect of penetrating keratoplasty using grafts of various sizes on keratoconic myopia and astigmatism. *J Cataract Refract Surg.* 1988;14: 541-547.
32. Mahjoub SB, Au YK. Astigmatism and tissue shape disparity in penetrating keratoplasty. *Ophthalmic Surg.* 1990;21:187-190.
33. Musch DC, Meyer RF, Sugar A, Soong HK. Corneal astigmatism after penetrating keratoplasty: the role of suture technique. *Ophthalmology.* 1989;96:698-703.
34. Assil KK, Zarnegar SR, Schanzlin DJ. Visual outcome after penetrating keratoplasty with double continuous or combined interrupted and continuous suture wound closure. *Am J Ophthalmol.* 1992;114:63-71.
35. Binder PS. Selective suture removal can reduce post keratoplasty astigmatism. *Ophthalmology.* 1985;92:1412-1416.
36. Van Meter WS, Gussler JR, Soloman KD, Wood TO. Postkeratoplasty astigmatism control: single continuous suture adjustment versus selective interrupted suture removal. *Ophthalmology.* 1991;98:177-183.

THE ANATOMICAL RECORD 290:1542–1550 (2007)

Comparative Study of Fibrillar Collagen Arrangement in the Corneas of Primates and Other Mammals

SALLY HAYES,[1] CRAIG BOOTE,[1] JENNIFER LEWIS,[1,2] JACK SHEPPARD,[1] MOHAMMAD ABAHUSSIN,[1] ANDREW J. QUANTOCK,[1] CHRISTINE PURSLOW,[1] MARCELA VOTRUBA,[1] AND KEITH M. MEEK[1]*

[1]Structural Biophysics Research Group, School of Optometry and Vision Institute, Cardiff University, Cardiff, United Kingdom

[2]Department of Ophthalmology, Havener Eye Institute, Ohio State University, Columbus, Ohio

ABSTRACT

This study is a comparative study of the relationship between corneal structure, morphology, and function in a range of mammalian species. X-ray scattering patterns were gathered at regular spatial intervals over the excised cornea (and in most cases also the scleral rim) of humans, marmosets, horses, cows, pigs, rabbits, and mice. All patterns were analyzed to produce quantitative information regarding the predominant orientation of fibrillar collagen throughout the tissue. The predominant direction of corneal collagen varies between mammals. This variation is not related to the size, shape, or thickness of the cornea or the frequency with which the animal blinks. A relationship does, however, appear to exist between corneal collagen arrangement and visual acuity. An excess of collagen directed toward one or both sets of opposing rectus muscles is a feature of animals that have an intermediate to high level of visual acuity. There is a significant variation in the arrangement of corneal collagen between different mammalian species. This finding may be related to differences in the frequency of action and the forces generated by the various extraocular muscles during eye movement and image fixation. Anat Rec, 290:1542–1550, 2007. © 2007 Wiley-Liss, Inc.

Key words: cornea; species; collagen; x-ray scattering

The cornea, often referred to as "the transparent window at the front of the eye," provides a tough external barrier to protect the contents of the eye from injury while also maintaining a precise curvature to enable light to be focussed onto the retina. The mammalian cornea is composed mainly of water and type I collagen fibrils, and it is the unique arrangement of this collagen that governs the strength, shape, and transparency of the tissue. The long, cylindrical collagen fibrils have a uniform diameter, a regular separation distance, and lie parallel to each other within layers (lamellae), which are themselves stacked parallel to the surface of the cornea. The diameter and separation distance of the fibrils differs between species but the proportion of the corneal stroma occupied by hydrated collagen fibrils remains constant (Meek and Leonard, 1993).

As initially proposed by Kokott (1938) and more recently confirmed using x-ray scattering (Meek et al., 1987; Aghamohammadzadeh et al., 2004; Boote et al., 2006), most lamellae in the central region of the human

Grant sponsor: Medical Research Council; Grant number: G0600755; Grant sponsor: the Central Laboratory of Research Councils.

*Correspondence to: Keith M. Meek, School of Optometry and Vision Institute, Carditt University, Maindy Road, Cardiff CF24 4LU UK. Fax: 44-(0)2920-874859. E-mail: meekkm@cf.ac.uk

Received 7 June 2007; Accepted 17 August 2007

DOI 10.1002/ar.20613

Published online 24 October 2007 in Wiley InterScience (www.interscience.wiley.com).

TABLE 1. Sample details

Species	Sample details	Source	Storage
Human *Homo sapiens sapiens*	Right cornea with 3-mm scleral rim. Tagged at superior. (n = 2)	Great Wall Hospital, Bejing, China	Fixed 10% formalin
Human *Homo sapiens sapiens*	Paired left and right cornea with 3mm scleral rim. (n = 2)	Manchester Eye Hospital, UK	Frozen −80°C
Human *Homo sapiens sapiens*	Left corneas with 3-mm scleral rim. Tagged at superior. (n = 2)	Bristol Eyebank, UK	Frozen −80°C
Common marmoset *Callithrix jaccus*	Paired left and right cornea with 0.5-mm scleral rim. Tagged at superior. (n = 20)	Oxford University, UK	Frozen −80°C
Horse *Equus caballus*	Cornea with a 2-mm scleral rim. Vertical meridian marked. (n = 3)	Abattoir, Bristol, UK	Frozen −80°C
Cow *Bos indicus*	Cornea with a 2-mm scleral rim. Vertical meridian marked. (n = 5)	Abattoir, Bristol, UK	Frozen −80°C
Pig *Sus scrofa domesticus*	Cornea with a 2-mm scleral rim. Tagged at superior. (n = 3)	Abattoir, Bristol, UK	Frozen −80°C
New Zealand White Rabbit *Oractolagus cuniculus*	Cornea with a 2-mm scleral rim. Tagged at superior. (n = 3)	Heath Hospital, Cardiff, UK	Frozen −80°C
Laboratory mouse *Mus musculus*	Cornea with a 0.25-mm scleral rim. Tagged at superior. (n = 13)	Cardiff University, UK	Frozen −80°C

cornea, particularly in the deeper layers of the stroma, lie in the superior–inferior and nasal–temporal directions. As the tensile strength of connective tissue is determined in part by the orientation of collagen fibrils in relation to the direction of stress (Jeronimidis and Vincent, 1984; Hukins and Aspden, 1985), this has prompted suggestions that the preferred orthogonal orientation of fibrils in the central human cornea may be necessary to resist the mechanical forces of the four rectus muscles that insert behind the limbus at opposing positions along each meridian (Kokott, 1938; Daxer and Fratzl, 1997; Newton and Meek, 1998). A limbal annulus of collagen surrounds the human cornea and is believed to provide additional reinforcement at the point where it meets the lesser curved sclera (Maurice, 1984; Newton and Meek, 1998; Aghamohammadzadeh et al., 2004).

Based on the birefringence properties of the bovine cornea, it was suggested that a nonrandom distribution of lamellae was also present in the bovine cornea (Kaplan and Bettleheim, 1972). Small-angle light scattering of bovine and rabbit cornea confirmed this to be the case in both species (McCally and Farrell, 1982), but the authors were unable to determine the precise orientation of the stromal lamellae. Of interest, analysis of single x-ray scatter patterns obtained from the central cornea of over 50 vertebrate species (which included primates), revealed the human cornea to be unique in possessing an arrangement of stromal collagen that is preferentially orientated along both the superior–inferior and nasal–temporal meridians (Meek et al., 1987).

X-ray scattering is a powerful technique for studying the gross orientation of collagen fibrils in the cornea. As corneal collagen molecules lie near axially within the fibrils, the high-angle equatorial x-ray scattering pattern arising from the lateral packing of the molecules in the stroma can be used to determine the preferred direction of the fibrils at that position in the cornea. In recent years, this method has been used successfully to map the predominant orientation of collagen at fine spatial intervals throughout the entire human and marmoset cornea and limbus (Aghamohammadzadeh et al., 2004; Boote et al., 2004, 2006).

Given the frequent use of nonhuman species in studies of corneal biomechanics and that the size and orientation of collagen fibrils largely contributes to biomechanical calculations (Jeronimidis and Vincent, 1984; Hukins and Aspden, 1985), it is clear that a greater knowledge of the precise arrangement of corneal collagen in species other than human is needed. Here, we have addressed this issue by using x-ray scattering to map the predominant orientation of corneal and limbal collagen in the human, marmoset, horse, cow, pig, rabbit, and mouse.

MATERIALS AND METHODS

Tissue Samples

All tissue samples used in this study (Table 1) were obtained in accordance with the tenets of the Declaration of Helsinki for the use of human tissue and the Association for Research in Vision and Ophthalmology (ARVO) statement for the use of animals in ophthalmic research.

In the majority of cases, the in vivo orientation was marked on the scleral rim at the 12 o'clock position by means of a nylon suture or a surgical skin marker pen. In the case of the horse, cow, and pig cornea, where the in vivo orientation was not known, the vertical meridian was identified by the elliptical shape of the cornea. To minimize tissue dehydration, frozen samples were wrapped in Clingfilm™ (Superdrug Stores Plc., Croydon, UK) before freezing in liquid nitrogen-cooled isopentane. Each sample was defrosted at room temperature immediately before data collection.

X-ray Scattering Data Collection

High-angle x-ray scatter patterns were collected from most samples on Station 14.1 at Daresbury Synchrotron Radiation Source (Warrington, UK), using a 200 × 200

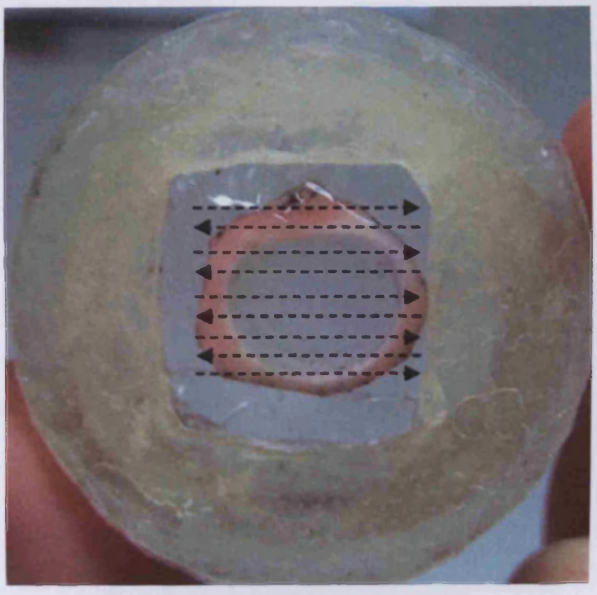

Fig. 1. A pig cornea (with scleral rim) enclosed within a sealed sample holder. X-ray scattering patterns were recorded at regular intervals across the cornea in the directions indicated by the arrows.

micron beam with a wavelength of 0.1488 nm. The images were recorded on a Quantum 4R CCD detector (ADSC, Poway, CA) placed 150 mm behind the sample. The rare opportunity to use the micro-focus x-ray beam (measuring 5 microns in diameter and with a wavelength of 0.984 nm) on Station ID-13 at the European Synchrotron Radiation Facility (Grenoble, France) was utilized to obtain comparable x-ray scattering data for an additional pig cornea.

Each cornea was placed in its correct orientation into a sealed sample holder enclosed between two sheets of Mylar (Dupont-Teijin, UK; Fig. 1). The sample holder was then carefully positioned onto a computer-operated translation stage (Newport Spectra-Physics Ltd., Newbury, UK) so that the most anterior side of the cornea faced the x-ray beam. X-ray scatter patterns resulting from an exposure time of 75 sec (human), 150 sec (marmoset), 30 sec (pig), and 45 sec (rabbit and mouse) were collected over the entire cornea and scleral rim of each specimen at regular intervals of 0.8 mm (human), 0.5 mm (marmoset), 1 mm (pig and rabbit), and 0.2 mm (mouse). Due to the large size of the horse and cow cornea and the limited capacity of the specimen holder, x-ray scatter patterns resulting from a 20-sec x-ray exposure were collected at 1-mm intervals over a 14-mm trephined corneal disc taken from the center of each cornea.

X-ray Diffraction Data Analysis

A circular x-ray scatter reflection, formed as a result of the interference of x-rays scattered by the collagen molecules within the fibrils, was present on each x-ray scatter pattern. In cases where the collagen was orientated equally in all directions within the plane of the tissue, a uniform ring of x-ray scatter was formed; however, when there was an excess of fibrils lying in a particular direction (Fig. 2A) or directions (Fig. 2B), lobes of increased scatter intensity were seen at right angles to the dominant orientation of the fibrils.

Using image analysis software (Optimas 6.5, Media Cybernetics, UK) and Microsoft Excel (UK), a 0–360 degree intensity distribution profile was produced for each x-ray pattern by measuring the intensity of x-ray scatter around the intermolecular reflection (Fig. 2C,D). Each intensity distribution profile was normalized against the exposure time and the average x-ray intensity during exposure (recorded by an ion chamber placed between the x-ray beam and the sample). At this point, the signal to noise ratio was improved by folding the intensity profile; this was possible without the loss of any data, due to the centrosymmetric nature of x-ray scatter patterns. The area under the intensity profile, which is proportional to the total amount of collagen through which the x-ray beam has passed, can be separated into two components—the scatter from collagen lying equally in all directions within the plane of the cornea (isotropic scatter) and the scatter from collagen fibrils that adopt a preferred orientation (aligned scatter) (Fig. 2C,D).

Removal of the isotropic scatter from the intensity profile leaves only the scatter from aligned fibrillar collagen. To ascertain the preferred orientation of these aligned fibrils, it was necessary to first shift the profile by 90 degrees to account for the fact that the high-angle equatorial reflection occurs at right angles to the fibril axis. Using statistical analysis software (Statistica 7, StatSoft Ltd., UK), the intensity profile was then converted into a vector plot (Fig. 2E,F), in which the distance from the center to the edge of the plot at any given angle is proportional to the intensity of x-ray scatter from aligned collagen molecules oriented in that direction. Individual vector plots were then compiled onto a grid relating to corneal position to show the preferred orientation of aligned collagen in each cornea.

The specific arrangement of corneal collagen in each species was examined alongside published values (where available) of corneal size, radius of curvature, and thickness as well as the frequency with which the animal blinks (shown as the interval between subsequent blinks) and its visual acuity (Table 2). Visual acuity, which is measured in cycles per degree of visual field, may be defined as the spatial resolving capacity of the visual system. It provides a measure of the eye's ability to distinguish one object from another in terms of degree angles of visual field.

As no values could be found in the literature for the blink interval of the pig, this value was measured by assessing videographic footage acquired from nine healthy Yorkshire/Landrace mix breed sows housed in single stalls for birthing. The time between subsequent blinks was recorded in several minute episodes using the video time counter, and the average blink interval was calculated.

RESULTS

Figure 3A shows the predominant direction of collagen in the human cornea. Within the central 5.6 mm, most fibrils lie in the superior–inferior and nasal–tem-

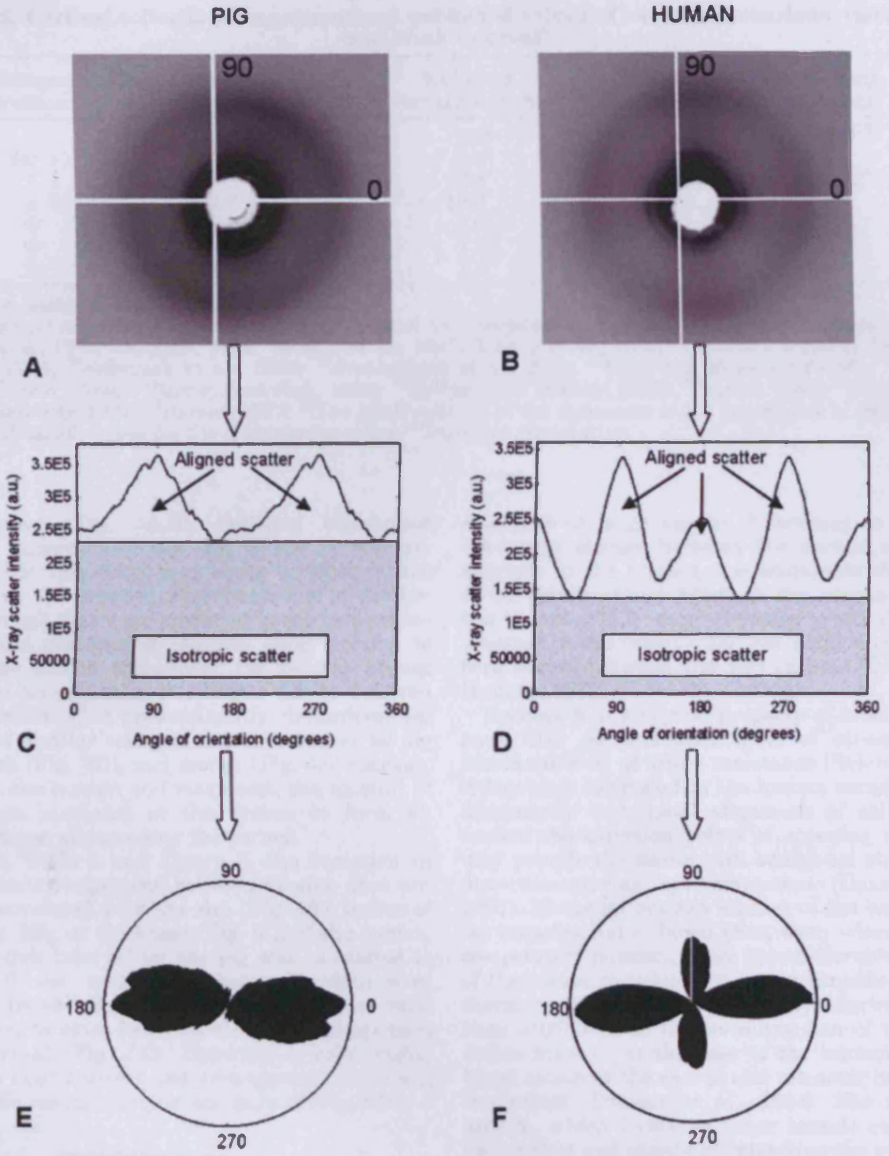

Fig. 2. **A,B:** High angle x-ray scattering patterns from the center of a pig (A) and a human cornea (B). **C,D:** The intensity of x-ray scatter around the intermolecular reflection was measured to produce a profile of total collagen scatter intensity as a function of angular position. **E,F:** The profile of x-ray scatter from aligned collagen only (isotropic scatter removed) is displayed as a vector plot, taking into account that x-rays are scattered at right angles to the fibril axis. The distance from the center of a vector plot in any given direction is representative of the amount of collagen fibrils preferentially orientated in that particular direction.

poral directions, giving rise to a characteristic cross-shaped vector plot (Newton and Meek, 2001; Aghamohammadzadeh et al., 2004; Boote et al., 2006). With increasing distance from the center of the cornea, the size of the vector plots increases, indicating that more collagen is highly aligned and the principal direction of collagen becomes increasingly tangential with respect to the edge of the cornea. A distinct annulus of aligned collagen measuring 1.6–2.0 mm spans the corneolimbal region.

A predominantly orthogonal orientation of collagen is rarely seen in the marmoset cornea (4 of 20 examined). In most cases (16 of 20 corneas examined) an excess of fibrils are oriented along the superior–inferior meridian (Fig. 3B). As with the human cornea, a well-defined limbal annulus measuring 0.5–1.2 mm is a common feature of the marmoset.

X-ray scatter patterns recorded from three equine corneas and three bovine corneas revealed that, in the central 14 mm, an excess of collagen is orientated along the

TABLE 2. Corneal collagen arrangement and published values of corneal dimensions, visual acuity and blink interval[a]

Species	Collagen direction[1]	Cornea size (horizontal × vertical) (mm)	Radius of curvature (mm)	Corneal thickness (mm)	Visual acuity (cycles/deg)	Blink interval (sec)
Human	+	11.7 × 10.6[2]	7.8[2]	0.55[9]	47.0–86.0[13]	2.8[18]
Marmoset	I (or +)	6.1 × 5.4[3]	3.5[3]	0.30[3]	30.0[3]	1.4[19,20]
Horse	I	35.0 × 28.5[4]	17.2[7]	0.81[10]	16.4–20.4[14]	2.3[19]
Cow	I (or O)	29.0 × 24.0[4]	15.8[7]	0.80[11]	12.4[15]	2.7[19]
Pig	O	15.5 × 12.5[4]	9.0[7]	0.85[9]	8.0[15]	3.8[21]
Rabbit	O	13.4 × 13.0[5]	7.3[5]	0.38[12]	4.3[16]	>30[19]
Mouse	O	3.5 horiz.[6]	1.4[8]	0.17[6]	0.5[17]	>30[19]

[a]The superscript numbers indicate the following:
[1]Corneal collagen arrangement is classified as orthogonal (+), vertical (I) or circumferential (O); [2]Tripathi and Tripathi, 1984; [3]Troilo et al., 1993; [4]Smythe, 1956; [5]Bozkir et al., 1997; [6]Zhang et al., 1996; [7]Coile and O'Keefe, 1988; [8]Schmucker and Schaeffel, 2004; [9]Wollensak et al., 2003; [10]Svaldeniene et al., 2004; [11]Scott and Bosworth, 1990; [12]Li et al., 1997; [13]Hirsch and Curcio, 1989; [14]Timney and Keil, 1992; [15]Heffner and Heffner, 1992; [16]Vaney, 1980; [17]Prusky et al., 2000; [18]Ponder and Kennedy, 1927; [19]Blount, 1927; [20]The blink interval of the marmoset is not known but is assumed to be similar to that of published values for the Sudanese monkey; [21]Personal observation.

vertical meridian (Fig. 4A,B). Collagen orientation appears to be tangential at the edge of the 14 mm trephined disks, but this effect may be an artefact caused by trephination. Of interest, examination of a further two bovine corneas that were prepared in the same manner revealed the presence of collagen lying parallel to the edge of the cornea throughout the central 14-mm region and this arrangement of collagen will be referred to as "circumferential." A predominantly circumferential arrangement of fibrillar collagen was observed in all pig (Fig. 4C), rabbit (Fig. 4D), and mouse (Fig. 4E) corneas, and as seen in the human and marmoset, the amount of aligned collagen increases at the limbus to form an annulus of collagen surrounding the cornea.

As shown in Table 2 and Figure 5, the variation in corneal collagen arrangement between species does not appear to be correlated with the size (Fig. 5A), radius of curvature (Fig. 5B), or thickness (Fig. 5C) of the cornea. The average blink interval for the pig was calculated to be 3.76 (± 2.0) sec, and when these new data were included with those taken from the literature, no relationship seemed to exist between collagen arrangement and blink interval (Fig. 5E). However, a relationship does appear to exist between the arrangement of corneal collagen and the visual acuity of the animal (Fig. 5D).

DISCUSSION

In this study, we have shown that major differences in corneal collagen arrangement exist between mammals and, as highlighted in the common marmoset and the cow, further structural differences may also exist between individuals of the same species. The observed variation in collagen arrangement does not, however, appear to be related to the size, radius of curvature or thickness of the cornea.

It has been suggested elsewhere that the presence of an annulus of aligned collagen at the limbus may play a role in maintaining the curvature of the cornea at the point where it meets the lesser curved sclera (Maurice, 1984; Aghamohammadzadeh et al., 2004; Boote et al., 2004). Of interest, a limbal annulus of circumferentially aligned collagen appears to be a common feature of all animals examined within this study group, despite the existence of large species differences in the amount of curvature change between the cornea and sclera. For example in the human, a considerable change in radius of curvature occurs between the cornea (7.8 mm) and the sclera (11.5 mm; Tripathi and Tripathi, 1984), whereas in the rabbit a far less notable change in curvature occurs between the two regions (7.5 and 9.8 mm; Hughes, 1972).

Because it is a typical property of most connective tissues that an increased level of stress produces an increased level of stress resistance (Reichel et al., 1989), it has been suggested in the human cornea that the predominantly orthogonal alignment of collagen, directed toward the insertion points of opposing rectus muscles, may provide the tissue with additional strength to resist distortion during eye movement (Daxer and Fratzl, 1997). Electrical activity studies of the human extraocular muscles have shown that, even when the eye is in the primary position, there is considerable activity in all of the rectus muscles (Bjork and Kugelberg, 1953). Furthermore, the retraction of the eye during blinking has been attributed to the co-contraction of the extraocular rectus muscles in the case of the human and the combined action of the rectus and retractor bulbi muscles in the rabbit (Evinger et al., 1984). The retractor bulbi muscle, which forms an inner muscle cone around the optic nerve and assists in retracting the globe, is present in the horse, cow, pig, rabbit, and mouse but exists only as a rudimentary structure in the monkey and is entirely absent in the human (Prangen, 1928). The presence of four extraocular rectus muscles are, however, common to all mammalian species, although the length, width, and position of insertion varies between animals (Prangen, 1928; Prince et al., 1960). For example, the rectus muscles of the monkey and human insert at locations much closer to the limbus than those of the rabbit and pig (Prangen, 1928). Despite all mammalian species possessing the same four extraocular rectus muscles, a predominantly orthogonal arrangement of corneal collagen is not a common feature of vertebrates and has only been observed in the human, a minority of marmosets (Boote et al., 2004), and the chicken (personal observation). It must be remembered at this point that x-ray scattering patterns provide an average measurement of

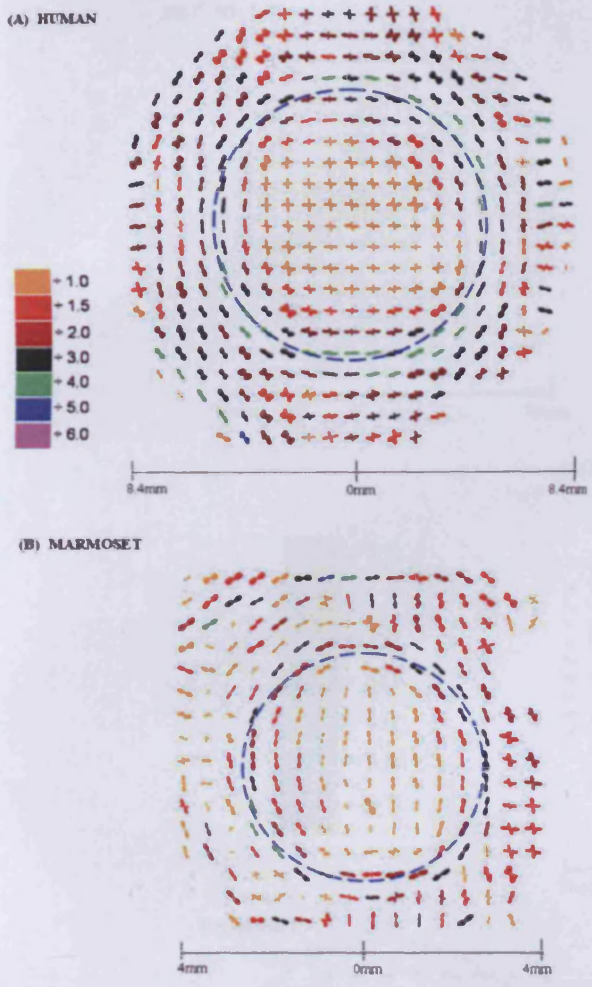

Fig. 3. **A,B:** Vector plot maps showing the predominant direction of stromal collagen in the human (A) and marmoset (B) cornea and scleral rim, sampled at 0.8-mm and 0.5-mm intervals, respectively. Vector plots are scaled down by the factors shown in the key. The position of the limbus is highlighted by a broken blue line.

collagen fibril orientation throughout the entire thickness of the cornea. It is possible therefore that other nonhuman species also possess an orthogonal arrangement of lamellae but as suggested by Gyi and colleagues (1987), they may be fewer in number or of a reduced thickness to those present in the human cornea and therefore contribute less to the overall x-ray scatter pattern. Indeed electron microscopy, a technique that can be used to provide detailed structural information at specific sites in a tissue, has provided evidence of some fibrils crossing at right angles to each other in the posterior stroma of the developing mouse cornea (Haustein, 1983), but x-ray scattering has revealed that, on average, most stromal collagen in the adult mouse cornea lie in a circumferential arrangement with respect to the edge of the cornea.

Here, we have shown that a relationship may exist between corneal collagen orientation and visual acuity (Fig. 5; Table 2). This apparent relationship may be due to animals with a higher level of visual acuity having an increased frequency of rectus muscle contraction as a result of finer eye movements (Prince et al., 1960). Primates are exclusive among mammals in their possession of a fovea—a small circular region of the retina that has a high cone photoreceptor density and affords the animal with a high level of visual acuity. The alignment of collagen in the human cornea toward the insertion points of the rectus muscles may play a role in maintaining a stable eye position during image fixation on the fovea and/or resisting corneal distortion caused by the co-contraction of antagonistic pairs of rectus muscles during blinking. It is worth noting here that, although marmosets possess a fovea, have a relatively high level of visual acuity (30 cycles/degree; Troilo et al., 1993) and likely (based on published values of the blink interval in the Sudanese monkey; Blount, 1927) blink at a similar frequency to humans, they rarely exhibit an orthogonal arrangement of corneal collagen. However, in contrast to the human retina, which shows a sharp decrease in cone density with distance from the fovea, the marmoset retina exhibits a much more gradual decline of cone density along the horizontal meridian (Troilo et al., 1993). The need for such precise horizontal eye movements during image fixation may therefore be reduced and the presence of a predominantly vertical arrangement of collagen may help to preferentially counteract the forces generated by the superior and inferior rectus muscles. It must also be considered that, if corneal collagen arrangement is indeed influenced by the stresses exerted on the cornea by the action of the extraocular muscles, then one might expect the corneas of animals born and raised in captivity to differ from their wild counterparts as a result of differences in their visual environment and, hence, the frequency and direction of eye movements. As suggested by Barmack (1976), deprivation of binocular vision in an animal that normally has excellent binocular vision may reduce the stiffness of the extraocular muscles and cause misalignments.

The need for accurate control of eye position is greatly reduced in animals that possess a retina with a visual streak (a broad strip of increased cone density), because the lateral position of their eyes affords a large field of view without the need for extensive eye movement (Prince et al., 1960; Barmack, 1976). The horse and cow possess an intermediate level of visual acuity (relative to the other species studied here), and in the majority of cases examined in this study have an excess of vertically orientated collagen within the central region of the cornea. A predominantly vertical arrangement of collagen in these species may help to counteract the forces of the superior and inferior rectus muscles, which act antagonistically to help maintain a stable retinal image on a horizontal visual streak. In lower visual acuity animals such as the pig, rabbit, and mouse, the predominantly circumferential direction of corneal collagen does not correspond to the insertion points of any of the rectus muscles. In these species, the frequency of rectus muscle contraction may be lower as a result of limited eye movement and the possession of a retractor bulbi muscle, which helps to retract the eye during blinking. Such a relationship between collagen

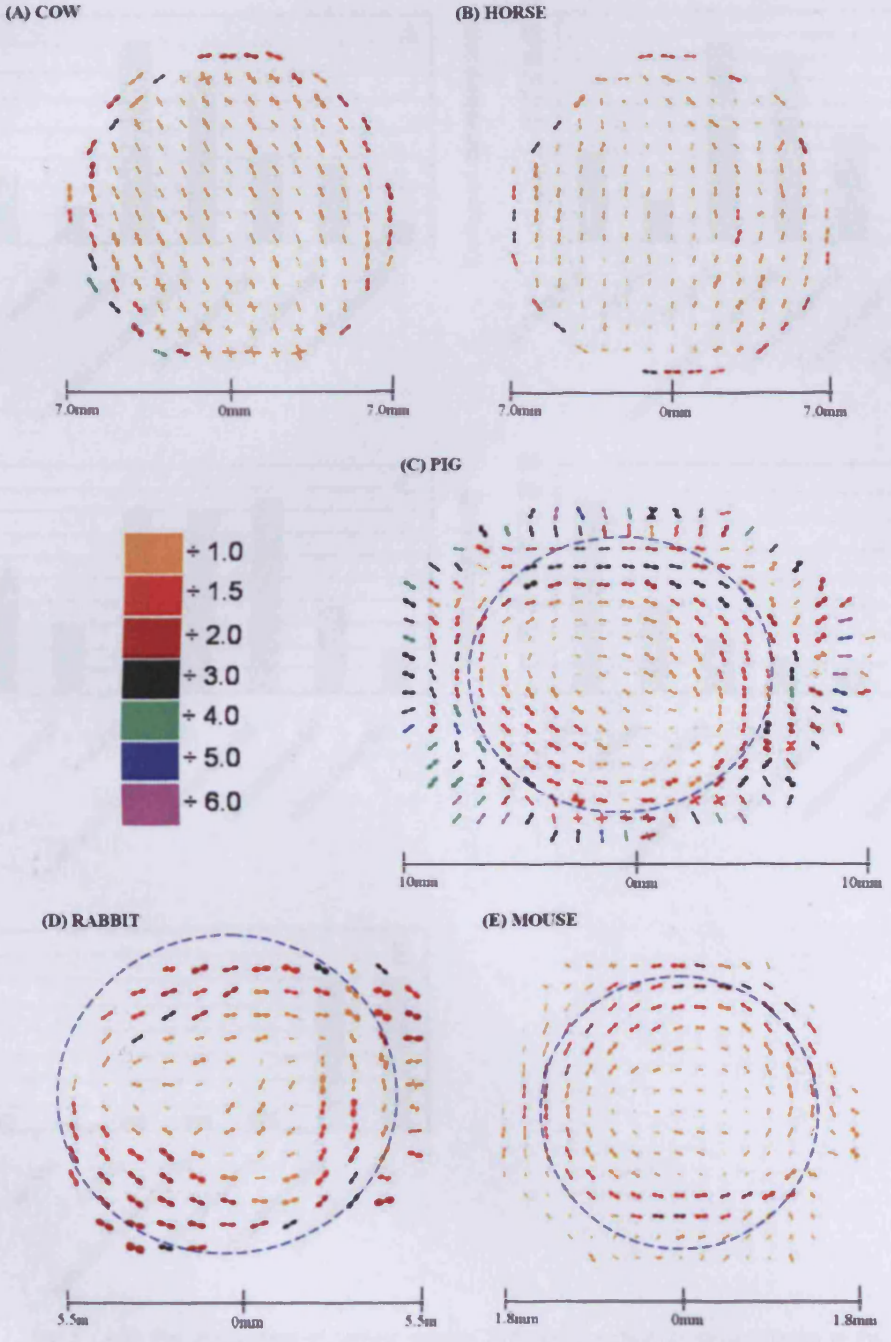

Fig. 4. **A–E:** Vector plot maps showing the predominant direction of stromal collagen in the central 14 mm of the cow (rotated anticlockwise 30 degrees off axis; A) and horse cornea (B) and in the cornea and scleral rim of a pig (C), rabbit (D), and mouse (E). Vector plots are scaled down by the factors shown in the key.

arrangement and eye movement is supported by the fact that the stiffness of both the cornea (Jue and Maurice, 1986) and the extraocular rectus muscles (Barmack, 1976) of the rabbit are far lower than that of the human.

This study has highlighted that major differences in corneal structure exist between mammalian species. These differences may be related to variations in the direction, frequency, and precision of eye movements, however, a functional study of corneal collagen arrange-

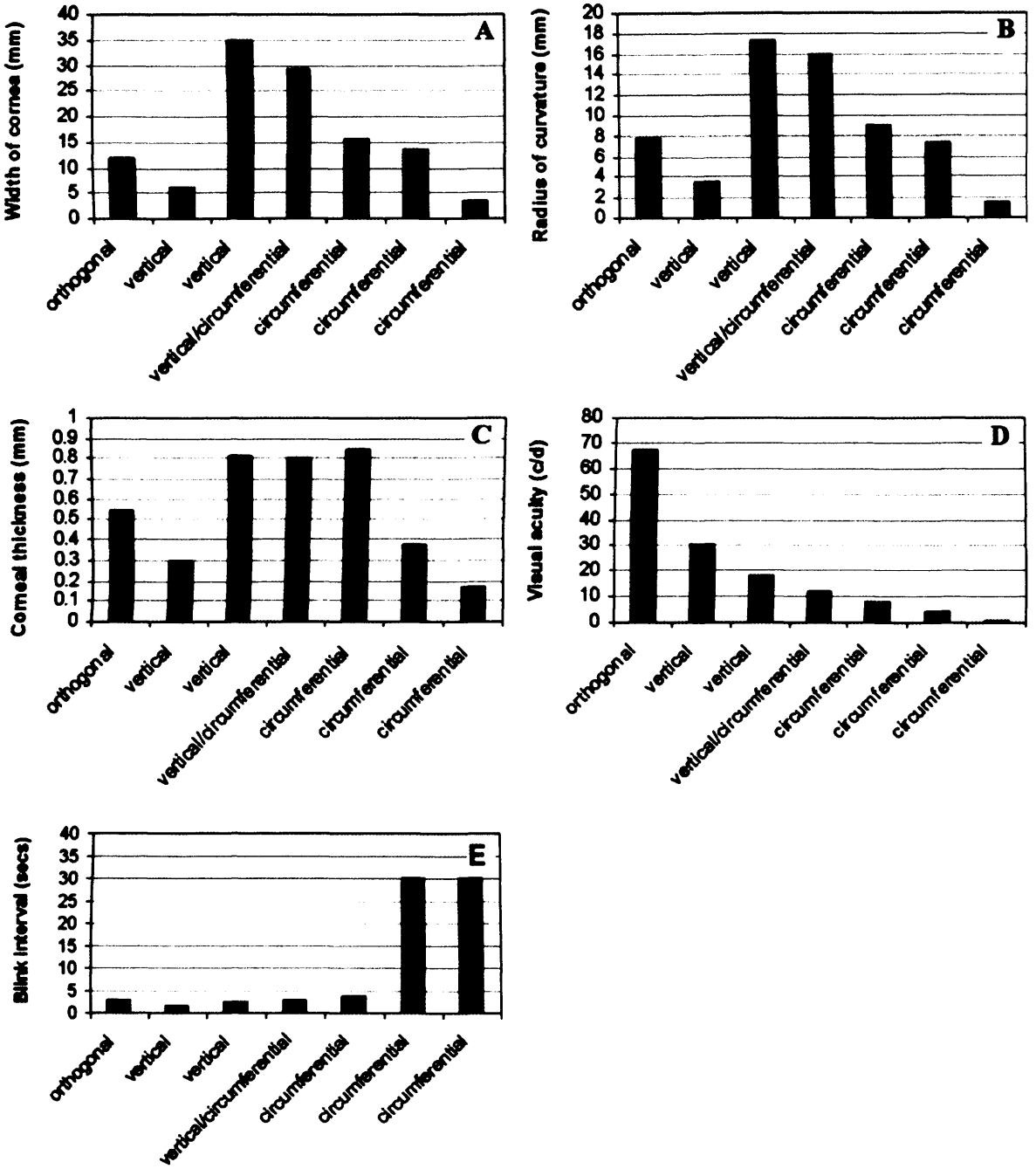

Fig. 5. **A–E:** The arrangement of corneal collagen (orthogonal, vertical, or circumferential) in the human, marmoset, horse, cow, pig, rabbit, and mouse (shown in order from left to right across each graph) is shown relative to published values of the size (A), radius of curvature (B), and thickness (C) of the cornea and the visual acuity (D) and blink interval (E) of each animal (as listed in Table 2).

ment and ocular muscle activity is needed to confirm this. As a consequence of such interspecies structural variation, one should be cautious in interpreting the clinical relevance of nonhuman corneal biomechanical studies.

ACKNOWLEDGMENTS

The authors thank Dr. Mike MacDonald, Dr. Manfred Burghammer, Clarke Maxwell, and Jon Ulmer for their help with data collection and Dr. Yifei Huang, Tom

Kelly, and Dr. Stuart Judge for the provision of specimens. Prof. Keith Meek is a Royal Society-Wolfson Research Merit Award Holder.

LITERATURE CITED

Aghamohammadzadeh H, Newton RH, Meek KM. 2004. X-ray scattering used to map the preferred collagen orientation in the human cornea and limbus. Structure 12:249–256.

Barmack NH. 1976. Measurements of stiffness of extraocular muscles of the rabbit. J Neurophysiol 39:1009–1019.

Bjork A, Kugelberg E. 1953. The electrical activity of the muscles of the eye and eyelids in various positions during eye movement. Electroencephalogr Clin Neurophysiol 5:595–602.

Blount WP. 1927. Studies of the movements of the eyelids of animals: blinking. Q J Exp Physiol 18:111–125.

Boote C, Dennis S, Meek KM. 2004. Spatial mapping of collagen fibril organisation in primate cornea- an X-ray diffraction investigation. J Struct Biol 146:359–367.

Boote C, Hayes S, Abahussin M, Meek KM. 2006. Mapping collagen organisation in the human cornea: left and right eyes are structurally distinct. Invest Ophthalmol Vis Sci 47:901–908.

Bozkir G, Bozkir M, Dogan H, Aycan K, Guler B. 1997. Measurements of axial length and radius of corneal curvature in the rabbit eye. Acta Med Okayama 51:9–11.

Coile D, O'Keefe LP. 1988. Schematic eyes for domestic animals. Ophthalmic Physiol Optics 8:215–220.

Daxer A, Fratzl P. 1997. Collagen fibril orientation in the human corneal stroma and its implications in keratoconus. Invest Ophthalmol Vis Sci 38:121–129.

Evinger C, Shaw MD, Peck CK, Manning MA, Baker R. 1984. Blinking and associated eye movements in humans, guinea pigs and rabbits. J Neurophysiol 52:323–339.

Gyi TJ, Elliott GF, Meek KM, Wall RS. 1987. Comparative structural studies of corneal stromas from a range of different species using synchroton x-ray-diffraction and electron-microscopy. Ophthalmic Res 19:32–32.

Haustein J. 1983. On the ultrastructure of the developing and adult mouse corneal stroma. Anat Embryol (Berl) 168:291–305.

Heffner RS, Heffner HE. 1992. Visual factors in sound localisation in mammals. J Comp Neurol 317:219–232.

Hirsch J, Curcio CA. 1989. The spatial resolution capacity of human foveal retina. Vision Res 29:1095–1101.

Hughes A. 1972. A schematic eye for the rabbit. Vision Res 12:123–128.

Hukins DWL, Aspden RM. 1985. Composition and properties of connective tissues. Trends Biochem Sci 10:260–264.

Jeronimidis G, Vincent JFV. 1984. Composite materials. In: Huykins DWL, editor. Connective tissue matrix. London: Macmillan. p 187–210.

Jue B, Maurice DM. 1986. The mechanical properties of the rabbit and human cornea. J Biomech 10:847–853.

Kaplan D, Bettleheim FA. 1972. On the birefringence of the bovine cornea. Exp Eye Res 13:219–226.

Kokott W. 1938. Ubermechanisch-funktionelle strikturen des auges. Albrecht von Graefes. Arch Ophthalmol 138:424–485.

Li HF, Petroll WM, Møller-Pedersen T, Maurer JK, Cavanagh HD, Jester JV. 1997. Epithelial and corneal thickness measurements by in vivo confocal microscopy through focusing (CMTF). Curr Eye Res 16:214–221.

Maurice DM. 1984. The cornea and sclera. In: Davson H, editor. The eye. London: Academic Press. p 30.

McCally RL, Farrell RA. 1982. Structural implications of small-angle light scattering from cornea. Exp Eye Res 34:99–113.

Meek KM, Leonard DW. 1993. Ultrastructure of the corneal stroma – a comparative study. Biophys J 64:273–280.

Meek KM, Blamires T, Elliot G, Gyi TJ, Nave C. 1987. The organisation of collagen fibrils in the human corneal stroma: a synchrotron x-ray diffraction study. Curr Eye Res 6:841–846.

Newton RH, Meek KM. 1998. Circumcorneal annulus of collagen fibrils in the human limbus. Invest Ophthalmol Vis Sci 39:1125–1134.

Newton RH, Meek KM. 2001. Mapping the orientations of the collagen fibrils in human cornea and sclera. Invest Ophthalmol Vis Sci 42:1517.

Ponder E, Kennedy WP. 1927. On the act of blinking. Q J Exp Physiol 18:89–110.

Prangen A. 1928. A study of the comparative anatomy of the extraocular muscles. Trans Am Ophthalmol Soc 26:353–380.

Prince JH, Diesem CD, Eglitis I, Ruskell GL. 1960. Anatomy and histology of the eye and orbit in domestic animals. Springfield, IL: Charles C Thomas.

Prusky GT, West PWR, Douglas RM. 2000. Behavioural assessment of visual acuity in mice and rats. Vision Res 40:2201–2209.

Reichel E, Miller D, Blanco E, Mastanduno R. 1989. The elastic modulus of central and perilimbal bovine cornea. Ann Ophthalmol 21:205–208.

Schmucker C, Schaeffel F. 2004. A paraxial schematic eye model for the growing C57BL/6 mouse. Vision Res 44:1857–1867.

Scott J, Bosworth T. 1990. A comparative biochemical and ultrastructural study of proteoglycan-collagen interactions in corneal stroma. Functional and metabolic implications. Biochem J 270:491–497.

Smythe RH. 1956. Veterinary ophthalmology. London: Bailliere, Tindall and Cox Ltd.

Svaldeniene E, Paunksniene M, Babrauskiene V. 2004. Ultrasonography study of equine eyes. Ultragarsas 4:49–51.

Timney B, Keil K. 1992. Visual acuity in the horse. Vision Res 32:2289–2293.

Tripathi RC, Tripathi BJ. 1984. The cornea and sclera. In: Davson H, editor. The eye. London: Academic Press. p 12.

Troilo D, Howland HC, Judge SJ. 1993. Visual optics and retinal cone topography in the common marmoset (callitrix jacchus). Vision Res 33:1301–1310.

Vaney DI. 1980. A quantitative comparison between the ganglion cell populations and axonal outflows of the visual streak and periphery of the rabbit retina. J Comp Neurol 189:215–233.

Wollensak G, Spoerl E, Seiler T. 2003. Stress-strain measurements of human and porcine corneas after riboflavin-ultraviolet-A-induced cross-linking. J Cataract Refract Sur 29:1780–1785.

Zhang EP, Schrunder S, Hoffmann F. 1996. Orthotopic corneal transplantation in the mouse-a new surgical technique with minimal endothelial cell loss. Graefes Arch Clin Exp Ophthalmol 234:714–719.